TUNING THE GROUND AND EXCITED STATE PROPERTIES OF A SERIES OF POLYMETALLIC TRIDENTATE COMPLEXES INCORPORATING Ru(II) OR Os(II) AS THE CHROMOPHORE
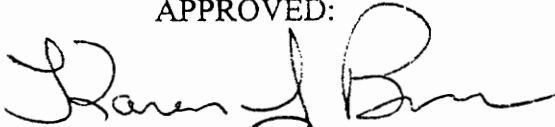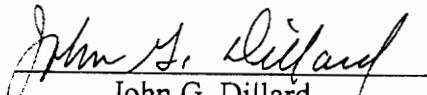
by

Lisa M. Vogler

A dissertation in partial fulfillment of
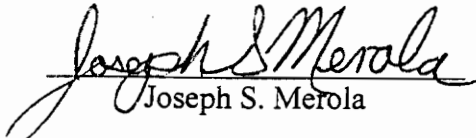the requirements for the degree of

DOCTOR OF PHILOSOPHY
IN
CHEMISTRY

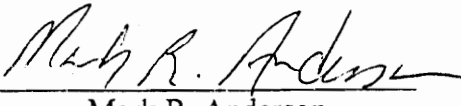VIRGINIA POLYTECHNIC INSTITUTE &
STATE UNIVERSITY

APPROVED:

Karen J. Brewer, chair

John G. Dillard

Joseph S. Merola

Brian E. Hanson

Mark R. Anderson

April 1995

Blacksburg, VA

Key Words: Tridentate, tpp, Polypyridyl, Electrochemistry, Spectroscopy, Excited-States, Photochemistry

c.2

TUNING THE GROUND AND EXCITED STATE PROPERTIES OF A SERIES OF TRIDENTATE COMPLEXES INCORPORATING Ru(II) OR Os(II) AS THE CHROMOPHORE

by

Lisa M. Vogler

Department of Chemistry

ABSTRACT

The work reported in this thesis involves the synthesis of a series of monometallic and polymetallic complexes incorporating the tridentate polypyridyl bridging ligand tpp (where tpp = 2,3,5,6-tetrakis(2-pyridyl)pyrazine) and an investigation of their ground and excited state properties. A series of ruthenium monometallic chromophore complexes has been prepared varying the ligands coordinated on the metal center. The systematic alteration of the ligands has enhanced the understanding of the electrochemical and spectroscopic properties of ruthenium polypyridyl tridentate complexes. In contrast to $[Ru(tpy)_2]^{2+}$ (where tpy = 2,2':6',2''-terpyridine), these monometallic complexes and many of the polymetallic systems emit in solution at room temperature. Methylation of one of the remote pyridine nitrogens on tpp has been accomplished forming a covalently coupled viologen that can potentially function as an electron acceptor.

Two classes of synthetically useful bimetallic complexes of the form $[(tpy)M(tpp)RuCl_3]^+$ and $[(tpy)M(tpp)Ru(tpp)]^{4+}$ have been prepared (where M = Ru(II) or Os(II)). Synthetic methods have been developed for the stepwise construction of tpp bridged systems by a building block approach. In all bimetallic complexes, the tpp bridging ligand is the site of localization of the LUMO. In the $[(tpy)M(tpp)RuCl_3]^+$ systems, the ruthenium metal coordinated to tpp and three chlorides is the easiest to oxidize and is the site of localization of the HOMO. In contrast, for the

$[(tpy)M(tpp)Ru(tpp)]^{4+}$ systems, the HOMO is localized on the metal being varied, either Ru or Os. This gives rise to complexes which possess a lowest lying excited state that is always a MLCT state involving tpp but can be tuned to involve Ru or Os metal centers. Bimetallic systems that incorporate this tpp ligand have long lived excited states in solution at room temperature ($\tau > 100$ ns). The bimetallic complex $[(tpy)Ru(tpp)IrCl_3]^{2+}$ has been studied and shown to be an electrocatalyst for the reduction of CO_2 to CO and formate.

The synthesis of the monometallic complexes has advanced the understanding of the ground and excited state properties of tridentate compounds. Incorporation of these complexes into bimetallic systems has aided in the understanding of the perturbations of these properties that occur upon formation of a polymetallic system.

because they didn't have the mind for it. These people provided all the impetus I needed to make it through the rough times throughout my graduate schooling.

I thank all my family and friends who have been supportive throughout all the many years I have spent in school, without these special people this degree would not mean as much. My sisters, Kristina and Julie, have been wonderful sources of encouragement and love throughout my many years of school and particularly in the past five years in graduate school. My parents, Anne and Roger Sheley, have always been there in times of crisis and despair and have always remained my main source of strength and love. My second set of parents, Martin and Michele Vogler, have always remained steadfast in their love and support. In addition, I thank Mark, who had to put up with all my moody spells and times of doubt. Without his support I do not know what I would have done.

TABLE OF CONTENTS

LIST OF TABLES

LIST OF ABBREVIATIONS

bpy	2,2'-Bipyridine
BL	Bridging Ligand
CT	Charge Transfer
dpb	2,3-Bis(2-pyridyl)benzoquinoxaline
dpp	2,3-Bis(2-pyridyl)pyrazine
dpq	2,3-Bis(2-pyridyl)quinoxaline
ES	Excited State
FAB MS	Fast Atom Bombardment Mass Spectroscopy
GS	Ground State
HOMO	Highest-Occupied Molecular Orbital
IC	Internal Conversion
IL	Internal Ligand
ISC	Intersystem Crossing
LF	Ligand Field
LMCT	Ligand-to-Metal Charge Transfer
LUMO	Lowest-Unoccupied Molecular Orbital
Medpp	2-[2-(1-Methylpyridiniumyl)-3-(pyridyl)pyrazine
Metpp	2-[2-(1-Methylpyridiniumyl)-3,5,6-Tris(2-pyridyl)pyrazine

mer	meridional
MLCT	Metal-to-Ligand Charge Transfer
MO	Molecular Orbital
NHE	Normal Hydrogen Electrode
TBAH	Tetrabutlyammonium hexafluorophosphate
tpy	2,2':6',2''-Terpyridine
tpp	2,3,5,6-Tetrakis(2-pyridyl)pyrazine
UV	Ultraviolet
VR	Vibrational Relaxation

DEDICATION

I dedicate this thesis to Mark, the love of my life, and to my parents.
Without the love and support of these important people
my dreams would have never come true.

Chapter I

Introduction

The main objective of this research is to investigate the ground and excited state properties of complexes incorporating a tridentate polypyridyl ligand, specifically, tpp as a bridging ligand, where tpp = 2,3,5,6-tetrakis(2-pyridyl)pyrazine).

t p p
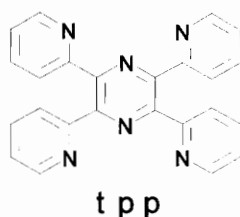
This involves the development of methods to synthesize these metal complexes as well as an investigation of their spectroscopic and electrochemical properties.

Principles of Molecular Photochemistry

Photochemistry can be defined as the chemistry induced by light on a chemical system. The first act of any photochemical or photophysical process is the absorption of a photon. When a molecule absorbs a photon and undergoes electronic excitation, an electron is promoted from the state in which it normally resides to a state of higher energy. This excited state is generally more chemically reactive than the ground state.[1] By absorbing a photon of light the ground state, A, is converted into a higher energy excited state, *A, as shown below:

Ground State (A)   Excited State (*A)
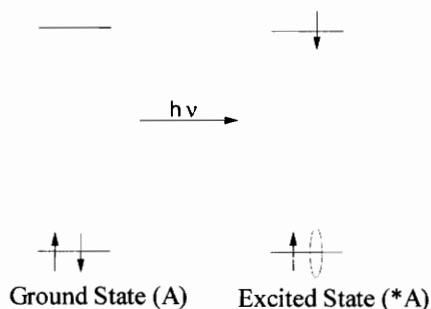
A necessary condition for excitation is that the photon energy matches the energy gap between the ground and excited states.[1] This energy gap for transition metal complexes often corresponds to light in the visible and ultraviolet. The photon energy, E, is equal to $h\nu$, where h = Planck's constant (6.626×10^{-34} Js) and ν is the frequency of the radiation with the units s^{-1}. The frequency can be converted into wavelength since ν is equal to c/λ where c is the speed of light (3×10^{8} ms^{-1}) and λ is the wavelength in meters. Generally wavelength is given in nm and will be expressed as such throughout this work. By matching the photon energy to the energy difference between molecular energy levels, molecules may be excited to higher electronic energy states.

The absorptivity of ultraviolet and visible light by a sample is given by the Beer-Lambert Law.[1] Absorbance, A, is directly proportional to the path length through the solution, l, and the concentration of the absorbing species, c. In the following equation, I_o and I are the light intensities at the front of the absorber and at a distance l, respectively.

$$I = I_o 10^{-\varepsilon cl} \text{ and } A = \varepsilon cl = \log_{10}(I_o/I)$$

The molar absorption coefficient, ε, depends on the molecule used, as well as the wavelength of light. Intensity decreases exponentially with concentration and with solution pathlength.

For a molecule to be excited, the photon energy must match the energy gap between the ground and excited states. In attempting to determine the likelihood and intensity of electronic transitions, one should realize that not all transitions occur with equal probability.[1,5] Two selection rules are particularly important and relate directly to photochemical processes: the Laporte selection rule and the spin selection rule. The probability of the absorption of photons is determined by selection rules for light absorption. The symmetry requirement for a transition is given by the following equation:

$$f \propto \left| \int_{-\infty}^{\infty} \Psi_{GS} M \Psi_{ES} \, dv \right|^2 = D$$

where f is the oscillator strength of integrated intensity and is equal to $4.315 \times 10^{-9} \int \epsilon dv$. In the equation Ψ_{GS} and Ψ_{ES} are the electronic wave functions for the ground and excited states, respectively, and M is the electronic dipole moment operator. Whenever D is not equal to zero, the transition is symmetry allowed and the electronic transition is observed. Transitions in molecules that lack a center of symmetry depend on the symmetries of the initial and final states. If the direct product of Ψ_{GS} and Ψ_{ES} with M_x, M_y, or M_z contains A_1, the transition is allowed. If all integrals are odd, the transition is forbidden. A simple example of this occurs in the case of formaldehyde when evaluating whether the $\pi \rightarrow \pi^*$ transition is symmetry allowed. The symmetry of this molecule is C_{2v}, the ground state belongs to A_1 since there are no unpaired electrons, and the excited state also belongs to A_1 ($B_1 \times B_1 = A_1$). From the character table for C_{2v} one finds that M_x corresponds to B_1, M_y to B_2, and M_z to A_1. The direct product of Ψ_{GS} and Ψ_{ES} with M_z will result in A_1, thus this is symmetry allowed. The direct product with M_x or M_y will result in an odd integral, thus these are forbidden transitions.

The Laporte selection rule for molecules possessing a center of symmetry states that allowed transitions are those accompanied by a change in parity. This rule requires that transitions between states must be either $u \rightarrow g$ or $g \rightarrow u$, but not $g \rightarrow g$ or $u \rightarrow u$. In this case g stands for gerade, German for even, and u stands for ungerade, meaning odd. The d and s orbitals are gerade whereas the p orbitals are ungerade. Therefore, $d \rightarrow d$ transitions in centrosymmetric complexes are forbidden.

For a transition to be spin allowed the spin multiplicity of the ground and excited states must be the same.[8] The spin quantum number for a state is given by the equation $m = 2S + 1$, where m is the spin multiplicity and S is the total spin of all electrons. In a singlet state, the spins are antiparallel ($\uparrow\downarrow$), the total spin of the electrons is zero, and the spin multiplicity is equal to one. In a species with two unpaired electrons having parallel spin, $\uparrow\uparrow$, $S = 1$ and the multiplicity is three, a triplet state. Transitions involving excitation into a state of different multiplicity are said to be forbidden and these are generally not observed in the absorption spectra because of their low intensity. In triplet

states the electrons must occupy different orbitals, since pairs of electrons with parallel spins are forbidden from occupying the same region of space (Pauli exclusion principle).

Forbidden transitions can be observed because of perturbations between states.[1] Two mechanisms by which a forbidden transition is observed are vibronic coupling and spin orbit coupling. The symmetry selection rule breaks down for complexes where vibronic coupling changes the symmetry of the molecule. If a vibration removes the center of symmetry of the complex, the g, u classification of the states is relaxed in the excited state. The spin selection rule breaks down for complexes where spin-orbit coupling occurs. An electron possesses spin, and therefore possesses a magnetic moment. A magnetic moment also arises from the orbital angular momentum of a charged nucleus circling the electron. This magnetic field can interact with the spin magnetic moment of the electron resulting in a spin-orbit interaction. The effect is that spin is no longer a valid quantum number. Therefore, a forbidden transition involving a spin flip is observable because of the coupling between the spin and orbital motion of an electron. Since the intensity of a spin forbidden transition is much smaller than that of a spin allowed transition, the spin forbidden transitions are often hidden in the absorption bands of the spin allowed transitions.

Vibrational levels are associated with the ground electronic state and with each excited electronic state.[9-12] Each nuclear vibration possesses a distinct energy and occupies a unique position on a vibrational energy scale. Figure 1 shows the electronic potential energy as a function of internuclear distance. In this diagram the ground and first excited electronic state potential energy wells are shown. In the formation of excited states, light absorption normally takes place from the lowest vibrational level of the ground electronic state. This generates the excited state in a high vibrational level. The excited state populated initially upon absorption is called the Franck-Condon excited state and possesses the geometry of the ground state, but with a new electronic structure. The vibrationally excited molecules disperse the excess vibrational energy quite rapidly via a vibrational relaxation, VR. Vibrational relaxation can be described as the loss of any excess vibrational energy associated with the molecule as a consequence of
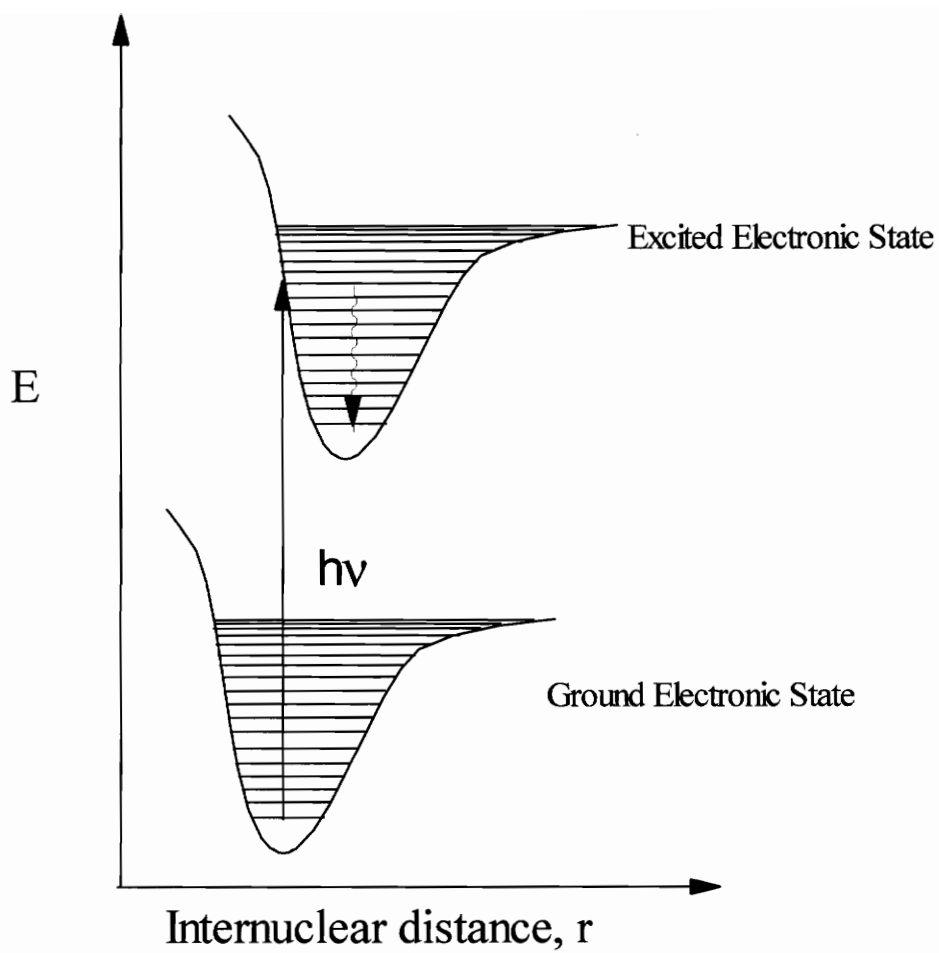
Figure 1. Morse Potential Energy Curves.

absorption. It is represented by a wavy arrow in the diagram. The lowest vibrational level of the electronically excited state is called the equilibrium, or thermally relaxed, excited state, the "thexi" state.[12] The energy corresponding to the equilibrated state is E_{00}, and represents the energy difference between the lowest vibrational level in the ground electronic state and the lowest vibrational level in the excited state.

A Jablonski (state) diagram, as shown in Figure 2, is a convenient layout to trace the pathways for the formation and decay of excited states. Shown on the left of the diagram are excited states of the same spin multiplicity. These are populated directly by optical excitation of the ground state, M. On the right side of the diagram are excited states of spin multiplicity, N, different than those initially obtained.

The excited states are unstable species of higher energy than the ground state and must undergo deactivation of some type. Four major processes can occur following excitation: luminescence, nonradiative decay, a photochemical reaction or a quenching process.[1,5] Luminescence is used when discussing the radiative process that leads to the generation of light , hv', upon relaxation to a lower energy state. Nonradiative decay refers to a process that releases heat to the environment upon relaxation. An excited state can also undergo a photochemical reaction resulting in the formation of chemical products that are not the original ground state. Quenching processes are bimolecular processes that involve the addition of another substance, a quencher. It can react with the excited state to yield the original ground state and/or other products.

Electronically excited molecules can return to the ground state by emitting a photon of light. This radiative deactivation can be separated into two classes, fluorescence and phosphorescence. Luminescence produced by an electronic transition in which the spin multiplicities of the initial and final states are the same, is called fluorescence. Phosphorescence is the emission that occurs with the relaxation from the excited state to a state with a different spin multiplicity.

There are also radiationless deactivation pathways to the ground state and these release energy to the environment in the form of heat. Nonradiative decay processes in which the initial and final states have the same spin multiplicity, are called internal
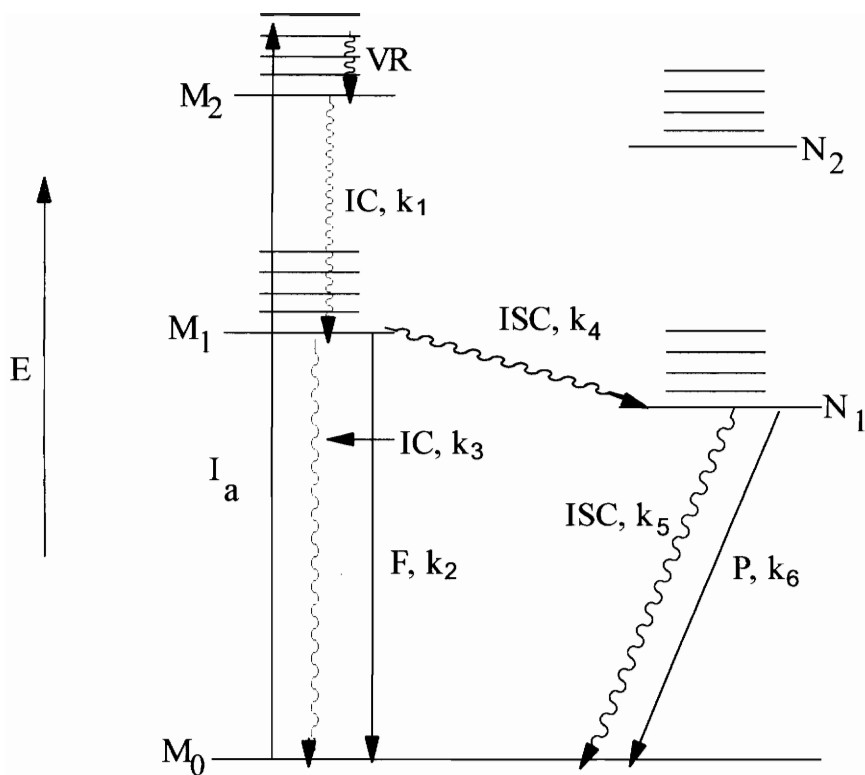
M = same spin multiplicity (1)

N = different spin multiplicity (3)

VR = Vibrational Relaxation

IC = Internal Conversion, k_1 or k_3

F = Fluorescence, k_2

ISC = Intersystem Crossing, k_4 or k_5

P = Phosphorescence, k_6

Figure 2. Jablonski Diagram

conversion, IC. Nonradiative decay to the manifold of triplet states, or decay between states of different spin multiplicities, is called intersystem crossing, ISC. Intersystem crossing, which involves a spin flip, usually results in the formation of a vibrationally excited state. Hund's rule states that spectroscopic states with higher spin multiplicities, triplet states, are lower in energy than those with lower spin multiplicities, or singlet states. Following ISC, rapid vibrational relaxation occurs forming N_1 in its lowest vibrational state releasing heat to the environment. In most d^6 platinum group coordination complexes of the type studied here, near unity population of this lowest lying state, N_1, occurs.[8,14] This rule comes from the general principal that radiationless decay from upper excited states is very fast, and relaxation to the lowest excited state occurs with nearly 100 % efficiency. The absence of fluorescence in these complexes arises from spin-orbit coupling accelerating intersystem crossing.

Quantum yield, Φ, is defined as the ratio of the moles of species produced (photons or molecules) divided by the number of moles of photons absorbed by the reaction system.[6,9,12] For each process one can calculate the quantum yield for the process. For a directly populated state, M_1 for example, the quantum yield is equal to the rate constant of the process of interest, divided by the sum of all the rate constants for deactivation, i.e., $\Phi_F = \kappa_2/(\kappa_2+\kappa_3+\kappa_4)$. For an indirectly populated state, N_1, the quantum yield is equal to the quantum yield for the population of that state, multiplied by the process of interest, divided by the sum of the rate constants for deactivation. The quantum yield of phosphorescence can be expressed as follows:

$$\Phi_P = \Phi_{ISC}[k_5/(k_5+k_6)]$$

where $\Phi_{ISC} = k_4/(k_2 + k_3 + k_4)$, the efficiency of the population of the emitting state from the state directly populated upon absorption.

Another expression that will be used is τ, the lifetime of the excited state. τ is equal to one divided by the sum of all the rate constants for the processes that correspond to the disappearance of the reactive excited state. The lifetime of M_1 is equal to $1/(k_2 + k_3 + k_4)$, whereas the lifetime of N_1 is equal to one divided by $k_5 + k_6$.

The relationship between the nonradiative rate constant and the emission energy is given by the energy gap law. The energy gap law predicts that for a series of related excited states based on the same chromophore, radiationless decay rates are determined largely by the orbital overlap between the ground and excited states.[22,45] If the basis for the chromophore and the nature of the deactivating, or acceptor vibration remain the same through the series, the nonradiative rate constant, k_{nr}, varies with the excited state energy as follows:

$$\ln k_{nr} \approx A - BE_{EM}$$

where k_{nr} is the nonradiative rate constant and E_{EM} is the energy of the emission. A and B are positive constants that depend on the magnitude of the vibrationally induced electronic coupling between the states, and the properties of the acceptor vibrations, respectively. Thus, as the energy gap decreases, the nonradiative rate constant increases. The validity of this is important in the design of photosensitizers. The MLCT excited state energy, and consequently the lifetime of this state, can be increased by designing complexes that have large energy gaps between the ligand and metal-based redox levels.

In constructing the electronic configuration of inorganic complexes using π acceptor ligands, it is useful to consider an octahedral complex, a prototype of many transition metal complexes, as shown in Figure 3. Molecular orbitals can be regarded as the linear combinations of the atomic orbitals of the atoms that comprise the molecule.[1-4] When two atomic orbitals of similar energy combine to form a molecular orbital, both bonding and antibonding molecular orbitals are formed. In a bonding situation the electron density is increased between the nuclei. In an antibonding case the electron density between nuclei is decreased, thus resulting in a node. On a vertical energy scale, the antibonding orbital lies at higher energy than the bonding orbital. Electrons residing within the atomic orbitals populate the newly formed molecular orbital, and the maximum number of electrons in one molecular orbital is two.

As shown in Figure 3, in transition metal complexes the molecular orbitals are made up of linear combinations of the s, p, and d atomic orbitals of the metal, and the s and p atomic orbitals of the ligands. The octahedral crystal field of the ligands splits the
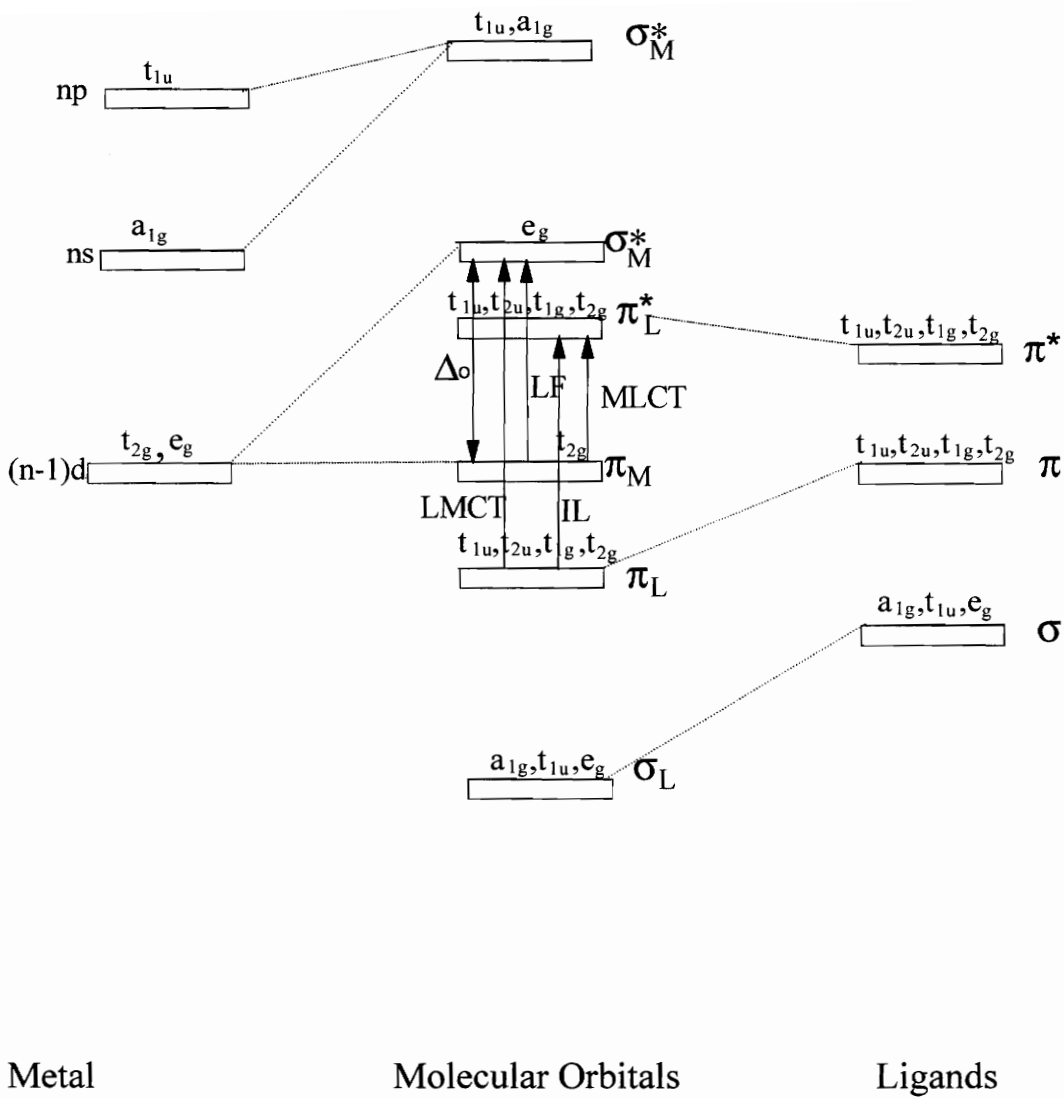
Figure 3. Molecular orbital diagram for an octahedral metal complex

five degenerate d orbitals, by an amount Δ_o, into a triply degenerate t_{2g} level and a doubly degenerate e_g level.[1-4] The triply degenerate t_{2g} symmetry set contains the d_{xy}, d_{xz}, d_{yz} orbitals that are directed between the ligands and are stabilized. The e_g symmetry set contains the d_{z^2} and $d_{x^2-y^2}$ orbitals that are directed towards the ligands and are destabilized. The t_{2g} symmetry set is suitable for bonding with the p orbitals of the ligands to form π bonds. Conversely, the e_g symmetry set combines with the σ orbitals of the ligands to generate σ bonds. The magnitude of the splitting is given by the crystal field splitting, Δ_o.[1-4,7] This is a particularly important parameter that is determined by the crystal field strength of the ligands and the central metal ion. If Δ_o is large (strong field/low spin) it is energetically more favorable to pair electrons in the t_{2g} level than to keep them unpaired by distributing them throughout the t_{2g} and e_g levels (Hund's Rule).

The absorption spectra of transition metal complexes contain several bands that correspond to the transitions illustrated in Figure 3. The spectroscopic states are derived from the various orbital configurations. The lowest energy excited state is one in which an electron is promoted from the highest-occupied molecular orbital (HOMO) to the lowest-unoccupied molecular orbital (LUMO). There are three types of excited states that can be classified as follows:[1-4,6]

1) Internal Ligand, IL, ligand localized excited states

2) Ligand Field, LF, metal localized excited states and

3) Charge Transfer, CT, metal and ligand localized excited states.

Transitions taking place between molecular orbitals with mainly ligand character are called internal ligand, IL, transitions. In transition metal complexes, these transitions are generally $\pi \rightarrow \pi^*$ transitions derived by promoting an electron from a π bonding orbital to a π^* orbital. These high energy absorptions are generally spin and symmetry allowed, with extinction coefficients on the order of 10^5-10^6 $M^{-1}cm^{-1}$.

In O_h symmetry, LF bands are low intensity, symmetry forbidden transitions that are generally observed in the visible region, if at all. In d^6 metal complexes, singlet and triplet $d \rightarrow d$ states arise by promoting a bonding t_{2g} electron to an e_g level ($t_{2g}^5 e_g^1$). A

problem with exciting low lying LF states is that the t_{2g} orbitals are bonding with respect to ligands while e_g orbitals tend to be antibonding. Thus, with d-d states of $t_{2g}^5 e_g^1$, it is observed that ligand loss and ligand substitution occur upon excitation. Because these transitions are symmetry forbidden, the extinction coefficients are on the order of $1\text{-}10^2\ M^{-1}cm^{-1}$.

Charge transfer states involve both the organic ligand and the metal. There are two types of CT excited states, ligand-to-metal charge transfer, LMCT, and metal-to-ligand charge transfer, MLCT, transitions. Ligand-to-metal charge transfer bands involve the transfer of electronic charge from the ligands towards the coordinating metal. LMCT involves promoting an electron from a ligand orbital to a metal orbital, $(\pi^{N-1}\sigma^{*1})$ or $(\sigma^{N-1}\sigma^{*1})$. MLCT transitions involve promoting an electron from a metal orbital to a ligand orbital $(t_2^5\pi^{*1})$. If the donor is an electron rich ligand (NH_3 or a halogen) and the acceptor is readily reduced, the transition is a LMCT. If the donor is an oxidizable metal such as Ru^{2+} or Os^{2+}, and the acceptor is an electron poor ligand such as bpy or phen, the transition is an MLCT. These bands are usually Laporte and spin allowed, thus giving rise to extinction coefficients on the order of $10^4\ M^{-1}cm^{-1}$. Since charge is being transferred, the photochemistry resulting from these transitions generally involves redox processes.[6,8] The excited state, following the charge transfer, is a stronger oxidizing and reducing agent than the ground state. This is due to the shift in electron density between the metal and the ligand.

Photoinduced Energy and Electron Transfer

In addition to the unimolecular processes described, the excited state can also participate in bimolecular processes. When the lifetime of the excited state is long enough for the excited molecule to encounter another molecule, *A can return to A. This is called a quenching process. The most important bimolecular processes are energy transfer[6,18-19] and electron transfer[6,16-18] reactions. During quenching, the sensitizer induces permanent or temporary chemical changes in surrounding ground-state molecules.

Energy transfer is the process by which excitation energy passes from a photoexcited molecule to an adjacent molecule in its ground state, a quencher. The quencher must have a thermodynamically accessible excited state, one with energy lower than that of the photoexcited molecule. In an energy transfer process, when the quencher receives the excess energy of the excited state, the quencher itself becomes excited and subsequently undergoes the same physical and chemical processes as if excited directly. As shown in the reaction below, *A, the excited state of the photosensitizer A, transfers its excitation energy to the quencher B, producing the excited state *B as *A relaxes to its ground state A.

$$A + h\nu \rightarrow \text{*A} \qquad \text{excitation}$$

$$\text{*A} + B \rightarrow A + \text{*B} \qquad \text{energy transfer}$$
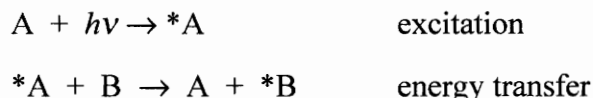
Photoinduced energy transfer occurs in systems that consist of a covalently linked photosensitizer and quencher. This phenomenon has been shown to occur in polymetallic systems composed of various metal centers.[25,38,45,55,57,69] As stated previously, the requirement for energy transfer to occur is that the quencher have an excited state of lower energy than the photosensitizer. Polymetallic complexes can be designed using metals possessing different excited states such that energy transfer occurs upon excitation. An example of a such a system involves the use of Ru(II) and Os(II) as the metal centers in a supramolecular complex $[(X_1tpy)Ru(tpy(ph)_n)tpy)Os(tpyX_2)]^{4+}$ (where X_1 and X_2 = Meph or MeO_2S, and n = 0, 1, and 2). In analogous monometallic

complexes, where only the metal is changed from Ru(II) to Os(II), it is found that the energy of the luminescent ^{3}MLCT level for the Os complexes is of lower energy than that of the Ru complexes. A polynuclear compound containing these monometallic components covalently linked through a bridging ligand will undergo energy transfer. If only one luminescent band is present, it is concluded that the ^{3}MLCT excited state of the ruthenium based component is quenched by the osmium based component.[69]

Electron transfer describes the process by which an electron is passed from an electron donor to an electron acceptor. The charge separation provides a way to convert the excitation energy of the excited molecule to chemical potential. In general, the excited state of a metal complex is both a stronger oxidant and reductant than the ground state from which it originates. In oxidative electron transfer, the excited state of the photosensitizer, *A, transfers an electron to B, the quencher, resulting in a singly oxidized photosensitizer and a singly reduced quencher. In reductive electron transfer, the quencher becomes oxidized and the photosensitizer becomes reduced. These two electron transfer processes are shown below:

$$A + h\nu \rightarrow {}^*A \qquad \text{excitation}$$

$$^*A + B \rightarrow A^+ + B^- \qquad \text{oxidative electron transfer}$$

$$^*A + B \rightarrow A^- + B^+ \qquad \text{reductive electron transfer}$$
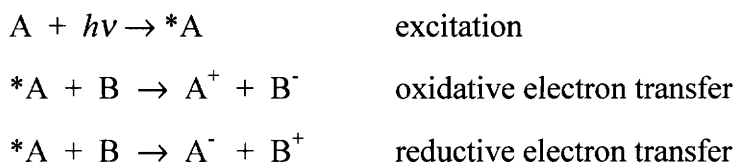
Photoinduced intramolecular electron transfer from a donor to a covalently attached acceptor can also occur. The photoinduced electron transfer processes in covalently linked donor-acceptor systems are optical electron transfer, photoinduced electron transfer, charge transfer emission, and thermal back-electron transfer. In the processes shown below, A is the donor of electronic energy, L is a linker, and B is the quencher. As discussed above, reductive quenching can also occur where electron transfer from a donor to a photoexcited acceptor occurs.

(1) $\quad$ A - L - B + $h\nu' \rightarrow$ A$^+$ - L - B$^-$ $\qquad$ optical electron transfer

(2) $\quad$ A - L - B + $h\nu'' \rightarrow$ *A - L - B $\qquad$ photoinduced electron transfer

$\qquad$ *A - L - B $\rightarrow$ A$^+$ - L - B$^-$ $\qquad\qquad$ (oxidative quenching)

(3) $A - L - B + hv'' \rightarrow *A - L - B$ photoinduced electron transfer

    $*A - L - B \rightarrow A^- - L - B^+$ (reductive quenching)

(4) $A^+ - L - B^- \rightarrow A - L - B$ thermal back electron transfer

    (charge recombination)
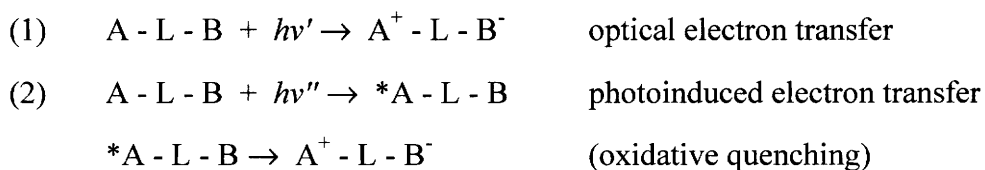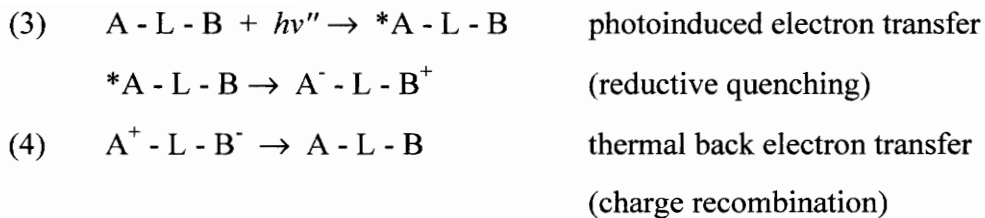
In covalently linked chromophore-quencher complexes, photoexcitation of the chromophore initiates forward electron transfer. This leads to the formation of the charge transfer state that can then undergo back electron transfer to regenerate the ground state. Variations of the distance separating the donor from the acceptor, as well as variations of the driving force for the electron transfer, influence the dynamics of intramolecular electron transfer.

In the classical Marcus-Hush theory, the initial nuclear geometry of the reactant state undergoes reorganization to a transition state prior to electron transfer. The energy of the transition state, ΔG^*, is gained by intermolecular collisions, in order to satisfy the conservation of energy and momentum. The rate for an electron transfer process is given by:[6,25,70,83]

$$k_{ET} = \kappa_{el}\nu_N \exp(-\Delta G^*/RT)$$

In these equations, k_{ET} is the rate of electron transfer, κ_{el} is the electronic transmission coefficient, and ν_N is the frequency of nuclear motion (approximately equal to 6×10^{12} s^{-1} at 25 ^{O}C), R is the gas constant, T is the temperature in Kelvin, and ΔG^* is the free energy of activation required to reorganize the reactants and surrounding medium prior to the electron transfer. The product of the electronic transmission coefficient and the frequency of nuclear motion is given by the equation

$$\kappa_{el}\nu_N = \{2H_{AB}^2/h\}\{\pi^3/\lambda k_B T\}^{1/2}$$

where k_B is the Boltzman constant, h is Planck's constant, H_{AB} is the donor-acceptor electronic coupling matrix, and λ is the reorganization energy. The free energy of activation is expressed as

$$\Delta G^* = (\lambda/4)(1+ \Delta G/\lambda)^2$$

where ΔG is the standard free energy change of the reaction, and λ is the nuclear reorganization energy. The reorganization energy has both inner, λ_i, and outer, λ_o, sphere components where λ_o is the predominant contribution. The outer sphere reorganization energy is given by

$$\lambda_o = e^2[1/2r_D + 1/2r_A - 1/r_{DA}][1/\varepsilon_{OP} - 1/\varepsilon_S]$$

In this equation, e is the charge transferred, r_D is the radius of the donor, r_A is the radius of the acceptor, and r_{DA} is the donor acceptor separation. ε_{OP} and ε_S are the optical and static dielectric constants of the solvent where ε_{OP} is generally given as the square of the refractive index. A plot of $\log k_{FET}$ versus ΔG_{FET} gives a value for the preexponential factor from which λ can then be estimated. The calculated values of λ are always larger than that those estimated values given by fitting the experimental data.

For a series of reactions having the same λ and κ values, a log k_{ET} versus ΔG plot is a bell shaped curve. This curve contains a normal region in which k_{ET} increases with driving force, region I, a maximum where $-\Delta G = \lambda$, II, and a region in which log k_{ET} decreases with increasing driving force, III. Region III, that in which an increase in the driving force is predicted to act against the rate of electron transfer, is called the Marcus inverted region($\Delta G < -\lambda$).
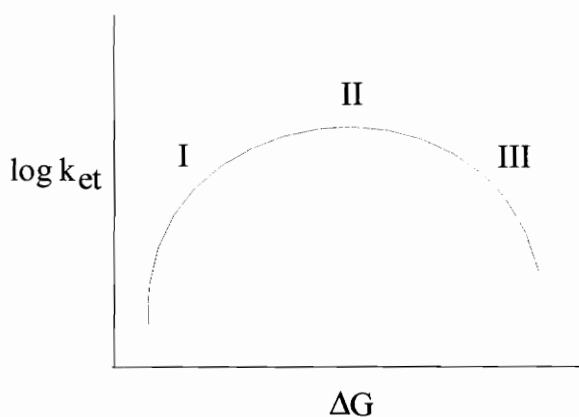
The total reorganization energy, λ, is made up of both inner and outer sphere components, $\lambda = \lambda_i + \lambda_o$. The inner sphere barrier, λ_i, corresponds to the reorganization energy due to changes in the bond lengths and angles within the two reaction partners.

λ_o is the outer sphere barrier, which corresponds to the reorganization energy within the surrounding solvent molecules. Values of k_{ET} can be calculated assuming ν_N, κ_{el}, and λ are invariant from complex to complex in a series.

By varying the length of a spacer bridge in supramolecular complexes, it is possible to study the distance dependence on the rate of electron transfer.[25,71,83] In a series of donor-acceptor complexes where the driving force, ΔG and the reorganization energy, λ, stay the same while distance between the electron acceptor and donor is varied, the rate constants can be found using the equation below.

$$k_{ET}(r) = k_{ET}(R_o)\exp[-\beta(r-R_o)]$$

In this equation, R_o is a reference distance, r is the center-to-center distance between the donor and acceptor, and β is an empirical parameter that expresses the attenuation of k_{ET} with increasing separation. Increasing the distance between the components accessible for charge separation may inhibit the fast back electron transfers thus allowing a more practical use for the molecule.

The activation energy for electron transfer, $\Delta G^{\ddagger}$, can be related to the driving force, ΔG, through the application Marcus and Hush theories. The thermodynamic driving force for forward and back electron transfer for reductive quenching $(A\text{-}B \rightarrow {}^*A\text{-}B \rightarrow A^-\text{-}B^+)$ can be estimated from the electrochemical and emission data using the following equations:[6,25,83]

$$\Delta G_{forward} \approx E_{1/2}(B/B^+) - E_{1/2}(A/A^-) - E_{00}$$

$$\Delta G_{back} \approx E_{1/2}(A/A^-) - E_{1/2}(B/B^+)$$

For oxidative quenching $(A\text{-}B \rightarrow {}^*A\text{-}B \rightarrow A^+\text{-}B^-)$

$$\Delta G_{forward} \approx E_{1/2}(B/B^-) - E_{1/2}(A/A^+) - E_{00}$$

$$\Delta G_{back} \approx E_{1/2}(A/A^+) - E_{1/2}(B/B^-)$$

where A is the chromophore and B is an electron donor in the reductive quenching case and an electron acceptor in the oxidative quenching case. In the equations, $E_{1/2}$ values are from the cyclic voltammetry and E_{00} is the energy of the zero-zero vibrational level

of the emissive state. $E_{1/2}$ (D/D$^+$) is the half-wave potential for the oxidation of the electron donor and $E_{1/2}$(A/A$^-$) is the half-wave potential for the reversible reduction of the electron acceptor. In a complex containing a covalently attached electron acceptor, $E_{1/2}$ (D/D$^+$) corresponds to the oxidation of the metal in the complex, and $E_{1/2}$ (A/A$^-$) corresponds to the reduction of the electron accepting moiety. Likewise, in a complex containing a covalently attached electron donor, $E_{1/2}$ (D/D$^+$) corresponds to the oxidation of the electron donating moiety, and $E_{1/2}$ (A/A$^-$) corresponds to the first reduction in the metal complex.

Nature of MLCT Excited States versus LF states

Ligand field state excitation involves the promotion of an electron from a metal $d\pi$ orbital into a metal $d\sigma^*$ orbital at higher energy.[1-4] This removes electron density from the metal localized, nonbonding, t_{2g} orbitals, and places it into an antibonding e_g metal localized orbital. Overall, this increases the electron density between the metal and ligand antibonding molecular orbitals that leads to the possibility of ligand loss. When the lowest excited state is LF, it undergoes fast radiationless deactivation to the ground state and/or ligand dissociation reactions. As a consequence, room temperature excited state lifetimes are very short and generally no luminescence is observed. Because of their Laporte forbidden nature, absorption bands arising from d $\rightarrow$ d transitions are weak and generally not observed in the absorption spectra of low spin d^6 O_h polypyridyl complexes.

Metal-to-ligand charge transfer transitions involve the excitation of an electron from a metal $d\pi$ orbital belonging to the t_{2g} symmetry set to a π^* antibonding ligand orbital.[1-4] The result is an oxidized metal and a reduced ligand. MLCT excited states are therefore both better oxidizing and reducing agents than the ground state. These types of transitions do not lead to ligand loss upon excitation. When the lowest excited state is

18

MLCT it does not undergo fast radiationless decay to the ground state and luminescence can usually be observed.

An estimate of the excited state redox potentials can be found from the redox potentials of the ground state and the spectroscopic excited state energy.[25,45,50] These potentials can be calculated using the following equations:

$$E^{\circ}(*M/M^-) = E^{\circ}(M/M^-) + E_{00}$$

$$E^{\circ}(*M/M^+) = E^{\circ}(M/M^+) - E_{00}$$

where $E^{\circ}(*M/M^-)$ and $E^{\circ}(*M/M^+)$ are the reduction and oxidation potentials of the excited state, respectively. $E^{\circ}(M/M^-)$ is the electrochemically measured reduction potential, $E^{\circ}(M/M^+)$ is the electrochemically measured oxidation potential, and E_{00} is the zero-zero energy of the emissive state.

The goal of this research is to design complexes in which the lowest excited state is a MLCT state, thus preventing photochemical instability. To control excited state properties, one must also control the relative energy of the states. The nature and energy of the lowest excited state must be such that the complexes have reasonably long lifetimes as well as being chemically and photochemically stable. Consequently, d-d states must be well above this MLCT excited state to prevent the thermal excitation of the LF state, thereby resulting in photochemical instability and rapid excited state decay.[8,11,22]

The complexes being studied contain either a ruthenium or osmium metal center with polypyridine ligands completing the coordination sphere. Ru^{2+} and Os^{2+} are d^6 metals. The polypyridine ligands coordinated to these metals are usually colorless possessing σ-donor orbitals localized on the nitrogen atoms and π donor and π^* acceptor orbitals more or less delocalized on the aromatic rings.[8,11,22] Spin-orbit coupling should be high resulting in relaxation of the spin selection rule. This allows the probability of emission to increase and radiative decay to compete more efficiently with radiationless decay. The excited state lifetime for many complexes with a MLCT transition is long enough to allow for quenching processes to take place.

A primary goal is to design complexes in which the d-d state is thermally inaccessible from the emitting MLCT state. This can be accomplished by increasing Δ. This can be accomplished by varying either the metal or the ligands coordinated. [1-4,7] The magnitude of Δ can be changed by using a metal that is in a lower row on the periodic chart. As you descend a column, Δ increases due to the larger size of the orbitals that extend further from the central atom. Second and third row transition metals have a high crystal field splitting. This makes complexes containing these metals of almost exclusively low spin (energy of Δ is larger than the pairing energy). In the case of Ru versus Os, Δ is much larger for Os resulting in a d-d excited state much higher in energy than the MLCT. The LF state becomes sufficiently above the MLCT excited state, thus preventing thermal excitation of the LF state and rapid excited state decay.

Another way to influence Δ is through the nature of the ligands coordinated to the metal center. Incorporating π bonding ligands(halides) increases the energy of the t_{2g} orbitals, thus decreasing Δ. Ligands containing $\pi*$ bonding have a high crystal field effect due to their ability to accept electron density from the metal. The use of π backbonding ligands stabilizes the t_{2g} set thus increasing Δ. The crystal field strength of the following ligands increases in the series for the metal ion of interest

$$Cl^- < py << bpy, phen < CN^- < CO.$$
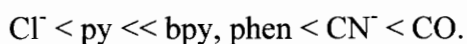
Polypyridyl ligands have vacant $\pi*$ orbitals that can accept electron density from the metal. The result is that complexes incorporating these ligands are strong field/low spin. The ability of these ligands to π-backbond allows the $d\pi$ orbitals to be stabilized, thus increasing Δ. Due to the increased aromaticity of the ligands used in this study relative to bpy and phen, as well as the enhanced ability to π-backbond, the ligands used in this study would be expected to lie between bpy, phen, and CN^-. The crystal field strength of the ligands dpp, dpq, dpb, and tpp should increase in the series dpp<tpp<dpq<dpb (see Figure 4 for the structure of the ligands). The σ donor strength would decrease and the π-backbonding ability would increase in this series.

The energy of the excited state is dependent upon both the metal and the ligands that are coordinated. If the ligands are to remain the same, substitution of a metal with one that is easier to oxidize lowers the energy of the MLCT transition. If the metal center, as well as the oxidation state of the metal, is kept the same, variation of the ligands with ones that are better π acceptors, stabilizes the π^* orbital and results in the lowering of the MLCT excited state energy. From these two variations it becomes apparent that the energy of the MLCT transition could be systematically tuned to contain the properties that are desired of the complex.

The following is an example where variation of the ligand has an effect on the emitting state and consequently on the lifetime of the complex. $[Ru(bpy)_3]^{2+}$ has a lowest lying absorbance at 450 nm, emission at 603 nm and a lifetime of 850 ns.[27,45,50] Replacing the bpy ligands with tpy ligands results in the formation of $[Ru(tpy)_2]^{2+}$.[51,52] This compound has a lowest lying absorbance at 474 nm and no emission intensity at room temperature. The absence of a room temperature emission for $[Ru(tpy)_2]^{2+}$ has been explained as a consequence of the LF excited state being in close proximity to the MLCT excited state. At 77 K, however, the emission for $[Ru(tpy)_2]^{2+}$ is observed at 620 nm with an excited state lifetime of 10 µs. This leads to the conclusion that the lowest energy excited state is the MLCT state, but at room temperature the thermal population of the LF state occurs, thus resulting without an emission. An idea of the energy gap separating the ^{3}MLCT and ^{3}LF state can be obtained through temperature dependent lifetime measurements. An activation energy of 1500 cm^{-1} has been obtained from an Arrhenius plot of -lnτ versus 1/T (T in Kelvin) which represents the barrier associated with crossing from the ^{3}MLCT to the short-lived ^{3}LF state.[54]
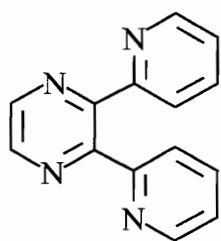
dpp = 2,3-bis(2-pyridyl)pyrazine
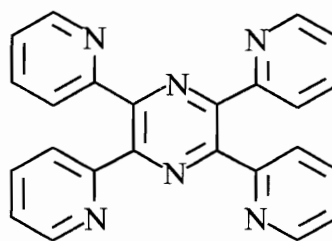
tpp = 2,3,5,6-tetrakis
(2'-pyridyl)pyrazine
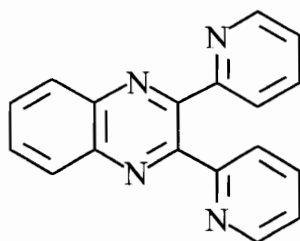
dpq = 2,3-bis(2-pyridyl)quinoxaline
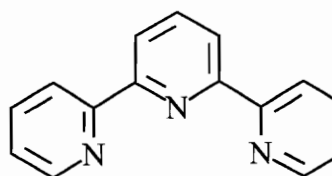
tpy = 2,2':6',2''-terpyridine
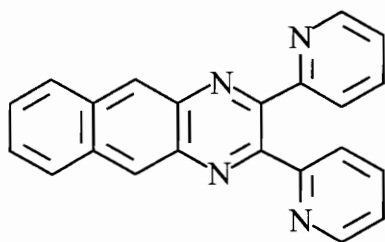
dpb = 2,3-bis(2-pyridyl)benzoquinoxaline
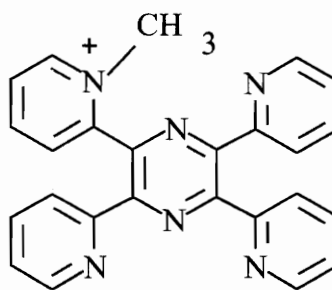
Metpp = 2-[2-(1-Methylpyridiniumyl)]-
3,5,6-tris(2-pyridyl)pyrazine

Figure 4. Polypyridyl Ligands Used in this Study

Polypyridyl Complexes

Since the discovery of $[Ru(bpy)_3]^{2+}$, many studies have concentrated on the utilization of the long lived metal-to-ligand charge transfer (MLCT) excited states in photochemical energy conversion schemes.[14,15,21-29,45,50] For $[Ru(bpy)_3]^{2+}$, the lowest excited state is relatively long lived ($\tau = 850$ ns) with a quantum yield for the formation of this state of near unity ($\Phi_{em} = 0.062$). The excited state of $[Ru(bpy)_3]^{2+}$ is long enough to encounter solute molecules and acts as an electron donor, electron acceptor, or energy donor.

Because of the electron transfer properties of $[Ru(bpy)_3]^{2+}$, research focused on the modification of bpy to other polypyridine ligands. Thus, a large number of polypyridine complexes have been synthesized, and their photochemical and photophysical properties have been investigated.[23-39] Many of these complexes are monometallic complexes of the general formula RuL_3^{2+}, where L represents a bidentate polypyridyl ligand that is a bpy derivative.

An important feature of polypyridyl complexes is the possibility of changing the various ground and excited state properties. This is accomplished through the variation of the ligands coordinated to the metal by using ligands having different π accepting and σ donating abilities. Consequently, such complexes possess easily tunable redox properties allowing them to be ideal components for excited state electron transfer processes.

The synthesis of mixed ligand complexes with more than one polypyridyl ligand allows one to probe the nature of the excited state. Numerous studies have investigated complexes of the type $[Ru(bpy)_2(BL)]^{2+}$, where BL = dpp, dpq, and dpb as shown in Figure 4.[8,25,36,40,41] In mixed ligand complexes of this type, the lowest excited state absorption is a MLCT transition from the $Ru(d\pi)$ to a ligand(π^*) orbital. The ligand where the CT is localized will be the ligand that is most easily reduced, which in the case of these ligands, is the ligand being varied, dpp, dpq, or dpb. In the series of complexes, the energy of the metal based orbital remains fairly constant, thus all differences between

the complexes are due to the nature of the ligand being varied. It has been shown that the addition of an electron withdrawing benzene group fused to the side of the pyrazine ring tends to stabilize the BL π^* orbital though the series. This shifts the energy of the MLCT to lower energy and results in a shorter excited-state lifetime.

The properties of ruthenium polypyridyl complexes spurred the investigation of the osmium analogs of these systems.[25,32,35,43,45] A desirable feature of osmium is that Δ_o is larger for Os than Ru. Consequently, the energy of the d-d states will be much higher than the MLCT excited states, thus resulting in more stable complexes upon excitation. In general, the Os(II) complexes are oxidized at less positive potentials than the Ru(II) complexes whereas the first reduction potential is almost the same in the two series of compounds. For these Os complexes, the HOMO-LUMO gap will be decreased resulting in lower energy transitions as well as shorter excited state lifetimes. For example, in going from $[Ru(bpy)_3]^{2+}$ to $[Os(bpy)_3]^{2+}$, the osmium complex is oxidized at a less positive potential (+ 0.82 V) than the Ru(II) complex (+ 1.29 V), whereas the first reduction potential is almost the same for the two complexes (- 1.26 and - 1.28 V, respectively).[25,50] As predicted from the electrochemistry, the absorption maximum of the ^{1}MLCT band for $[Ru(bpy)_3]^{2+}$ (450 nm) lies at a higher energy than that for $[Os(bpy)_3]^{2+}$ (475 nm). Consequently, the emission energy for the ruthenium complex is higher than the osmium complex and has an excited-state lifetime of 580 ns versus 60 ns for $[Os(bpy)_3]^{2+}$. The osmium complex is much less emissive than the ruthenium complex because the energy of its MLCT state is lower than the ruthenium complex due to the lower energy emission, thus decay to the ground state is more efficient as predicted by the energy gap law.

The drawback to using $[Ru(bpy)_3]^{2+}$ or its many monometallic analogs in electron and energy transfer processes is that the excited state species is required to collide with the quencher during the lifetime of the excited state. Consequently, these processes are often inefficient. Covalently attaching the quencher to the photosensitizer could increase the efficiency of these processes.

The introduction of polyazine bridging ligands has led to the study of supramolecular compounds. These systems incorporate ruthenium and osmium polypyridine complexes covalently linked to other components through the utilization of the bridging capability of these ligands.[8,14,38-47] To design polymetallic systems with tunable ground and excited states, it is necessary to investigate the properties of the individual components. The nature of these excited states has prompted a series of studies investigating the light absorbing and photochemical reaction properties of such systems. These systems generally consist of two or more metal centers linked together by bridging ligands. The properties of these complexes differ from the monometallic fragments.[8,14,50] In general, upon formation of the bimetallic complex from the monometallic complex, the lowest energy MLCT band is shifted to lower energy in the bimetallic complex. Addition of an electron withdrawing metal center to the vacant nitrogen sites on the bridging ligand would be expected to stabilize the π^* orbital on the ligand. The result is a decreasing energy difference between the metal and ligand orbital. Consequently, the emission energy of the bimetallic complex also shifts to longer wavelength and the excited state lifetime is decreased. For example, the monometallic complexes $[Ru(bpy)_3]^{2+}$ and $[Ru(bpy)_2(dpp)]^{2+}$ have lowest lying absorbances at 450 nm and 464 nm, emissions at 603 nm and 660 nm, with excited state lifetimes of 850 ns and 226 ns, respectively.[50] Formation of the bimetallic complex $[(bpy)_2Ru(dpp)Ru(bpy)_2]^{4+}$ shifts the lowest lying absorbance to 523 nm, the emission to 746 nm and the lifetime is decreased to 80 ns.[40] It has been found that perturbations in the photochemical and redox properties in going from monometallic to polymetallic complexes occurs for each metal subunit in the polynuclear systems. This allows for new processes to occur within the framework. Mixed metal systems make possible the development of supramolecular complexes having widely varied functions at the different metal centers.

Balzani and coworkers have synthesized many large polymetallic complexes containing bidentate ligands with Ru(II) and/or Os(II) as the metal ions, 2,3- and/or 2,5-dpp as the bridging ligands, and bpy or 2,2'-biquinoline (biq) as the terminal ligands.[8,14,38] Species with a nuclearity up to 22 metals, that consist of different metals,

bridging ligands, and terminal ligands, have been synthesized. All complexes emit in solution at room temperature. Variation of the components in these systems allows the direction of energy transfer in these complexes to be dictated.

Recent interest has focused on the covalent coupling of electron donors and electron acceptors to polypyridyl Ru(II) and Os(II) complexes.[6,72,73] The covalent attachment of electron donors and/or acceptors has been utilized to allow MLCT excited states to undergo intramolecular electron transfer. This leads to more spatially separated, charge separated states. These systems generally consist of a photosensitizer as well as the electron donor/acceptor. In order to obtain photoinitiated charge separation, the photosensitizer must be capable of transferring an electron to another component. Two component complexes (dyads) are composed of the light absorber and either the electron donor or acceptor. Generally the back electron transfer in these systems is too fast and the initial ground state complex is reformed.

Balzani and coworkers have synthesized a series of complexes and have investigated the photoinduced charge separation processes.[73] Dyads that contain the photosensitizer covalently linked to an electron donor have been synthesized as well as ones where the photosensitizer is linked to the electron acceptor. A triad has also been synthesized in which the photosensitizer is covalently linked to both the electron donor and acceptor. The electron acceptor used in these studies is methylviologen, MV^{2+}, and the electron donor is either di-p-anisylamine, DPPA, or phenothiazine, PTZ. The dyads incorporating the electron donor were shown to have properties essentially the same as the photosensitizer without the donor attached. This was due to the charge separated state occurring at higher energy than the luminescent level. The dyads incorporating the electron acceptor had a charge separated state at lower energy than the luminescent state of the photosensitizer alone, and the intensity of the emission was reduced dramatically. The triad, where the donor was PTZ, behaved just as the electron acceptor dyad. For the triad where the donor was DPAA the emission intensity is reduced even further than in the dyad incorporating the acceptor. The luminescence energy of these complexes is shifted to slightly lower energy with a marked decrease in the intensity of this emission and the excited state lifetime is reduced dramatically.

Tridentate versus Bidentate Ligands

The complexes discussed in this thesis contain tridentate ligands coordinated to the metal centers, thus allowing for added stability due to the chelate effect.[1-4] The chelate effect deals with the enhanced stability of a system containing chelate rings compared to the stability of a system that is as similar as possible but contains none or fewer rings.

Tris-chelated species have the possibility of existing as Δ or Λ stereoisomers. Upon incorporation into supramolecular complexes, this yields a mixture of stereoisomers that are typically not separated. In addition, these systems often have short excited state lifetimes. One approach to the elimination of the multiple stereoisomers found in supramolecular complexes built using tris-chelated complexes is to incorporate tridentate ligands such as tpy or tpp (tpy = 2,2':6',2''-terpyridine and tpp = 2,3,5,6-tetrakis(2-pyridyl)pyrazine).[34,48-56] Tridentate ligands are advantageous in that they coordinate to three sites thus limiting the number of stereoisomers possible upon coordination of other ligands. The use of the tridentate ligands tpy and tpp eliminates the Δ and Λ isomers possible when using bidentate ligands since these tridentate ligands coordinate in a *mer* fashion.

Although substantial attention has focused on the utilization of bidentate bridging ligands in polymetallic systems, little work has involved the incorporation of tridentate ligands. Most polymetallic systems similar to those discussed in this work utilize tris-chelated complexes. These are then covalently linked through a bridging ligand to other parts of the supramolecular architecture as was discussed in the previous section.

Interest in the use of tridentate ligands has been hindered by the short excited-state lifetime and absence of a room temperature emission for $[Ru(tpy)_2](PF_6)_2$.[51-53] Hecker et. al. synthesized a $[Ru(tpy)_2]^{2+}$ analog containing phenyl substituents on the 4,4',4'' positions, para to the nitrogen, on the tpy ligand.[54] Introducing these substituents

Hecker et. al. synthesized a $[Ru(tpy)_2]^{2+}$ analog containing phenyl substituents on the 4,4',4'' positions, para to the nitrogen, on the tpy ligand.[54] Introducing these substituents enhanced the excited state lifetime of this analog. It is reasoned that the aryl groups conjugate with the low lying π^* orbital of tpy stabilizing the ^{3}MLCT emissive state. Through the various studies conducted on $[Ru(tpy)_2]^{2+}$ and its analogs, it is now well known that this is due to the quenching of the ^{3}MLCT emission by the thermally populated ^{3}LF state giving rise to rapid nonradiative deactivation of the MLCT state.

Only recently have tridentate polypyridyl bridging ligands, such as tpp, been used in the building of polymetallic systems. In the late 1980s, Petersen[50] and Thummel et. al.[58] reported the synthesis and characterization of $[Ru(tpy)(tpp)]^{2+}$ and $[(tpy)Ru(tpp)Ru(tpy)]^{4+}$. Due to what appears to be a purification problem, the work by Thummel et. al. did not contain the properties one would expect of such complexes. Petersen reported that the emitting state for $[Ru(tpy)(tpp)]^{2+}$ is the ^{3}MLCT state with an excited-state lifetime of 91 ns. In the bimetallic complex the ^{3}MLCT emitting state is shifted to lower energy with an excited state lifetime of 100 ns. Petersen also reported that $[Ru(tpp)_2]^{2+}$ also possesses a ^{3}MLCT emitting state with an excited state lifetime of 80 ns.

In 1989, Ruminski and coworkers synthesized two sets of complexes utilizing tpp as a bridging ligand.[49] In the first report $Rh(tpp)Cl_3$ and $Cl_3Rh(tpp)RhCl_3$ were synthesized. The synthesis of $[Ru(tpp)(NH_3)_3]^{2+}$ and $[(NH_3)_3Ru(tpp)Ru(NH_3)_3]^{4+}$ have also been reported. In these studies tpp was investigated as a bridging ligand. It was concluded that tpp affords direct metal-metal communication through the central pyrazine group as well as through the remote pyridine based nitrogens.

In 1993, Arana and Abruña reported the preparation of a series of mono-, bi-, and trimetallic complexes of Ru and Os using tpp as the bridging ligand and tpy as the terminal ligand.[59] The monometallic complexes $[M(tpy)(tpp)]^{2+}$ and $[M(tpp)_2]^{2+}$, where M = Ru and Os, emitted in fluid solution at room temperature. Excited state lifetimes were not measured. As predicted the ^{3}MLCT transitions for the osmium monometallic complexes are shifted to lower energy than the analogous ruthenium complexes.

In 1994, Brewer and coworkers synthesized a series of osmium (II) complexes incorporating tpp.[56] The ligands coordinated to the other three sites on the metal center were varied using both polypyridine as well as phosphine ligands. Two of the complexes that were investigated are particularly important to this work, $[Os(tpy)(tpp)]^{2+}$ and $[Os(tpp)_2]^{2+}$. The excited-state lifetimes of these complexes were 260 and 600 ns, respectively. It has been found that the presence of water or oxygen will quench the excited state of $[Os(tpp)_2]^{2+}$.[80]

Sauvage and coworkers[57] prepared and characterized homo- and heterobimetallic complexes using both tpy and ttpy (4'-p-tolyl-2,2':6',2''-terpyridine) as the terminal ligands. The bridging ligands used in these studies are two tpy ligands linked back-to-back via the 4' position (tpy-tpy), as well as using phenyl spacers allowing the bridging ligand length to vary, tpy-ph-tpy and tpy-ph$_2$-tpy. Upon studying the luminescence of these complexes it is concluded that there is an electronic interaction observed between the Os and Ru components when there is no phenyl spacer that is reduced when a single phenyl spacer is incorporated in the bridging ligand. When two phenyl spacers are inserted, the absorption and Os based luminescence properties vary little from a 1:1 mixture of $[Ru(ttpy)_2]^{2+}$ and $[Os(ttpy)_2]^{2+}$, i.e., the two metal centers do not interact. In 1993 Sauvage and coworkers utilized tpp as a bridging ligand to prepare $[(ttpy)Ru(tpp)Ru(ttpy)]^{4+}$.[57] It is concluded that there is strong metal-metal communication through the bridging ligand. No excited state properties were given.

Statement of Problem

The goal of this research is to investigate the ground and excited state properties of complexes incorporating tridentate polypyridyl ligands. Specifically, the use of tpp as a bridging ligand is investigated. This involves the development of a method to synthesize these metal complexes, as well as the study of their spectroscopic and electrochemical properties. Systematic variations of the ligands coordinated to the metal centers, variation of the metal centers, incorporation of a covalently attached electron acceptor, and the formation of bimetallic systems, have allowed for a wide variety of complexes to be studied. These compounds could be applicable to electrocatalysis of CO_2 reduction and photoinitiated charge separation. The synthesis of the monometallic compounds will advance the understanding of the ground and excited state properties of tridentate compounds. Incorporation of these complexes into bimetallic systems will aid in the understanding of the perturbations of these properties that occur upon formation of polymetallic systems.

Chapter II

Experimental

Materials

All chemicals were reagent grade and used without further purification unless otherwise specified. Deionized water was used throughout this work. $RuCl_3 \cdot 3H_2O$, $OsCl_3 \cdot 3H_2O$, and $IrCl_3 \cdot 3H_2O$ were received from Johnson Matthey through the precious metal loan program. The ligand 2,3,5,6-tetrakis(2'-pyridyl)pyrazine, tpp, was first prepared by Goodwin and Lions[62] and is now available commercially from GFS Chemicals. The ligands 2,3-bis(2-pyridyl)pyrazine (dpp) and 2,2':6',2"-terpyridine (tpy) as well as trimethyloxoniumtetrafluoroborate, $[(CH_3)_3OBF_4]$, 2,2'-pyridil, *o*-phenylenediamine, 2,3-diaminonaphthalene, and potassium hexafluorophosphate were purchased from Aldrich Chemical Company. The ligand TRIPHOS, bis(2-diphenylphosphinoethyl)phenylphosphine) or PPP, (^{31}P spectrum given in Appendix Figure A-I on page 170) was purchased from Strem Chemicals. The adsorption alumina used for the purification of the metal complexes was obtained from Fisher Scientific. The size exclusion resin, Sephadex LH-20, used was purchased from Pharmacia. The UV grade acetonitrile and dimethylformamide solvents (Burdick and Jackson) used in the electrochemical and spectroelectrochemical experiments were dried over activated molecular sieves. All other chemicals were obtained from Fisher Scientific.

Synthesis of Ligands

The ligand 2,3- bis(2-pyridyl)quinoxaline (dpq) was synthesized according to the published method of Goodwin and Lions reacting *o*-phenylenediamine and 2,2'-pyridil in ethanol.[62] Similarly, the ligand 2,3-bis(2-pyridyl)benzoquinoxaline (dpb) was synthesized substituting 2,3-diaminonaphthalene for *o*-phenylenediamine.[62-64] The

ligands dpq and dpb must be recrystallized several times from hot ethanol to remove any unreacted starting materials, namely 2,2'-pyridil that can act as a ligand also. A simplified method for the purification of dpb is to use alumina adsorption chromatography with 1:1 (v/v) acetonitrile/methylene chloride as the eluent. All the starting materials stay at the top with only the pure dpb flowing through. This is brought to dryness using rotary evaporation, dissolved in hot ethanol, and crystals form that can be separated by vacuum filtration.

Synthesis of Electrolyte

The tetrabutylammonium hexafluorophosphate (TBAH) used in this study was either purchased from BioAnalytical Systems or synthesized by the metathesis of tetrabutylammonium bromide, Bu_4NBr, with potassium hexafluorophosphate, KPF_6. To a saturated solution of KPF_6 in water was added a saturated solution of Bu_4NBr in water. A white precipitate formed which was collected by vacuum filtration. Purification was achieved through repeated recrystallization from hot ethanol. This was dried under vacuum and stored in a dessicator prior to use.

Purification of Complexes

All monometallic and most bimetallic systems were purified by alumina chromatography as described in the procedure for the synthesis of each complex. $[(tpy)Ru(tpp)IrCl_3]^{2+}$ was purified by size exclusion chromatography using a Sephadex LH-20 resin. This method also allows for quantitative estimates of the size of our complexes. All the bimetallic systems studied eluted prior to the monometallic systems from which they were prepared consistent with their larger size. Electronic absorption spectroscopy was performed on fractions taken during the purification procedure for all complexes to establish separation. Cyclic voltammetry was also used to check for purity of the desired complex. All other compounds that contain the metals or ligands used in this study that could be possible impurities would be electroactive and would be detected

in the cyclic voltammogram if present in significant amounts, ca.> 5 %. Fast Atom Bombardment Mass Spectroscopy (FAB MS) was used to study [(tpy)Ru(tpp)IrCl$_3$](PF$_6$)$_2$, [(tpy)Ru(tpp)RuCl$_3$](PF$_6$), [(tpy)Ru(tpp)Ru(tpp)](PF$_6$)$_4$, [(tpy)Os(tpp)RuCl$_3$](PF$_6$), and [(tpy)Os(tpp)Ru(tpp)](PF$_6$)$_4$ in order to further confirm the identity of these complexes. Abruña et. al.[59] performed the pioneering application of this technique to tpp bridged systems. Because the ligands generally do not fragment, one observes pieces of the bimetallic systems as well as intact bridged systems. In general, the FAB mass spectra of the bimetallic complexes contained numerous peaks with isotopic distributions very close to calculated values. The results are given following the synthetic procedure for each complex and shown in Appendix Figures A-XI, A-XII, A-XIII, A-XIV, and A-XV (pages 180-184) and summarized in Appendix Table A-1 (page 192). The isotropic distribution calculations for the assigned peaks are given in Appendix Figures A-XVI, A-XVII, A-XVIII, and A-XIX,(pages 185-188).

Synthesis of Metal Complexes

Trichloro(2,2':6',2"-terpyridine)ruthenium(III), Ru(tpy)Cl$_3$[65], and trichloro(2,2':6',2"-terpyridine)osmium(III), Os(tpy)Cl$_3$[66], were prepared according to the literature methods, reacting MCl$_3$·3H$_2$O with tpy stirring at reflux, under argon, for three hours. The solid was separated by vacuum filtration, washed with ethanol, and dried under vacuum. Tetrachloro(2,2'-bipyridine)ruthenium(IV), Ru(bpy)Cl$_4$, was synthesized following the published procedure by Krause,[67] reacting RuCl$_3$·3H$_2$O and excess bpy in 1.0 N HCl for nine days at room temperature. This was filtered and washed with deionized water. The preparation of the precursor complexes Ru(PPh$_3$)$_3$Cl$_2$[77], [Ru$_2$(μ-Cl)$_3$(PPP)$_2$]Cl·2H$_2$O[78], and [Ru(PPP)(CH$_3$CN)$_3$](CF$_3$SO$_3$)$_2$[78] were accomplished as previously reported with slight modifications of the published syntheses for [Ru$_2$(μ-Cl)$_3$(PPP)$_2$]Cl·2H$_2$O and [Ru(PPP)(CH$_3$CN)$_3$](CF$_3$SO$_3$)$_2$.

Monometallic Complexes

Trichloro(2,3,5,6-tetrakis(2-pyridyl)pyrazine)iridium(III)

Preparation of Ir(tpp)Cl$_3$ was achieved by adding solid IrCl$_3$·3H$_2$O (0.515 g, 0.161 mmol) to a solution of the ligand tpp (0.705 g, 0.181 mmol) in 25 mL of ethylene glycol.[55] The solution was heated near reflux for approximately 25 minutes and filtered while hot. The red crystalline product was washed with 60 mL of water, 60 mL of ethanol, and 75 mL of anhydrous diethyl ether and dried under vacuum. X-ray quality crystals were obtained by recrystallization from hot dimethylamide. A blood red crystal was obtained. A typical yield for the reaction was 45 %.

(2,2':6', 2''-Terpyridine)(2,3,5,6-tetrakis(2-pyridyl)pyrazine)ruthenium(II) Hexafluorophosphate

[Ru(tpy)(tpp)](PF$_6$)$_2$ was first prepared by Thummel et al.[58] For our work a modification of the procedure was performed.[55] This compound was synthesized by adding solid Ru(tpy)Cl$_3$ (0.152 g, 0.345 mmol) to a solution of tpp (0.413 g, 1.06 mmol) and 1.5 mL of triethylamine in 30 mL of 2:1 (v/v) ethanol/distilled water mixture. This was heated at reflux and stirred under argon for 5 hours. The complex was precipitated by the addition of saturated, aqueous KPF$_6$ (20 mL) and separated by vacuum filtration. Purification was performed by column chromatography on adsorption alumina in 2:1 (v/v) toluene/acetonitrile. The first band to elute was yellow, unreacted tpp. The second band to elute was orange and was the product of interest. A minor purple band was the third to elute, this was found to be [(tpy)Ru(tpp)Ru(tpy)]$^{4+}$. The orange band was collected and concentrated by rotary evaporation. This was dissolved in a minimum amount of acetonitrile and precipitated by addition to a stirring solution of diethyl ether. The product was separated by vacuum filtration and dried under vacuum. A typical yield for this reaction was 82 %.

Bis(2,3,5,6-tetrakis(2-pyridyl)pyrazine)ruthenium(II) Hexafluorophosphate

$[Ru(tpp)_2](PF_6)_2$ was synthesized by a modification of the previously published procedure.[59] This was prepared by adding approximately seven equivalents of tpp (6.124 g, 15.7 mmol) and one equivalent of $RuCl_3 \cdot 3H_2O$ (0.576 g, 2.20 mmol) to 150 mL of 95% ethanol. This was heated at reflux and stirred under argon for 48 hours. The complex was precipitated by the addition of saturated, aqueous KPF_6 (150 mL) and separated by vacuum filtration. Purification was performed by column chromatography on adsorption alumina using 3:2 (v/v) toluene/acetonitrile as the eluent. The desired product, an orange band, was the second band to elute after excess tpp starting material. It was collected and concentrated by rotary evaporation, dissolved in a minimum amount of acetonitrile and precipitated by addition to a stirring solution of diethyl ether. The product was separated by vacuum filtration and dried under vacuum. A typical yield for this reaction was 64 %.

Trisaquo(2,2':6', 2''-terpyridine)osmium(III) Hexafluorophosphate

Preparation of $[Os(tpy)(H_2O)_3](PF_6)_3$ was achieved by reacting $[Os(tpy)Cl_3]$ (0.079 g, 0.149 mmol) with $AgCF_3SO_3$ (0.386 g, 1.50 mmol) in 50 mL of deionized water. The solution was heated at reflux and stirred under argon for approximately 48 hours. The suspension goes from a brown/black to a blue color. The solution volume was decreased to approximately 25 mL by rotary evaporation. The resulting solution was added to a saturated, aqueous solution of KPF_6 to induce precipitation. The blue solid was separated by vacuum filtration and dried under vacuum. A typical yield for this reaction was 63 %.

(2,2':6', 2''-Terpyridine)(2,3,5,6-tetrakis(2-pyridyl)pyrazine)osmium(II) Hexafluorophosphate

To alleviate purification problems encountered through the published syntheses by Abruña et al.[59] and Brewer et al.[56], $[Os(tpy)(tpp)]^{2+}$ was synthesized using $[Os(tpy)(H_2O)_3]^{3+}$ (0.106 g, 0.138 mmol) and tpp (0.065 g, 0.168 mmol). These were reacted in 30 mL of ethylene glycol and heated near reflux for 30 minutes with stirring

under argon. The reaction solution goes from a blue to a brown color. The resulting solution was removed from the heat and a saturated, aqueous solution of KPF_6 was added to induce precipitation. This was separated by vacuum filtration. Purification of the product was achieved by column chromatography on adsorption alumina using 2:1 (v/v) toluene/acetonitrile solution. As with the ruthenium analog, the first band to elute was unreacted tpp. The second band to elute, the brown band, was collected. This was concentrated by rotary evaporation, dissolved in a minimum amount of acetonitrile and precipitated in diethyl ether. The product was separated by vacuum filtration and dried under vacuum. A cyclic voltammogram was performed in which it was apparent there were minor impurities attributed to $[Os(tpy)_2](PF_6)_2$ and $[Os(tpp)_2)](PF_6)_2$. A second column was performed in a similar manner, this time collecting the middle portion of the brown band that contained the product of interest. Purity was checked by cyclic voltammetry. A typical yield for this reaction was 75 %.

Bis(2,3,5,6-tetrakis(2-pyridyl)pyrazine)osmium(II) Hexafluorophosphate

$[Os(tpp)_2](PF_6)_2$ was prepared as published by Abruña et al.[59], a similar procedure to the synthesis of $[Ru(tpp)_2]^{2+}$, substituting $OsCl_3 \cdot 3H_2O$ (0.701 g, 2.00 mmol) for $RuCl_3 \cdot 3H_2O$. Purification was achieved by column chromatography on adsorption alumina using 3:2 (v/v) toluene/acetonitrile. The desired product, a brown band, was the second to elute after excess tpp starting material. This was concentrated by rotary evaporation, dissolved in a minimum amount of acetonitrile and precipitated in diethyl ether. The product was collected by vacuum filtration and dried under vacuum. A typical yield for this reaction was 70 %.

{2-[2-(1-Methylpyridiniumyl)]-3,5,6-tris(2-pyridyl)pyrazine}(2,2':6',2''-terpyridine)ruthenium(II) Hexafluorophosphate

$[Ru(tpy)(Metpp)](PF_6)_3$ can be prepared by two different methods both using trimethyloxoniumtetrafluoroborate as the methylating agent. The first method is a modification of the procedure Serroni and Denti used to methylate dpp in the design of

multimetallic systems.[68] $[Ru(tpy)(Metpp)]^{3+}$ was synthesized by adding $[Ru(tpy)(tpp)]^{2+}$ (0.098 g, 0.109 mmol) and $(CH_3)_3OBF_4$ (0.052 g, 0.350 mmol) to 50 mL of 1,2-dichloroethane. This was refluxed and stirred for 3 hours under argon. The product was separated by vacuum filtration. Purification was performed by column chromatography on adsorption alumina in 3:2 (v/v) acetonitrile/toluene solvent mixture. The first band to elute, light orange, was unreacted $[Ru(tpy)(tpp)]^{2+}$ and the second band that contained the product of interest, a darker orange, eluted when a 2:1 (v/v) acetonitrile/methanol solution was used. It was collected and concentrated by rotary evaporation. This was dissolved in a minimum amount of acetonitrile and precipitated by addition to a stirring solution of diethyl ether. The product was separated by vacuum filtration and dried under vacuum. A typical yield for this reaction was 32 %.

The second method is similar in design yet has an improved yield. The methylated complex was prepared by adding $(CH_3)_3OBF_4$ (0.012 g, 0.081 mmol) and $[Ru(tpy)(tpp)](PF_6)_2$ (0.070 g, 0.069 mmol) to a 100 mL three-necked round bottom fitted with an argon inlet. Using a syringe, 50 mL of distilled dichloromethane was added to the mixture. This was heated at reflux with stirring under argon for approximately 3 hours then cooled to room temperature. The solid was isolated by vacuum filtration and purified as described as above. A typical yield for this reaction was 71 %.

The ^1H NMR spectra of this methylated complex is consistent with the proposed structure. The ^1H and ^{13}C NMR spectra are shown in the Appendix Figures AIV-AVII (pages 173-176) for $[Ru(tpy)(tpp)]^{2+}$ and $[Ru(tpy)(Metpp)]^{3+}$. Upon methylation a new ^1H resonance appears at 4.58 for $[Ru(tpy)(Metpp)]^{3+}$. This is in agreement with the ^1H resonance at 4.08 ppm for the methyl protons in Medpp found by Serroni and Denti.[68] Integration yields a ratio of 27 phenyl protons to 3 methyl protons, excluding the acetonitrile protons, for $[Ru(tpy)(Metpp)]^{3+}$. The integration is consistent with a singly methylated product. The ^1H NMR spectra show methylation occurs at the pyridyl nitrogen as would be expected due to its greater nucleophilicity compared to the pyrazine nitrogen.

(2,2'-Bipyridine)chloro(2,3,5,6-tetrakis(2-pyridyl)pyrazine)ruthenium(II) Hexafluorophosphate

To Ru(bpy)Cl$_4$ (0.152 g, 0.381 mmol) and tpp (0.185 g, 0.477 mmol) was added 40 mL of 1:1 (v/v) ethanol/water solution and 2 mL triethylamine. This was refluxed while stirring under argon for four hours then cooled to room temperature. The crude product was formed following precipitation of the solution with a saturated, aqueous solution of KPF$_6$. The crude solid was separated through vacuum filtration and purified by column chromatography on adsorption alumina using 2:1 (v/v) toluene/acetonitrile solution as the eluent. The first band to elute was tpp starting material. [Ru(bpy)(tpp)Cl](PF$_6$), the red band, was the second to elute. This was collected and brought to dryness by rotary evaporation. A minimum amount of acetonitrile was added to the flask and the product precipitated upon addition to a stirring solution of diethyl ether. The product was separated by vacuum filtration and dried under vacuum. The chromatographic purification was repeated twice to ensure product purity. A typical yield for this reaction was 83 %.

Acetonitrile(2,2'-bipyridine)(2,3,5,6-tetrakis(2-pyridyl)pyrazine)ruthenium(II) Hexafluorophosphate

A solution of [Ru(bpy)(tpp)Cl]$^+$ (0.104 g, 0.126 mmol) and a large excess of AgPF$_6$ (0.319 g, 1.26 mmol) in 25 mL acetonitrile and 25 mL water was heated at reflux with stirring for 6 hours under argon. The AgCl was removed by vacuum filtration and the acetonitrile removed by rotary evaporation. On addition to an aqueous solution of saturated KPF$_6$ a precipitate was obtained; it was filtered and purified by alumina adsorption chromatography using 1:1 (v/v) toluene/acetonitrile solution as the eluent. The first band to elute was unreacted [Ru(bpy)(tpp)Cl]$^+$. The second band to elute was yellow, [Ru(bpy)(tpp)(CH$_3$CN)](PF$_6$)$_2$. This was collected and concentrated by rotary evaporation. To the flask was added a minimum amount of acetonitrile and the product precipitated by addition to a stirring solution of diethyl ether. The solid was separated by vacuum filtration and dried under vacuum. A typical yield for this reaction was 95 %.

Acetonitrile(2,2'-bipyridine){2-[2-(1-Methylpyridiniumyl)]-3,5,6-tris(2-pyridyl)pyrazine}ruthenium(II) Hexafluorophosphate

The methylation of $[Ru(bpy)(tpp)(CH_3CN)](PF_6)_2$ was achieved following the procedure for the methylation of $[Ru(tpy)(tpp)]^{2+}$. To $[Ru(bpy)(tpp)(CH_3CN)]^{2+}$ (0.477 g, 0.049 mmol) and $(CH_3)_3OBF_4$ (0.028 g, 0.189 mmol) was added 50 mL distilled dichloromethane. The mixture was heated at reflux and stirred under argon for 3 hours. The solid was collected by vacuum filtration and purified by adsorption alumina chromatography using 3:2 (v/v) acetonitrile/toluene solution. The first band to elute (yellow) was the unreacted starting metal complex whereas the second band was the methylated complex $[Ru(bpy)(Metpp)(CH_3CN)](PF_6)_3$ (yellow/orange). The second band was collected and concentrated by rotary evaporation. This was dissolved in a minimum amount of acetonitrile and precipitated by addition to a stirring solution of diethyl ether. The product was separated by vacuum filtration and dried under vacuum. A typical yield for this reaction was 80 %.

Upon methylation, a new ^1H resonance appears at 4.56 ppm for $[Ru(bpy)(Metpp)(CH_3CN)]^{3+}$ in agreement with previously published results on Medpp[59] as well as $[Ru(tpy)(Metpp)]^{3+}$. Integration yields a ratio of 24 phenyl protons and 3 methyl protons, excluding the acetonitrile protons. This is consistent with a singly methylated product.

(2,3-Bis(2-pyridyl)pyrazine)chloro(2,2':6',2"-terpyridine)ruthenium(II) Hexafluorophosphate

$[Ru(tpy)(dpp)Cl](PF_6)$ was prepared by adding solid $Ru(tpy)Cl_3$ (0.824 g, 1.87 mmol) to a solution of the ligand dpp (0.599 g, 2.56 mmol) in 100 mL of 2:1 (v/v) ethanol/deionized water mixture with 8 mL of triethylamine as a reducing agent.[34] The solution was heated near reflux with stirring for approximately 5 hours under argon. The complex was precipitated by the addition of saturated, aqueous KPF_6 and separated by vacuum filtration. Purification was achieved by column chromatography on adsorption alumina in 3:2 (v/v) toluene/acetonitrile. The red product was the first one to elute. This band was collected, concentrated by rotary evaporation,

and precipitated by addition to diethyl ether. The precipitate was separated by vacuum filtration and dried under vacuum. A typical yield for this reaction was 79%.

(2,3-Bis(2-pyridyl)quinoxaline)chloro(2,2':6',2"-terpyridine)ruthenium(II) Hexafluorophosphate

[Ru(tpy)(dpq)Cl](PF$_6$) was synthesized by an analogous procedure to that of [Ru(tpy)(dpp)Cl]$^+$ substituting the ligand dpq (0.820 g, 1.86 mmol) for the ligand dpp.[34] Purification was as described above. The product was the first to elute and was purple. A typical yield for this reaction was 65%.

(2,3-Bis(2-pyridyl)benzoquinoxaline)chloro(2,2':6',2"-terpyridine) ruthenium(II) Hexafluorophosphate

[Ru(tpy)(dpb)Cl](PF$_6$) was prepared by an analogous procedure to that of [Ru(tpy)(dpp)Cl](PF$_6$) substituting the ligand dpb (0.863 g, 2.58 mmol) for the ligand dpp.[34] A 2:1 toluene/acetonitrile eluent was used and the product band was blue. A typical yield for this reaction was 63%.

(2,3-Bis(2-pyridyl)pyrazine)pyridine(2,2':6',2"-terpyridine)ruthenium(II) Hexafluorophosphate

[Ru(tpy)(dpp)(py)](PF$_6$)$_2$ was prepared by adding 1 mL of pyridine to a stirring solution of [Ru(tpy)(dpp)Cl](PF$_6$) (0.117 g, 0 156 mmol) in 20 mL of 1:1 (v/v) ethanol/distilled water.[34] This mixture was heated at reflux while stirring under argon for approximately 20 hours. The complex was precipitated by the addition of a saturated, aqueous KPF$_6$ solution and separated by vacuum filtration. Purification was performed as described for the chloride substituted complexes. The desired product was the orange band that eluted second, after unreacted [Ru(tpy)(dpp)Cl]$^+$. The second band was collected and concentrated by rotary evaporation. This was dissolved in a minimum amount of acetonitrile and precipitated by addition to a stirring solution of diethyl ether. The product was separated by vacuum filtration and dried under vacuum. A typical yield for this reaction was 85%.

(2,3-Bis(2-pyridyl)quinoxaline)pyridine(2,2':6',2"-terpyridine)ruthenium(II) Hexafluorophosphate

$[Ru(tpy)(dpq)(py)](PF_6)_2$ was synthesized by an analogous procedure to that of $[Ru(tpy)(dpp)(py)]^{2+}$ substituting $[Ru(tpy)(dpq)Cl](PF_6)$ (0.113 g, 0.142 mmol) for the analogous dpp complex.[34] The desired product eluted second and was red in color. A typical yield for this reaction was 82%.

(2,3-Bis(2-pyridyl)benzoquinoxaline)pyridine(2,2':6',2"-terpyridine)ruthenium(II) Hexafluorophosphate

$[Ru(tpy)(dpb)(py)](PF_6)_2$ was prepared by an analogous procedure to that of $[Ru(tpy)(dpp)(py)]^{2+}$ substituting $[Ru(tpy)(dpb)Cl](PF_6)$ (0.127 g, 0.150 mmol) for the analogous dpp complex.[34] The desired product eluted second as a purple band. A typical yield for this reaction was 81%.

(Bis(2-diphenylphosphinoethyl)phenylphosphine))ruthenium(II) (μ-Cl)₃ruthenium(II)(bis(2-diphenylphosphinoethyl)phenylphosphine)) Chloride.

$[(Ru_2(\mu\text{-}Cl)_3(PPP)_2]Cl\cdot2H_2O$ was synthesized using a 250 mL three necked flask, fitted with a nitrogen inlet and reflux condenser containing TRIPHOS (1.13 g, 2.09 mmol) and 30 mL of benzene.[78] A suspension of $Ru(PPh_3)_3Cl_2$ (2.03 g, 4.09 mmol) in benzene was added. This mixture was heated at reflux, stirring, for 12 hours. The volume was reduced to approximately 20 mL by rotary evaporation and a yellow crude product was precipitated with ether. This product was separated by vacuum filtration then dissolved in ethanol. The solution was filtered, concentrated to a small volume followed by precipitation with ether. The yellow solid was separated by vacuum filtration and used without further purification. A typical yield was 63 %.

Trisacetonitrile(bis-(2-diphenylphosphinoethyl)phenylphosphine)ruthenium(II) Triflate.

[Ru(PPP)(CH$_3$CN)$_3$](CF$_3$SO$_3$)$_2$ was prepared by reacting [Ru$_2$(μ-Cl)$_3$(PPP)$_2$]Cl·2H$_2$O (0.0427 g, 0.298 mmol) synthesized above and AgCF$_3$SO$_3$ (0.406 g, 1.58 mmol) in 20 mL of freshly distilled acetonitrile.[78] This was heated at reflux, under argon, for 24 hours then cooled to room temperature. The AgCl formed was separated by vacuum filtration and the filtrate was concentrated to dryness. The solid was dissolved in minimal acetonitrile and filtered to remove all remaining AgCl. Ether was added to the solution to induce precipitation and a white solid formed. The solid was separated by vacuum filtration and used in the synthesis of [Ru(tpp)(PPP)]$^{2+}$. A typical yield for this reaction was 92 %.

(2,2':6',2''-Terpyridine)(bis(2-diphenylphosphinoethyl)phenylphosphine) ruthenium(II) Hexafluorophosphate.

[Ru(tpy)(PPP)]$^{2+}$ was synthesized by adding TRIPHOS (0.453 g, 0.833 mmol) to a solution of Ru(tpy)Cl$_3$ (0.122 g, 0.277 mmol), 50 mL 2:1 (v/v) ethanol/H$_2$O, and 2 mL triethylamine that had been brought to reflux and allowed to cool to room temperature. This mixture was heated at reflux for five hours then precipitated in a saturated, aqueous solution of KPF$_6$. The crude product was separated by vacuum filtration. Purification was achieved by column chromatography on adsorption alumina using a 2:1 (v/v) toluene/acetonitrile solvent mixture. The desired yellow band was eluted when the solvent mixture was switched to 3:2 (v/v) toluene/acetonitrile. The solvent was removed by rotary evaporation. The solid was dissolved in a minimum amount of acetonitrile and precipitated in ether. A typical yield for this reaction was 84 %. The ^{31}P spectrum is shown in Figure A-II in the Appendix (page 171). E$_{1/2}$ = + 1.63 V, - 1.19 V, - 1.49 V. λ_{max}^{abs} = 390 nm, λ_{max}^{em} = 500 nm.

(2,3,5,6-Tetrakis(2-pyridyl)pyrazine)(bis(2-diphenylphosphinoethyl) phenylphosphine)ruthenium(II) Hexafluorophosphate.

$[Ru(PPP)(CH_3CN)_3](CF_3SO_3)_2$ (0.170 g, 0.159 mmol) and tpp (0.253 g, 0.652 mmol) were placed in a three necked round bottom fitted with an argon inlet. To this solid mixture, 40 mL of ethylene glycol was added. This was heated at reflux approximately 25 minutes. The cooled solution was precipitated using a saturated, aqueous solution of KPF_6 and the solid was removed by vacuum filtration. Purification was achieved through alumina adsorption chromatography using 2:1 (v/v) toluene/acetonitrile solvent mixture. The second band to elute (yellow) was collected and evaporated to dryness. A minimum amount of acetonitrile was added and precipitation was induced with ether. Using emission spectroscopy it was apparent this was not a pure complex so further purification was performed. Using the same solvent mixture, another alumina column was employed and fractions taken. Fraction 4 came off when the solvent mixture was switched to 1:1 (v/v) toluene/acetonitrile and gave a single emission peak signifying purity. A typical yield for this reaction was 63 %. The ^{31}P spectrum is shown in Figure A-III in the Appendix (page 172).

$E_{1/2} = + 1.68$ V, $- 0.88$ V, $- 1.31$ V. $\lambda_{max}^{abs} = 418$ nm, $\lambda_{max}^{em} = 525$ nm.

(2,2':6',2''-Terpyridine) ruthenium(II)[μ-2,3,5,6-tetrakis(2-pyridyl)pyrazine]iridium(III) Trichloride Hexafluorophosphate

[(tpy)Ru(tpp)IrCl$_3$](PF$_6$)$_2$ was prepared by reacting solid Ru(tpy)Cl$_3$ (0.150 g, 0.340 mmol) and Ir(tpp)Cl$_3$ (0.096 g, 0.140 mmol) in a mixture of 10 mL of dimethylformamide and 10 mL of absolute ethanol.[55] The solution was heated at reflux with stirring for 4 hours. Next, the ethanol was removed by rotary evaporation. The complex was precipitated by addition of a saturated, aqueous KPF$_6$ solution (20 mL) and separated by vacuum filtration. Purification was achieved by size-exclusion column chromatography on a Sephadex LH-20 (Pharamacia) column developed with a 2:1 (v/v) ethanol/acetonitrile solvent mixture. The first band eluted was dark purple and contained the product of interest. It was collected and concentrated by rotary evaporation. This was dissolved in a minimum amount of acetonitrile and precipitated by addition to a stirring solution of diethyl ether. The product was separated by vacuum filtration and dried under vacuum. This purification process was repeated twice, and purity was established by thin layer chromatography. A typical yield for this reaction was 62 %.

Appendix Figure XI (page 180) shows the fast atom bombardment mass spectrum of this complex. A number of informative ions are observed. The highest mass/charge ions at m/z = 1166 and 1020 correspond to the loss of one and then two PF$_6^-$ counter ions forming [(tpy)Ru(tpp)IrCl$_3$](PF$_6$)$^+$ and [(tpy)Ru(tpp)IrCl$_3$]$^+$, respectively. This establishes the formation of the bimetallic cation. Predicted isotropic distributions for these ions are shown in Appendix Figure A-XVI (page 185). These data are consistent with the observed patterns. The ions at m/z = 985, 950, and 915 correspond to the sequential loss of the chloride ligands forming [(tpy)Ru(tpp)IrCl$_2$]$^+$, [(tpy)Ru(tpp)IrCl]$^+$, and [(tpy)Ru(tpp)Ir]$^+$. The peak at m/z = 722 corresponds to [(tpy)Ru(tpp)]$^+$, and those at m/z = 655 and 615 to [(tpp)IrCl$_2$]$^+$ and [(tpp)IrCl]$^+$, respectively. Assignment of these peaks is possible due to the tpp ligand remaining intact.

(2,2':6',2''-Terpyridine)ruthenium(II)[μ-2,3,5,6-tetrakis(2-pyridyl)pyrazine] trichlororuthenium(II) Hexafluorophosphate

[(tpy)Ru(tpp)RuCl$_3$](PF$_6$) was synthesized using our building block approach by reacting [Ru(tpy)(tpp)]$^{2+}$ (0.069 g, 0.068 mmol) with RuCl$_3$·3H$_2$O (0.127 g, 0.490 mmol). The RuCl$_3$·3H$_2$O was heated in approximately 30 mL of absolute ethanol at reflux while stirring under argon. The [Ru(tpy)(tpp)]$^{2+}$ was heated in approximately 15 mL of hot absolute ethanol, with 5 mL acetonitrile to allow it to go completely into solution. The [Ru(tpy)(tpp)]$^{2+}$ solution was added to the RuCl$_3$. The solution went from an orange/brown to a green color. This was heated at reflux for 1.5 hours and no further color changes occurred. The flask was then removed from the heat and the volume was reduced to dryness. This was dissolved in a minimum amount of acetonitrile and added to a saturated solution of aqueous KPF$_6$ (50 mL) with stirring to induce precipitation. The blue solid was separated by vacuum filtration. This precipitate was dissolved in a minimum amount of acetonitrile, precipitated in ether, and filtered by vacuum filtration to remove starting materials. No further purification was needed. A typical yield for this reaction was 88 %.

A second method for the synthesis of this Ru/Ru bimetallic was reacting [Ru(tpy)(tpp)]$^{2+}$ (0.056 g, 0.055 mmol) with RuCl$_3$·3H$_2$O (0.101 g, 0.387 mmol) in 50 mL of absolute ethanol. The solution was heated at reflux with stirring under argon for 24 hours. The flask was then removed from the heat. The solution volume was reduced by rotary evaporation to approximately 20 mL. A saturated solution of aqueous KPF$_6$ (50 mL) was then added to induce precipitation. The precipitate was collected by vacuum filtration. This was purified by column chromatography on a Sephadex LH-20 column developed with a 2:1 (v/v) ethanol/acetonitrile solvent mixture. The first band to elute was a purple trimetallic. The desired blue band was collected in fractions each being monitored by UV-Vis spectroscopy. This pure fractions were combined and concentrated by rotary evaporation. This was dissolved in a minimum amount of acetonitrile and precipitated by addition to a stirring solution of diethyl ether. The product was separated by vacuum filtration and dried under vacuum. A typical yield for

this reaction was 47 %. The first procedure is the improved synthetic method using this building block approach. From the two different syntheses, it appears that the presence of water causes this reaction to fail resulting in the formation of the trimetallic complex, $[(tpy)Ru(tpp)Ru(tpp)Ru(tpy)]^{6+}$.

Appendix Figure A-XII (page 181) shows the FAB MS of $[(tpy)Ru(tpp)RuCl_3](PF_6)$. As in $[(tpy)Ru(tpp)IrCl_3](PF_6)_2$, the fragmentation pattern is indicative of the desired bimetallic complex. Contrary to the Ru/Ir bimetallic complex, the first fragmentation produces an ion at $m/z = 1039$ corresponds to loss of a chloride ligand forming $[(tpy)Ru(tpp)RuCl_2](PF_6)^+$. The next highest peak at $m/z = 894$ corresponds to the loss of the PF_6^- counterion forming $[(tpy)Ru(tpp)RuCl_2]^+$. Once again, the peak at $m/z = 722$ corresponds to $[(tpy)Ru(tpp)]^+$. Predicted isotropic distributions for these ions are shown in Appendix Figure A-XVI (page 185). These data are consistent with the observed patterns.

(2,2':6',2''-Terpyridine)osmium(II)[μ-2,3,5,6-tetrakis(2-pyridyl)pyrazine] trichlororuthenium(II) Hexafluorophosphate

$[(tpy)Os(tpp)RuCl_3](PF_6)$ was prepared by an analogous procedure to that of $[(tpy)Ru(tpp)RuCl_3]^+$ substituting $[Os(tpy)(tpp)]^{2+}$ (0.078 g, 0.070 mmol) for $[Ru(tpy)(tpp)]^{2+}$. The blue/green solid was separated by vacuum filtration. A similar procedure was used to remove unreacted starting materials. A typical yield for this reaction was 77 %.

$[(tpy)Os(tpp)RuCl_3](PF_6)$ was also prepared as in the second method above substituting $[Os(tpy)(tpp)]^{2+}$ (0.061 g, 0.056 mmol) for $[Ru(tpy)(tpp)]^{2+}$. The first band to elute was a blue/purple trimetallic species. The greenish/blue product band was the second to elute and once again this was taken in fractions and monitored spectroscopically. All fractions were collected, concentrated by rotary evaporation, dissolved in a minimum amount of acetonitrile followed by precipitation in stirring diethyl ether. The pure product was collected by vacuum filtration. A typical yield for

this reaction was 43 %. Once again, first procedure is the improved synthetic method using this building block approach.

Appendix Figure A-XIV (page 183) shows the FAB MS of $[(tpy)Os(tpp)RuCl_3]^+$. As in $[(tpy)Ru(tpp)RuCl_3](PF_6)$, the fragmentation pattern is indicative of the desired bimetallic complex with a similar fragmentation pattern being observed. The molecular ion peak appearing at m/z = 1128 corresponds to $[(tpy)Os(tpp)RuCl_2](PF_6)^+$. The peak at m/z = 985 corresponds to the loss of the PF_6^- counterion forming $[(tpy)Os(tpp)RuCl_2]^+$. The peaks at m/z = 956, 825, and 811 correspond to the $[(tpy)Os(tpp)](PF_6)^+$, $[Os(tpp)Ru](PF_6)^+$, and $[(tpy)Os(tpp)]^+$ ions, respectively. Predicted isotropic distributions for these ions are shown in Appendix Figure A-XIII (page 187). These data are consistent with the observed patterns.

(2,2',2''-Terpyridine)ruthenium(II)[μ-2,3,5,6-tetrakis(2-pyridyl) pyrazine]ruthenium(II)(2,2',2''-terpyridine) Hexafluorophosphate

$[(tpy)Ru(tpp)Ru(tpy)](PF_6)_4$ was prepared through a modification of previously published procedures[58,59] using three equivalents of $Ru(tpy)Cl_3$ (0.264 g, 0.600 mmol) and one equivalent of tpp (0.093 g, 0.240 mmol). To this was added 2 mL triethylamine and 50 mL of 2:1 (v/v) ethanol/water solution. This was heated at reflux and stirred under argon for 24 hours. To induce precipitation, the solution was added to a saturated, aqueous solution of KPF_6. The solid was separated by vacuum filtration. This was purified by alumina column chromatography developed a with 1:1 (v/v) toluene/acetonitrile solvent mixture. The first band to elute was the orange monometallic complex, $[Ru(tpy)(tpp)]^{2+}$. The purple band, the second to elute, was the desired bimetallic complex. This was concentrated by rotary evaporation, dissolved in a minimum amount of acetonitrile followed by precipitation in stirring diethyl ether. The pure product was collected by vacuum filtration and dried under vacuum. A typical yield for this reaction was 73 %.

(2,2':6',2''-Terpyridine)ruthenium(II)[μ-2,3,5,6-tetrakis(2-pyridyl)pyrazine] ruthenium(II)[2,3,5,6-tetrakis(2-pyridyl)pyrazine] Hexafluorophoshate

$[(tpy)Ru(tpp)Ru(tpp)]^{4+}$ has been prepared previously following a different synthetic procedure.[59] Using the building block approach developed in this laboratory, $[(tpy)Ru(tpp)Ru(tpp)]^{4+}$ was prepared by reacting one equivalent of $[(tpy)Ru(tpp)RuCl_3]^+$ (0.027 g, 0.025 mmol) and seven equivalents of tpp (0.068 g, 0.175 mmol) in 50 mL of absolute ethanol. The solution was heated at reflux with stirring under argon for 1.5 hours. The solution volume was reduced to approximately 20 mL by rotary evaporation. Precipitation was induced when the reaction solution was added dropwise to a stirring saturated, aqueous solution of KPF_6. The precipitate was then collected using vacuum filtration. The product was isolated by column chromatography on adsorption alumina using 3:2 (v/v) toluene/acetonitrile solution. The first and second bands to elute were unreacted tpp and unreacted bimetallic starting materials. The product of interest was the third to elute, the purple band, and isolated when the solvent solution was switched to a 2:3 (v/v) toluene/acetonitrile solution. This was concentrated to dryness using rotary evaporation, dissolved in a minimum amount of acetonitrile and precipitated in diethyl ether. The pure product was collected by vacuum filtration and dried under vacuum. A typical yield for this reaction was 86 %.

Appendix Figure A-XIII (page 182) shows the fast atom bombardment mass spectrum of this complex. The highest mass/charge ion at m/z = 1501 corresponds to loss of two PF_6^- counterions while that at m/z = 1356 corresponds to loss of three PF_6^- counterions forming $[(tpy)Ru(tpp)Ru(tpp)](PF_6)^+$. This establishes the formation of the bimetallic cation. The other ions correspond to the loss of the forth PF_6^- counterion forming $[(tpy)Ru(tpp)Ru(tpp)]^+$ at m/z = 1211, as well as peaks at m/z = 877, 722, and 606 that correspond to $[Ru(tpp)_2]^+$, $[(tpy)Ru(tpp)]^+$, and $[(tpy)Ru(tpp)Ru(tpp)]^{2+}$, respectively. Predicted isotropic distributions for these ions are shown in Appendix Figure A-XVII (page 186). These data are consistent with the observed patterns.

(2,2':6',2''-Terpyridine)osmium(II)[μ-2,3,5,6-tetrakis(2-pyridyl)pyrazine] ruthenium(II)[2,3,5,6-tetrakis(2-pyridyl)pyrazine] Hexafluorophoshate

[(tpy)Os(tpp)Ru(tpp)](PF$_6$)$_4$ was prepared by an analogous procedure to that of [(tpy)Ru(tpp)Ru(tpp)]$^{4+}$ substituting [(tpy)Os(tpp)RuCl$_3$]$^+$ (0.080 g, 0.068 mmol) for [(tpy)Ru(tpp)RuCl$_3$]$^+$ and reacting with tpp (0.199 g, 0.513 mmol) in 50 mL absolute ethanol. Purification was performed by column chromatography on adsorption alumina using a 3:2 (v/v) toluene/acetonitrile solution. Once again the third band to elute, the purple band, was the desired product. A typical yield for this reaction was 83 %.

Appendix Figure A-XV (page 184) shows the fast atom bombardment mass spectrum of this complex. The highest mass/charge ion at m/z = 1735 corresponds to loss of a PF$_6^-$ counterion forming [(tpy)Os(tpp)Ru(tpp)](PF$_6$)$_3$$^+$, that at m/z = 1590 to loss of two PF$_6^-$ counterions forming [(tpy)Os(tpp)Ru(tpp)](PF$_6$)$_2$$^+$, the peak at m/z = 1445 to loss of three PF$_6^-$ counterions forming [(tpy)Os(tpp)Ru(tpp)](PF$_6$)$^+$, and the peak at 1300 to loss of all four PF$_6^-$ counterions forming [(tpy)Os(tpp)Ru(tpp)](PF$_6$)$^+$. This establishes the formation of this bimetallic complex. The other fragment ions at m/z = 877, 811, and 578 correspond to [Ru(tpp)$_2$]$^+$, [(tpy)Os(tpp)]$^+$, and [Os(tpp)]$^+$, respectively. Predicted isotropic distributions for these ions are shown in Appendix Figure A-XIX (page 188). These data are consistent with the observed patterns.

Instrumentation

Electrochemistry. Cyclic voltammograms were recorded on a BioAnalytical Systems l00W electrochemical analyzer. The three electrode system utilized in these studies consisted of a platinum disk working electrode, a platinum wire auxiliary electrode, and a silver/silver chloride reference electrode (0.286 V vs. NHE). The reference electrode was calibrated versus the Fc/Fc^+ couple (0.665 V vs. NHE).[81] The platinum disk working electrode was cleaned prior to each scan. The solvent used was a high purity acetonitrile or dimethylformamide dried over activated molecular sieves. The supporting electrolyte was 0.1 M tetrabutylammonium hexafluorophosphate. Prior to each scan, the solutions were deoxygenated by bubbling with argon for 20 minutes and blanketed with argon during each scan.

Electronic Absorption Spectroscopy. A Hewlett Packard 8452A diode array spectrophotometer (resolution 2 nm) interfaced to a Hewlett Packard Vectra ES computer was used to obtain absorption spectra in the wavelength range of 190 - 820 nm. All spectra were recorded as acetonitrile solutions (Burdick and Jackson high purity) at room temperature in a 1 cm x 1 cm square quartz cuvette. Samples used to calculate molar extinction coefficients (ε) were prepared gravimetrically.

Spectroelectrochemistry. Electronic absorption spectra of electrogenerated oxidation states were recorded using the cell shown in Figure 5. The working electrode was either carbon cloth or a platinum mesh cylinder, the reference electrode was the Ag/AgCl gel electrode used in the electrochemical measurements and the auxiliary electrode was a platinum mesh cylinder. The potential was controlled by a BAS 100W electrochemical analyzer. Cyclic voltammograms were obtained prior to the spectroelectrochemical measurements. All experiments were carried out in 0.1 M TBAH acetonitrile solution except for the reductive spectroelectrochemistry of $[Ru(tpy)(tpp)]^{2+}$, $[Ru(tpy)(Metpp)]^{3+}$, and $[(tpy)Ru(tpp)IrCl_3]^{2+}$ that were performed in dimethylformamide
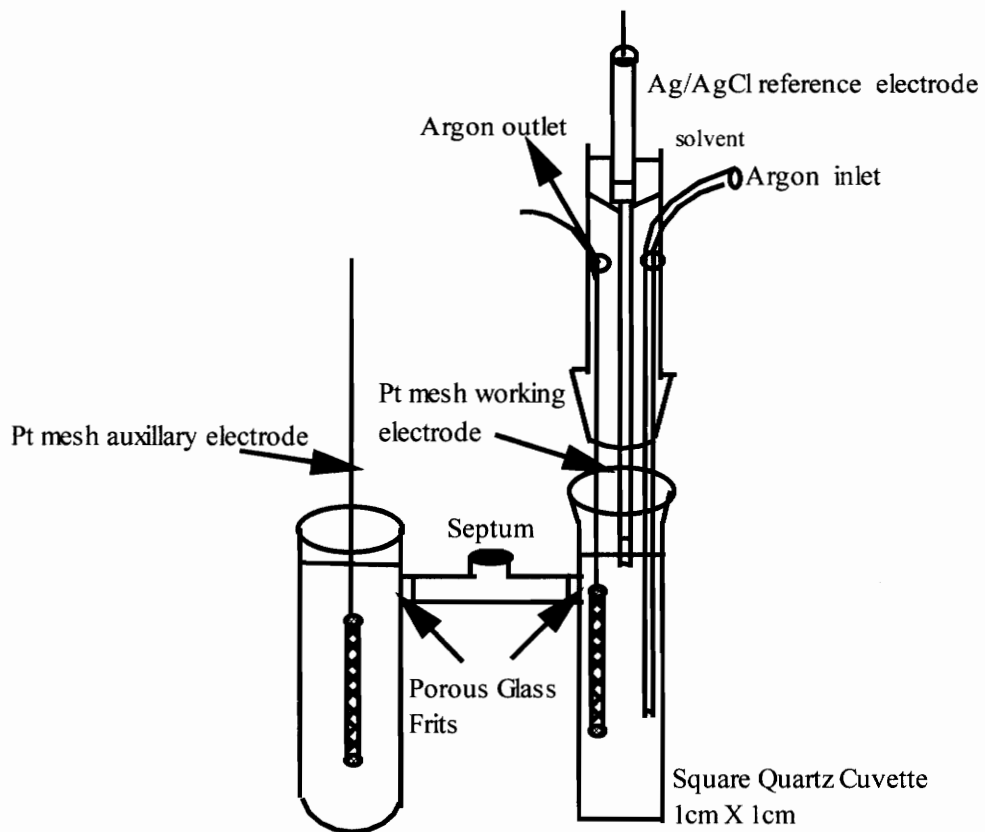
Figure 5. Cell used in Spectroelectrochemical Experiments

solution to improve reversibility. The working compartment was deoxygenated by bubbling with argon prior to and during each experiment. The spectra presented in each figure are from the same solution and are presented so that relative intensity of the observed transitions is as illustrated.

Emission spectroscopy. Emission spectra were recorded at room temperature in deoxygenated Burdick and Jackson high purity acetonitrile solution and obtained on a Photon Technology Inc. MSIII spectrofluorometer utilizing a 150-W mercury arc lamp excitation source and a thermoelectrically cooled Hamamatsu R666-S photomultiplier tube utilizing a single photon-counting detection system. In general, 15 scans were repeated and averaged. All spectra were corrected for photomultiplier response.

Spectroscopic quantum yields were calculated using $[Ru(bpy)_3](PF_6)_2$ as the reference in preparing absorbance matched solutions for those complexes in which the quantum yields were calculated. The emission spectrum of the reference in deoxygenated solution was obtained followed by the measurement of the emission spectra of the samples without changing any settings on the experimental setup. These measurements were obtained at room temperature. The emission quantum yields were calculated using the following equation:[72]

$$\Phi_1 = \Phi_2[(A_1 I_2)]/[(A_2)(I_1)]$$

Where Φ is the emission quantum yield of the reference and sample (subscript 1 or 2 respectively), I is the integrated sum of the emission intensity (the area under the emission curve), and A is the absorbance in a 1 cm x 1 cm cell of the reference and sample. The known quantum yield of the $[Ru(bpy)_3]^{2+}$ reference was $\Phi_{em} = 0.062$ in acetonitrile.[79]

Low temperature emission spectra were recorded on deoxygenated absorbance matched ethanol solutions prepared in quartz tubes. Using an optical dewar containing liquid nitrogen, the tubes were frozen while obtaining the spectra.

Lifetime measurements. Solutions for the excited-state lifetime measurements were prepared using high purity acetonitrile (Burdick and Jackson). These samples were deoxygenated employing the freeze-pump-thaw degassing method, repeating the process five times. The glass tubes were then sealed under vacuum. Upon returning to room temperature, the samples were ready for lifetime measurements.

Excited- state lifetime measurements were obtained using a Photon Technology Inc. PL 2300 nitrogen laser equipped with a PL 201 continuously tunable dye laser (360 - 900 nm) as the excitation source. The excitation pulse passes through an optical trigger prior to entering the sample compartment. The emission from the excited state is detected at a right angle. The emission passes through a PTI 1200 L/mm grating monochromator and is detected by a Hamamatsu R928 photomultiplier tube. The raw data were fit to equation $[Y = A + Bexp(-X/c)]$ following the removal of the initial data that included the optical delay and rise time of the system, where c is the lifetime of the complex. The configuration for excited-state lifetime measurements is shown in Figure 6.

Low temperature lifetime measurements were performed on deoxygenated ethanol solutions prepared in quartz tubes. The solution was prepared, placed in the quartz tube, and sonicated for 20 minutes. The tube was quickly placed in an optical dewar filled with liquid nitrogen and frozen for 10 minutes. The optical dewar containing liquid nitrogen as well as the quartz sample tube were placed in the sample compartment and the lifetime measured.

Transient Absorbance. Transient absorption measurements were conducted with a system described elsewhere.[80]

Electrocatalysis. The solution used for electrocatalysis was prepared by measuring the appropriate amount of sample to make approximately a 1 mM solution. The solid was diluted with 0.1 M TBAH in high purity acetonitrile to the appropriate

PTI PL 2300
Nitrogen Laser

PTI PL 201
Dye Head

PTI Optical
Trigger

LeCroy 6880B
Digitizer

Sample
Chamber

Hamamatsu R-928 PMT
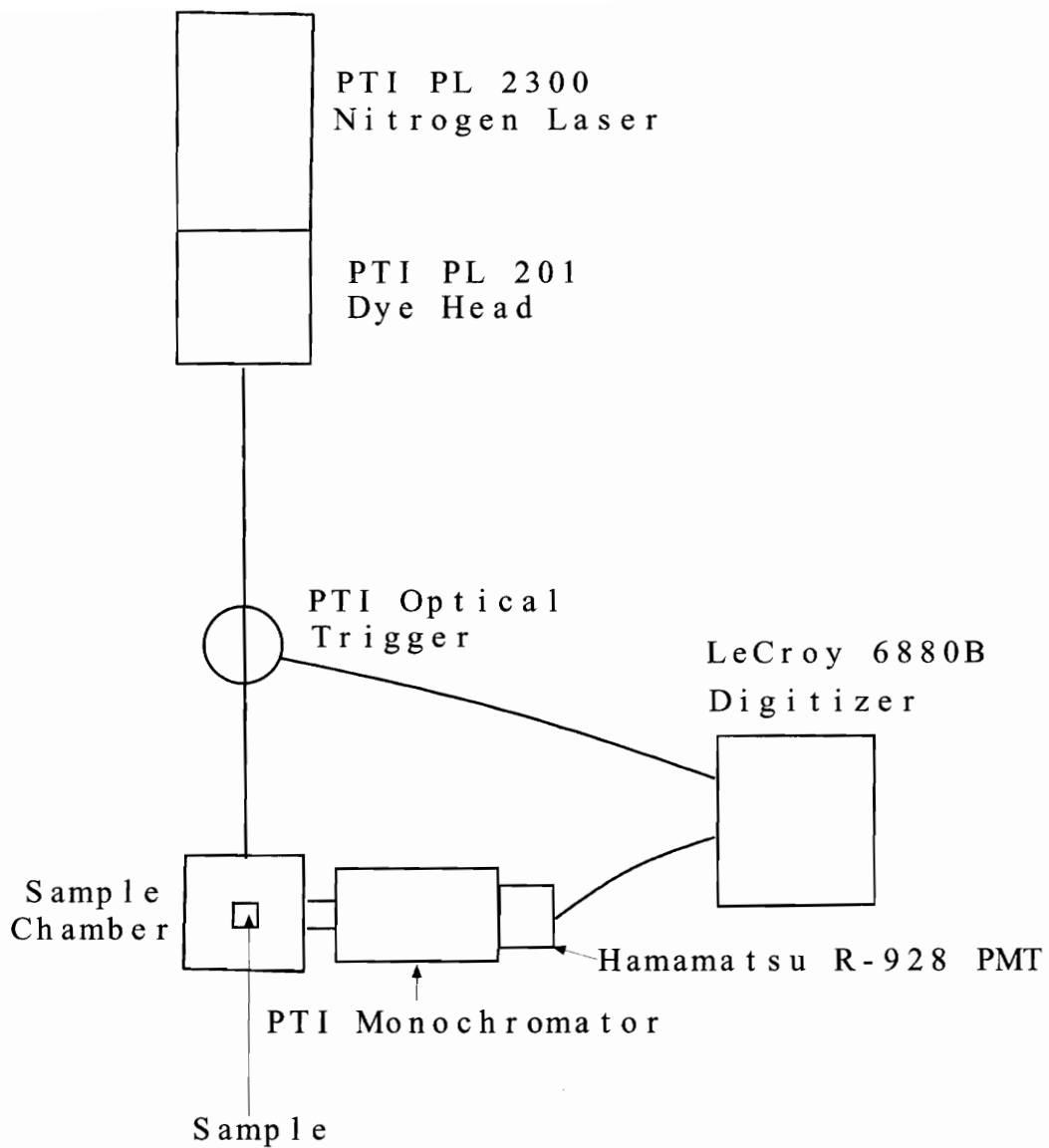
PTI Monochromator

Sample

Figure 6. Schematic of the Laser-Induced Emission Lifetime System

volume. The controlled potential electrolysis experiments were performed using the cell described previously.[74] In one compartment was the working electrode, carbon cloth clipped to a platinum wire, and the Ag/AgCl reference electrode, and a carbon cloth auxiliary electrode was in the other compartment. This was connected to the electrochemical analyzer. Prior to electrolysis, the solutions were deoxygenated by bubbling with CO_2 for 30-45 minutes. The solution in the auxiliary compartment was bubbled with CO_2 during electrolysis. Complete details for the electrocatalysis experiment as well as the determination of the products are described elsewhere.[74]

NMR Spectroscopy. ^1H and ^{13}C NMR measurements were made on saturated solutions in CD_3CN using a Varian Unity 400-MHz instrument.

Crystal Growth and Analysis. X-ray quality crystals for the complex $Ir(tpp)Cl_3$ were obtained by recrystallization from hot dimethylformamide. The system used for the determination and analysis of the crystal structure has been described elsewhere.[55,75]

Fast Atom Bombardment Mass. Spectroscopy. Mass Spectral data was obtained on a Fisions VG Quattro Triple-Stage Quadupole Mass Spectrometer. The bimetallic complexes were dissolved in a liquid matrix of neat 3-nitrobenzyl alcohol and placed on a FAB probe tip. The typical conditions included an electron impact ionization energy of 70 eV with a 200° C source energy using methane as the reagent gas for chemical ionization and 20 kV Cesium ions for liquid secondary ionization.

Chapter III
Results and Discussion

Synthetic Route

The complexes synthesized in this work are unique compared to most polypyridyl complexes studied in that they incorporate the tridentate ligands tpy and tpp. Terpyridine (tpy) is a heterocyclic nitrogen ligand that generally binds in a tridentate fashion with *mer* stereochemistry. We have used the tridentate nitrogen aromatic heterocyclic ligand tpp (2,3,5,6-tetrakis(2-pyridyl)pyrazine), which also binds in a mer fashion, as the bridging ligand when synthesizing the bimetallic complexes. The bidentate ligands dpp (2,3-bis(2-pyridyl)pyrazine), dpq (2,3-bis(2-pyridyl)quinoxaline), and dpb (2,3-bis (2-pyridyl)benzoquinoxaline), which can serve as bridging ligands, have been used in the synthesis of monometallic complexes. The use of these ligands allows for the systematic variation of the properties of these complexes.

In addition to acting as a bridging ligand, upon methylation, tpp can potentially act as an electron accepting moiety. Covalently attaching this moiety may result in the MLCT excited state undergoing intramolecular electron transfer leading to a spatially separated charge separated state with an oxidized metal and reduced viologen. Two types of methylated complexes have been synthesized, $[Ru(tpy)(Metpp)]^{3+}$ and $[Ru(bpy)(Metpp)(CH_3CN)]^{3+}$. In the latter complex, the bidentate ligand bpy (2,2'-bipyridine) has been substituted for tpy opening up a site where an electron donor could be covalently attached. In this case, the charge separated state would contain an oxidized electron donor and a reduced electron acceptor.

The procedures for the synthesis of the monometallic complexes that have been prepared in this study are shown in Figure 7 (those complexes incorporating tpy) and Figure 8 (those complexes incorporating bpy). The first step involves the synthesis of $M(tpy)Cl_3$ where M = Ru[33a] or Os[33b] or Ru(bpy)Cl$_4$[34] assembling the terminal part of the
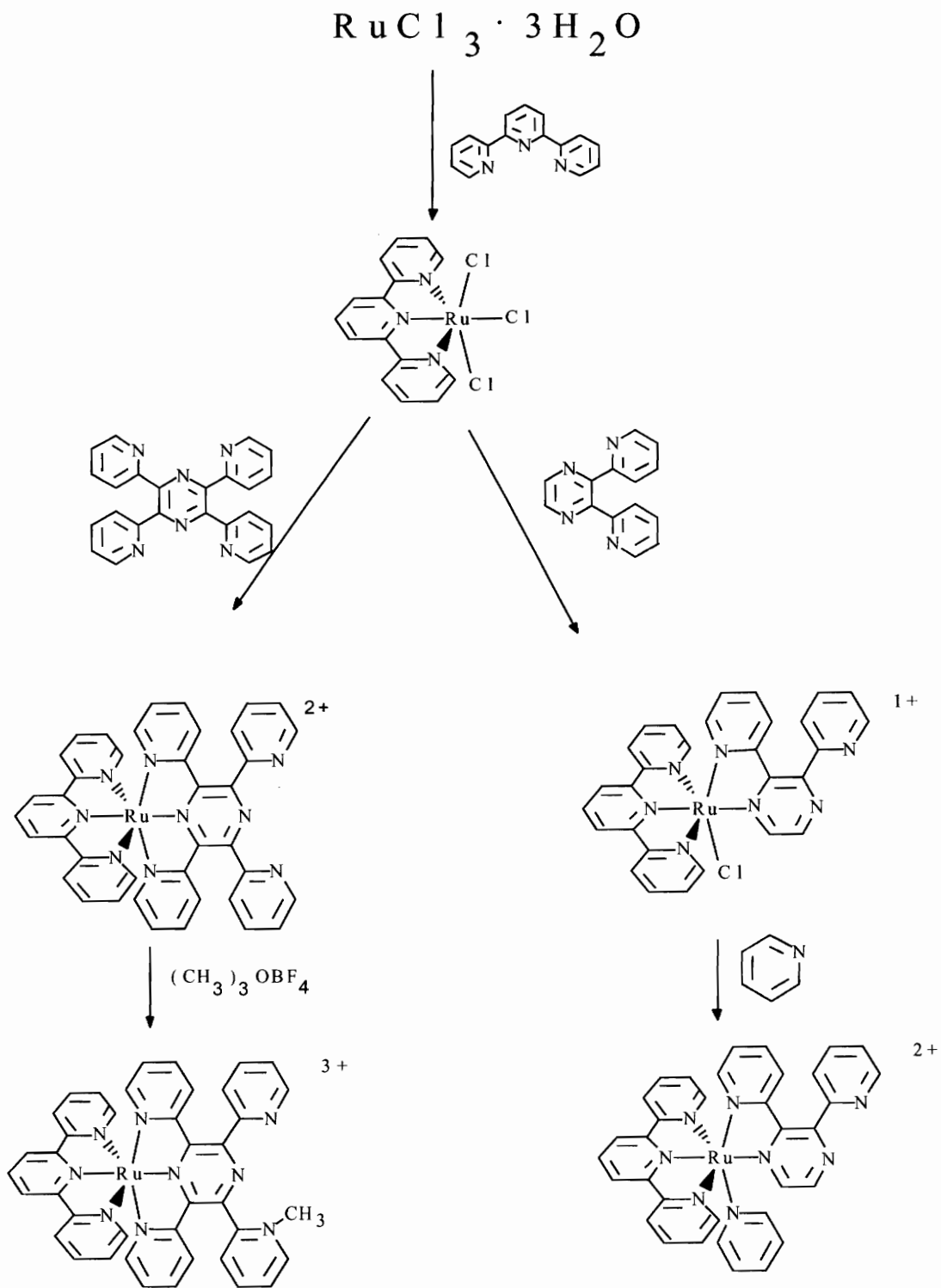
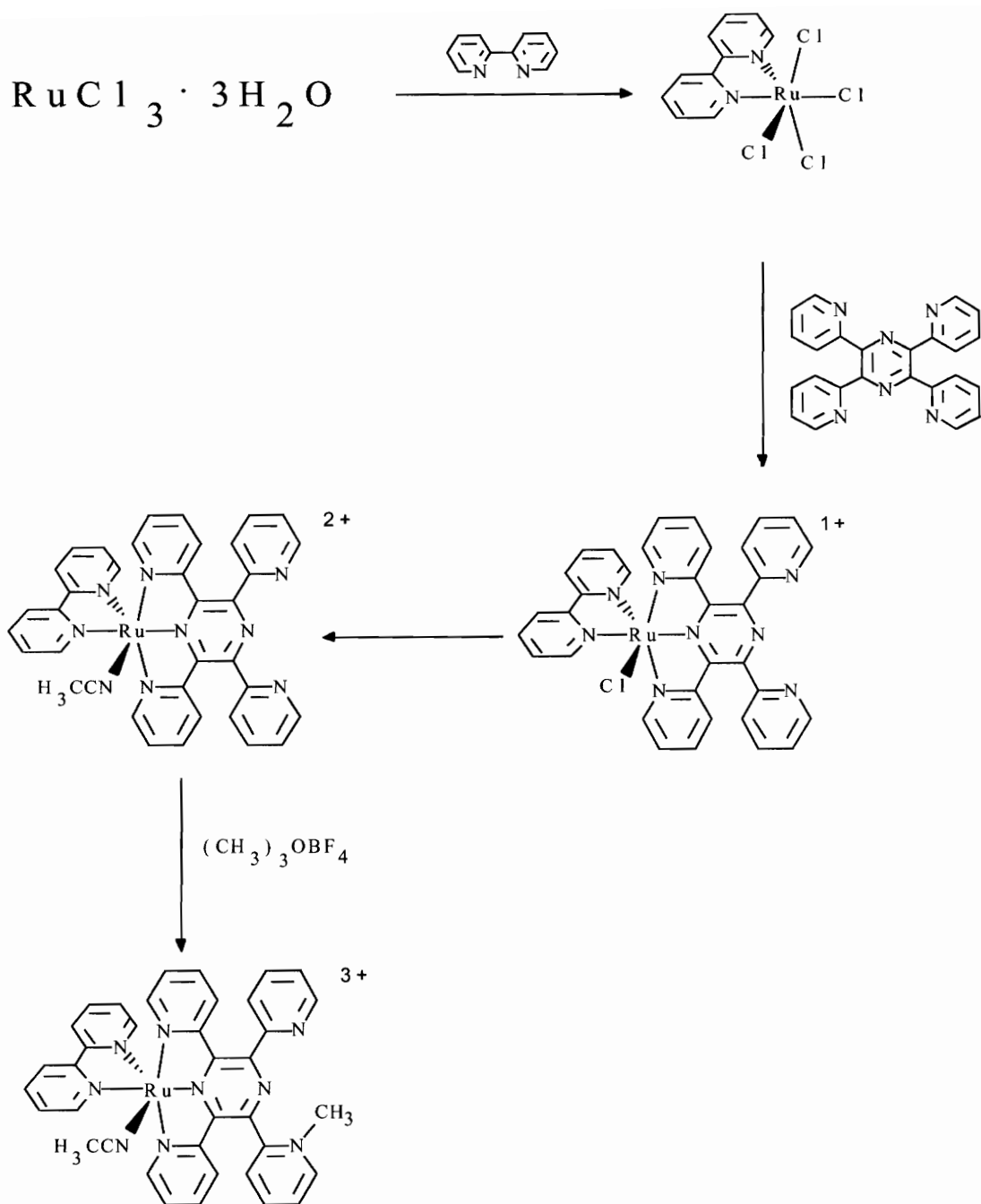Figure 7. Synthesis of ruthenium monometallic complexes incorporating tpy.

Figure 8. Synthesis of ruthenium monometallic complexes incorporating bpy

molecule. The bridging ligand is added to this starting material for the preparation of the desired monometallic complex. For the complexes of the type $[Ru(tpy)(BL)Cl]^+$, where BL = dpp, dpq, or dpb, the attachment of pyridine (py) was accomplished replacing the chloride, synthesizing the $[Ru(tpy)(BL)(py)]^{2+}$ complexes. Figure 8 shows the synthesis of this group of complexes where BL = dpp, however the dpq and dpb complexes are made following the same procedure. The synthesis of the methylated complexes is shown in Figures 7 and 8 for the two different types of complexes. Methylation of one of the remote nitrogens forms a covalently coupled viologen that can potentially function as an electron acceptor. Synthesizing a complex containing a LUMO that is localized on the remote viologen portion of the Metpp ligand is desired to make intramolecular electron transfer quenching is thermodynamically favored.

The series of bimetallic complexes has been prepared using our building block approach outlined in Figure 9. As in designing the monometallic complexes, the first step is to synthesize $M(tpy)Cl_3$. The ligand tpp is added to the $M(tpy)Cl_3$ starting material, forming the monometallic building blocks $[M(tpy)(tpp)]^{2+}$. This step is followed by the attachment of a $RuCl_3$ moiety to the tpp ligand utilizing the bridging capability of tpp. This adds the next metal center to form the bimetallic complex $[(tpy)M(tpp)RuCl_3]^+$. The attachment of a second tpp ligand to form the $[(tpy)M(tpp)Ru(tpp)]^{4+}$ complexes was accomplished by substituting the chlorides on the added Ru with tpp. This general stepwise approach to the construction of these molecules allows further extension of the molecular design by these methodologies. This also allows for the systematic construction of a wide variety of mixed-metal, stereochemically defined larger supramolecular systems of variable but known length and composition.

The mixed-metal bimetallic $[(tpy)Ru(tpp)IrCl_3]^{2+}$ was initially synthesized using the method shown in Figure 10. This complex is the first example of a mixed-metal tpp bridged system and contains metals that can function as both a light absorber, ruthenium, and a catalytic center, iridium. After the development of the method for the synthesis of
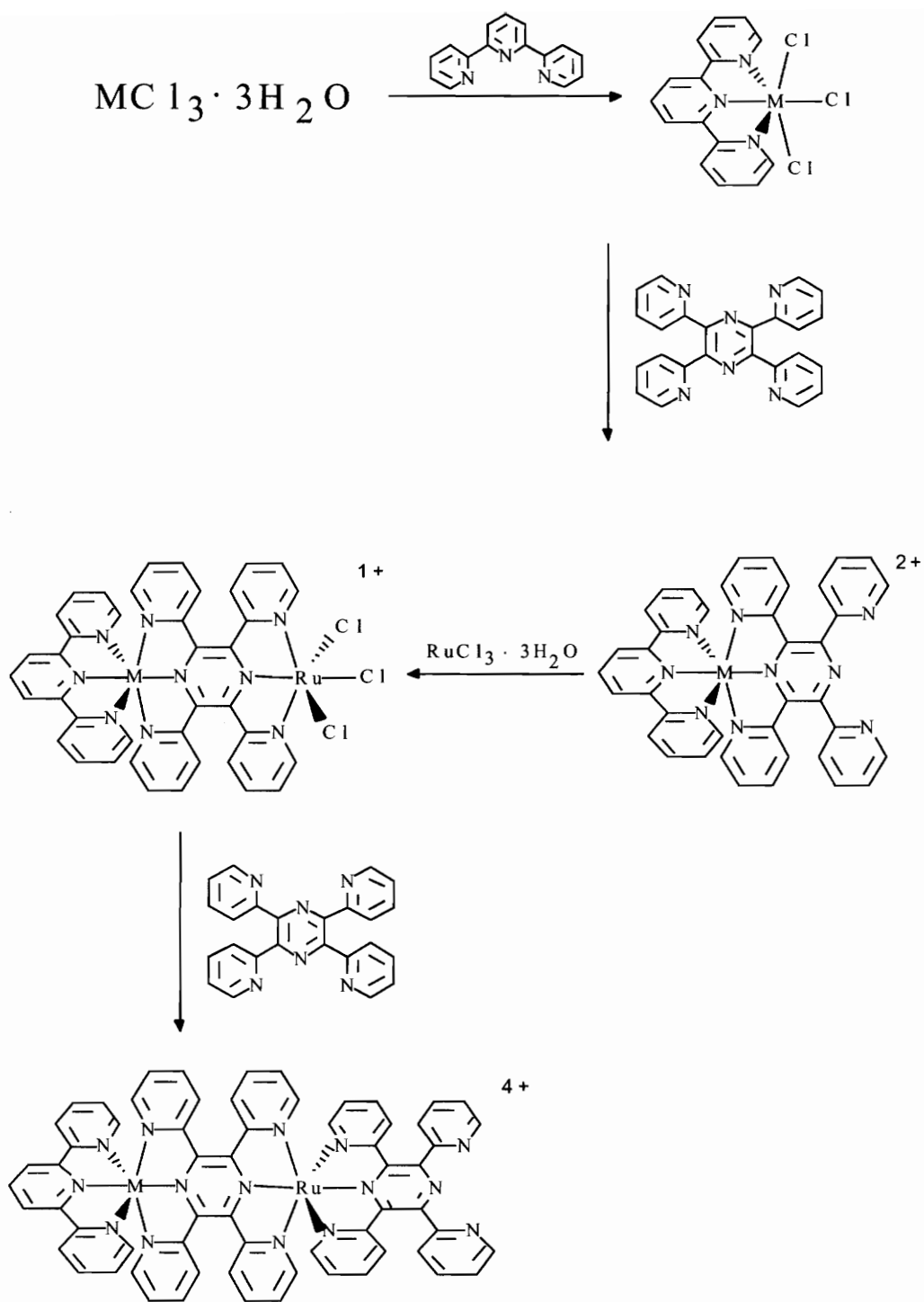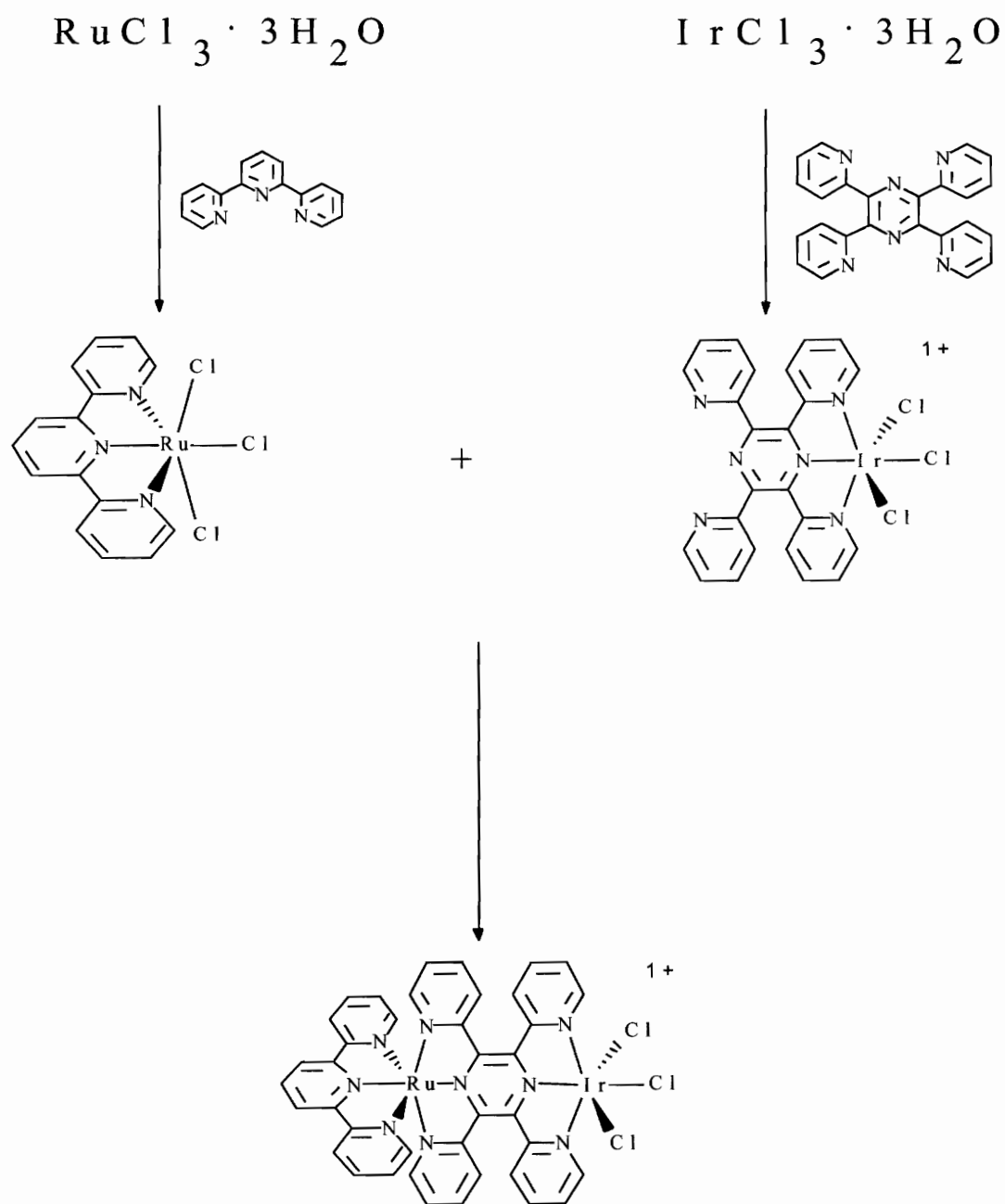
Figure 9. Synthesis of bimetallic complexes.

Figure 10. Synthesis of [(tpy)Ru(tpp)IrCl₃]²⁺.

the bimetallic complexes shown in Figure 9, the synthesis of this Ru/Ir bimetallic, substituting $IrCl_3$ with $RuCl_3$, was also successful.

Electrochemistry

Free Ligands

The free ligands bpy, tpy, tpp, dpp, dpq, and dpb used in this study have been characterized previously.[36,62-64] Table I contains the cyclic voltammetric data for the series of ligands used in this study. The ligand tpp is easier to reduce than either tpy or bpy and will thus contain the or lowest-unoccupied molecular orbital (LUMO) on mixed-ligand complexes of these ligands. All the bidentate bridging ligands, dpp, dpq, and dpb are easier to reduce than tpy. In addition, the ligands become easier to reduce within the series dpp, dpq, dpb. This is a result of the addition of the fused phenyl ring giving rise to a stabilization of the π^* LUMO.

Monometallic Complexes

All of the monometallic complexes prepared contain numerous electroactive moieties. The electrochemistry of polypyridyl complexes is typically discussed using the assumption that the MOs are largely ligand or metal in character. This localized MO description will be used throughout this discussion. The electrochemical properties of transition metal polypyridine complexes typically show metal based oxidations and a series of ligand based reductions localized on each ligand. In complexes of this type, the HOMO is metal based with the metal oxidation potential being sensitive to the coordination environment of the metal center.[8,14,25-37,50,55-60] Oxidatively, reversible waves ($i_p^c/i_p^a = 1$ and $E_p^a - E_p^c = 59.0/n$ (mV) where n is the number of electrons) corresponding to the 2+/3+ couple for both Ru and Os and the 3+/4+ couple for Ir are observed. Reductively, reversible ligand localized reductions are observed with their potential depending on the type of ligand reduced. The complexes display ΔE_P

Table I. Cyclic Voltammetric Data for the Series of Polyazine Ligands Used in this Study (where bpy = 2,2'-bipyridine, tpy = 2,2':6',2''-terpyridine, tpp = 2,3,5,6-tetrakis(2-pyridyl)pyrazine, dpp = 2,3-bis(2-pyridyl)pyrazine, dpq = 2,3-bis(2-pyridyl)quinoxaline, and dpb = 2,3-bis(2-pyridyl)benzoquinoxaline).[a]

Ligand	$E_{1/2}$ (V)	Assignment
bpy	- 2.28 V	bpy/bpy⁻
tpy	- 2.10 V	tpy/tpy⁻
dpp	- 1.80 V	dpp/dpp⁻
tpp	- 1.63 V	tpp/tpp⁻
dpq	- 1.43 V	dpq/dpq⁻
dpb	- 1.14 V	dpb/dpb⁻

[a] Potentials reported in CH_3CN solution with 0.1 M TBAH vs. Ag/AgCl (0.29 V vs. NHE) and a scan rate of 200 mV/sec.

($\Delta E_P = E_p{}^a - E_p{}^c$) values greater than the expected value of 59 mV, similar to the value of 75 mV exhibited by ferrocene under similar conditions. Electrochemical reduction of Ir(III) to Ir(I) is irreversible resulting from the generation of an iridium(I) d^8 square planar system, which loses two chlorides.[37,76] Tables II-IV summarize the cyclic voltammetric data for the monometallic complexes. Table II contains the cyclic voltammetric data for $[Ru(tpp)_2]^{2+}$, $[Ru(tpy)(tpp)]^{2+}$, $[Ru(tpy)(Metpp)]^{3+}$, and $[Os(tpy)(tpp)]^{2+}$, Table III for $Ir(tpp)Cl_3$, $[Ru(bpy)(tpp)Cl]^+$, $[Ru(bpy)(tpp)(CH_3CN)]^{2+}$, and $[Ru(bpy)(Metpp)(CH_3CN)]^{3+}$, and Table IV for $[Ru(tpy)(dpp)Cl]^+$, $[Ru(tpy)(dpq)Cl]^+$, $[Ru(tpy)(dpb)Cl]^+$, $[Ru(tpy)(dpp)(py)]^{2+}$, $[Ru(tpy)(dpq)(py)]^{2+}$, and $[Ru(tpy)(dpb)(py)]^{2+}$. All potentials reported are measured in acetonitrile and reported versus a Ag/AgCl reference electrode (0.29 V vs. NHE) calibrated against the Fc/Fc$^+$ couple (0.665 V vs. NHE).[81]

As shown in Figure 11, $Ir(tpp)Cl_3$ exhibits one oxidation and two reductions. The quasi-reversible oxidation of $Ir(tpp)Cl_3$ at + 1.74 V is assigned as an Ir(III)/Ir(IV) metal based process. The first reduction at - 0.78 V is assigned as a tpp ligand based reduction. The second reduction at - 1.35 V is irreversible and assigned as an Ir(III)/Ir(I) metal based process. Irreversible Ir reductions are often observed for systems containing iridium(III).[37, 76] These processes are normally irreversible two electron metal based reductions which result in the generation of an iridium(I) d^8 system. This d^8 system rearranges from an octahedral to a square planar ligand environment in our complex by loss of two chloride ligands. In $Ir(tpp)Cl_3$ the HOMO is an iridium based dπ orbital and the LUMO is a tpp ligand based π^* orbital.

The electrochemistry for $[Ru(tpy)(tpp)]^{2+}$ was studied previously by Thummel et. al.[58] The potentials given in Table II for $[Ru(tpy)(tpp)]^{2+}$ are for our sample studied under our conditions for comparison. The cyclic voltammogram for this complex is shown in Figure 12. $[Ru(tpy)(tpp)]^{2+}$ exhibits one reversible oxidation and three reversible reductions. The oxidation at + 1.40 V is assigned as a Ru(II)/Ru(III) metal based process and the first reduction at - 0.97 V as a tpp based reduction. The second reduction at - 1.38 V is assigned as a tpy/tpy⁻ ligand centered process. The third

Table II. Cyclic Voltammetric Data for a Series of Ru(II) and Os(II) Complexes Incorporating the Tridentate Polypyridyl Bridging Ligand tpp (where tpp = 2,3,5,6-tetrakis(2-pyridyl)pyrazine, tpy = 2,2':6',2''-terpyridine, and Metpp = 2-[2-(1-Methylpyridiniumyl)]-3,5,6-tris(2-pyridyl)pyrazine).[a]

Compound	$E_{1/2}$ (V)	Assignment
$[Ru(tpp)_2]^{2+}$	+ 1.57 V	Ru(II)/Ru(III)
	− 0.82 V	tpp/tpp⁻ (pyrazine)
	− 1.10 V	tpp/tpp⁻ (pyrazine)
$[Ru(tpy)(tpp)]^{2+}$ [b]	+ 1.40 V	Ru(II)/Ru(III)
	− 0.97 V	tpp/tpp⁻ (pyrazine)
	− 1.38 V	tpy/tpy⁻
	− 1.60 V	tpp⁻/tpp²⁻
$[Ru(tpy)(Metpp)]^{3+}$	+ 1.55 V	Ru(II)/Ru(III)
	− 0.65 V	Metpp⁺/Metpp (viologen)
	− 0.80 V	Metpp/Metpp⁻ (pyrazine)
	− 1.46 V	tpy/tpy⁻
$[Os(tpy)(tpp)]^{2+}$ [c]	+ 1.06 V	Os(II)/Os(III)
	− 0.97 V	tpp/tpp⁻ (pyrazine)
	− 1.39 V	tpy/tpy⁻
	− 1.74 V	tpp⁻/tpp²⁻

[a] Potentials reported in CH_3CN solution with 0.1 M TBAH vs. Ag/AgCl (0.29 V vs. NHE) with a scan rate of 200 mV/sec.

[b] Reference 55.

[c] Reference 56.

Table III. Cyclic Voltammetric Data for a Series of Ru(II) Complexes as well as Ir(tpp)Cl$_3$ Incorporating the Tridentate Polypyridyl Bridging Ligand tpp (where tpp = 2,3,5,6-tetrakis(2-pyridyl)pyrazine, bpy = 2,2'-bipyridine, and Metpp = 2-[2-(1-Methylpyridiniumyl)]-3,5,6-tris(2-pyridyl)pyrazine). [a]

Compound	$E_{1/2}$ (V)	Assignment
[Ru(bpy)(tpp)Cl]$^+$	+ 0.97 V	Ru(II)/Ru(III)
	- 1.06 V	tpp/tpp$^-$ (pyrazine)
[Ru(bpy)(tpp)(CH$_3$CN)]$^{2+}$	+ 1.36 V	Ru(II)/Ru(III)
	- 0.97 V	tpp/tpp$^-$ (pyrazine)
	- 1.48 V	bpy/bpy$^-$
[Ru(bpy)(Metpp)(CH$_3$CN)]$^{3+}$	+ 1.54 V	Ru(II)/Ru(III)
	- 0.51 V	Metpp$^+$/Metpp (viologen)
	- 0.72 V	Metpp/Metpp$^-$ (pyrazine)
Ir(tpp)Cl$_3$ [b]	+ 1.74 V	Ir(III)/Ir(IV)
	- 0.78 V	tpp/tpp$^-$ (pyrazine)
	- 1.35 V	Ir(III)/Ir(I)

[a] Potentials reported in CH$_3$CN solution with 0.1 M TBAH vs. Ag/AgCl (0.29 V vs. NHE) with a scan rate of 200 mV/sec.

[b] Reference 55.

Table IV. Cyclic Voltammetric Data for a Series of Ru(II) Complexes Incorporating the Tridentate Ligand tpy and the Bidentate Polypyridyl Bridging Ligands dpp, dpq, and dpb (where tpy = 2,2':6',2''-terpyridine, dpp = 2,3-bis(2-pyridyl)pyrazine, dpq = 2,3-bis(2-pyridyl)quinoxaline, and dpb = 2,3-bis(2-pyridyl)benzoquinoxaline).[a,b]

Compound	$E_{1/2}$ (V)	Assignment
$[Ru(tpy)(dpp)Cl]^+$	+ 1.04 V	Ru(II)/Ru(III)
	- 1.07 V	dpp/dpp⁻
	- 1.27 V	tpy/tpy⁻
$[Ru(tpy)(dpq)Cl]^+$	+ 1.06 V	Ru(II)/Ru(III)
	- 0.77 V	dpq/dpq⁻
	- 1.27 V	tpy/tpy⁻
$[Ru(tpy)(dpb)Cl]^+$	+ 1.02 V	Ru(II)/Ru(III)
	- 0.61 V	dpb/dpb⁻
	- 1.25 V	tpy/tpy⁻
$[Ru(tpy)(dpp)(py)]^{2+}$	+ 1.42 V	Ru(II)/Ru(III)
	- 1.04 V	dpp/dpp⁻
	- 1.35 V	tpy/tpy⁻
$[Ru(tpy)(dpq)(py)]^{2+}$	+ 1.41 V	Ru(II)/Ru(III)
	- 0.75 V	dpq/dpq⁻
	- 1.34 V	tpy/tpy⁻
$[Ru(tpy)(dpb)(py)]^{2+}$	+ 1.44 V	Ru(II)/Ru(III)
	- 0.59 V	dpb/dpb⁻
	- 1.34 V	tpy/tpy⁻

[a] Potentials reported in CH_3CN solution with 0.1 M TBAH vs. Ag/AgCl (0.29 V vs. NHE) with a scan rate of 200 mV/sec.
[b] Reference 34.
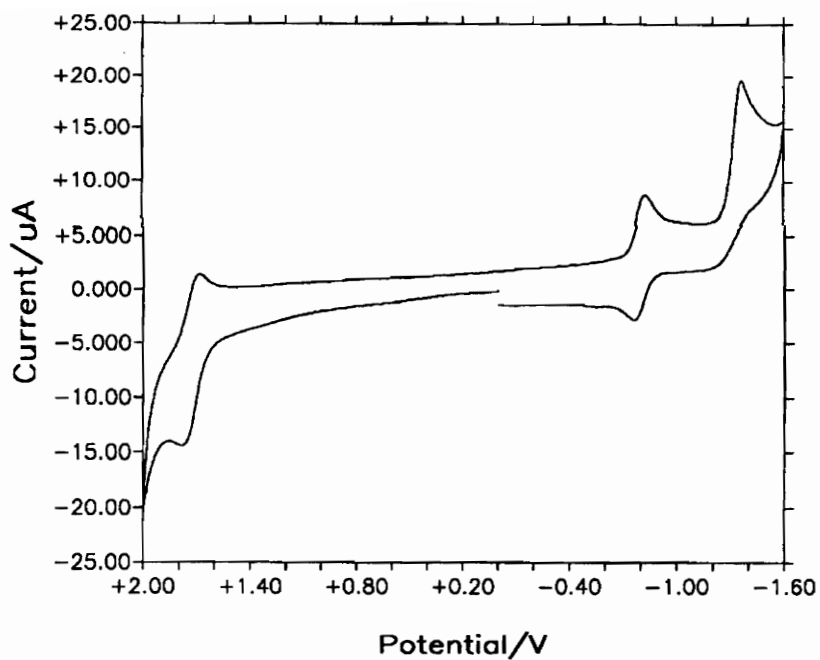
Figure 11. Cyclic Voltammogram of Ir(tpp)Cl$_3$ (where tpp = 2,3,5,6-tetrakis(2-pyridyl)pyrazine and using a Ag/AgCl reference electrode (0.29 V vs. NHE) with a scan rate of 200 mV/sec).

Figure 12. Cyclic Voltammogram of $[Ru(tpy)(tpp)]^{2+}$ (where tpy = 2,2':6',2''-terpyridine, tpp = 2,3,5,6-tetrakis(2-pyridyl)pyrazine and using a Ag/AgCl reference electrode (0.29 V vs. NHE) with a scan rate of 200 mV/sec).

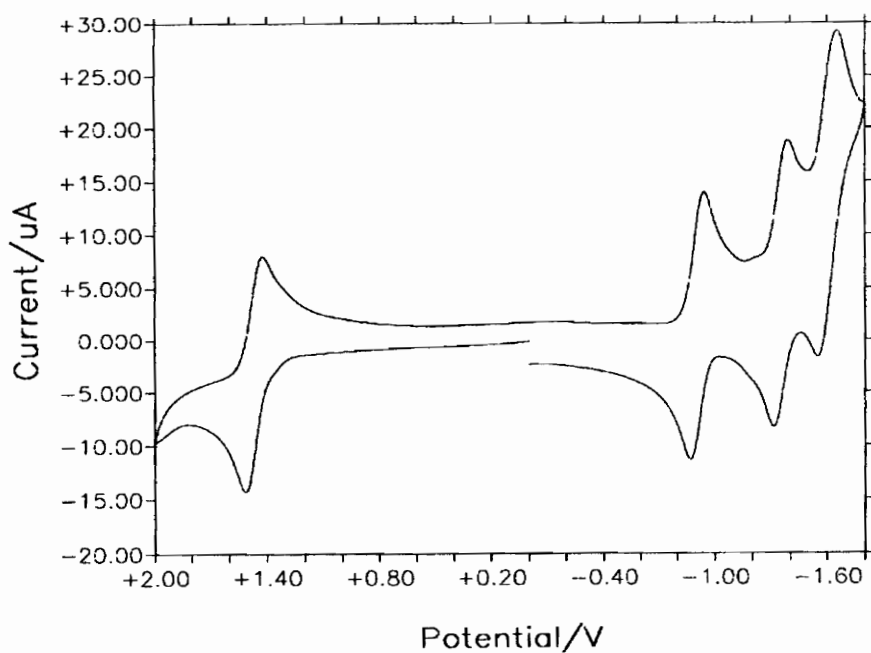reduction at - 1.60 V is assigned as a second tpp based reduction (tpp⁻/tpp^{2-}) on the basis of the reductions observed in the free ligands tpp and tpy.[49-53] In [Ru(tpy)(tpp)]$^{2+}$, the HOMO is a ruthenium based dπ orbital and the LUMO is a tpp ligand based π* orbital.

The electrochemistry of [Os(tpy)(tpp)]$^{2+}$ was previously reported.[56,59] The potentials given in Table II (page 65) are for our sample studied under our conditions for comparison. The osmium analog to [Ru(tpy)(tpp)]$^{2+}$ would be expected to exhibit similar electrochemical properties with the oxidation now being osmium based rather than ruthenium based. In the monometallic [Os(tpy)(tpp)]$^{2+}$, the oxidation at + 1.06 V was assigned as an Os(II)/Os(III) metal based process. The ligand localized reductions at - 0.97 and - 1.39 V are assigned as tpp/tpp⁻ and tpy/tpy⁻ based processes. The second tpp reduction occurs at - 1.74 V in this monometallic complex. Comparison of the ruthenium monometallic to the osmium analog, one observes that osmium oxidizes at a less positive potential than ruthenium. Osmium is expected to have dπ orbitals higher in energy than ruthenium leading to a metal that is more easily oxidized. The first tpp and tpy reductions in these two complexes appear to be insensitive to the nature of the coordinated metal leading to the conclusion that the reductions are largely ligand localized. In [Os(tpy)(tpp)]$^{2+}$, the HOMO is an osmium based dπ orbital and the LUMO is a tpp ligand based π* orbital.

The electrochemical data for [Ru(tpy)(Metpp)]$^{3+}$ is summarized in Table II (page 65). [Ru(tpy)(Metpp)]$^{3+}$ exhibits one reversible oxidation and three reversible reductions. Figure 13 contains the cyclic voltammogram of [Ru(tpy)(Metpp)]$^{3+}$. The methylated analog of [Ru(tpy)(tpp)]$^{2+}$, [Ru(tpy)(Metpp)]$^{3+}$, has a ruthenium oxidation at + 1.55 V and a series of reductions at - 0.65, - 0.80, and - 1.46 V. Upon methylation, the ruthenium metal becomes harder to oxidize by 150 mV. This is due partly to the increased π accepting ability of the Metpp ligand compared to tpp leaving the metal less electron rich. Part of this shift may also result from the complex's net charge being increased from 2+ to 3+.

If one were to align the Ru(II)/Ru(III) couple it is evident that there is a new reductive process that appears in the methylated complex prior to the first tpp reduction
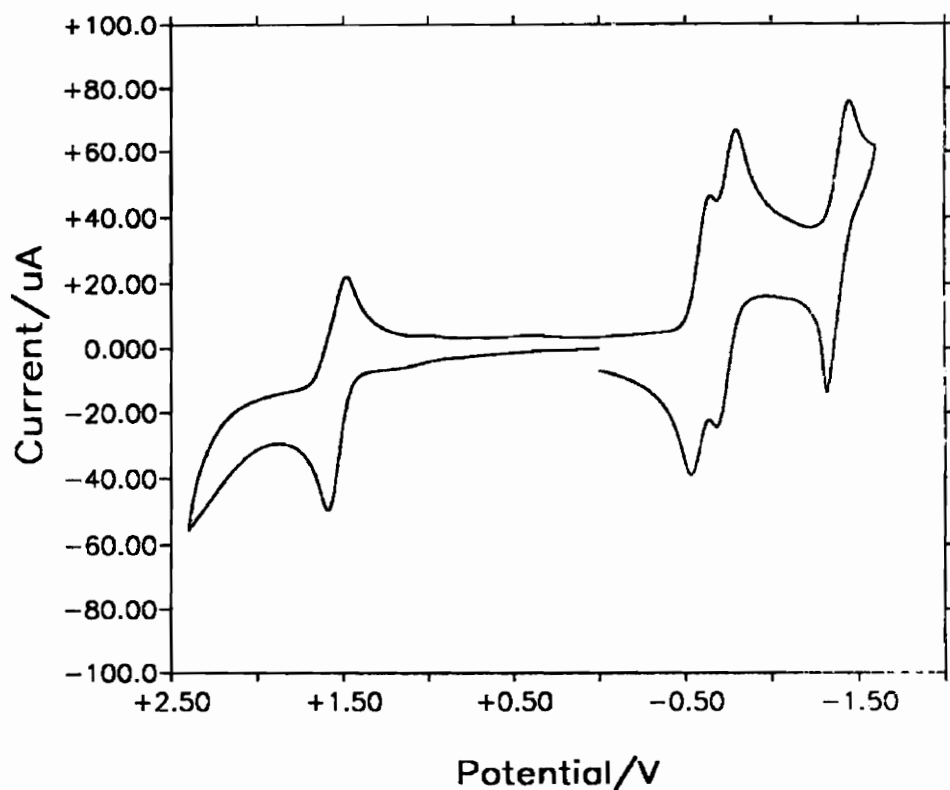
Figure 13. Cyclic Voltammogram of $[Ru(tpy)(Metpp)]^{3+}$ (where tpy = 2,2':6',2''-terpyridine, Metpp = 2-[2-(1-Methylpyridiniumyl)]-3,5,6-tris(2-pyridyl)pyrazine and using a Ag/AgCl reference electrode (0.29 V vs. NHE) with a scan rate of 200 mV/sec).

Figure 14. Cyclic Voltammograms of (——) $[Ru(tpy)(tpp)]^{2+}$ and
(------) $[Ru(tpy)(Metpp)]^{3+}$ (where tpy = 2,2':6',2''-terpyridine, tpp =
2,3,5,6-tetrakis(2-pyridyl)pyrazine, Metpp = 2-[2-(1-Methylpyridiniumyl)]-
3,5,6-tris(2-pyridyl)pyrazine and using a Ag/AgCl reference electrode
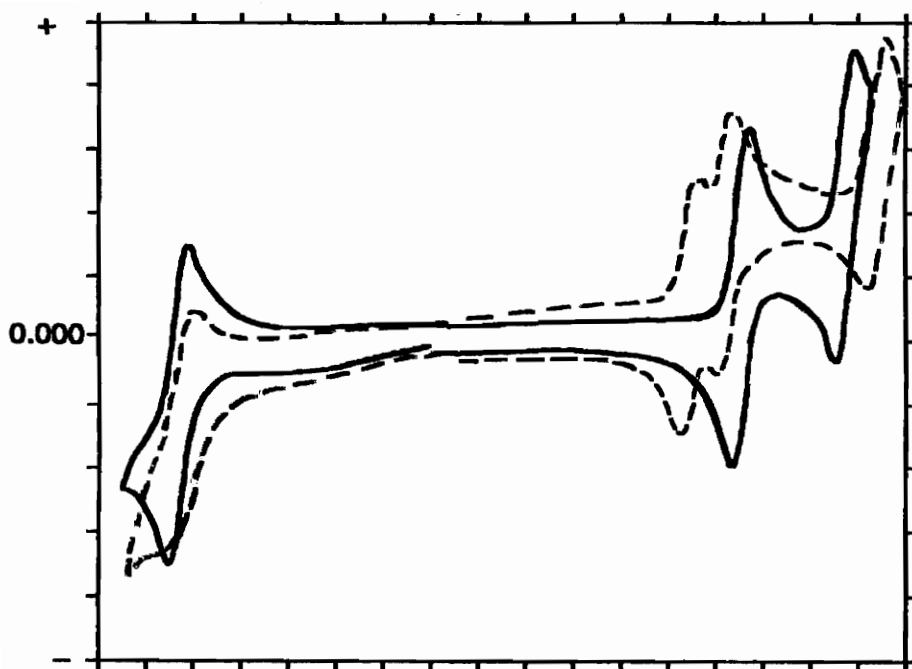(0.29 V vs. NHE) with a scan rate of 200 mV/sec).

as shown in Figure 14. In this figure, the Ru(II)/Ru(III) oxidations are aligned, thus, the scale on the x axis is an arbitrary potential in volts. The new reductive process is assigned as reduction of the viologen portion of the Metpp ligand. It has been shown previously by ESR that Os complexes incorporating the tpp ligand possess a one electron reduction that is localized on the pyrazine portion of the tpp ligand.[56] Thus, the second reduction of [Ru(tpy)(Metpp)]$^{3+}$ is assigned as a reduction that is based on the pyrazine portion of the tpp ligand. This occurs at a slightly more positive potential than the unmethylated analog, [Ru(tpy)(tpp)]$^{2+}$ and is primarily due to the electron withdrawing effect of the viologen substituent. The third reduction of [Ru(tpy)(Metpp)]$^{3+}$ at - 1.46 V most likely represents the reduction of the tpy ligand. In [Ru(tpy)(Metpp)]$^{3+}$, the HOMO is a ruthenium based dπ orbital and the LUMO is a Metpp ligand based π^* orbital localized on the remote viologen portion of the ligand.
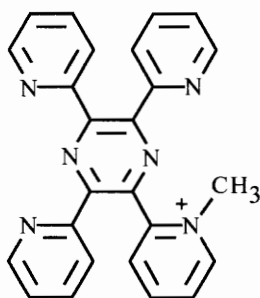
The design of this system was to have a pyrazine based π^* orbital for optical excitation and a MQ (monoquat) based acceptor orbital to localize the charge. The pyrazine is bound to the metal and thus has significant overlap with the metal dπ orbitals allowing for optical excitation. The MQ is bound to the pyrazine to allow electron transfer from the pyrazine based π^* orbital to the lowest lying MQ$^+$ based acceptor orbital. The MQ is not bound to the metal. This is intended to slow back electron transfer (BET) due to a lack of orbital overlap as well as maintain the spectroscopic properties of the Ru^{II}(tpp) moiety. This is shown as follows:
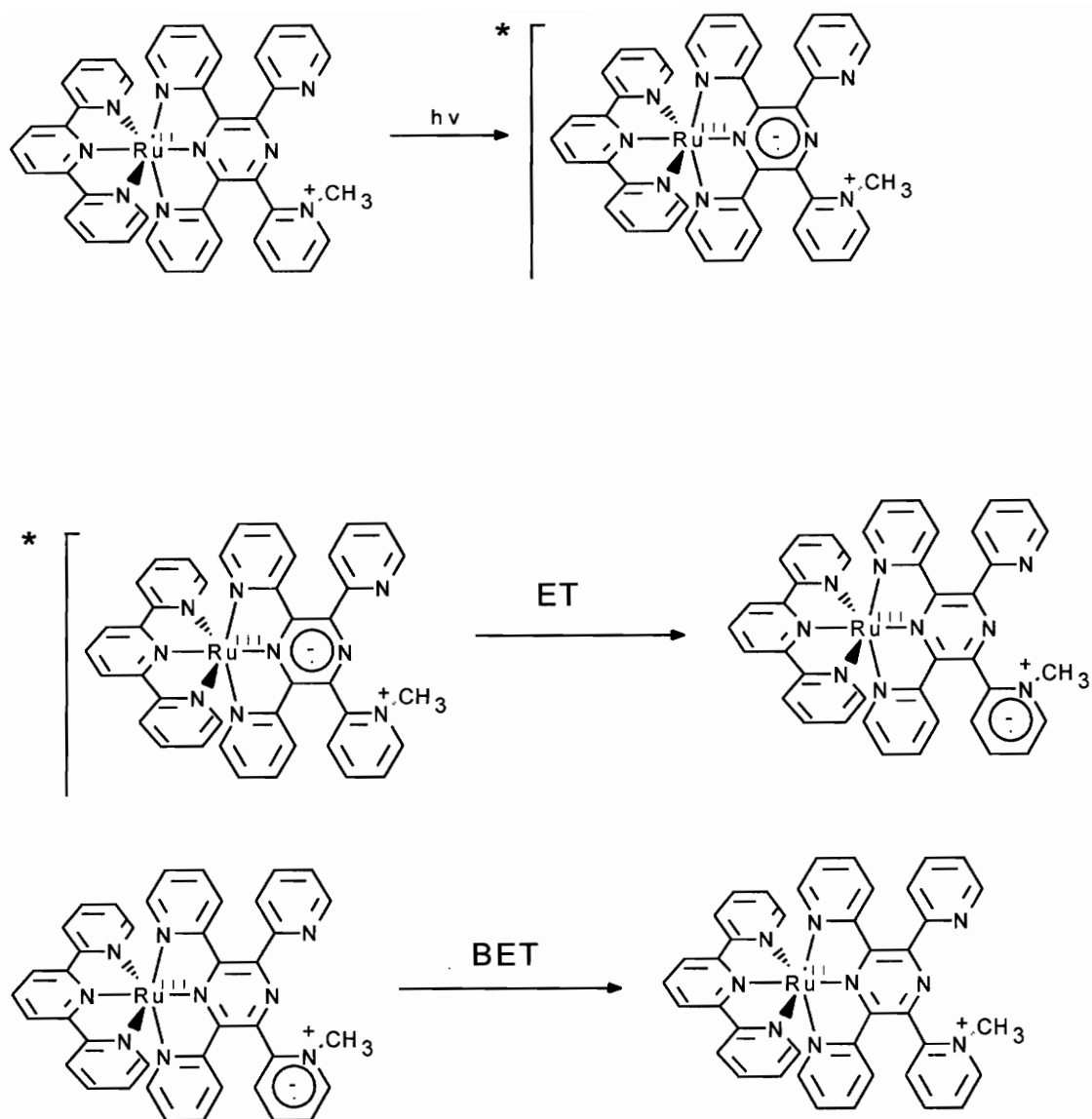
In the case of $[Ru(bpy)(tpp)Cl]^+$, a single reduction is reported in Table III (page 66) due to the complex becoming neutral after this process and adsorbing to the electrode surface. The ruthenium oxidation occurs at $+ 0.97$ V and the tpp reduction at $- 1.06$ V. The shift of the ruthenium oxidation of $[Ru(bpy)(tpp)Cl]^+$ to less positive potentials relative to $[Ru(tpy)(tpp)]^{2+}$ is indicative of the better σ-donation and weaker π-accepting ability of the chloride ligand relative to a polypyridine ligand. This provides a

more electron rich metal that is substantially easier to oxidize. The tpp reduction shifts to more negative potential in $[Ru(bpy)(tpp)Cl]^+$ relative to $[Ru(tpy)(tpp)]^{2+}$. This is the result of the more electron rich Ru metal center having an increased π-backbonding interaction with the tpp ligand. In $[Ru(bpy)(tpp)Cl]^+$, the HOMO is a ruthenium based $d\pi$ orbital and the LUMO is a tpp ligand based π^* orbital.

The electrochemical data for $[Ru(bpy)(tpp)(CH_3CN)]^{2+}$ is summarized in Table III (page 66). This complex contains one reversible oxidation and two reversible reductions. The Ru(II)/Ru(III) oxidation occurs at $+ 1.36$ V, the tpp/tpp⁻ reduction at $- 0.97$ V and the bpy/bpy⁻ reduction at $- 1.48$ V. Substitution of the chloride ligand on $[Ru(bpy)(tpp)Cl]^+$ with an acetonitrile solvent molecule to produce $[Ru(bpy)(tpp)(CH_3CN)]^{2+}$ results in a complex that is harder to oxidize by 390 mV consistent with the lower σ-donating and better π-accepting ability of the coordinated acetonitrile ligand. The tpp reduction in the solvato complex occurs 90 mV more positive than the chloride complex. This substitution of the chloride with acetonitrile leaves the ruthenium center less electron rich decreasing the degree of π backbonding to the tpp ligand giving rise to the observed shift in the tpp based reduction potential. In $[Ru(bpy)(tpp)(CH_3CN)]^{2+}$, the HOMO is a ruthenium based $d\pi$ orbital and the LUMO is a tpp ligand based π^* orbital.

In comparing the methylated and nonmethylated complexes $[Ru(bpy)(tpp)(CH_3CN)]^{2+}$ and $[Ru(bpy)(Metpp)(CH_3CN)]^{3+}$ one would expect to find the results similar to those discussed above for $[Ru(tpy)(tpp)]^{2+}$ and $[Ru(tpy)(Metpp)]^{3+}$. $[Ru(bpy)(Metpp)(CH_3CN)]^{3+}$ exhibits one reversible oxidation and two reversible reductions. Upon methylation the ruthenium again becomes harder to oxidize, $+ 1.54$ V for $[Ru(bpy)(Metpp)(CH_3CN)]^{3+}$ versus $+ 1.36$ V for $[Ru(bpy)(tpp)(CH_3CN)]^{2+}$. A new reductive process is observed at -0.51 V for the methylated complex and represents reduction of the viologen portion of the tpp ligand The second reduction of $[Ru(bpy)(Metpp)(CH_3CN)]^{3+}$ represents reduction of the pyrazine portion of the tpp ligand and occurs at $- 0.72$ V. The reduction of the bpy ligand is not observed presumably due to the formation of a neutral metal complex that adsorbs to the electrode

surface. In [Ru(bpy)(Metpp)(CH$_3$CN)]$^{3+}$, the HOMO is a ruthenium based dπ orbital and the LUMO is a tpp ligand based π* orbital localized on the remote viologen portion of the ligand.

To summarize, the results of the electrochemical studies for the methylated versus the nonmethylated compounds indicate that all of the complexes prepared possess ruthenium (dπ) based HOMOs. The nature of the LUMO varies as a function of structure. The unmethylated complexes [Ru(tpy)(tpp)]$^{2+}$ and [Ru(bpy)(tpp)(CH$_3$CN)]$^{2+}$ possess LUMOs that are localized on the pyrazine portion of the tpp ligand. Methylation to yield [Ru(tpy)(Metpp)]$^{3+}$ and [Ru(bpy)(Metpp)(CH$_3$CN)]$^{3+}$ produces complexes in which the LUMO is localized on the remote viologen portion of the Metpp ligand. This indicates that intramolecular electron transfer quenching of the Ru(dπ) $\rightarrow$ tpp(π*) MLCT state is thermodynamically favored to produce a reduced viologen acceptor, consistent with the molecular design.

The electrochemical data for the series of complexes [Ru(tpy)(BL)Cl]$^+$ and [Ru(tpy)(BL)(py)]$^{2+}$ (where BL = dpp, dpq, or dpb) is summarized in Table IV (page 67). All six complexes exhibit one reversible oxidation and two reductions. Within each series, the oxidation corresponding to a Ru(II)/Ru(III) couple occurs at a similar potential in the three complexes. In the series [Ru(tpy)(BL)Cl]$^+$, the Ru(II)/Ru(III) oxidation occurs at + 1.04 V when BL = dpp, + 1.06 V when BL = dpq, and + 1.02 V when BL = dpb. The first reductive process varies as a function of the bridging ligand shifting to more positive potential on going from dpp to dpq to dpb. This supports its assignment as being BL based. In this series of complexes [Ru(tpy)(BL)Cl]$^+$, the BL/BL$^-$ reduction occurs at - 1.07 V when BL = dpp, - 0.77 V when BL = dpq, and - 0.61 V when BL = dpb. In this series of complexes, the tpy/tpy$^-$ reduction occurs at - 1.27 V when BL = dpp, - 1.27 V when BL = dpq, and - 1.25 V when BL = dpb. This supports the assignment of the second reduction as being tpy based. In these complexes, the highest-occupied molecular orbital (HOMO) is a ruthenium based dπ orbital and the lowest-unoccupied molecular orbital (LUMO) is a bridging ligand based π* orbital.

The cyclic voltammograms for the $[Ru(tpy)(BL)(py)]^{2+}$ series are shown in Figure 15. Figure 16 contains the cyclic voltammograms of $[Ru(tpy)(dpq)Cl]^{+}$ and $[Ru(tpy)(dpp)(py)]^{2+}$ demonstrating the effects of the substitution of the chloride with pyridine at the sixth coordination site. Substitution of the chloride ligand with pyridine to produce complexes of the type $[Ru(tpy)(BL)(py)]^{2+}$ results in complexes that are harder to oxidize by ca. 400 mV consistent with the decreased σ donating and increased π accepting ability of the pyridine ligand. This is remarkably similar to the 390 mV shift in the $[Ru(bpy)(tpp)Cl]^{+}$ system. In the series $[Ru(tpy)(BL)(py)]^{2+}$, the Ru(II)/Ru(III) oxidation occurs at + 1.42 V when BL = dpp, + 1.41 V when BL = dpq, and + 1.44 V when BL = dpb. The magnitude of the shift of the BL/BL⁻ reduction is essentially independent of the formulation of the complex, i.e. Cl⁻ or py in the sixth coordination site. In this set of complexes, the BL/BL⁻ reduction occurs at - 1.04 V when BL = dpp, - 0.75 V when BL = dpq, and - 0.59 V when BL = dpb. The change from dpp to dpq results in a 300 mV shift for the Cl⁻ series and 290 mV for the py series. The second reductive process occurs at a relatively constant potential within each series. This reduction is not as well behaved due to the overall charge on the complex becoming zero. In the series $[Ru(tpy)(BL)(py)]^{2+}$, the tpy/tpy⁻ reduction occurs at - 1.35 V, - 1.34 V, and - 1.34 V for BL = dpp, dpq, and dpb, respectively. It is interesting to note that this tpy based reduction shifts to slightly more negative potential upon substitution of pyridine for the chloride within this framework while the BL based reductions remain relatively unchanged. The difference in the response of these two ligands to substitution of the Cl⁻ by pyridine could be a result of the stereochemistry of the system. Namely, the BL is trans to the ligand being substituted while the tpy is cis to the site of substitution. Similar stereochemical effects on redox potentials of polyazine ligands have been observed in the past.[56] As in the series discussed above, the highest-occupied molecular orbital (HOMO)
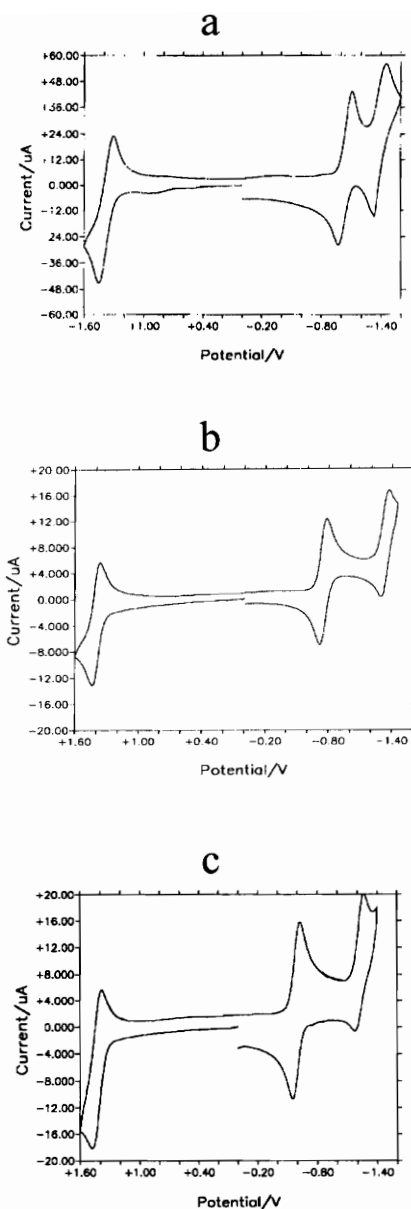
Figure 15. Cyclic Voltammograms of [Ru(tpy)(BL)(py)]$^+$ polypyridyl complexes where BL = (a) dpp, (b) dpq, or (c) dpb (where dpp = 2,3-bis (2-pyridyl)pyrazine), dpq = 2,3-bis(2-pyridyl)quinoxaline), dpb = 2,3-bis (2-pyridyl)benzoquinoxaline, tpy = 2,2':6',2''-terpyridine, py = pyridine and using a Ag/AgCl reference electrode (0.29 V vs. NHE) with a scan rate of 200 mV/sec).

a

b
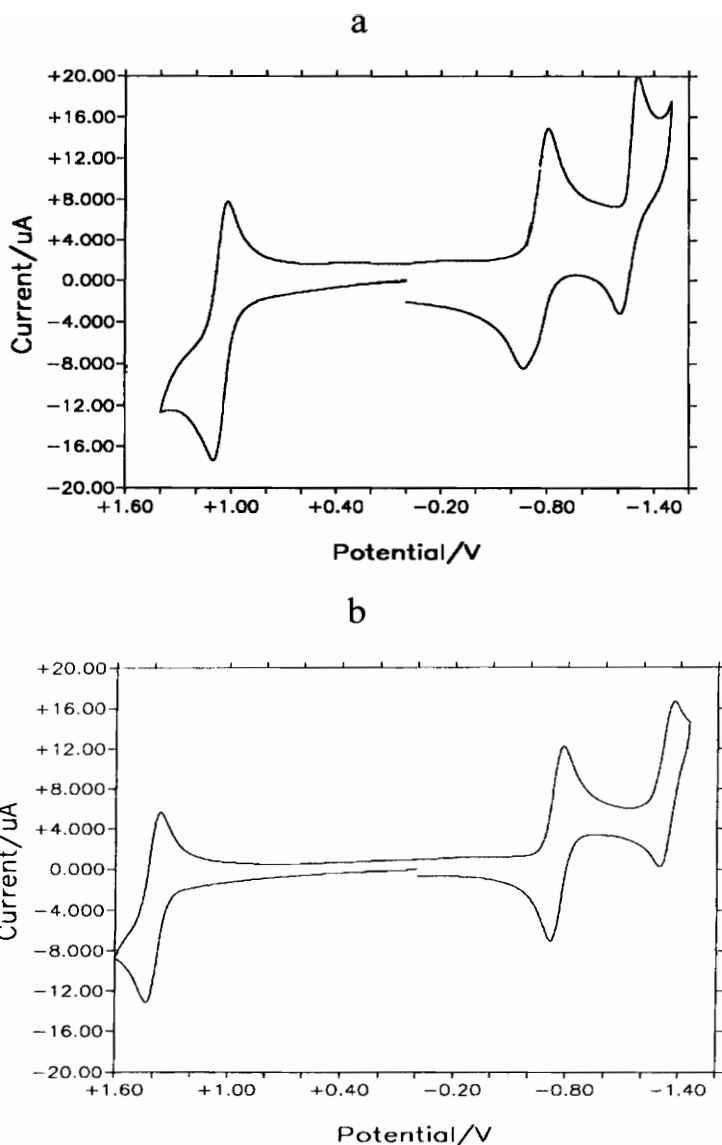
Figure 16. Cyclic Voltammograms of ruthenium polypyridyl complexes
(a) $[Ru(tpy)(dpq)Cl]^+$ and (b) $[Ru(tpy)(dpq)(py)]^{2+}$ (where dpp = 2,3-bis
(2-pyridyl)pyrazine), dpq = 2,3-bis(2-pyridyl)quinoxaline), dpb = 2,3-bis
(2-pyridyl)benzoquinoxaline, tpy = 2,2':6',2''-terpyridine, py = pyridine
and using a Ag/AgCl reference electrode (0.29 V vs. NHE) with a scan rate
of 200 mV/sec.

79

is a ruthenium based $d\pi$ orbital and the lowest-unoccupied molecular orbital (LUMO) is a bridging ligand based π^* orbital.

Bimetallic Complexes

The cyclic voltammetric data for the bimetallic complexes is summarized in Table V. Upon formation of a bimetallic, one would expect to see a sum of all the electrochemical processes observed in the monometallic fragments with perturbations introduced by the formation of the bridged system. The main perturbation results from the stabilization of the bridging ligand π^* orbitals upon formation of a bimetallic system and often gives rise to two sequential one electron reductions of the bridging ligand prior to reduction of other electroactive moieties.[38-47,50,55,56] A shift in the oxidation potentials of bimetallic complexes compared to the monometallic fragments is expected due to the electron withdrawing effect of the additional metal center upon formation of the additional metal center and the enhanced π back-bonding ability of the bridging ligand.

The cyclic voltammogram of $[(tpy)Ru(tpp)IrCl_3]^{2+}$ is shown in Figure 17. This complex exhibits two reversible oxidations, two reversible reductions, and one irreversible reduction. The oxidations in the bimetallic complex are metal based processes with the one at $+1.92$ V assigned as an Ir(III)/Ir(IV) oxidation and the one at $+1.56$ V being assigned as a Ru(II)/Ru(III) oxidation. As expected, a shift by 160 mV in the Ru(II)/Ru(III) oxidation for the bimetallic complex compared to $[Ru(tpy)(tpp)]^{2+}$ is observed due to the electron withdrawing effect of the additional metal center and the enhanced π backbonding ability of the tpp ligand. A 180 mV shift is observed for the Ir(III)/Ir(IV) oxidation in the bimetallic system as compared to Ir(tpp)Cl$_3$. This shift can be attributed in part to the addition of the Ru^{II}tpy moiety. Another factor that can contribute to this shift is the charge on the complex prior to the iridium oxidation. Since the ruthenium metal is oxidized first in the bimetallic complex, an additional $1+$ charge is added making the charge on this complex $3+$ versus 0 for Ir(tpp)Cl$_3$ prior to the

Table V. Cyclic Voltammetric Data for a Series of Ru(II), Os(II), and Ir(III) Bimetallic Complexes Incorporating the Tridentate Polypyridyl Bridging Ligand tpp (where tpy = 2,2':6',2''-terpyridine and tpp = 2,3,5,6-tetrakis(2-pyridyl)pyrazine). [a]

Compound	$E_{1/2}$ (V)	Assignment
$[(tpy)Ru(tpp)IrCl_3]^{2+}$	+ 1.92 V	Ir(III)/Ir(IV)
	+ 1.56 V	Ru(II)/Ru(III)
	- 0.29 V	tpp/tpp$^-$
	- 0.83 V	tpp$^-$/tpp^{2-}
	- 1.42 V	Ir(III)/Ir(I)
$[(tpy)Ru(tpp)\mathbf{Ru}Cl_3]^+$	+ 1.61 V	Ru(II)/Ru(III)
	+ 0.73 V	**Ru**(II)/**Ru**(III)
	- 0.60 V	tpp/tpp$^-$
	- 1.10 V	tpp$^-$/tpp^{2-}
	- 1.50 V	tpy/tpy$^-$
$[(tpy)Os(tpp)RuCl_3]^+$	+ 1.32 V	Os(II)/Os(III)
	+ 0.66 V	Ru(II)/Ru(III)
	- 0.59 V	tpp/tpp$^-$
	- 1.07 V	tpp$^-$/tpp^{2-}
	- 1.47 V	tpy/tpy$^-$

Compound	$E_{1/2}$ (V)	Assignment
[(tpy)**Ru(tpp)**Ru(tpp)]$^{4+}$	+ 1.86 V	Ru(II)/Ru(III)
	+ 1.51 V	**Ru(II)/Ru(III)**
	- 0.30 V	**tpp/tpp⁻**
	- 0.82 V	**tpp⁻/tpp²⁻**
	- 1.10 V	tpp/tpp⁻
[(tpy)**Os(tpp)**Ru(tpp)]$^{4+}$	+ 1.81 V	Ru(II)/Ru(III)
	+ 1.17 V	**Os(II)/Os(III)**
	- 0.36 V	**tpp/tpp⁻**
	- 0.81 V	**tpp⁻/tpp²⁻**
	- 1.07 V	tpp/tpp⁻
[(tpy)Ru(tpp)Ru(tpy)]$^{4+}$	+ 1.76 V	Ru(II)/Ru(III)
	+ 1.44 V	Ru(II)/Ru(III)
	- 0.35 V	tpp/tpp⁻
	- 0.84 V	tpp⁻/tpp²⁻
	- 1.30 V	tpy/tpy⁻

[a] Potentials reported in CH_3CN solution with 0.1 M TBAH and reported vs. Ag/AgCl (0.29 V vs. NHE) with a scan rate of 200 mV/sec.
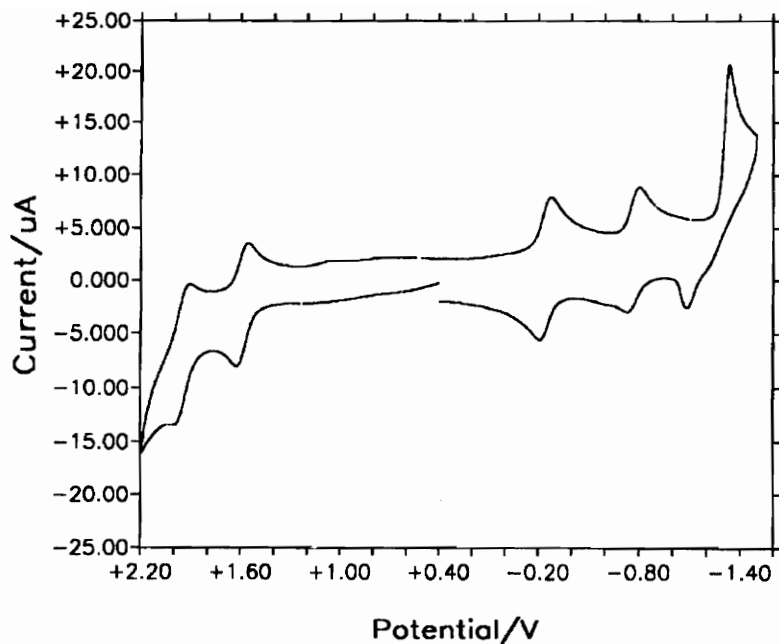
Figure 17. Cyclic Voltammogram of [(tpy)Ru(tpp)IrCl$_3$]$^{2+}$ (where tpy = 2,2':6',2''-terpyridine, tpp = 2,3,5,6-tetrakis(2-pyridyl)pyrazine and using a Ag/AgCl reference electrode (0.29 V vs. NHE) with a scan rate of 200 mV/sec).

Ir(III)/Ir(IV) oxidation. The first two reductions at - 0.29 V and - 0.83 V are assigned as sequential one electron reductions of the tpp ligand. The third reduction at - 1.42 V is an irreversible reduction and is thus assigned as an Ir(III)/Ir(I) metal based process. The tpy reduction is shifted beyond the solvent window. This results in a complex with a ruthenium based HOMO and a bridging tpp based LUMO.

The cyclic voltammogram of $[(tpy)Ru(tpp)RuCl_3]^+$ is shown in Figure 18 and the data summarized in Table V (page 81). Upon attachment of a $RuCl_3$ moiety to $[Ru(tpy)(tpp)]^{2+}$ producing $[(tpy)Ru(tpp)RuCl_3]^+$, an additional oxidation is observed and the first reduction is shifted to more positive potentials. The two oxidations are assigned as Ru(II)/Ru(III) metal based processes. The first oxidation at + 0.73 V is assigned as being the ruthenium that is coordinated to tpp and three chloride ligands. This metal would be more electron rich since chloride is a better π donor while tpy is a π acceptor. The second oxidation at + 1.61 V is assigned as the ruthenium coordinated to tpy and tpp. This ruthenium becomes harder to oxidize relative to the monometallic analog due to the enhanced π backbonding to the tpp upon bimetallic formation. The two reductions at - 0.60 and - 1.10 V are assigned as being sequential tpp reductions which is typical for polyazine bridged systems of this type. These reductions occur at more positive potentials due to the stabilization of the tpp π^* orbitals upon addition of a second metal center as the tpp acts as a bridging ligand. A shift in the tpp reduction potential by 370 mV occurs in the bimetallic complex relative to the monometallic complex $[Ru(tpy)(tpp)]^{2+}$. This is consistent with a metal that is more electron rich increasing the π backbonding to the tpp ligand. The third reduction at - 1.50 V is assigned as a tpy/tpy⁻ reduction. This yields a complex, $[(tpy)Ru(tpp)RuCl_3]^+$, in which the HOMO is based on the ruthenium bound to the three chlorides and the LUMO is based on the bridging tpp ligand.

Substitution of the chlorides on $[(tpy)Ru(tpp)RuCl_3]^+$ by tpp produces $[(tpy)Ru(tpp)Ru(tpp)]^{4+}$. The cyclic voltammogram of this bimetallic complex is shown in Figure 19 and the results summarized in Table V (page 81). This complex exhibits two reversible oxidations and three reversible reductions. The first oxidation of this
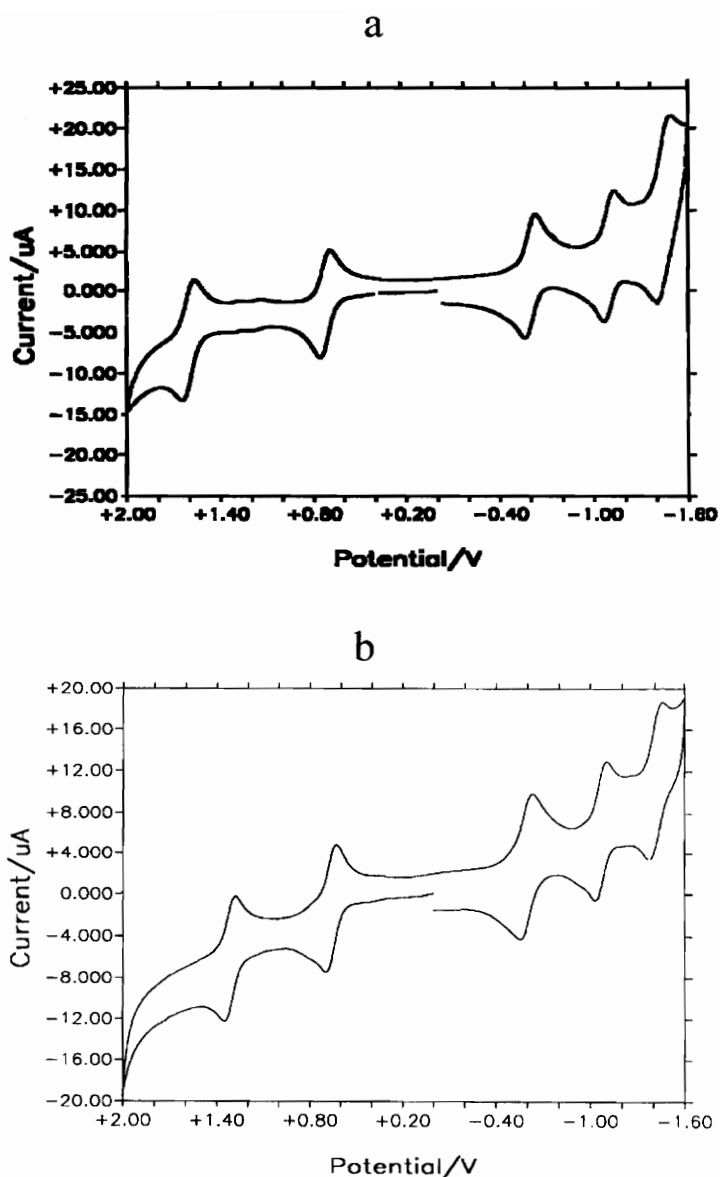
Figure 18. Cyclic Voltammograms of (a) [(tpy)Ru(tpp)RuCl$_3$]$^+$ and (b) [(tpy)Os(tpp)RuCl$_3$]$^+$ (where tpy = 2,2':6',2''-terpyridine, tpp = 2,3,5,6-tetrakis(2-pyridyl)pyrazine and using a Ag/AgCl reference electrode (0.29 V vs. NHE) with a scan rate of 200 mV/sec).
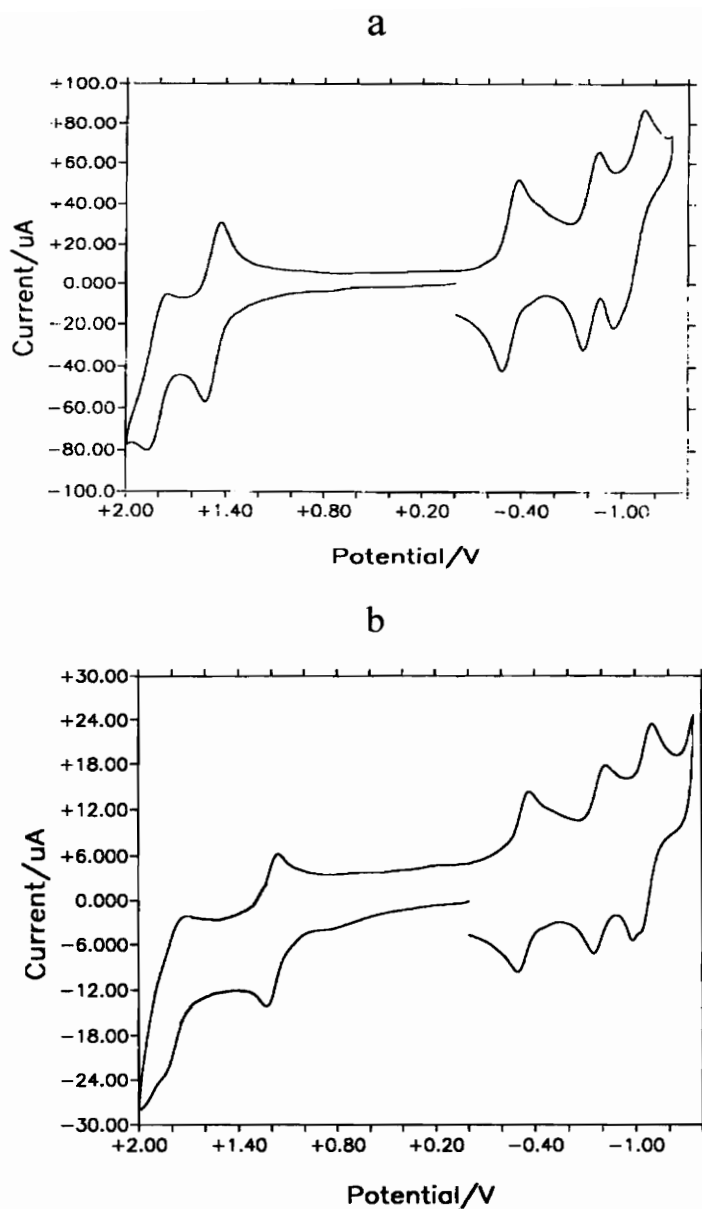
Figure 19. Cyclic Voltammograms of (a) [(tpy)Ru(tpp)Ru(tpp)]$^{4+}$ and (b) [(tpy)Os(tpp)Ru(tpp)]$^{4+}$ (where tpy = 2,2':6',2''-terpyridine, tpp = 2,3,5,6-tetrakis(2-pyridyl)pyrazine and using a Ag/AgCl reference electrode (0.29 V vs. NHE) with a scan rate of 200 mV/sec).

complex is shifted to more positive potentials relative to $[(tpy)Ru(tpp)RuCl_3]^+$. As reported in Table II (page 65) and previously by other authors, $[Ru(tpp)_2]^{2+}$ has a Ru(II)/Ru(III) oxidation at + 1.57 V followed by reduction of the two tpp ligands at - 0.82 and - 1.07 V.[50,59] Thus $[Ru(tpp)_2]^{2+}$ is harder to oxidize than $[Ru(tpy)(tpp)]^{2+}$ by 170 mV. This is consistent with tpp having an increased π acidity relative to tpy leaving the metal center less electron rich. Consequently, the first oxidation at + 1.51 V in $[(tpy)Ru(tpp)Ru(tpp)]^{4+}$ represents the Ru(II)/Ru(III) processes that is centered on the ruthenium coordinated to both tpp and tpy whereas the second oxidation at + 1.86 V is the Ru(II)/Ru(III) couple for the ruthenium coordinated to two tpp ligands. The two reductions at - 0.30 and - 0.82 V correspond to the expected sequential reduction of bridging tpp ligand. The tpp bridging ligand is stabilized more when bound to $Ru^{II}(tpp)$ than $Ru^{II}Cl_3$. As discussed, the tpp reduction in $[(tpy)Ru(tpp)RuCl_3]^+$ is shifted by 370 mV relative to the monometallic complex. In $[(tpy)Ru(tpp)Ru(tpp)]^{4+}$, this orbital is stabilized by 670 mV. This can be attributed to the increased π backbonding when the ruthenium is bound to the chlorides. The third reduction is assigned as the tpp/tpp⁻ reductive process localized on the terminal tpp ligand. This yields a complex in which the HOMO is based on the ruthenium site bound to tpy and the LUMO is based on the bridging tpp ligand.

The symmetric bimetallic $[(tpy)Ru(tpp)Ru(tpy)]^{4+}$ was prepared as an analog to $[(tpy)Ru(tpp)(Ru(tpp)]^{4+}$. This bimetallic complex has been prepared previously and the electrochemistry studied.[50,59] The potentials given in Table V (page 81) are for our sample studied under our conditions for comparison. This bimetallic exhibits two reversible oxidations and three reversible reductions. The first Ru(II)/Ru(III) oxidation occurs at + 1.44 V with the second oxidation occurring at + 1.76 V. The other metal, Ru(II), becomes harder to oxidize relative to the first due to the enhanced π backbonding to the tpp as well as the overall charge on the complex being 5+ prior to this process. Because this complex is symmetric, the two ruthenium oxidations should occur at the same potential in the absence of any interaction between the metal centers. The difference in the oxidation potentials between the two ruthenium centers leads to the

conclusion that metal-metal communication through the tpp ligand is significant. The complex $[(tpy)Ru(tpp)Ru(tpy)]^{4+}$ exhibits three reversible one electron ligand based reductions. The reduction at - 0.35 V is the one electron reduction of tpp (tpp/tpp⁻) whereas the one at - 0.84 V can be attributed to the second reduction of tpp (tpp⁻/tpp²⁻). The third reduction at - 1.30 V is assigned as the tpy/tpy⁻ reduction. The sequential tpp reductions in $[(tpy)Ru(tpp)Ru(tpy)]^{4+}$ and $[(tpy)Ru(tpp)Ru(tpp)]^{4+}$ occur at essentially the same potentials leading to the conclusion that substitution of a terminal tpp ligand with tpy does not have an effect on the nature of the bridging ligand. This results in a complex with ruthenium based HOMO and a bridging tpp based LUMO. The difference in the oxidation potentials between this bimetallic and $[(tpy)Ru(tpp)Ru(tpp)]^{4+}$ are not surprising. The oxidation of the Ru bound to two tpp ligands would be expected to occur at a higher potential than that of a Ru coordinated to tpy and tpp due to the better π accepting ability of tpp. It is interesting to note that $[(tpy)Ru(tpp)Ru(tpy)]^{4+}$ has a $\Delta E_{1/2}$ that is not much less than the $[(tpy)Ru(tpp)Ru(tpp)]^{4+}$ system.

Due to the similarities of the osmium and ruthenium monometallic precursor complexes, similar results are expected for the osmium analog of $[(tpy)Ru(tpp)RuCl_3]^+$. Upon incorporation of $RuCl_3$ to the remote nitrogens on the tpp ligand of $[Os(tpy)(tpp)]^{2+}$ to produce $[(tpy)Os(tpp)RuCl_3]^+$, an additional oxidation is observed and the first reduction shifts to more positive potentials. Based on the assignments for $[(tpy)Ru(tpp)RuCl_3]^+$, the first oxidation for $[(tpy)Os(tpp)RuCl_3]^+$ at + 0.66 V is assigned as the Ru(II)/Ru(III) oxidation. The ruthenium metal will be more electron rich than the osmium due to its coordination environment. Interestingly, this ruthenium based oxidation occurs at a 60 mV less positive potential in this heterobimetallic complexes relative to the all ruthenium analog. This likely results from the enhanced π-backbonding ability of the Os metal center giving rise to a decreased π-accepting ability of the tpp ligand. This gives a more electron rich $(tpp)RuCl_3$ moiety in the heterobimetallic complex relative to the all ruthenium analog. The second oxidation at +1.32 V is assigned as an Os(II)/Os(III) metal based process. This metal is harder to oxidize than the analogous monometallic complex $[Os(tpy)(tpp)]^{2+}$. This results from the

increased π acceptor ability of the bridging tpp ligand leading to a less electron rich metal. As predicted by the electrochemical properties of the monometallic fragments, the osmium oxidation occurs at a lower potential than the similarly coordinated ruthenium in the Ru/Ru bimetallic. The first two reductions at - 0.59 and - 1.07 V are assigned as sequential tpp reductions, and the third reduction at - 1.47 V as tpy reduction. This system, $[(tpy)Os(tpp)RuCl_3]^+$, has a ruthenium based HOMO and a tpp based LUMO.

Substitution of the chlorides in $[(tpy)Os(tpp)RuCl_3]^+$ by tpp to form $[(tpy)Os(tpp)Ru(tpp)]^{4+}$ leads to a reversal in the order of the metal centered oxidations. The first oxidation at + 1.17 V is assigned as being an Os(II)/Os(III) oxidation with the second oxidation at + 1.81 V being a Ru(II)/Ru(III) metal based oxidation. The osmium oxidation is slightly shifted relative to the monometallic due to the electron withdrawing effect of the additional ruthenium center and the enhanced π backbonding ability of the bridging tpp. As expected, the osmium oxidation occurs at a lower potential than the similarly coordinated ruthenium in $[(tpy)Ru(tpp)Ru(tpp)]^{4+}$. The second oxidation in $[(tpy)Os(tpp)Ru(tpp)]^{4+}$ corresponds to the Ru(II)/Ru(III) couple and occurs at 50 mV less positive potential in $[(tpy)Os(tpp)Ru(tpp)]^{4+}$ than the Ru/Ru bimetallic. This more electron rich ruthenium site results once again from an enhanced π backbonding of the osmium metal to the tpp ligand relative to the ruthenium analog. This gives rise to a lower degree of π-backbonding from the ruthenium site making it more electron rich. The ligand reductions at - 0.36 and - 0.81 V are assigned as tpp/tpp$^-$ and tpp$^-$/tpp^{2-} reductive processes consistent with a bridging tpp ligand whereas that at - 1.07 V is the tpp/tpp$^-$ reduction localized on the terminal tpp ligand. This results in a complex with an osmium based HOMO and a bridging tpp based LUMO.

Electronic Absorption Spectroscopy

There are numerous studies that have been performed that correlate metal-to-ligand charge transfer energies to the difference between the oxidation and reduction potentials found electrochemically.[8,14,21,23,25,27,84] Through electrochemistry, one can determine the nature of the highest-occupied molecular orbital as well as that of the lowest-unoccupied molecular orbital. These orbitals will be the ones involved in the lowest-lying spectroscopic transition. The redox orbital involved in the oxidation is identical with the orbital from which the electronic transition occurs, whereas the redox orbital involved in the reduction is the same as the orbital that becomes populated upon excitation. If the metal is held constant and only the ligands are varied, the MLCT excitation energies correlate with the reduction potential of the coordinated ligand and the energy of this transition can be tuned to the desired energy.[8,14,34-60] $\Delta E_{1/2}$ is the electrochemically measured energy gap between the one electron oxidation, the HOMO, and one electron reduction, the LUMO. $\Delta E_{1/2}$ is not exactly equal to the energy of the optically populated excited state, E_{op}, because of the difference of the timescale of the experiments. In absorption spectroscopy, the excited state that is formed upon promotion of an electron is a vibrationally excited state which then relaxes down to the lowest energy vibrational level for that state. In electrochemistry, the timescale is much greater allowing the molecule to rearrange to its ideal configuration prior to electron transfer. If one were to add in the inner and outer reorganization energies of the charge transfer state, E_{op} would be equal to $\Delta E_{1/2}$.

Free ligands

The free ligands bpy, tpy, tpp, dpp, dpq, and dpb used in this study have been characterized previously.[36,55,59,62-64] The free ligand spectra are dominated by intense $n \rightarrow \pi^*$ and $\pi \rightarrow \pi^*$ transitions in the ultraviolet. In the bidentate bridging ligands, these transitions shift to lower energy on going from dpp to dpq to dpb. This is a result of the addition of the fused aromatic rings increasing the conjugation of the ligand and

stabilizing the π^* orbital. The free ligand spectra for bpy, tpy, and tpp are shown in Figure 20. The terminal ligands bpy and tpy have a lowest energy absorption at and 265 and 278 nm, respectively. The bridging ligands tpp, dpp, dpq, and dpb have a λ_{max}^{abs} for their lowest lying optical transition at 308, 284, 332, and 378 nm. This order is the same as the order of the $E_{1/2}$ for reduction.

Monometallic Complexes

The electronic absorption spectra of polypyridyl transition metal complexes would be expected to contain transitions that are observed in the free ligands as well as transitions that occur between the metal and the coordinated ligands. In metal complexes of these ligands, the ultraviolet region consists primarily of ligand based n $\rightarrow \pi^*$ and $\pi \rightarrow \pi^*$ transitions localized on each ligand.[8,14,37-60] The n $\rightarrow \pi^*$ ligand based transitions exhibit a large shift upon coordination to a metal. The visible region of the electronic absorption spectra for polypyridyl metal complexes contains bands that are assigned as metal-to-ligand charge transfer, MLCT, transitions terminating on each acceptor ligand.[8,14,37-60] The relative energy of the lowest lying excited states in complexes of this type is dominated by the shift in the bridging ligand based π^* LUMO.[8,14,34-47] The results of the electronic absorption spectroscopy for the monometallic complexes are summarized in Table VI and Table VII.

The electronic absorption spectrum of $Ir(tpp)Cl_3$ is shown in Figure 21. The monometallic system displays a series of transitions throughout the ultraviolet and visible regions of the spectrum. The lowest energy band at 558 nm is assigned as an $Ir(d\pi) \rightarrow tpp(\pi^*)$ [3]MLCT, while the more intense band at 424 nm is assigned as the $Ir(d\pi) \rightarrow tpp(\pi^*)$ [1]MLCT transition. A less intense transition at 498 nm is also observed and may represent another [3]MLCT transition. Due to the significant amount of spin-orbit coupling observed for iridium systems, transitions which are normally spin forbidden, such as [3]MLCT transitions, can be observed in the absorption spectrum and will be of low intensity. The remaining peaks in the ultraviolet region are assigned as n $\rightarrow \pi^*$ and
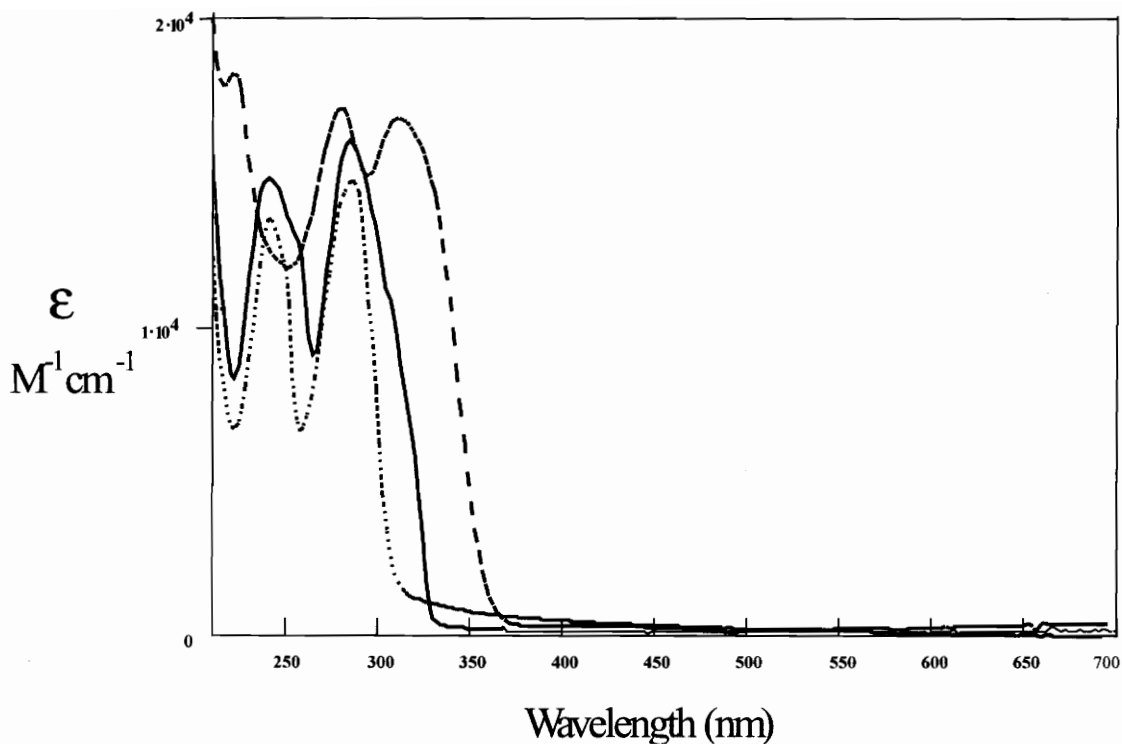
Figure 20. Electronic Absorption Spectra (acetonitrile solutions) for the Polypyridyl Ligands Used in this study (·····) bpy, (——) tpy, and (----) tpp (where bpy = 2,2'-bipyridine, tpy = 2,2':6',2''-terpyridine and tpp = 2,3,5,6-tetrakis(2-pyridyl)pyrazine).

Table VI. Electronic Absorption Spectroscopy and Photophysical Data for a Series of Ru(II), Os(II), and Ir(III) Complexes Incorporating the Tridentate Polypyridyl Bridging Ligand tpp (where bpy = 2,2'-bipyridine, tpy = 2,2':6',2''-terpyridine, tpp = 2,3,5,6-tetrakis(2-pyridyl)pyrazine), and Metpp = 2-[2-(1-Methylpyridiniumyl)]-3,5,6-tris(2-pyridyl)pyrazine).

Compound	λ_{max}^{abs} (nm)[a]	λ_{max}^{em} (nm)[b]	τ (ns)
$[Ru(tpp)_2]^{2+}$	480	648	80[d]
$[Ru(tpy)(tpp)]^{2+}$ [c]	474	665	30
$[Ru(tpy)(Metpp)]^{3+}$	474	700	38
$[Os(tpy)(tpp)]^{2+}$	468	775[d]	260[e]
$[Ru(bpy)(tpp)Cl]^{+}$	504	818	21
$[Ru(bpy)(tpp)(CH_3CN)]^{2+}$	456	700	62
$[Ru(bpy)(Metpp)(CH_3CN)]^{3+}$	458	712	70
$Ir(tpp)Cl_3$ [c]	558	632	1300

[a] Reported for the lowest energy [1]MLCT.

[b] Measured in deoxygenated acetonitrile solution at room temperature.

[c] Reference 55.

[e] Reference 50.

[d] Reference 56.

Table VII. Electronic Absorption Spectroscopy and Photophysical Data for a Series of Ru(II) Complexes Incorporating the Bidentate Polypyridyl Bridging Ligands dpp, dpq, and dpb (where tpy = 2,2':6',2''-terpyridine, dpp = 2,3-bis(2-pyridyl)pyrazine, dpq = 2,3-bis(2-pyridyl)quinoxaline, dpb = 2,3-bis(2-pyridyl)benzoquinoxaline, and py = pyridine).

Compound	λ_{max}^{abs} (nm)[b]	λ_{max}^{em} (nm)[c]	τ (ns)
[Ru(tpy)(dpp)Cl]$^+$	514	760	20
[Ru(tpy)(dpq)Cl]$^+$	564	d	d
[Ru(tpy)(dpb)Cl]$^+$	592	d	d
[Ru(tpy)(dpp)(py)]$^{2+}$	478	760	80
[Ru(tpy)(dpq)(py)]$^{2+}$	518	800	28
[Ru(tpy)(dpb)(py)]$^{2+}$	554	860	< 20

[a] Reference 34.

[b] Reported for the lowest energy ^{1}MLCT.

[c] Measured in deoxygenated acetonitrile solution at room temperature.

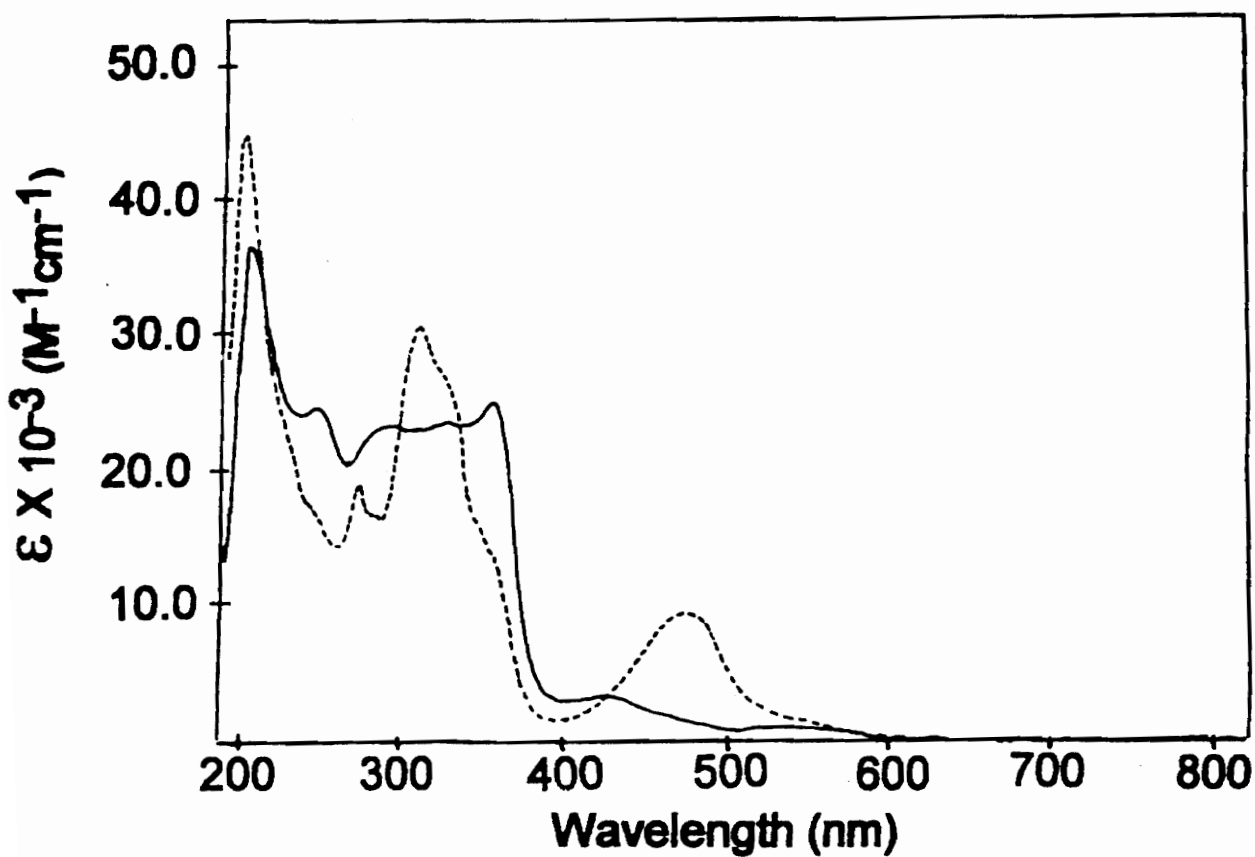[d] No emission was observable on our system.

Figure 21. Electronic Absorption Spectra (acetonitrile solutions) for Iridium(III) and Ruthenium(II) Monometallic Complexes Incorporating the Tridentate Polypyridyl Ligand tpp: (——) Ir(tpp)Cl$_3$ and (----) [Ru(tpy)(tpp)]$^{2+}$ (where tpy = 2,2':6',2''-terpyridine and tpp = 2,3,5,6-tetrakis(2-pyridyl)pyrazine).

$\pi \rightarrow \pi^*$ ligand localized transitions on the basis of their extinction coefficients.

The monometallic complex, [Ru(tpy)(tpp)]$^{2+}$ has been prepared previously and the electronic absorption spectrum studied.[50,59] The results given in Table VI are for our sample studied under our conditions for comparison purposes. The mixed ligand complex, [Ru(tpy)(tpp)]$^{2+}$, has a complicated spectrum consisting of both ligand based $\pi \rightarrow \pi^*$ and metal-to-ligand charge transfer bands. The electrochemical data for this system indicate both tpp and tpy based π^* orbitals are present at relatively low energy. The band at 474 nm can be assigned as two overlapping MLCT transitions, Ru(dπ) $\rightarrow$ tpy(π^*) and Ru(dπ) $\rightarrow$ tpp(π^*), with the tpp based MLCT occurring at slightly lower energy. Both tpp and tpy n $\rightarrow \pi^*$ and $\pi \rightarrow \pi^*$ transitions, as well as higher energy MLCT transitions are observed in the ultraviolet.

Figure 22 contains the electronic absorption spectra of [Ru(tpy)(tpp)]$^{2+}$ and [Ru(tpy)(Metpp)]$^{3+}$, the results are summarized in Table VI. Comparison of the electronic absorption spectroscopy of the two complexes reveals some interesting features. These spectra are virtually identical despite the very different electrochemistry. The lowest energy transition for both [Ru(tpy)(tpp)]$^{2+}$ and [Ru(tpy)(Metpp)]$^{3+}$ is at 474 nm. The energy of this transition remains the same upon methylation indicating that the acceptor orbital for this transition in both the methylated and nonmethylated complexes is the same, i.e. the pyrazine portion of the tpp ligand. This lowest energy absorption has a high energy shoulder attributed to the Ru(dπ) $\rightarrow$ tpy(π^*) MLCT transition.[55,58,59] Both of these transitions are solvatochromic, consistent with the assignment as being MLCT in nature. One does not observe a Ru(dπ) $\rightarrow$ viologen CT transition presumably due to a lack of sufficient orbital overlap. Both the methylated and nonmethylated complexes possess the same lowest lying spectroscopically accessible excited state that is Ru $\rightarrow$ tpp MLCT in nature. Consequently, optical population of this MLCT state will occur and should be followed by intramolecular electron transfer for the Metpp systems to produce a reduced viologen and an oxidized ruthenium.
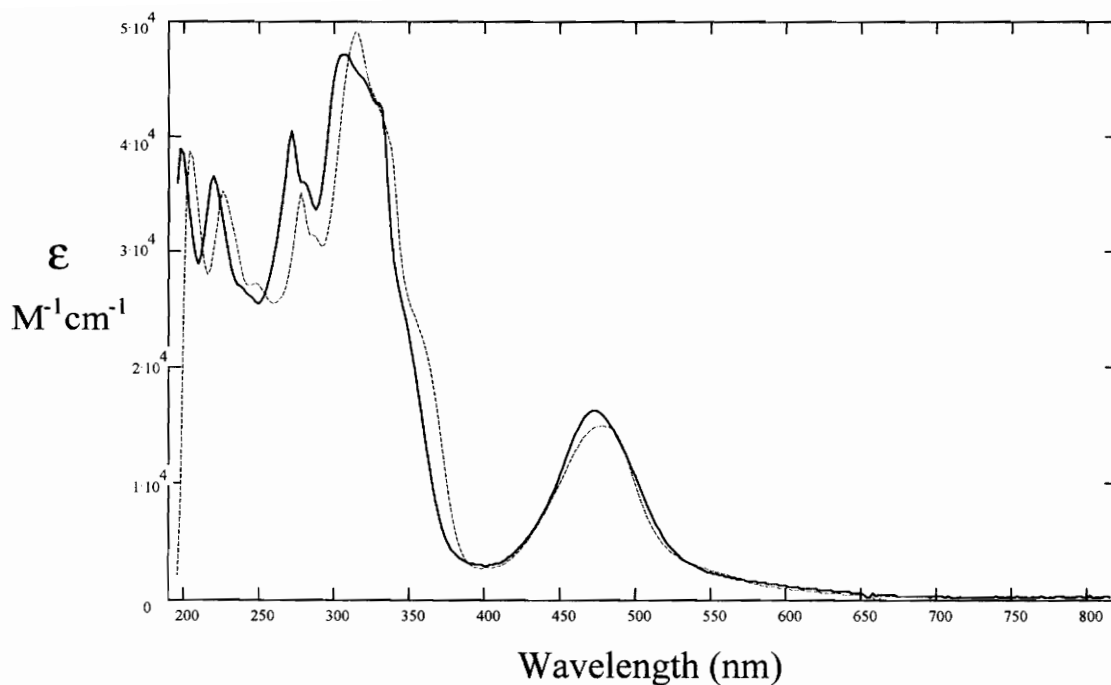
Figure 22. Electronic Absorption Spectra (acetonitrile solutions) for
(——) [Ru(tpy)(tpp)]$^{2+}$ and (----) [Ru(tpy)(Metpp)]$^{3+}$ (where tpy =
2,2':6',2''-terpyridine, tpp = 2,3,5,6-tetrakis(2-pyridyl)pyrazine, and
Metpp = 2-[2-(1-Methylpyridiniumyl)]-3,5,6-tris(2-pyridyl)pyrazine).

Comparison of the electronic absorption spectroscopy of the complexes containing bpy and tpp shows some interesting trends. The electronic absorption spectra are shown in Figure 23. [Ru(bpy)(tpp)Cl]$^+$ has a lowest lying absorbance at 504 nm that is assigned as a Ru(dπ) $\rightarrow$ tpp(π*) MLCT transition. The energy of the Ru(dπ) $\rightarrow$ tpp(π*) MLCT is shifted to higher energy upon substitution of the chloride with an acetonitrile solvent molecule. This is consistent with the electrochemical results which indicate the ruthenium is stabilized upon substitution of the chloride.

Comparison of the electronic absorption spectra of [Ru(bpy)(tpp)(CH$_3$CN)]$^{2+}$ and [Ru(bpy)(Metpp)(CH$_3$CN)]$^{3+}$ in Figure 23 shows some interesting features. Once again, the spectroscopy of the methylated [Ru(bpy)(Metpp)(CH$_3$CN)]$^{3+}$ and nonmethylated complex [Ru(bpy)(tpp)(CH$_3$CN)]$^{2+}$ is quite similar. The lowest energy transition corresponds to a Ru(dπ) $\rightarrow$ tpp(π*) MLCT terminating on the pyrazine portion of the tpp ligand. Hence, both the methylated and nonmethylated complexes possess the same lowest lying spectroscopically accessible excited state that is Ru $\rightarrow$ tpp MLCT in nature. This result, coupled to the electrochemical analysis, indicates that optical population of this MLCT state will occur and should be followed by intramolecular electron transfer for the Metpp systems to produce a reduced viologen and an oxidized ruthenium. The Ru $\rightarrow$ tpp MLCT in the chloro complex is red shifted relative to the acetonitrile complex consistent with the smaller electrochemically measured energy gap.

The electronic absorption spectra of the ruthenium compounds, [Ru(tpy)(BL)Cl]$^+$ and [Ru(tpy)(BL)(py)]$^{2+}$ (BL = dpp, dpq, or dpb) are shown in Figures 24 and 25, respectively, and summarized in Table VII, page 94. The [Ru(tpy)(BL)Cl]$^+$ complexes exhibit n $\rightarrow$ π* and π $\rightarrow$ π* transitions in the UV region which are both tpy and BL based.

In addition, metal-to-bridging ligand and metal-to-tpy charge transfer bands are present in the visible. The addition of the fused benzene ring to the bridging ligand extends the aromatic system and stabilizes the π* orbital thus shifting the transition to lower energy as dpq and dpb are substituted for dpp. For this reason the peaks at 514, 564 and 592 nm are assigned as the singlet Ru(dπ) $\rightarrow$ BL(π*) MLCT transitions.
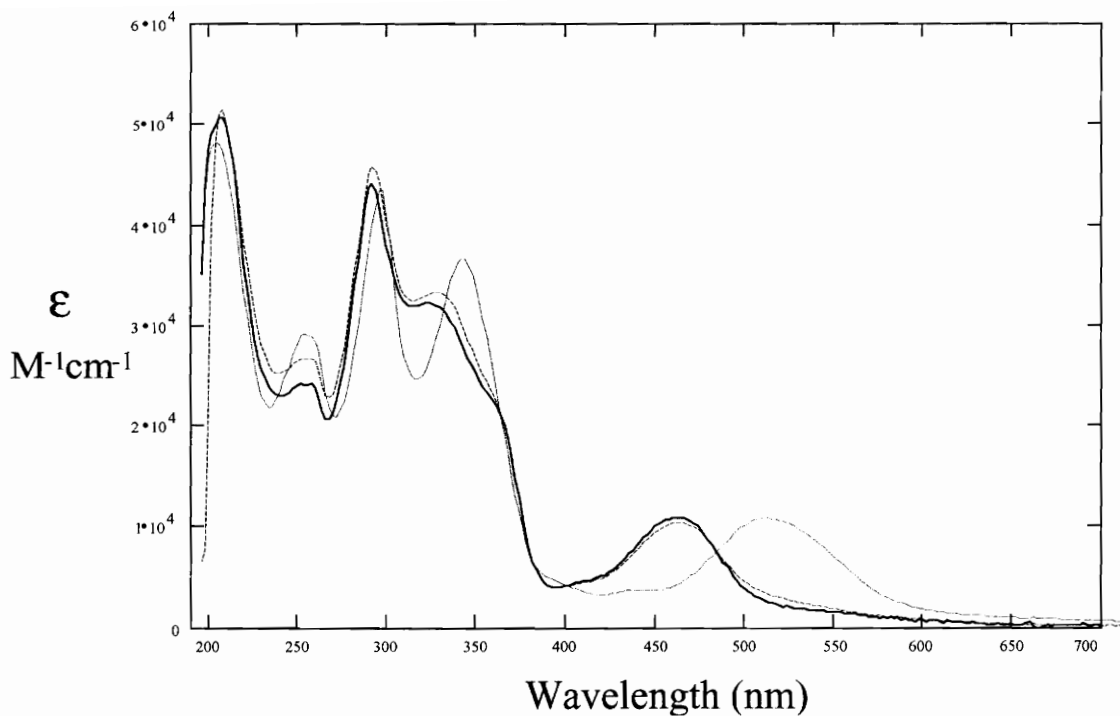
Figure 23. Electronic Absorption Spectra (acetonitrile solutions) for (——) [Ru(bpy)(tpp)Cl]$^+$, (----) [Ru(bpy)(tpp)(CH$_3$CN)]$^{2+}$, and (-.-.-) [Ru(bpy)(Metpp)(CH$_3$CN)]$^{3+}$ (where bpy = 2,2'-bipyridine, tpp = 2,3,5,6-tetrakis(2-pyridyl)pyrazine, and Metpp = 2-[2-(1-Methylpyridiniumyl)]-3,5,6-tris(2-pyridyl)pyrazine).

The band at approximately 450 nm is assigned as a Ru → tpy MLCT transition for the three complexes based on the results of the electrochemical studies.

The electronic absorption spectra of the $[Ru(tpy)(BL)(py)]^{2+}$ complexes contains transitions similar to those in the spectra of the $[Ru(tpy)(BL)Cl]^{+}$ series. The $[Ru(tpy)(BL)(py)]^{2+}$ complexes also exhibit n → π* and π → π* transitions in the UV region which are both tpy and BL based. Based on the reasons discussed above for the complexes with the Cl⁻ substituted, the peaks at 478, 518, and 554 nm are assigned as the singlet $Ru(d\pi) \rightarrow BL(\pi^*)$ MLCT transitions. This is as would be predicted since the substitution of the chloride with pyridine should result in a stabilization of the $Ru(d\pi)$ orbitals, leading to a blue shift of the Ru → BL MLCT. The Ru → tpy MLCT transition for the three complexes appears at approximately 450 nm. Once again, this is as predicted from the electrochemistry since the ruthenium oxidation and the tpy reduction remain at about the same potential throughout the series of complexes.

It has been assigned previously that $[Os(tpy)(tpp)]^{2+}$ contains n → π* and π → π* transitions for both tpy and tpp the ultraviolet region of the electronic absorption spectrum.[56,59] As in $[Ru(tpy)(tpp)]^{2+}$, the electrochemical data for this system indicate both tpp and tpy based π* orbitals are present at relatively low energy. The lowest energy transition at 468 nm has been assigned as overlapping $Os(d\pi) \rightarrow tpp(\pi^*)$ and $Os(d\pi) \rightarrow tpy(\pi^*)$ MLCT transitions with the tpp based transition at lower energy. The osmium and ruthenium complexes look remarkably similar when coordinated to two tridentate ligands. This has been attributed to the more covalent character of the metal-ligand interaction in the osmium complex.

The photochemistry of these types of complexes is dominated by the nature of the lowest lying excited state. Thus, the ability to synthetically manipulate the nature of this state is very important in molecular design. The nature of the lowest lying spectroscopically accessible excited state of the monometallic complexes, where the electron is localized on the pyrazine portion of the tpp ligand upon excitation, is
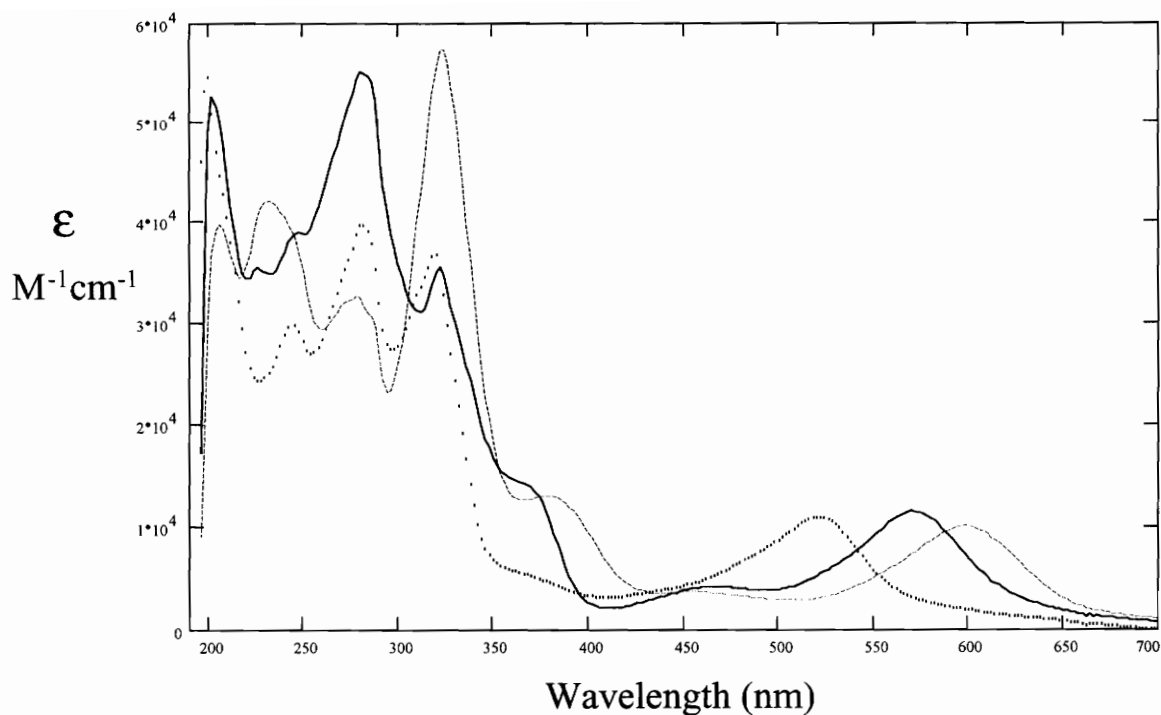
Figure 24. Electronic Absorption Spectra (acetonitrile solutions) for a series of ruthenium complexes of the general formula [Ru(tpy)(BL)Cl]$^+$: BL = (⋯⋯) dpp, (——) dpq, and (----) dpb (where dpp = 2,3-bis(2-pyridyl)pyrazine, dpq = 2,3-bis(2-pyridyl)quinoxaline, dpb = 2,3-bis(2-pyridyl)benzoquinoxaline, and tpy = 2,2':6',2''-terpyridine).
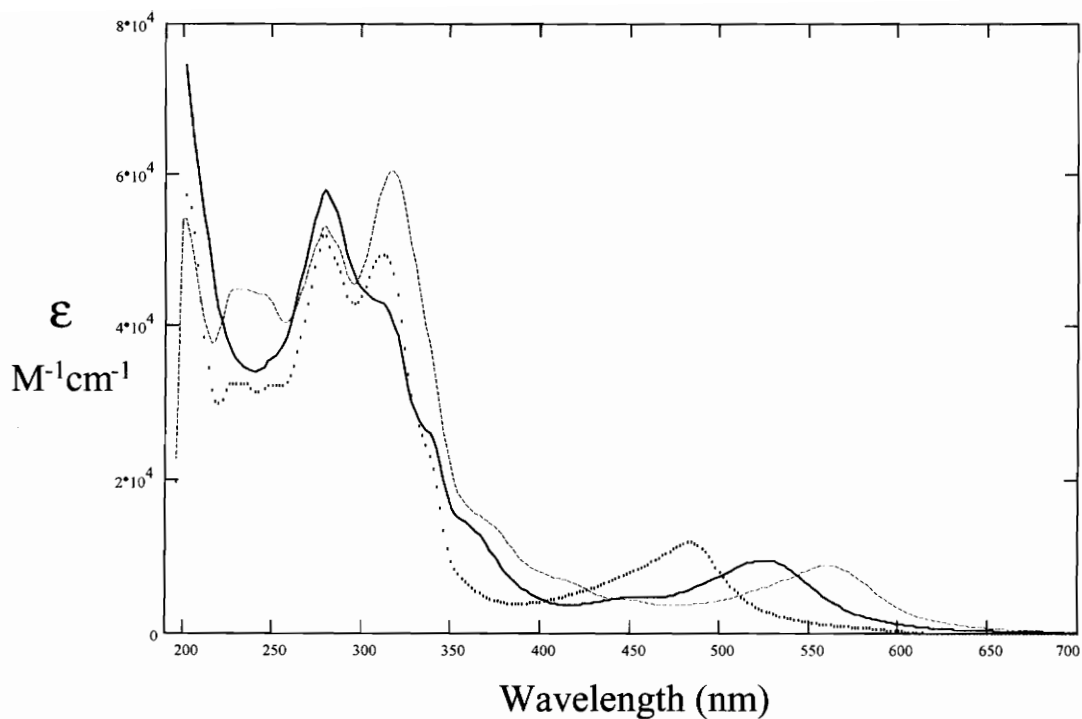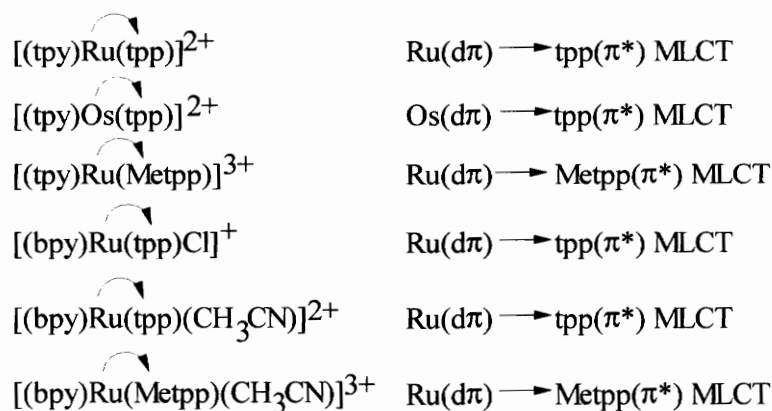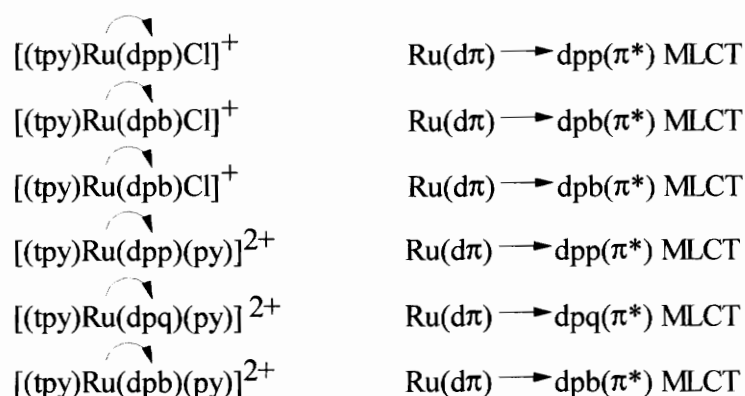
Figure 25. Electronic Absorption Spectra (acetonitrile solutions) for a series of ruthenium complexes of the general formula $[Ru(tpy)(BL)(py)]^{2+}$: BL = ($\cdots\cdots$) dpp, (——) dpq, and (- - - -) dpb (where dpp = 2,3-bis (2-pyridyl)pyrazine, dpq = 2,3-bis(2-pyridyl)quinoxaline, dpb = 2,3-bis (2-pyridyl)benzoquinoxaline, py = pyridine and tpy = 2,2':6',2''-terpyridine).

illustrated below. Hence, optical excitation will shift electron density towards the vacant nitrogens on tpp to which other components can be bound.

$[(tpy)Ru(tpp)]^{2+}$ $Ru(d\pi) \longrightarrow tpp(\pi^*)$ MLCT

$[(tpy)Os(tpp)]^{2+}$ $Os(d\pi) \longrightarrow tpp(\pi^*)$ MLCT

$[(tpy)Ru(Metpp)]^{3+}$ $Ru(d\pi) \longrightarrow Metpp(\pi^*)$ MLCT

$[(bpy)Ru(tpp)Cl]^{+}$ $Ru(d\pi) \longrightarrow tpp(\pi^*)$ MLCT

$[(bpy)Ru(tpp)(CH_3CN)]^{2+}$ $Ru(d\pi) \longrightarrow tpp(\pi^*)$ MLCT

$[(bpy)Ru(Metpp)(CH_3CN)]^{3+}$ $Ru(d\pi) \longrightarrow Metpp(\pi^*)$ MLCT

In the $[Ru(tpy)(BL)Cl]^{+}$ and $[Ru(tpy)(BL)(py)]^{2+}$ complexes (where BL = dpp, dpq, and dpb) the lowest lying spectroscopically accessible excited state is always localized on the bridging ligand that is being varied. This is important and shows that electron density will always shift towards the other components that can be bound to the free nitrogens on the bridging ligands. The nature of the MLCT state is illustrated below:

$[(tpy)Ru(dpp)Cl]^{+}$ $Ru(d\pi) \longrightarrow dpp(\pi^*)$ MLCT

$[(tpy)Ru(dpb)Cl]^{+}$ $Ru(d\pi) \longrightarrow dpb(\pi^*)$ MLCT

$[(tpy)Ru(dpb)Cl]^{+}$ $Ru(d\pi) \longrightarrow dpb(\pi^*)$ MLCT

$[(tpy)Ru(dpp)(py)]^{2+}$ $Ru(d\pi) \longrightarrow dpp(\pi^*)$ MLCT

$[(tpy)Ru(dpq)(py)]^{2+}$ $Ru(d\pi) \longrightarrow dpq(\pi^*)$ MLCT

$[(tpy)Ru(dpb)(py)]^{2+}$ $Ru(d\pi) \longrightarrow dpb(\pi^*)$ MLCT

Bimetallic Complexes

The electronic absorption spectra for the bimetallic complexes are shown in Figures 26, 27, and 28 and summarized in Table VIII. When comparing the monometallic complexes with the bimetallic complexes one notices that the lowest energy MLCT transition is shifted to lower energy in the bimetallic complexes. The addition of an electron withdrawing metal center onto the bridging ligand will stabilize

the π* orbital, reducing the energy difference between the metal and ligand orbital as shown in the electrochemical data.

The electronic absorption spectra of $[(tpy)Ru(tpp)IrCl_3]^{2+}$ and its monometallic fragments are shown in Figure 26. In the mixed-metal bimetallic, $[(tpy)Ru(tpp)IrCl_3]^{2+}$, a broad peak is seen in the visible region of the spectrum between 480 and 630 nm which is composed of many transitions. By analogy to the monometallic fragments, the lowest energy component at ca. 660 nm, which has a relatively low extinction coefficient, can be assigned as the $Ir(d\pi) \rightarrow tpp(\pi*)$ [3]MLCT transition. The intense portion of this peak between 480 and 610 nm is expected to contain three [1]MLCT bands, the $Ru(d\pi) \rightarrow tpp(\pi*)$ [1]MLCT, the $Ru(d\pi) \rightarrow tpy(\pi*)$ [1]MLCT, and the $Ir(d\pi) \rightarrow tpp(\pi*)$ [1]MLCT. Both the ruthenium and iridium bridging ligand based MLCT bands should shift to lower energy upon formation of the bimetallic complex due to the stabilization of the bridging ligand based π^* orbital. According to the electrochemical results, the magnitude of this shift is expected to be similar for both Ru and Ir. Consequently, the relative ordering of the bridging ligand based MLCT transitions should not change upon formation of the bridged system. The lowest energy component of these overlapping [1]MLCT bands should be $Ru(d\pi) \rightarrow tpp(\pi*)$ transition. In the bimetallic complex, the ruthenium backbonding to the bridging ligand is increased which will give rise to a blue shift of the $Ru(d\pi) \rightarrow tpy(\pi*)$ MLCT. Thus the shoulder observed at 425 nm is assigned as the $Ru(d\pi) \rightarrow tpy(\pi*)$. The magnitude of the shifts experienced by the Ru → tpp and Ir → tpp bands should be quite similar since the same bridging ligand based π^* orbital should be involved in both transitions. The intense peaks in the ultraviolet region, are assigned as ligand based n → π* and π → π* transitions for both tpy and tpp.

Figure 27 contains the electronic absorption spectra of the bimetallic complexes $[(tpy)Ru(tpp)RuCl_3]^+$ and $[(tpy)Os(tpp)RuCl_3]^+$. The Ru/Ru bimetallic will be discussed first. The addition of $RuCl_3$ to the three vacant sites on tpp of $[Ru(tpy)(tpp)]^{2+}$ to form $[(tpy)Ru(tpp)RuCl_3]^+$ results in two major bands appearing in the visible, one at 470 nm and another at 612 nm. The band at 470 nm is assigned as the $Ru(d\pi) \rightarrow tpy(\pi*)$ MLCT

Table VIII. Electronic Absorption Spectroscopy and Photophysical Data for a Series of Ru(II), Os(II), and Ir(III) Bimetallic Complexes Incorporating the Tridentate Polypyridyl Bridging Ligand tpp (where tpy = 2,2':6',2''-terpyridine and tpp = 2,3,5,6-tetrakis(2-pyridyl)pyrazine).

Compound	λ_{max}^{abs} (nm)[a]	λ_{max}^{em} (nm)[b]	τ (ns)
[(tpy)Ru(tpp)IrCl$_3$]$^{2+}$	660	810	22
[(tpy)Ru(tpp)RuCl$_3$]$^{+}$	612	c	c
[(tpy)Os(tpp)RuCl$_3$]$^{+}$	678	c	c
[(tpy)Ru(tpp)Ru(tpp)]$^{4+}$	548	833	100
[(tpy)Os(tpp)Ru(tpp)]$^{4+}$	546	820	120
[(tpy)Ru(tpp)Ru(tpy)]$^{4+}$	550	826	100

[a] Reported for the lowest energy ^{1}MLCT.

[b] Measured in deoxygenated acetonitrile solution at room temperature.
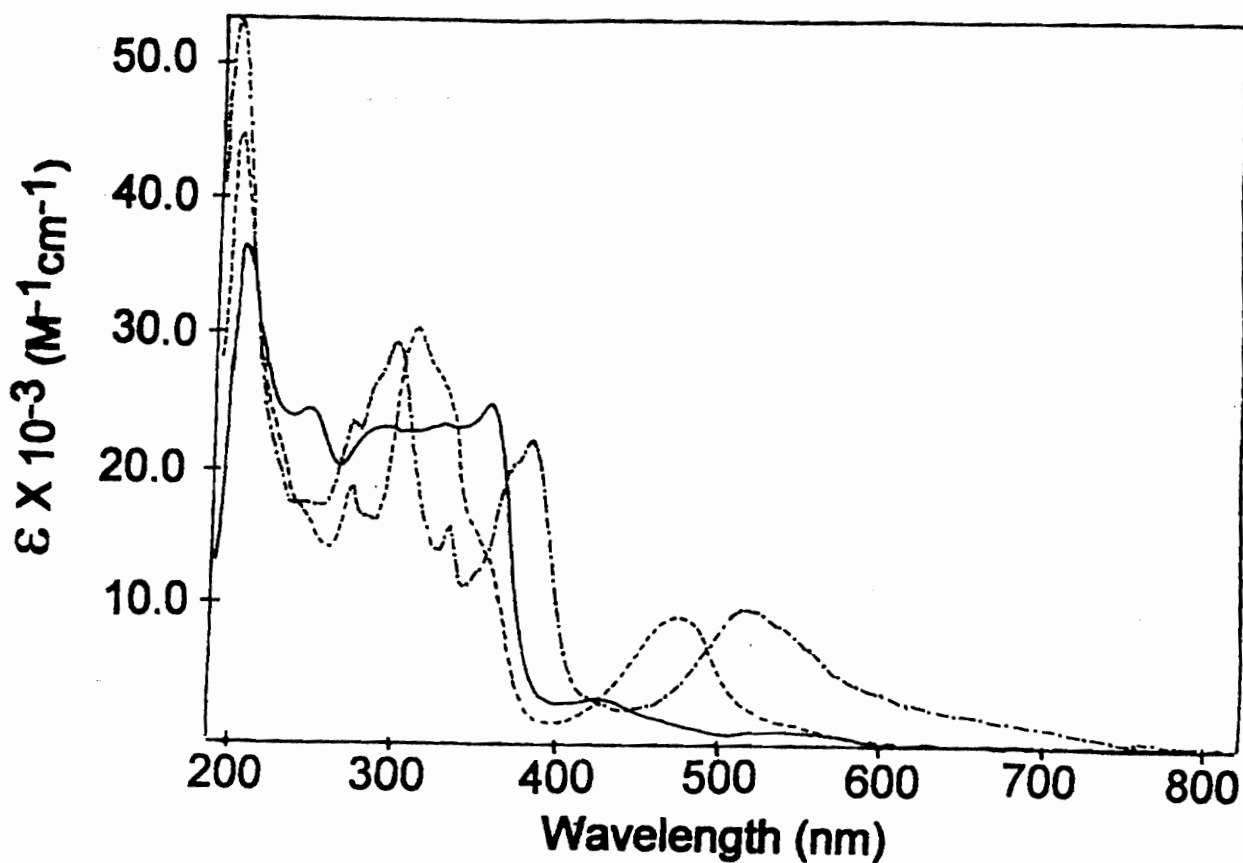
[c] No emission was observable on our system.

Figure 26. Electronic Absorption Spectra (acetonitrile solutions) for Iridium(III) and Ruthenium(II) Complexes Incorporating the Tridentate Polypyridyl Ligand tpp: (——) Ir(tpp)Cl$_3$,(----) [Ru(tpy)(tpp)]$^{2+}$ and (-.-.-.) [(tpy)Ru(tpp)IrCl$_3$]$^{2+}$(where tpy = 2,2':6',2''-terpyridine and tpp = 2,3,5,6-tetrakis(2-pyridyl)pyrazine).
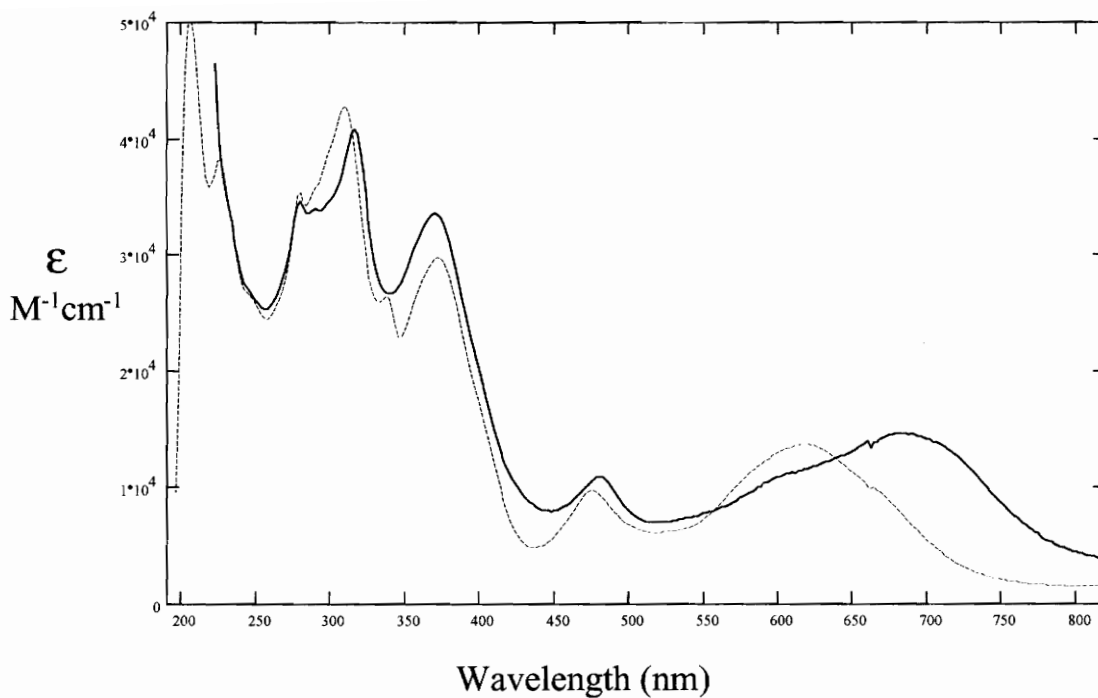
Figure 27. Electronic Absorption Spectra (acetonitrile solutions) of
Bimetallic Complexes Incorporating the Tridentate Polypyridyl Bridging
Ligand tpp (where tpp = 2,3,5,6-tetrakis(2-pyridyl)pyrazine):
(——) [(tpy)Os(tpp)RuCl$_3$]$^+$ and (-----) [(tpy)Ru(tpp)RuCl$_3$.

centered on the ruthenium coordinated to tpy and tpp. This transition is relatively unchanged upon bimetallic formation because the metal added is an electron rich $Ru^{II}Cl_3$ fragment. The $Ru(d\pi) \to tpp(\pi^*)$ MLCT transition centered on the Ru coordinated to tpy and tpp is at ca. 525 nm. This peak is shifted to lower energy compared to the monometallic $[Ru(tpy)(tpp)]^{2+}$. This red shift is expected since tpp now serves as a bridging ligand resulting in the stabilization of the π^* orbitals. The broad transition at 612 nm is assigned as a $Ru(d\pi) \to tpp(\pi^*)$ MLCT transition centered on the ruthenium metal coordinated to tpp and three chlorides. This yields a lowest lying excited state that is $Ru \to tpp$ MLCT in nature consistent with the electrochemical properties. The intense peaks in the ultraviolet are assigned as ligand-based $n \to \pi^*$ and $\pi \to \pi^*$ transitions for both tpp and tpy.

Figure 27 contains the electronic absorption spectrum of $[(tpy)Os(tpp)RuCl_3]^+$. This complex is similar to $[(tpy)Ru(tpp)RuCl_3]^+$ in the ultraviolet with some differences in the visible. The coordination of $RuCl_3$ to the vacant sites on tpp to form $[(tpy)Os(tpp)RuCl_3]^+$ results in three bands in the visible at 474, 606, and 678 nm. The band at 474 nm is assigned as a $Os(d\pi) \to tpy(\pi^*)$ MLCT transition. Due to tpp now serving as a bridging ligand, the π^* orbitals on tpp are stabilized, resulting in the MLCT transitions involving tpp shifting to the red, consistent with the electrochemistry. The band at 606 nm is assigned as the $Os(d\pi) \to tpp(\pi^*)$ MLCT transition. The band at 678 nm represents the $Ru(d\pi) \to tpp(\pi^*)$ CT transition as well as some contribution from the $Os \to tpp$ ^{3}MLCT. One might expect the spectrum of this Os/Ru system to look more like its Ru/Ru analog with minor increases in the intensity at high wavelengths due to the ^{3}MLCT states. The shift in the $Ru \to tpp$ CT transition is quite unusual. The electrochemically measured HOMO-LUMO gap for the two complexes, $[(tpy)Ru(tpp)RuCl_3]^+$ and $[(tpy)Os(tpp)RuCl_3]^+$, is 1.33 and 1.25 V respectively (Table V, page 81). This would predict a red shifted lowest lying MLCT for $[(tpy)Os(tpp)RuCl_3]^+$ versus the all ruthenium analog. The degree of red shift of this transition is somewhat surprising. The Os(II)/Os(III) oxidation occurs at a lower

potential than the analogous Ru(II)/Ru(III) oxidation (1.32 versus 1.61 V respectively). Thus, the presence of the Os based orbitals in close proximity to the Ru based orbitals (the ruthenium coordinated to tpp and three chlorides) may result in an interaction between the two which could lead to the shift of the Ru → tpp CT transition. This mixing could also result in increased intensity to the ^{3}MLCT band associated with this ruthenium metal center As expected, the intense peaks in the UV are n → π and π → π* transitions for both tpy and tpp.

The symmetric bimetallic, [(tpy)Ru(tpp)Ru(tpy)]$^{4+}$ has been prepared as an analog to [(tpy)Ru(tpp)(Ru(tpp)]$^{4+}$. Figure 28 contains the electronic absorption for this complex as well as those of [(tpy)Ru(tpp)Ru(tpp)]$^{4+}$ and [(tpy)Os(tpp)Ru(tpp)]$^{4+}$. This bimetallic complex has been prepared previously and the electronic absorption spectroscopy studied.[50,59] The electronic absorption spectrum is shown in Figure 26 and summarized in Table VIII, page 105, for all three bimetallic complexes. The spectra of the three bimetallic complexes are remarkably similar. In the symmetric bimetallic complex, [(tpy)Ru(tpp)Ru(tpy)]$^{4+}$, the peak at 550 nm is assigned as overlapping Ru(dπ) → tpp(π*) MLCT transitions for each metal. This peak is shifted significantly to lower energy compared to the monometallic [Ru(tpy)(tpp)]$^{2+}$. This is as anticipated since tpp is now serving as a bridging ligand resulting in the stabilization of the π* orbitals on tpp reducing the HOMO-LUMO gap. The two Ru → tpy MLCT transitions are located at 372 nm. The shift to higher energy of these transitions from 474 nm in the monometallic complex is as predicted by the electrochemistry. In addition, the ultraviolet region contains ligand centered n → π* and π → π* transitions localized on both tpp and tpy as well as higher energy MLCT transitions.

As shown in Figure 28, substitution of the chlorides on [(tpy)Ru(tpp)RuCl$_3$]$^+$ with tpp to form [(tpy)Ru(tpp)Ru(tpp)]$^{4+}$ results in a major band at 548 nm. This band is assigned as two overlapping Ru(dπ) → tpp(π*) MLCT transitions involving the bridging tpp. The Ru → tpp CT based on the (tpy)Ru^{II}(tpp) moiety should occur at slightly lower energy than the similar transition for the (tpp)Ru^{II}(tpp) moiety. The band at 360 nm is
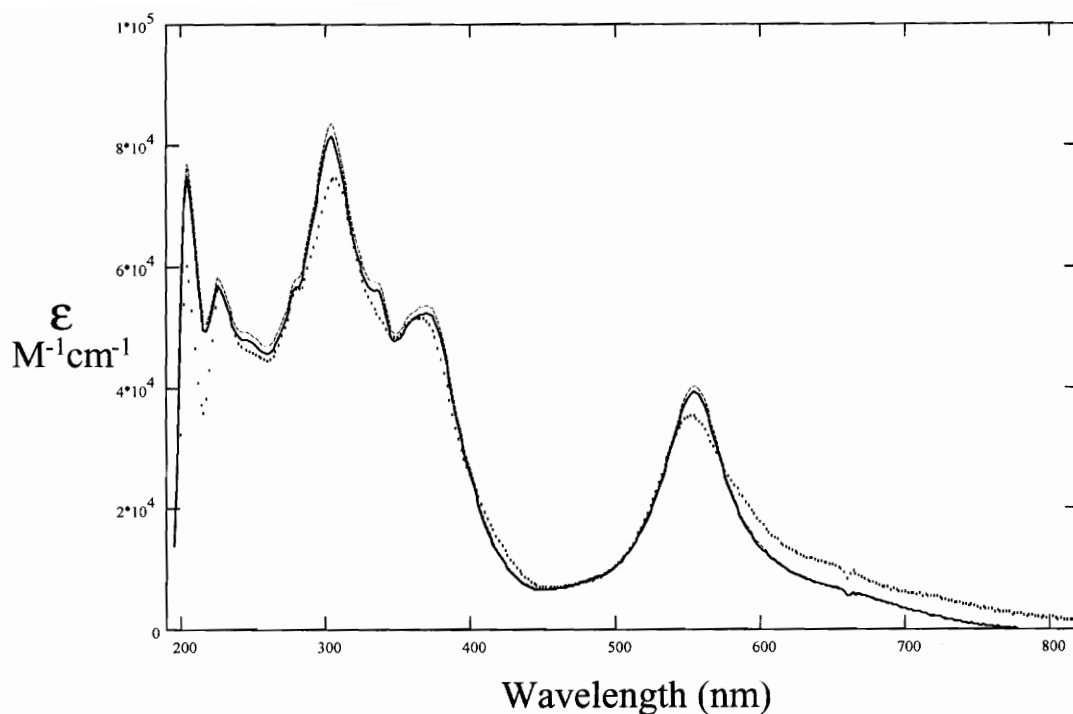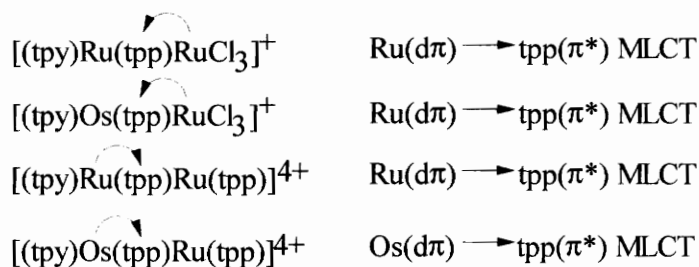
Figure 28. Electronic Absorption Spectra (acetonitrile solutions) of
Bimetallic Complexes Incorporating the Tridentate Polypyridyl Bridging
Ligand tpp (where tpp = 2,3,5,6-tetrakis(2-pyridyl)pyrazine):
(——) [(tpy)Ru(tpp)Ru(tpp)]$^{4+}$, (······) [(tpy)Os(tpp)Ru(tpp)]$^{4+}$, and
(-----)[(tpy)Ru(tpp)Ru(tpy)]$^{4+}$.

assigned as a Ru($d\pi$) $\rightarrow$ tpy(π^*) transition overlapping with a Ru($d\pi$) $\rightarrow$ tpp(π^*)

transition involving the terminal tpp ligand. These CT transitions should occur at higher

energy than the MLCT transitions to the bridging tpp ligand as indicated by the

electrochemistry. The ultraviolet consists of n $\rightarrow$ π^* and π $\rightarrow$ π^* transitions that are tpp

and tpy based.

Substitution of the chlorides on [(tpy)Os(tpp)RuCl$_3$]$^+$ with tpp to form

[(tpy)Os(tpp)Ru(tpp)]$^{4+}$ results in a major band at 546 nm with a tail at lower energy and

a peak at approximately 360 nm. The band at 546 nm is assigned as overlapping

Ru($d\pi$) $\rightarrow$ tpp(π^*) and Os($d\pi$) $\rightarrow$ tpp(π^*) MLCT transitions based on the bridging tpp

with the Os($d\pi$) $\rightarrow$ tpp(π^*) MLCT being the lower energy component. The tailing at

lower energy can be assigned as Os($d\pi$) $\rightarrow$ tpp(π^*) ^{3}MLCT transition due to the high

degree of spin orbit coupling in osmium. The peak at 360 nm can be assigned as the

Os($d\pi$) $\rightarrow$ tpy(π^*) MLCT transition overlapping with the Ru($d\pi$) $\rightarrow$ tpp(π^*) MLCT

transition involving the terminal tpp ligand. Interestingly, the spectra for

[(tpy)Ru(tpp)Ru(tpp)]$^{4+}$, [(tpy)Os(tpp)Ru(tpp)]$^{4+}$, and [(tpy)Ru(tpp)Ru(tpy)]$^{4+}$ are almost

identical due to the similar components in each of these systems. This would be

expected since the transitions in each bimetallic are based upon the same orbitals. The

spectra of [(tpy)Ru(tpp)Ru(tpp)]$^{4+}$ and [(tpy)Os(tpp)Ru(tpp)]$^{4+}$ are virtually identical

except for the ^{3}MLCT transitions that occur at lower energy than the ^{1}MLCT in the

Os/Ru bimetallic complex. This would be expected since the spectra of the

monometallic fragments that compose these complexes, i.e., [Ru(tpy)(tpp)]$^{2+}$ and

[Os(tpy)(tpp)]$^{2+}$ were quite similar. This similarity in the electronic absorption

spectroscopy of osmium and ruthenium based systems of the tridentate ligands is

somewhat surprising due to the much smaller electrochemical energy gap between the

HOMO and LUMO for the osmium based systems. The principle differences are in the

intensity of the bands in the ultraviolet on account of this being the region where the

π $\rightarrow$ π^* transitions for the ligands occur. Differences will also appear in the intensity of

the Ru $\rightarrow$ tpy and Ru $\rightarrow$ tpp MLCT transition due to the varying number of these

transitions in the group of complexes and in the triplet region for the Os/Ru bimetallic complex.

The photochemistry of these types of polypyridyl complexes is dominated by the nature of the lowest lying excited state. Thus, the ability to synthetically manipulate the nature of this state is very important in molecular design. In the two series of complexes [(tpy)M(tpp)RuCl$_3$]$^+$ and [(tpy)M(tpp)Ru(tpp)]$^{4+}$, where M = Ru(II) or Os(II), the nature of the lowest lying excited state varies as a function of metal center and coordination environment. The nature of this state is illustrated below.

[(tpy)Ru(tpp)RuCl$_3$]$^+$ Ru(dπ) $\longrightarrow$ tpp(π*) MLCT

[(tpy)Os(tpp)RuCl$_3$]$^+$ Ru(dπ) $\longrightarrow$ tpp(π*) MLCT

[(tpy)Ru(tpp)Ru(tpp)]$^{4+}$ Ru(dπ) $\longrightarrow$ tpp(π*) MLCT

[(tpy)Os(tpp)Ru(tpp)]$^{4+}$ Os(dπ) $\longrightarrow$ tpp(π*) MLCT

In the systems with a terminal Ru^{II}Cl$_3$ moiety, the lowest excited state is Ru $\rightarrow$ tpp CT based on this metal. When the three chloride ligands are replaced by a terminal tpp ligand, the lowest lying excited state now involves the other metal and can be either Os $\rightarrow$ tpp or Ru $\rightarrow$ tpp CT in nature. This is useful since the HOMO is on the tpy side of the molecule so, in theory, one can attach an acceptor, like Rh^{III}, to the other tpp sites and get charge separation over a long distance in a stereochemically defined multimetallic system.

Correlation of the Spectroscopy and Electrochemistry

A correlation can be drawn between the spectroscopic and electrochemical energy gap within similar complexes if the same orbitals are involved in both of these processes.[8,14,25,30-40] It has been reported that a linear relationship between E_{abs}, the energy of the lowest lying MLCT transition in eV, and $\Delta E_{1/2}$ the difference between the oxidation and reduction potentials, exists that can be approximated by[84]

$$E_{abs} = a\Delta E_{1/2}(redox) + constant$$

where the constant collects all the solvation and reorganization terms together and the slope, a, is unity. Deviation of the slope from unity is attributed to configuration interaction. The scatter in the plot is a result of variation in the solvation and reorganization energies as well as configuration interaction. A slope of unity would indicate that the free energy for electron transfer from the reduced to oxidized species as well as the reorganization energies are negligible. For a slope to be unity would require that the reduction potential be invariant with the oxidation state of the metal. This requires that the energy of the $d\pi$ orbitals must stay fairly constant in order for E_{abs} to track the reduction potential of the ligand. Deviations from unity could be indicative of the energy of the π^* orbitals of the other ligands coordinated to the metal being close to that of the π^* orbitals of the bridging ligand (LUMO).

A plot of the energy of the lowest lying spectroscopic transition (E_{abs} in eV) versus the difference in redox potentials between the first oxidation and first reduction, $\Delta E_{1/2} = E_{1/2}(Ru^{II}/Ru^{III}) - E_{1/2}(BL/BL^-)$, for the different sets of complexes gave a linear correlation. Table IX lists the $\Delta E_{1/2}$(redox) potentials as well as the calculated E_{abs} values that were used to make the plots shown in Figures 29 and 30. In the two series $[Ru(tpy)(BL)Cl]^+$ and $[Ru(tpy)(BL)(py)]^{2+}$ where BL = dpp, dpq, or dpb, the plot yielded $E_{abs} = 0.61\Delta E_{1/2} + 1.1$ with a correlation coefficient of 0.97 as shown in Figure 29a. If one were to plot only the $[Ru(tpy)(BL)Cl]^+$ complexes the slope is 0.67, intercept is 0.99 and the correlation coefficient is 1.0 (Figure 29b). The $[Ru(tpy)(BL)(py)]^{2+}$ complexes

Table IX. Calculated values of $\Delta E_{1/2}$ and E_{abs} for all monometallic and bimetallic complexes used in Figures 27 and 28 (where bpy = 2,2'-bipyridine, tpy = 2,2':6',2''-terpyridine, tpp = 2,3,5,6-tetrakis(2-pyridyl)pyrazine, Metpp = 2-[2-(1-Methylpyridiniumyl)]-3,5,6-tris(2-pyridyl)pyrazine, and py = pyridine).

| Compound	$\Delta E_{1/2}$ (V)	E_{abs} (eV)
$[Ru(tpy)(dpp)Cl]^+$	2.11	2.41
$[Ru(tpy)(dpq)Cl]^+$	1.83	2.20
$[Ru(tpy)(dpb)Cl]^+$	1.63	2.09
$[Ru(tpy)(dpp)(py)]^{2+}$	2.46	2.59
$[Ru(tpy)(dpq)(py)]^{2+}$	2.16	2.39
$[Ru(tpy)(dpb)(py)]^{2+}$	2.03	2.24
$[Ru(tpp)_2]^{2+}$	2.39	2.58
$[Ru(tpy)(tpp)]^{2+}$	2.37	2.62
$[Ru(tpy)(Metpp)]^{3+}$	2.35	2.62
$[Ru(bpy)(tpp)Cl]^+$	2.03	2.46
$[Ru(bpy)(tpp)(CH_3CN)]^{2+}$	2.33	2.72
$[Ru(bpy)(Metpp)(CH_3CN)]^{3+}$	2.26	2.71
$[(tpy)Ru(tpp)IrCl_3]^{2+}$	1.85	1.88
$[(tpy)Ru(tpp)RuCl_3]^+$	1.33	2.02
$[(tpy)Os(tpp)RuCl_3]^+$	1.25	1.83
$[(tpy)Ru(tpp)Ru(tpp)]^{2+}$	1.81	2.26
$[(tpy)Ru(tpp)Ru(tpy)]^{2+}$	1.79	2.25

114
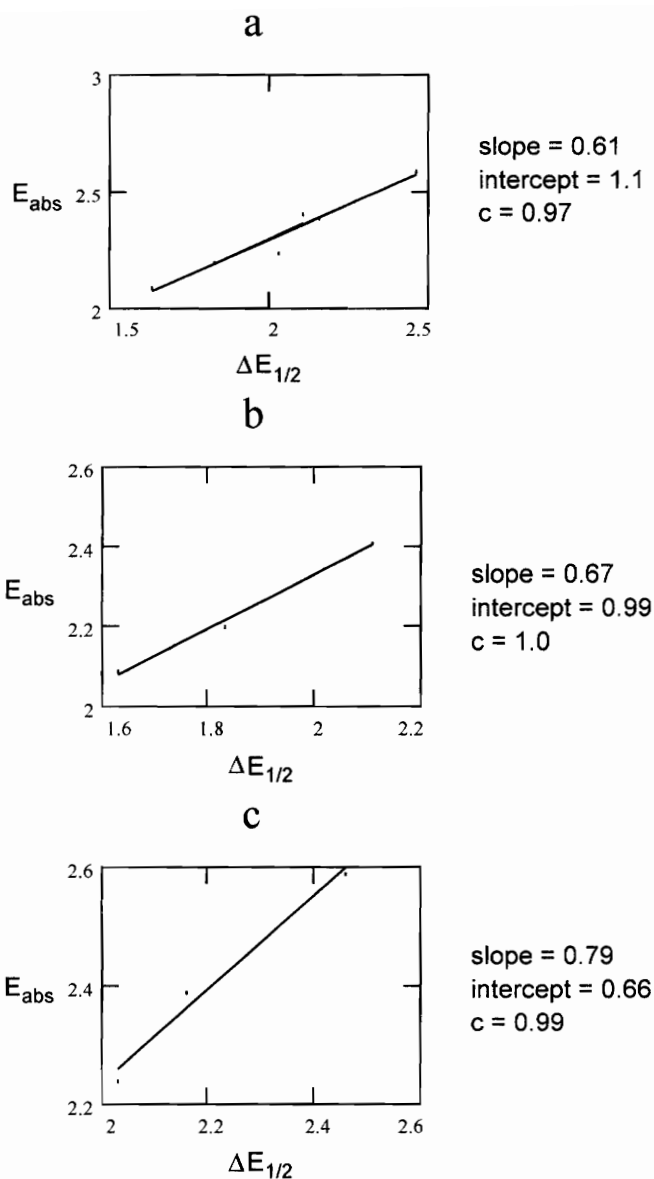
Figure 29. Plot of energies of the lowest energy absorption band (eV) versus $\Delta E_{1/2}$ (V) (a) Ruthenium monometallic complexes $[Ru(tpy)(BL)Cl]^+$ and $[Ru(tpy)(BL)(py)]^{2+}$ where BL = dpp, dpq, or dpb, (b) Ruthenium monometallic complexes $[Ru(tpy)(BL)Cl]^+$, and (c) Ruthenium monometallic complexes $[Ru(tpy)(BL)(py)]^{2+}$.

yielded a slope of 0.79, an intercept of 0.66 and a correlation coefficient of 0.99 (Figure 29c). Thus, the investigation of each series of complexes individually results in a line that is closer to unity with less scatter about the line. That the slope is not unity is a consequence of configuration interaction.

The ruthenium monometallic complexes $[Ru(tpp)_2]^{2+}$, $[Ru(tpy)(tpp)]^{2+}$, $[Ru(tpy)(Metpp)]^{3+}$, $[Ru(bpy)(tpp)Cl]^+$, $[Ru(bpy)(tpp)(CH_3CN)]^{2+}$, $[Ru(bpy)(Metpp)(CH_3CN)]^{3+}$ as well as the bimetallic complexes $[(tpy)Ru(tpp)IrCl_3]^{2+}$, $[(tpy)Ru(tpp)RuCl_3]^+$, $[(tpy)Os(tpp)RuCl_3]^+$, $[(tpy)Ru(tpp)Ru(tpp)]^{4+}$, and $[(tpy)Ru(tpp)Ru(tpy)]^{4+}$ were grouped together, where $\Delta E_{1/2}$ for the methylated complexes was the difference between the Ru oxidation and the Metpp/Metpp⁻ reduction that would be localized on the pyrazine ring. A plot of E_{abs} versus $\Delta E_{1/2}$ for all monometallic and bimetallic complexes incorporating tpp and Metpp has a slope of 0.73, an intercept of 0.92, and a correlation coefficient of 0.90 as shown in Figure 30a. In the graph it appears as though a point is far off the line that corresponds to the bimetallic complex $[(tpy)Ru(tpp)IrCl_3]^{2+}$. The $[(tpy)Ru(tpp)IrCl_3]^{2+}$ system has a MLCT transition that is difficult to locate since all the Ir transitions overlap. This same plot without this complex has a slope of 0.69, an intercept of 1.03, and a much better correlation coefficient of 0.97 as shown in Figure 30b. Once again, the slopes do not approach unity and the intercept is about the same.

The results shown in Figures 29 and 30 indicate that same $d\pi$-π^* orbitals are involved in both the electrochemical and spectroscopic processes. This supports the assignment of the lowest energy absorption being MLCT in nature involving the bridging ligand based acceptor orbitals. In all the plots, the slopes do not approach unity, rather they are all approximately 0.70. This may be a result of the lowest energy MLCT band not being purely a transition from the HOMO to the LUMO but actually is assigned as overlapping transitions for all complexes. The deviation from unity may result from significant configuration in these systems. The intercept in all the plots is approximately 1 that can be interpreted as the solvation and reorganization energies in all systems being equivalent. The graph of E_{abs} versus $\Delta E_{1/2}$ shown in Figure 30c, for all
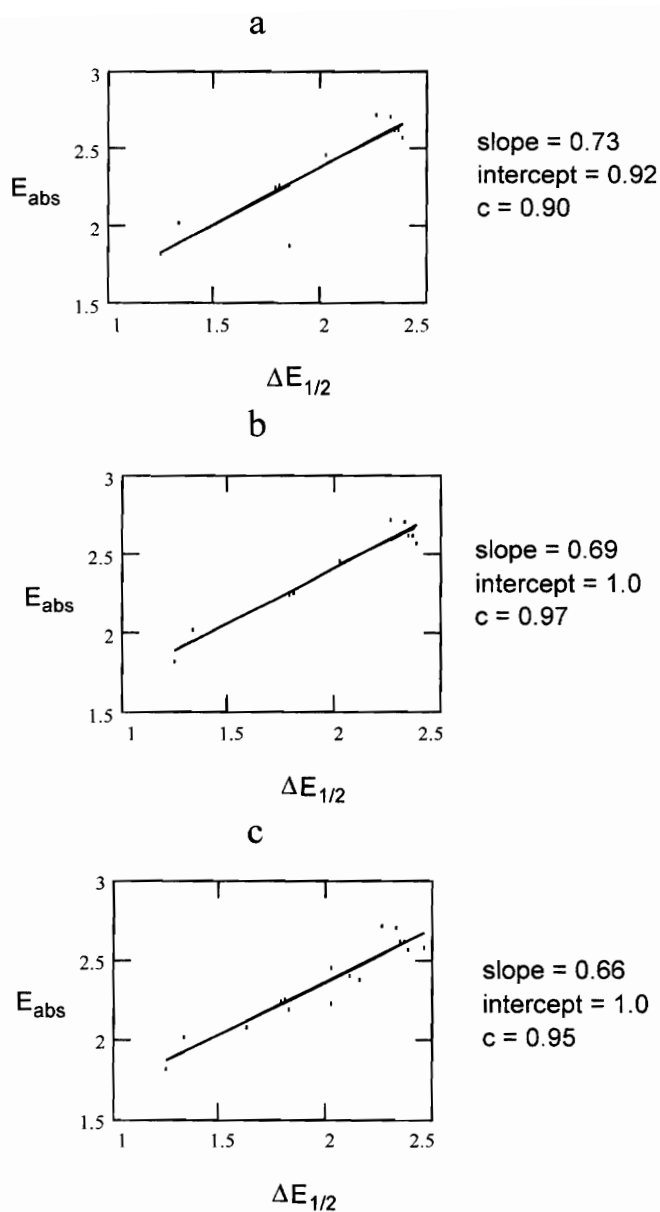
a

slope = 0.73
intercept = 0.92
c = 0.90

b

slope = 0.69
intercept = 1.0
c = 0.97

c

slope = 0.66
intercept = 1.0
c = 0.95

Figure 30. Plot of energies of the lowest energy absorption band (eV) versus $\Delta E_{1/2}$ (V) for (a) $[Ru(tpp)_2]^{2+}$, $[Ru(tpy)(tpp)]^{2+}$, $[Ru(tpy)(Metpp)]^{3+}$, $[Ru(bpy)(tpp)Cl]^{+}$, $[Ru(bpy)(tpp)(CH_3CN)]^{2+}$, $[Ru(bpy)(Metpp)(CH_3CN)]^{3+}$, $[(tpy)Ru(tpp)IrCl_3]^{2+}$, $[(tpy)Ru(tpp)RuCl_3]^{+}$, $[(tpy)Os(tpp)RuCl_3]^{+}$, $[(tpy)Ru(tpp)Ru(tpp)]^{4+}$, and $[(tpy)Ru(tpp)Ru(tpy)]^{4+}$ (b) all the above complexes except $[(tpy)Ru(tpp)IrCl_3]^{2+}$, and (c) all complexes except $[(tpy)Ru(tpp)IrCl_3]^{2+}$.

117

monometallic and bimetallic complexes except $[(tpy)Ru(tpp)IrCl_3]^{2+}$, supports these conclusions and has a slope is 0.66, the intercept is 1.0 with a correlation coefficient of 0.94. Once again, the Ru/Ir bimetallic system does not fit into the plot due to this system having a transition that is difficult to locate since all the Ir transitions overlap.

Spectroelectrochemistry

Spectroelectrochemistry is used to correlate the electronic transitions to the electrochemical redox processes. In the spectroelectrochemical experiments performed in this study, the complex is either oxidized or reduced at a potential that corresponds to a one or two electron process. Monitoring this by electronic absorption spectroscopy aids in the interpretation of the spectroscopy and electrochemistry of these complexes.

Electrogeneration of many different oxidation states of these complexes was possible. Electronic spectroscopy of these complexes in various stable oxidation states has been performed, and the results of these spectroelectrochemical studies are shown in Figures 31-38 for $[Ru(tpy)(tpp)]^{2+}$, $[Ru(tpy)(Metpp)]^{3+}$, $[(tpy)Ru(tpp)IrCl_3]^{2+}$, $[(tpy)Ru(tpp)RuCl_3]^{+}$, $[(tpy)Os(tpp)RuCl_3]^{+}$, $[(tpy)Ru(tpp)Ru(tpy)]^{4+}$, $[(tpy)Ru(tpp)Ru(tpp)]^{4+}$, and $[(tpy)Os(tpp)Ru(tpy)]^{4+}$, respectively. The spectra shown are obtained from the same solution and relative intensities for the transitions are as illustrated.

Generally, reduction of the bridging ligand will cause transitions involving this redox orbital to shift to a different energy. For example, Berger has studied $[Ru(bpy)_2(dpp)]^{2+}$ using spectroelectrochemistry.[82] In $[Ru(bpy)_2(dpp)]^{2+}$ the first reduction occurs at the dpp ligand whereas the second and third occur at the bpy ligands. In the visible region, a broad band appears at approximately 470 nm upon reduction of dpp. This transition has been assigned as being due to the Ru $\rightarrow$ bpy transitions shifting to lower energy as well as $\pi \rightarrow \pi^*$ dpp transitions. Reduction of dpp causes an electron to go into the π^* orbital that decreases the backbonding between the metal and dpp. Consequently, the $d\pi$ metal orbitals will increase in energy, decreasing the energy

difference between the metal and bpy orbitals. This decrease accounts for the shifting of the Ru $\rightarrow$ bpy MLCT transition to lower energy.

When tpp is reduced to - 1.70 V, new $\pi^* \rightarrow \pi^*$ transitions appear in the visible. The spectroelectrochemical results are shown in Figure A-VIII in the Appendix (page 177). In the spectroelectrochemical results for the complexes incorporating tpp, this will be expected to obscure the changes for MLCT transitions in this region. Electrogeneration of the one electron reduced species is reversible with > 90 % regeneration of the original oxidation state.

Figure 31a shows the results for the oxidative spectroelectrochemistry of $[Ru(tpy)(tpp)]^{2+}$. As one would predict, the Ru $\rightarrow$ tpy and Ru $\rightarrow$ tpp transitions at 474 nm are lost upon the one electron oxidation of the ruthenium metal, consistent with these being metal centered transitions. Electrogeneration of the oxidized complexes is possible with >95 % regeneration of the original oxidation state. In Figure 31b, the reductive spectroelectrochemistry of $[Ru(tpy)(tpp)]^{2+}$ is shown. The regeneration of the original oxidation state from the one electron reduced species was reversible to approximately 80 %. As expected, there is a decrease in intensity at 330 nm in this monometallic complex as well as the appearance of transitions similar to those when the free tpp ligand is reduced by one electron. This confirms our assignment of this peak as a tpp based $\pi \rightarrow \pi^*$ transition. At lower energy (660-730 nm) there is a band that appears in the spectra of the one electron reduced Ru monometallic. This most likely represents a LMCT transition (tpp $\rightarrow$ Ru).

Figure 32a shows the results for the oxidative spectroelectrochemistry of $[Ru(tpy)(Metpp)]^{3+}$. As expected, the oxidation of ruthenium results in a similar spectrum as that of the nonmethylated complex, $[Ru(tpy)(tpp)]^{2+}$. The band at 474 nm that has been assigned as overlapping Ru $\rightarrow$ tpy and Ru $\rightarrow$ tpp MLCT transitions losses intensity upon metal oxidation. Electrogeneration of the oxidized complexes is possible with >95 % regeneration of the original oxidation state. In Figure 32b are shown the
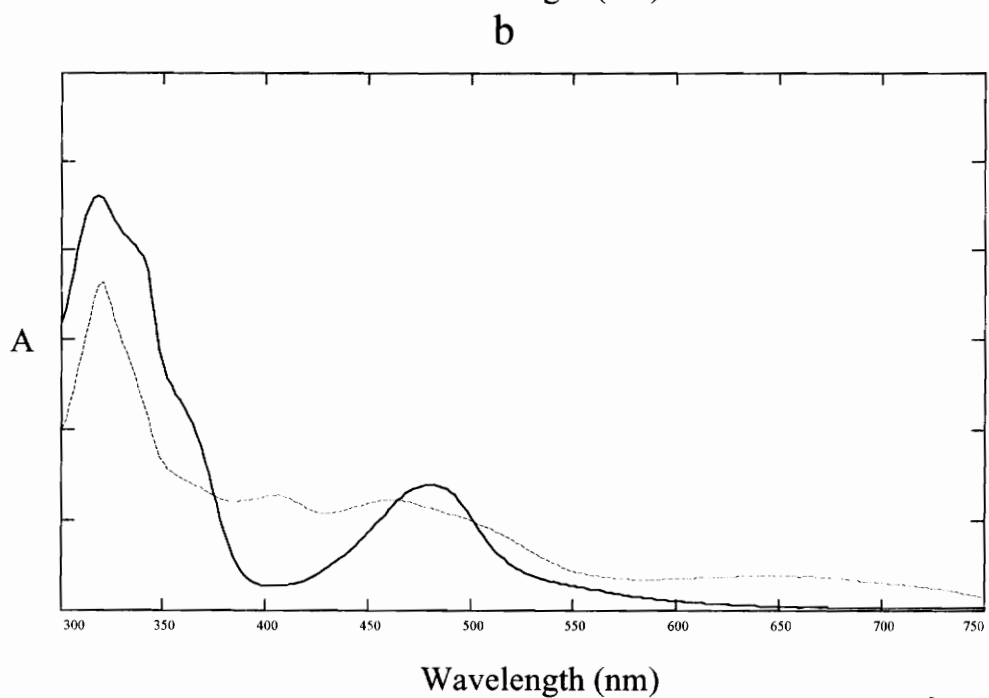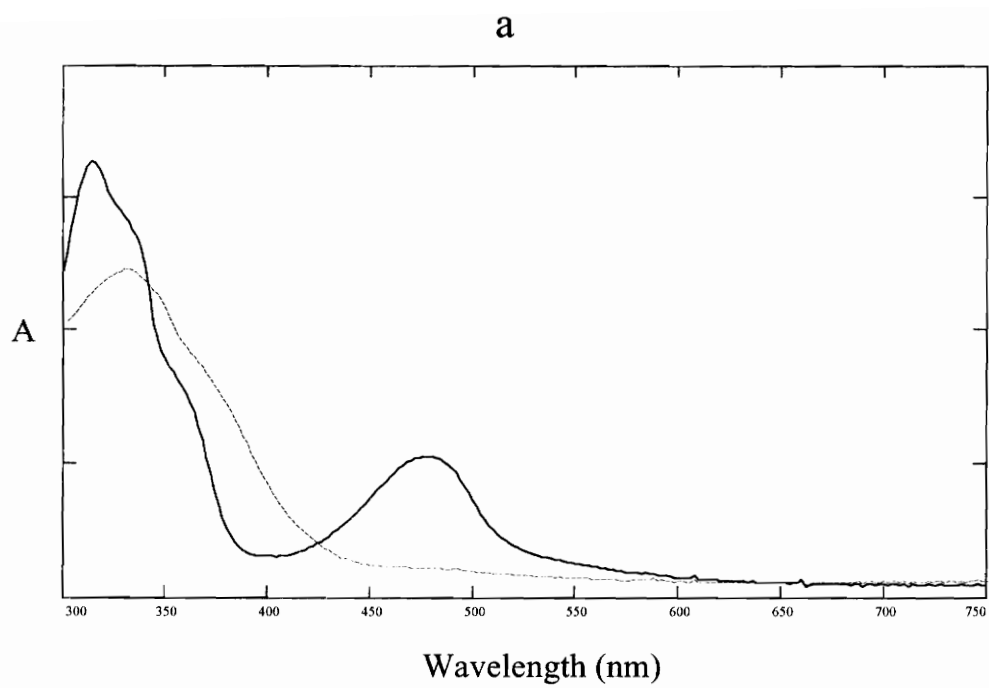
a

Wavelength (nm)

b

Wavelength (nm)

Figure 31. Spectroelectrochemical results for $[Ru(tpy)(tpp)]^{2+}$ (where tpy = 2,2':6',2''-terpyridine and tpp = 2,3,5,6-tetrakis(2-pyridyl)pyrazine].
(a) (——) Original oxidation state and (----) 1 electron oxidation.
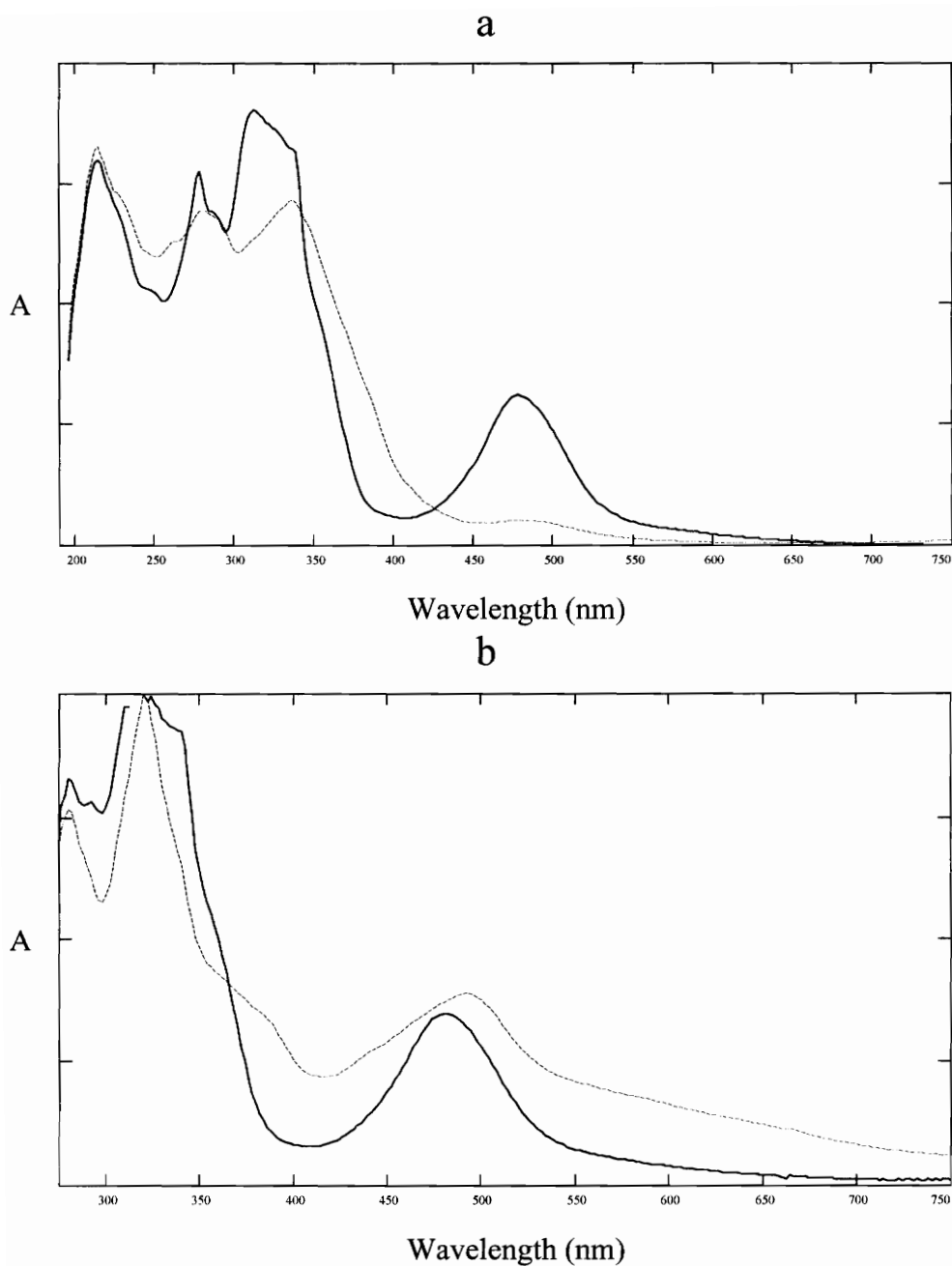(b) (——) Original oxidation state and (----) 1 electron reduction.

Figure 32. Spectroelectrochemical results for [Ru(tpy)(Metpp)]³⁺ (where tpy = 2,2':6',2''-terpyridine and Metpp = {2-[2-(1-Methylpyridiniumyl)]-3,5,6-tris(2-pyridyl)pyrazine}]. (a) (——) Original oxidation state and (----) 1 electron oxidation. (b) (——) Original oxidation state and (----) 1 electron reduction.

absorption spectra for $[Ru(tpy)(Metpp)]^{3+}$ and its one-electron reduced form. Electrogeneration of the one electron reduced species is reversible with > 95 % regeneration of the original oxidation state. It has been noted by Meyer and coworkers that the one-electron reduction of MQ^+ (where MQ^+ = N-methyl-4,4'-bipyridinium cation) results in a visible absorption spectrum containing a band at 535 nm.[72g] This corresponds to reduction of the viologen portion of this ligand. In metal complexes incorporating this ligand, increases in the same region occur at 358, 480, and 595 nm. Thus, similar behavior would be expected upon one electron reduction of $[Ru(tpy)(Metpp)]^{3+}$ since this is assigned as reduction of the viologen portion of the Metpp ligand. One electron reduction of this complex resulted in increases in a major band appearing at 485 nm as well as increased intensity at 375 nm and at wavelengths greater than 575 nm. This result is inconsistent with the reduction of the pyrazine portion of tpp as in the complex $[Ru(tpy)(tpp)]^{2+}$ as shown in Figure 31b. The spectrum of the one electron reduced species of $[Ru(tpy)(Metpp)]^{3+}$ is similar to what was found by Meyer and coworkers on complexes incorporating MQ^+ upon one electron reduction. This further confirms the assignment of the first reduction in this complex as being viologen based.

Figure 33a shows the results for the oxidative spectroelectrochemistry of $[(tpy)Ru(tpp)IrCl_3]^{2+}$. Electrogeneration of the oxidized complexes is possible with >95 % regeneration of the original oxidation state. In this system, the one electron oxidation results in a loss of the ruthenium based MLCT transitions (425 and 500 - 580 nm) with retention of the iridium based processes (500 and 600 - 700 nm). This observation is consistent with a ruthenium based oxidation and inconsistent with an iridium based process. It is interesting to note that the visible portion of the spectrum for the one electron oxidized form of the bimetallic is quite similar to the iridium monometallic $Ir(tpp)Cl_3$ (see Figure 21, p. 95), with the transitions in the mixed metal system being shifted to lower energy due to the stabilization of the π^* orbitals on the tpp. When both metals are oxidized, all of the transitions in the 500 - 700 nm regions are lost
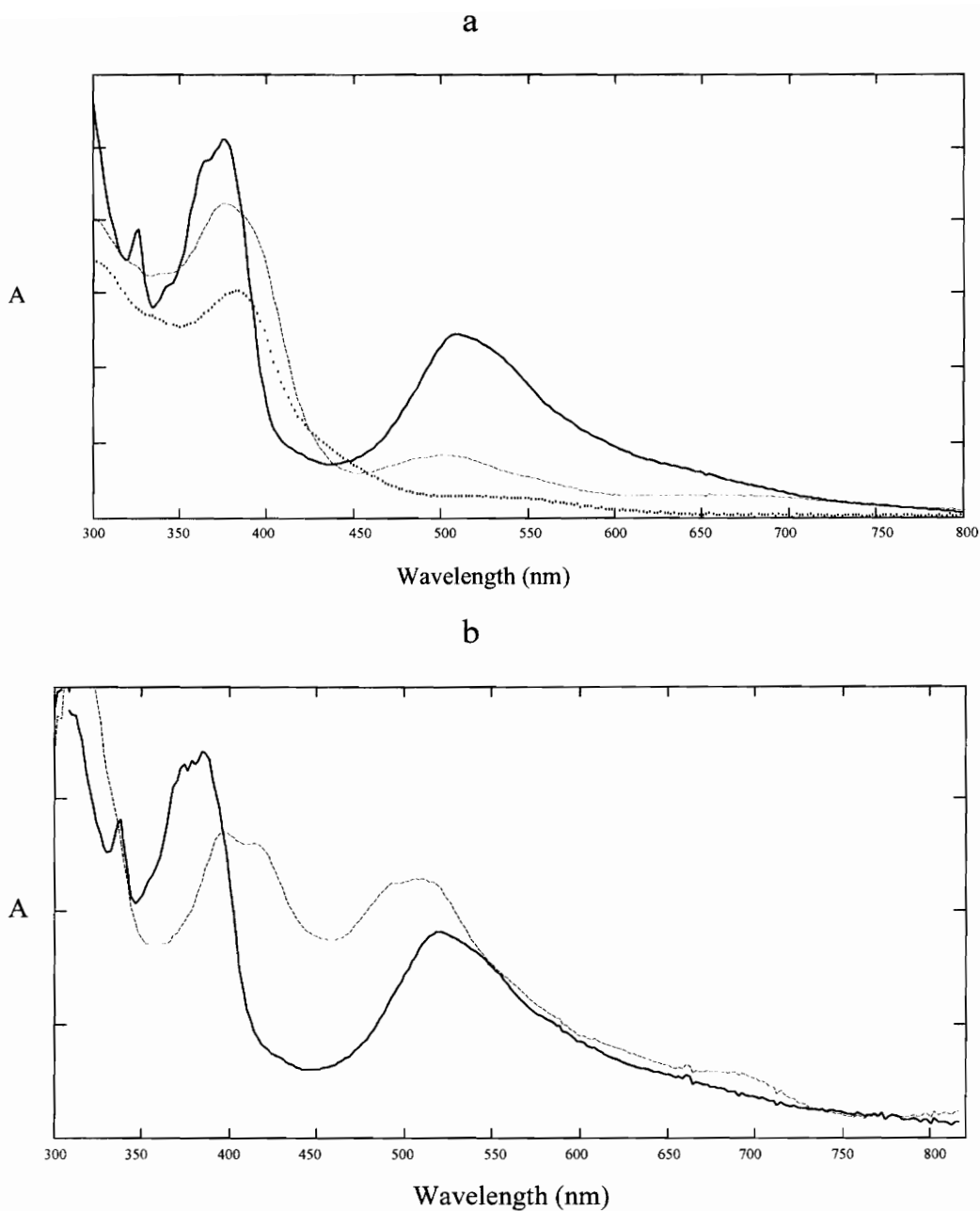
a

Wavelength (nm)

b

Wavelength (nm)

Figure 33. Spectroelectrochemical results for [(tpy)Ru(tpp)IrCl$_3$]$^{2+}$ (where tpy = 2,2':6',2''-terpyridine and tpp = 2,3,5,6-tetrakis(2-pyridyl)pyrazine). (a) (——) Original oxidation state, (----) 1 electron oxidation, (.......) 2 electron oxidation. (b) (——) Original oxidation state and (----) 1 electron reduction.

due to their MLCT nature. The oxidative spectroelectrochemistry of the bimetallic system shows a loss of the transitions at 332 and 368 nm when both metals are oxidized indicating their MLCT nature. In Figure 33b the reductive spectroelectrochemistry of $[(tpy)Ru(tpp)IrCl_3]^{2+}$ is shown. The transition at 390 nm that disappears when the tpp is reduced can be assigned as a $\pi \rightarrow \pi^*$ transition. The two shoulders at 332 and 368 nm also appear to be lost upon one electron reduction of tpp. New transitions involving the redox orbital appear in the spectra of the reduced bimetallic system between 350 and 550 nm. The Ru $\rightarrow$ tpy MLCT transition would be expected to red shift and should also be a component of this band. The new band present in the singly reduced complex between 680 and 720 nm can be assigned as a tpp $\rightarrow$ Ru LMCT transition. The two electron reduction of the bimetallic complex simply results in the decrease in the intensity of the $\pi^* \rightarrow \pi^*$ transitions and therefore is not shown. Electrogeneration of the one electron reduced species is reversible with > 90 % regeneration of the original oxidation state.

Figure 34 shows the spectroelectrochemical results for $[(tpy)Ru(tpp)RuCl_3]^+$. On the basis of the spectroelectrochemical results for the ruthenium monometallic, the transitions in the Ru/Ru mixed metal bimetallic can be assigned. Electrogeneration of the oxidized complexes is possible with >95 % regeneration of the original oxidation state. However, the one electron reduced species is reversible with > 50 % regeneration of the original oxidation state that could be a result of water being present in the solvent. Figure 34a shows the results for the oxidative spectroelectrochemistry of $[(tpy)Ru(tpp)RuCl_3]^+$. In this system, the first oxidation has been assigned as being due to the oxidation of the ruthenium bound to the bridging tpp ligand and three chlorides. Oxidation of this ruthenium should lead to the disappearance of the transitions involving this metal center. The one electron oxidation results in a loss of the low energy component of the broad MLCT band at 612 nm. The peak at 470 nm has been assigned as the Ru $\rightarrow$ tpy MLCT transition with the Ru $\rightarrow$ tpp transition occurring at 525 nm. The Ru $\rightarrow$ tpp transition would be expected to red shift upon oxidation of the other ruthenium
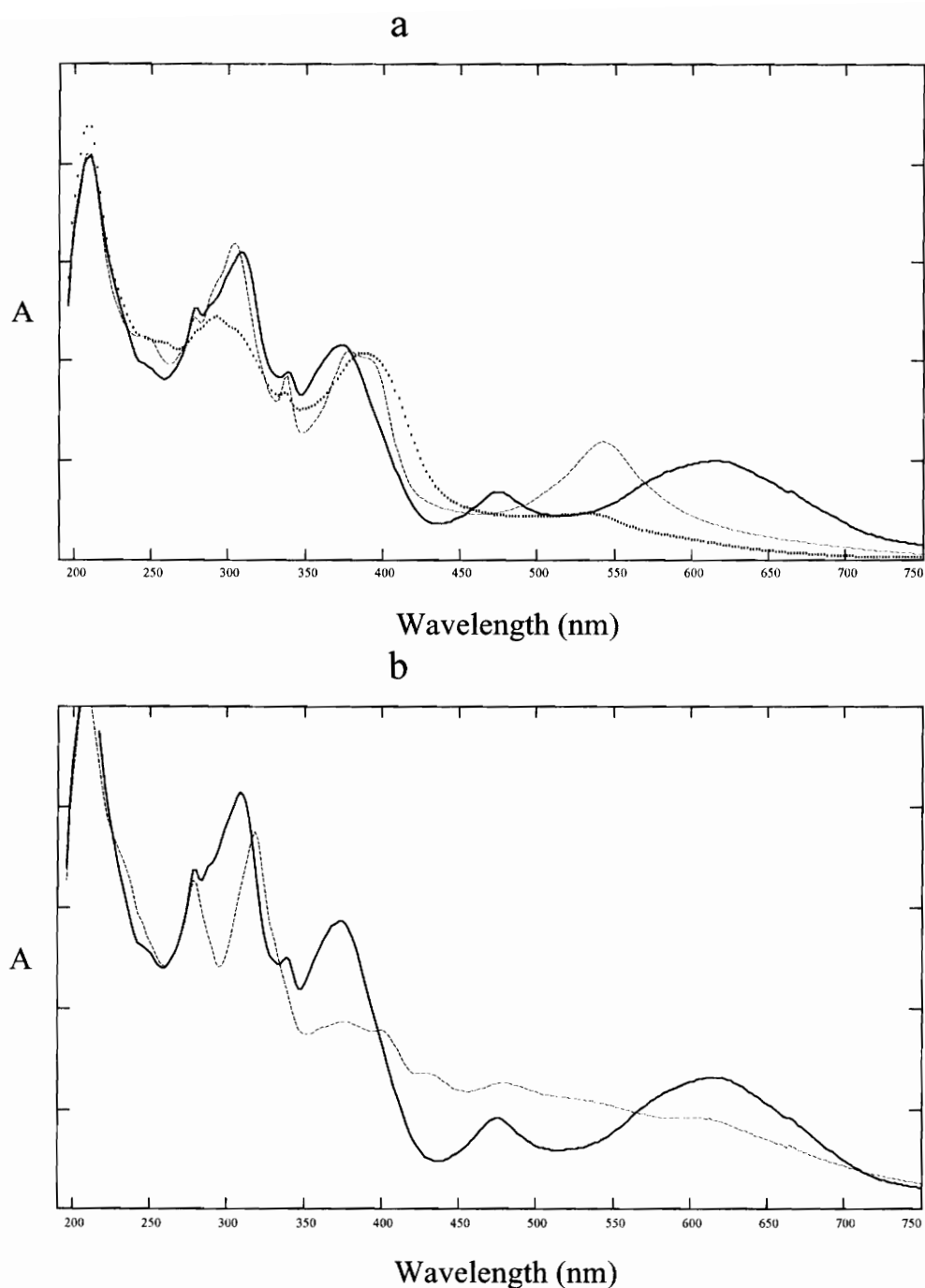
Figure 34. Spectroelectrochemical results for [(tpy)Ru(tpp)RuCl₃]⁺ (where tpy = 2,2':6',2''-terpyridine and tpp = 2,3,5,6-tetrakis(2-pyridyl)pyrazine). (a) (——) Original oxidation state, (----) 1 electron oxidation, (.......) 2 electron oxidation. (b) (——) Original oxidation state and (----) 1 electron reduction.

125

metal to Ru(III). The band at about 545 nm is attributed to the shifting of the Ru $\rightarrow$ tpp MLCT from 525 nm in the original oxidation state. The peaks between 360 - 390 nm would be expected to contain intensity from the Ru $\rightarrow$ tpy MLCT that would be expected to blue shift upon oxidation to the other ruthenium metal. This observation is consistent with a ruthenium based oxidation that is localized on the ruthenium that is not coordinated to tpy. It is interesting to note that the visible portion of the spectrum for the one electron oxidized form of this bimetallic is quite similar to $[(tpy)Ru(tpp)Ru(tpp)]^{4+}$. This indicates that the stabilizing effect on the tpp π^* orbitals of Ru^{II}tpy is about equal to that of $Ru^{III}Cl_3$. When both metals are oxidized, all of the transitions in the visible region are lost due to their MLCT nature. The oxidative spectroelectrochemistry of this bimetallic system also shows the characteristic loss of the higher energy MLCT transitions that have been discussed for the other systems. In the one electron reduced species shown in Figure 34b, the $\pi^* \rightarrow \pi^*$ transitions appearing in the visible make identification of any changes in the spectrum difficult as does the poor reversibility. The transitions in the UV that have been assigned as overlapping tpp and tpy $\pi \rightarrow \pi^*$ transitions lose intensity upon reduction of tpp and shift to lower energy.

Figure 35 shows the spectroelectrochemical results for $[(tpy)Os(tpp)RuCl_3]^+$. The first oxidation for this complex has been assigned as the Ru(II)/Ru(III) oxidation and the second as the Os(II)/Os(III) oxidation. Oxidation of the ruthenium should lead to the disappearance of the ruthenium based transitions similar to what is found for $[(tpy)Ru(tpp)RuCl_3]^+$ upon one electron oxidation. The one electron oxidation results in a loss of the band at 678 nm, verifying the assignment of this band as a Ru $\rightarrow$ tpp MLCT transition. The peak at 474 nm has been assigned as a Os $\rightarrow$ tpy MLCT with the Os $\rightarrow$ tpp transition occurring at 606 nm. The Os $\rightarrow$ tpy transition would be expected to blue shift upon oxidation of the Ru metal center and would be part of the intensity between 360 - 390 nm. The Os $\rightarrow$ tpp transition would be expected to red shift upon ruthenium oxidation. The band at 520 nm is attributed to the shifting of the Os $\rightarrow$ tpp MLCT from 606 nm in the original oxidation state. When both metals are oxidized, all
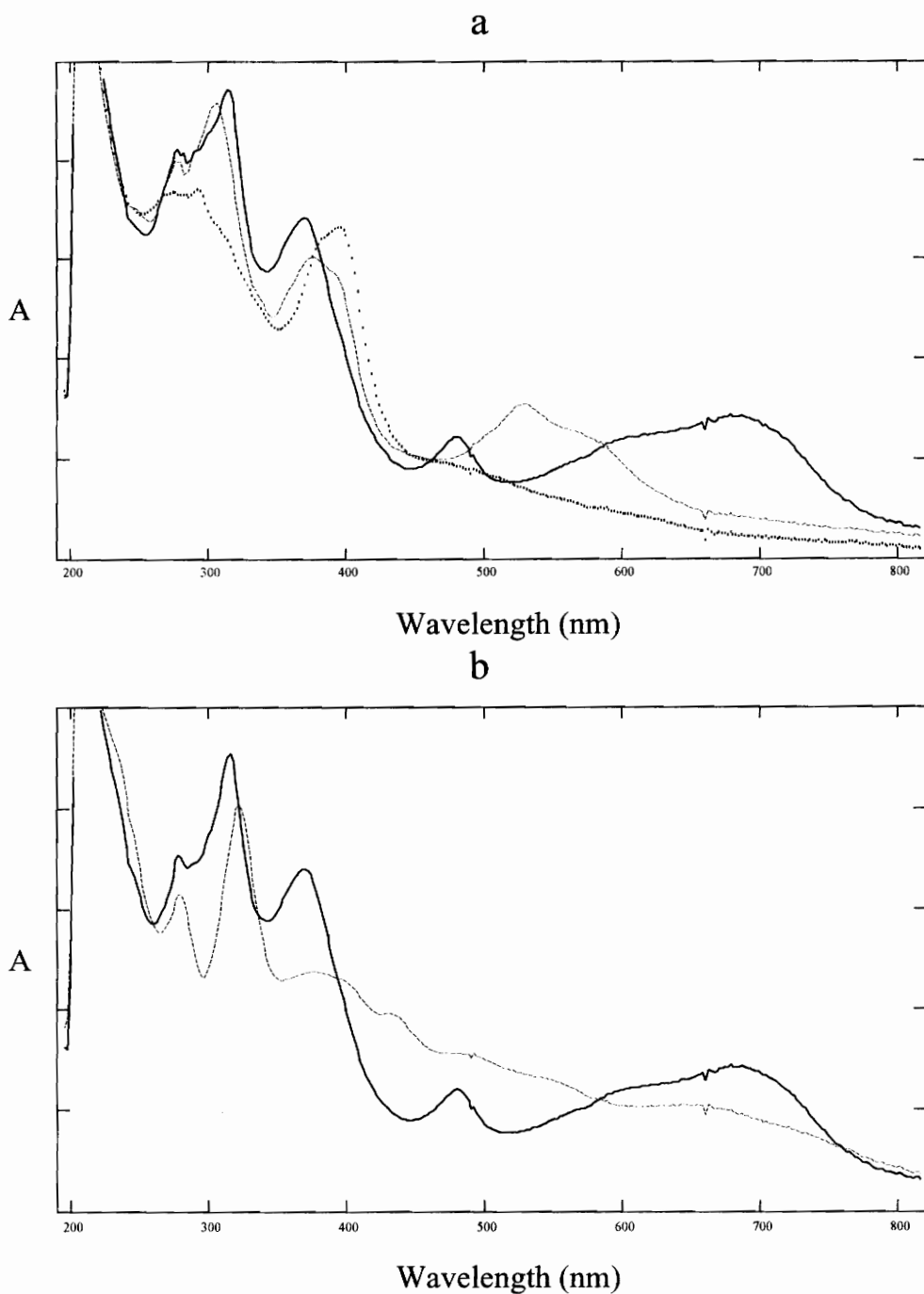
a

Wavelength (nm)

b

Wavelength (nm)

Figure 35. Spectroelectrochemical results for [(tpy)Os(tpp)RuCl$_3$]$^+$ (where tpy = 2,2':6',2''-terpyridine and tpp = 2,3,5,6-tetrakis(2-pyridyl)pyrazine). (a) (——) Original oxidation state, (----) 1 electron oxidation, (.......) 2 electron oxidation. (b) (——) Original oxidation state and (----) 1 electron reduction.

127

the transitions in the visible region are lost due to their MLCT nature. In the one electron reduced species shown in Figure 35b, a similar spectrum to that of the analogous Ru/Ru bimetallic complex is observed.

Figure 36a shows the oxidative spectroelectrochemical results for $[(tpy)Ru(tpp)Ru(tpy)]^{4+}$. Oxidation of the first ruthenium metal decreases the intensity of the MLCT at 540 nm with the remaining transition being due to the unoxidized ruthenium metal. This intensity is decreased further upon oxidation of the second metal center. Electrogeneration of the oxidized complexes is possible with >95 % regeneration of the original oxidation state. The reductive spectroelectrochemical results are shown in Figure 36b for the symmetric bimetallic $[(tpy)Ru(tpp)Ru(tpy)]^{4+}$. The Ru → tpy MLCT would be expected to red shift upon tpp reduction. The transition at 400 nm can be assigned as a Ru → tpy MLCT transition. The peak that grows in at 540 nm is similar to what is found in the Ru/Ir bimetallic complex and represents a tpp $\pi^* \to \pi^*$ transition. The new band from 620 to 720 nm can be assigned as a tpp → Ru LMCT transition. Electrogeneration of the one electron reduced species is reversible with > 90 % regeneration of the original oxidation state.

Figure 37 contains the spectroelectrochemical results for $[(tpy)Ru(tpp)Ru(tpp)]^{4+}$. Electrogeneration of the one electron oxidized and reduced complexes is possible with > 95 % regeneration of the original oxidation state. Figure 37a shows the oxidative spectroelectrochemical results for this bimetallic complex. The band at 548 nm has been assigned as two overlapping Ru → tpp MLCT transitions involving the bridging ligand, with the lower energy component being attributed to the Ru → tpp MLCT localized on the $(tpy)Ru^{II}(tpp)$ moiety. The first oxidation has been assigned as oxidation of the ruthenium metal that is coordinated to both tpy and tpp. Generation of the $(tpy)Ru^{III}(tpp)Ru^{II}(tpp)$ species results in the lower energy component of the band disappearing with the remaining band at 540 nm being the Ru → tpp MLCT transition involving the ruthenium coordinated to two tpp ligands. The Ru → tpy transition shifts slightly to higher energy. Figure 37b shows the reductive spectroelectrochemical results
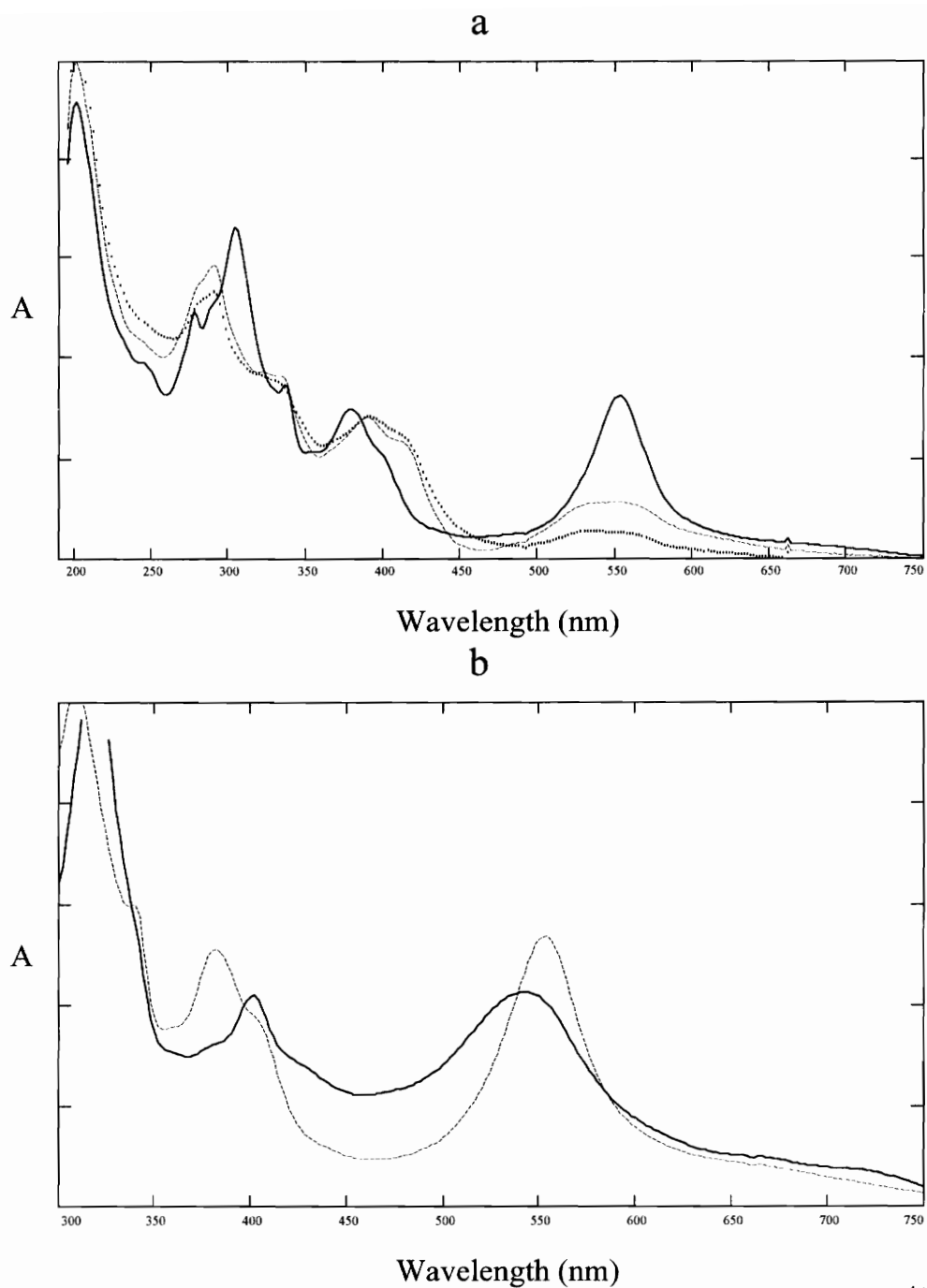
a

b

Figure 36. Spectroelectrochemical results for [(tpy)Ru(tpp)Ru(tpy)]$^{4+}$ (where tpy = 2,2':6',2''-terpyridine and tpp = 2,3,5,6-tetrakis(2-pyridyl)pyrazine). (a) (——) Original oxidation state, (----) 1 electron oxidation, (.......) 2 electron oxidation. (b) (----) Original oxidation state and (——) 1 electron reduction.
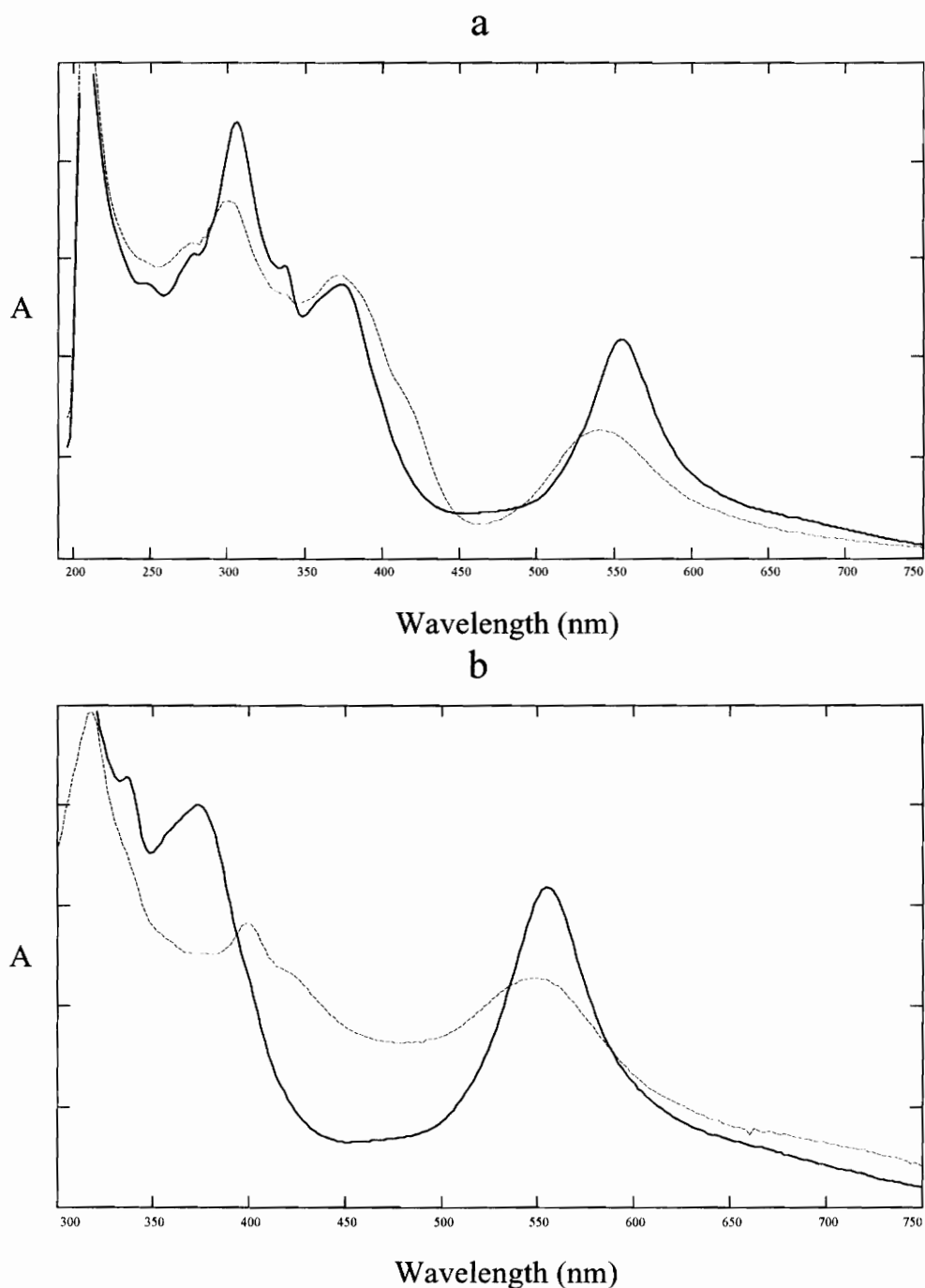
a

A

Wavelength (nm)

b

A

Wavelength (nm)

Figure 37. Spectroelectrochemical results for [(tpy)Ru(tpp)Ru(tpp)]$^{4+}$ (where tpy = 2,2':6',2''-terpyridine and tpp = 2,3,5,6-tetrakis(2-pyridyl)pyrazine). (a) (——) Original oxidation state and (----) 1 electron oxidation. (b) (——) Original oxidation state and (----) 1 electron reduction.

for $[(tpy)Ru(tpp)Ru(tpp)]^{4+}$. As expected, the band at 548 nm disappears upon reduction of the tpp bridging ligand. The Ru → tpy and Ru → tpp MLCT transition localized on the terminal ligands would be predicted to red shift upon reduction of the bridging tpp ligand. The transitions at 410 and 420 nm are assigned as the Ru → tpp and Ru → tpy MLCT transitions respectively. The peak that grows in at 550 nm is similar to what has been found previously and represents the tpp $\pi^* → \pi^*$ transition. This verifies the assignment of the HOMO as the ruthenium metal coordinated to tpy and tpp and the LUMO as the bridging tpp ligand.

Figure 38 shows the spectroelectrochemical results for $[(tpy)Os(tpp)Ru(tpp)]^{4+}$. Electrogeneration of the one electron oxidized and reduced complexes is possible with > 95 % regeneration of the original oxidation state. The band at 546 nm has been assigned as overlapping Ru → tpp and Os → tpp MLCT transitions involving the bridging tpp ligand with the lower energy component being the osmium based transition. The first oxidative process has been assigned as the Os(II)/Os(III) oxidation. Electrogeneration of this state should result in a spectrum that matches that of the one electron oxidized species of $[(tpy)Ru(tpp)Ru(tpp)]^{4+}$ shown in Figure 37a. As expected, the lower energy component of the band at 546 nm disappears with the remaining band at 540 nm being assigned as the Ru → tpp MLCT localized on the bridging tpp ligand. In comparing the one electron oxidized species of $[(tpy)Os(tpp)Ru(tpp)]^{4+}$ and $[(tpy)Ru(tpp)Ru(tpp)]^{4+}$, it is clear the two are virtually identical verifying the assignments made. Upon one electron reduction, Figure 38b, a spectrum similar to that of the Ru/Ru analog is generated. The tpp based MLCT transitions disappear and the new tpp $\pi^* → \pi^*$ transition grows in.

a

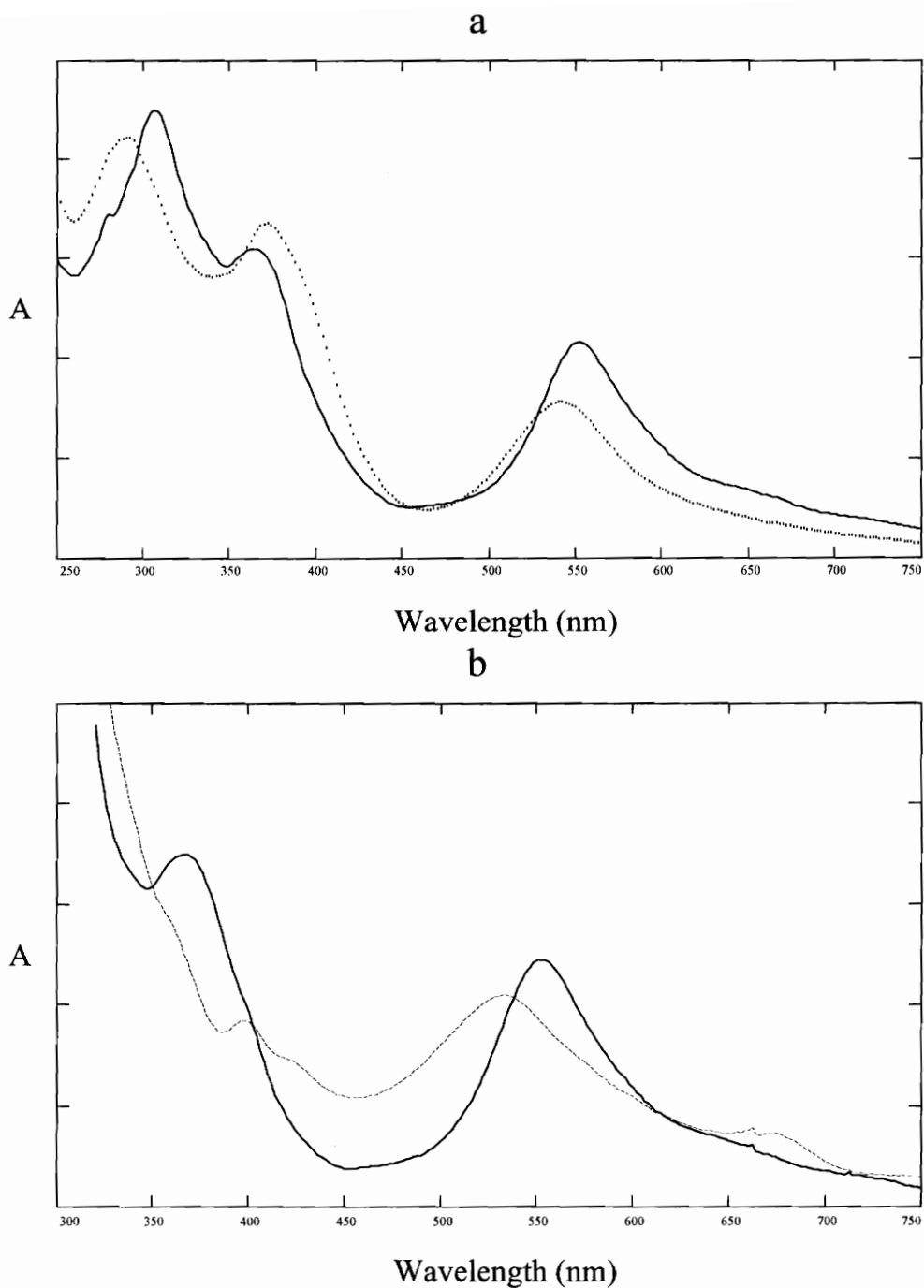Wavelength (nm)

b

Wavelength (nm)

Figure 38. Spectroelectrochemical results for $[(tpy)Os(tpp)Ru(tpp)]^{4+}$ (where tpy = 2,2':6',2''-terpyridine and tpp = 2,3,5,6-tetrakis(2-pyridyl)pyrazine). (a) (——) Original oxidation state and (----) 1 electron oxidation. (b) (——) Original oxidation state and (----) 1 electron reduction.

Emission Spectroscopy and Excited-State Lifetime Measurements

One way to probe the lowest lying excited state is through emission spectroscopy and excited state lifetime measurements. It has been reported that in polypyridyl complexes, visible light absorption is generally into a [1]MLCT whereas emission occurs from the more stabilized [3]MLCT state.[8,14,25,38-52] These emissions will occur at a lower energy than the absorptions due to the absorption being a [1]MLCT transition whereas the emission arises from the [3]MLCT state. It is also possible to measure the lifetimes of the emissive states of these complexes at room temperature in deoxygenated solution. The emission and excited-state lifetime results are summarized in Tables VI-VIII (pages 93, 94, and 105).

Monometallic Complexes

Ir(tpp)Cl$_3$ emits from a [3]MLCT excited state with a λ_{max}^{em} at 632 nm and an excited state lifetime of 1300 ns. The emission spectra for both [Ru(tpy)(tpp)]$^{2+}$ and [Os(tpy)(tpp)]$^{2+}$ have been published previously[50,55,56,59] with emission bands at 670 nm (30 ns) and 775 nm (260 ns), respectively. These peaks have been assigned as arising from the [3]MLCT excited states. Although the emission energies have been previously reported, comparison of the two complexes has not been performed. The energy gap decreases in the osmium system relative to the ruthenium complex. This typically results in significantly shorter excited state lifetimes in osmium versus ruthenium systems of analogous polypyridine ligands.[25,32,35,45,56,60] The much shorter lifetime of [Ru(tpy)(tpp)]$^{2+}$ results from the low lying LF state that can be thermally populated at room temperature from the emissive MLCT state. The osmium system, [Os(tpy)(tpp)]$^{2+}$ does not possess this low lying LF state and hence deactivation is only from the [3]MLCT state leading to the longer observed excited state lifetime. This is a unique example of an osmium complex having a lifetime that is longer than the analogous ruthenium complex. Table X contains the excited-state lifetimes of [Ru(tpy)$_2$]$^{2+}$, [Ru(tpy)(tpp)]$^{2+}$, [Ru(tpy)(Metpp)]$^{3+}$, and [Os(tpy)(tpp)]$^{2+}$, as well as the bimetallic complexes

Table X. Photophysical Data for $[Ru(tpy)_2]^{2+}$, $[Ru(tpy)(tpp)]^{2+}$, $[Ru(tpy)(Metpp)]^{3+}$, $[Os(tpy)(tpp)]^{2+}$, $[(tpy)Ru(tpp)Ru(tpp)]^{4+}$ and $[(tpy)Os(tpp)Ru(tpp)]^{4+}$ (where tpy = 2,2':6',2''-terpyridine, tpp = 2,3,5,6-tetrakis(2-pyridyl)pyrazine, and Metpp = 2-[2-(1-Methylpyridiniumyl)]-3,5,6-tris(2-pyridyl)pyrazine).

Compound	$\lambda_{max}em$ $(nm)^a$	τ^a (ns)	τ^b (ns)
$[Ru(tpy)_2]^{2+\ c}$	620	0.25	10000
$[Ru(tpy)(tpp)]^{2+}$	665	30	7100
$[Ru(tpy)(Metpp)]^{3+}$	700	38	3000
$[Os(tpy)(tpp)]^{2+}$	775	260	3800
$[(tpy)Ru(tpp)Ru(tpp)]^{4+}$	833	100	480
$[(tpy)Os(tpp)Ru(tpp)]^{4+}$	820	120	460

[a] Measured in deoxygenated acetonitrile solution at room temperature.

[b] Measured in an ethanolic glass at 77 K.

[c] References 54 and 61.

[(tpy)Ru(tpp)Ru(tpp)]$^{4+}$ and [(tpy)Os(tpp)Ru(tpp)]$^{4+}$ at room temperature and 77 K. The excited-state lifetime of [Ru(tpy)(tpp)]$^{2+}$ increases dramatically at 77 K (7 µs) supporting the rational behind the short excited-state lifetime of this complex at room temperature. Decreasing the temperature to 77 K would freeze out the thermal population of the ^{3}LF state resulting in deactivation being only from the Ru $\rightarrow$ tpp ^{3}MLCT excited state, leading to the enhanced lifetime of the complex. Consequently, the lifetime of [Ru(tpy)(tpp)]$^{2+}$ at 77 K is longer than the bimetallic systems as would be predicted by the emission energies for the two complexes.

The photophysical data for [Ru(tpy)(tpp)]$^{2+}$, [Ru(tpy)(Metpp)]$^{3+}$, [Ru(bpy)(tpp)Cl]$^+$, [Ru(bpy)(tpp)(CH$_3$CN)]$^{2+}$ and [Ru(bpy)(Metpp)(CH$_3$CN)]$^{3+}$ is summarized in Table VI, page 93. In agreement with the absorption spectroscopy, substitution of the coordinated chloride in [Ru(bpy)(tpp)Cl]$^+$, by an acetonitrile solvent molecule to form [Ru(bpy)(tpp)(CH$_3$CN)]$^{2+}$, leads to a higher energy emission. When comparing the methylated and nonmethylated systems, slight shifts in the emission maxima to lower energy occur upon methylation. [Ru(tpy)(tpp)]$^{2+}$ emits at 665 nm (15.0 kK) whereas [Ru(tpy)(Metpp)]$^{3+}$ emits at 700 nm (14.3 kK). Similar results are found in [Ru(bpy)(tpp)(CH$_3$CN)]$^{2+}$ and [Ru(bpy)(Metpp)(CH$_3$CN)]$^{3+}$ where the emission occurs at 700 nm (14.3 kK) and 712 nm (14.0 kK), respectively. All of the complexes studied emit from the Ru(dπ) $\rightarrow$ tpp(π*) ^{3}MLCT state in which the acceptor orbital is localized on the pyrazine portion of the ligand. The slightly lower energy emission of the Metpp complexes results from the stabilization of this pyrazine based orbital by the introduction of the electron withdrawing viologen substituent. This is shown in the Jablonski diagrams in Figure 39.

Based on the electrochemical studies one would expect to see intramolecular electron transfer quenching of the ^{3}MLCT excited state that is localized on the pyrazine ring in the systems possessing the Metpp ligand. This would generate a charge separated state with a reduced viologen and oxidized ruthenium. This intramolecular electron transfer should quench the emission of the ^{3}MLCT state in the Metpp systems.

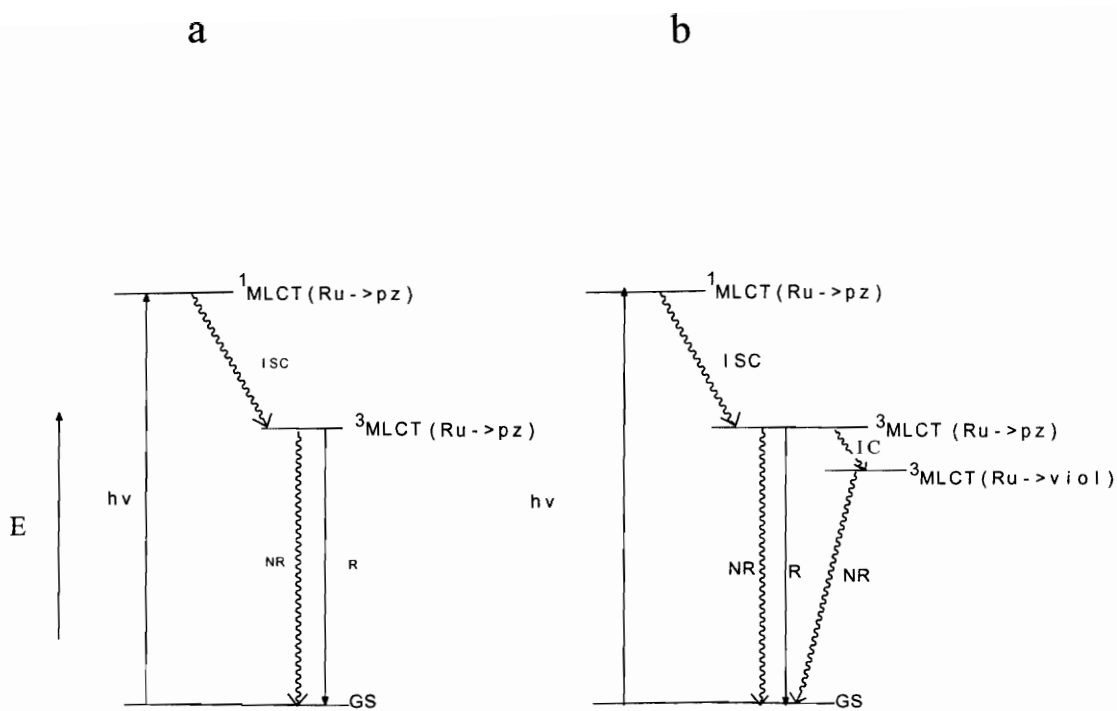Figure 39. Jablonski Diagrams for (a) [Ru(tpy)(tpp)]$^{2+}$ and
(b) [Ru(tpy)(Metpp)]$^{3+}$ (where tpy = 2,2':6',2''-terpyridine, tpp = 2,3,5,6-tetrakis(2-pyridyl)pyrazine, and Metpp = 2-[2-(1-Methylpyridiniumyl)]-3,5,6-tris(2-pyridyl)pyrazine).

The excited-state lifetimes of the ruthenium complexes are as follows: [Ru(tpy)(tpp)]$^{2+}$ is 30 ns, [Ru(tpy)(Metpp)]$^{3+}$ is 40 ns, [Ru(bpy)(tpp)(CH$_3$CN)]$^{2+}$ is 60 ns, and [Ru(bpy)(Metpp)(CH$_3$CN)]$^{3+}$ is 70 ns. As discussed, an emission at room temperature for [Ru(tpy)$_2$]$^{2+}$ is not observed due to the quenching of the ^{3}MLCT emission by the thermally populated ^{3}LF state resulting in rapid nonradiative deactivation of the MLCT state. In the complexes synthesized in this study, the ^{3}MLCT state is stabilized relative to this ^{3}LF state. However, the short lifetime can be attributed to the LF state still lying in close enough proximity to the MLCT state to be thermally populated, but at a slower rate. This is shown schematically in Figure 40. The methylated and nonmethylated complexes exhibit very similar emission maxima and band shapes. This would indicate a similar emissive state, consistent with the emissive state being the aforementioned Ru(dπ) $\rightarrow$ tpp(π*) ^{3}MLCT state localized on the pyrazine portion of the tpp ligand.

Table XI gives Φ_{EM}, k_R, and k_{NR} for the methylated and nonmethylated series of complexes. The emission quantum yields, Φ_{EM}, for each series of complexes have been calculated using the equation given in the experimental section (page 52). The nonmethylated complexes, [Ru(tpy)(tpp)]$^{2+}$ and [Ru(bpy)(tpp)(CH$_3$CN)]$^{2+}$ have quantum yields equal to 7.9 x 10^{-4} and 6.8 x 10^{-4} respectively. Upon methylation, the emission quantum yield decreases to about half that of the nonmethylated complexes, 3.7 x 10^{-4} for [Ru(tpy)(Metpp)]$^{3+}$ and 3.3 x 10^{-4} for [Ru(bpy)(Metpp)(CH$_3$CN)]$^{3+}$. This seems to indicate that this emission is quenched upon addition of an electron accepting moiety. This provides evidence of the desired intramolecular electron transfer.

Determination of the relative quantum yield of the methylated and nonmethylated systems in a frozen glass has also be performed. In an ethanolic glass at 77 K, it is expected that intramolecular electron transfer quenching will not occur if free rotation is needed to accommodate electron transfer.[72] Meyer and coworkers have performed studies on a series of complexes of the type [(4,4'-(X)$_2$-bpy)Re(CO)$_3$(MQ$^+$)]$^{2+}$ (X = C(O)OEt, H, NH$_2$) where MQ$^+$ is the covalently attached electron acceptor. From the electrochemical measurements, ΔG for intramolecular electron transfer quenching is
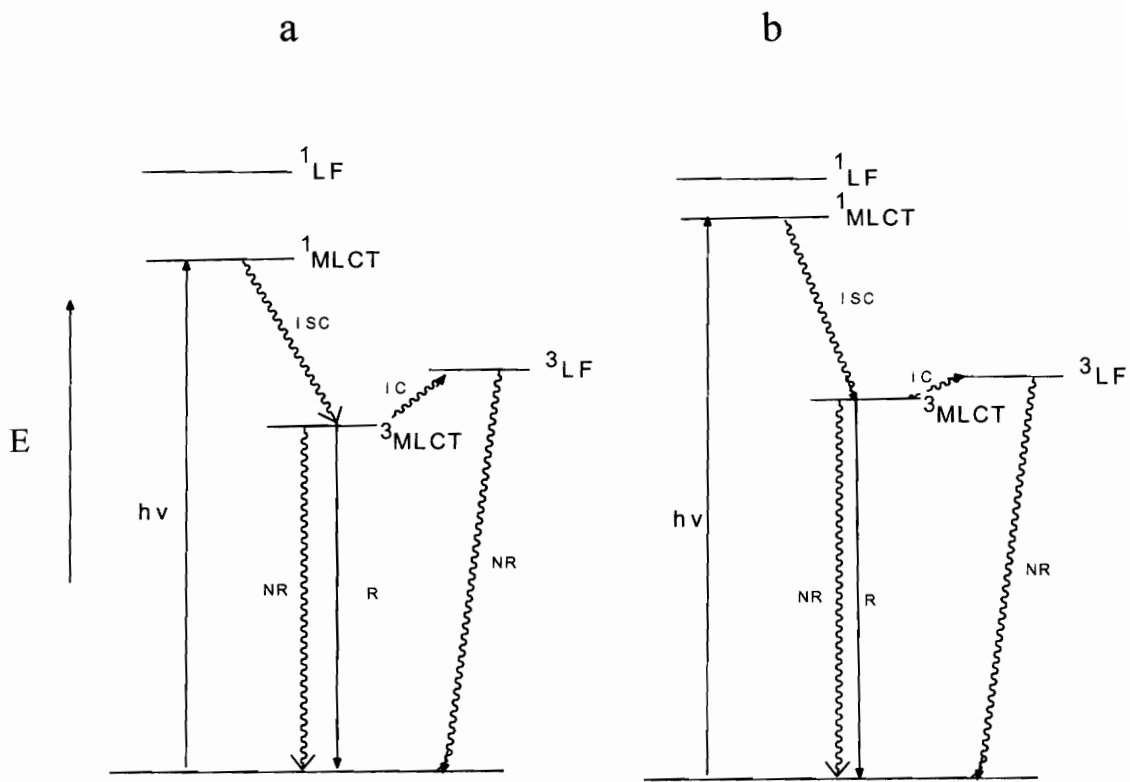
Figure 40. Jablonski Diagrams for (a) [Ru(tpy)(tpp)]$^{2+}$ and
(b) [Ru(tpy)$_2$]$^{2+}$ (where tpy = 2,2':6',2''-terpyridine and tpp = 2,3,5,6-
tetrakis(2-pyridyl)pyrazine).

Table XI. Emission Quantum Yields and Rate Constants for the Nonmethylated and Methylated Complexes [Ru(tpy)(tpp)]$^{2+}$, [Ru(tpy)(Metpp)]$^{3+}$, [Ru(bpy)(tpp)(CH$_3$CN)]$^{2+}$, and [Ru(bpy)(Metpp)(CH$_3$CN)]$^{3+}$ (where bpy = 2,2'-bipyridine, tpy = 2,2':6',2''-terpyridine, tpp = 2,3,5,6-tetrakis(2-pyridyl)pyrazine), and Metpp = 2-[2-(1-Methylpyridiniumyl)]-3,5,6-tris(2-pyridyl)pyrazine).[a]

Compound	Φ_{EM}	k_R (s^{-1})	k_{NR} (s^{-1})	k_{ET} (s^{-1})
[Ru(bpy)$_3$]$^{2+}$ [b]	6.2 x 10^{-2}	7.1 x 10^4	1.1 x 10^6	
[Ru(tpy)(tpp)]$^{2+}$	7.9 x 10^{-4}	2.6 x 10^4	3.3 x 10^7	
[Ru(tpy)(Metpp)]$^{3+}$	3.7 x 10^{-4}	2.6 x 10^4	3.3 x 10^7	3.8 x 10^7
[Ru(bpy)(tpp)(CH$_3$CN)]$^{2+}$	6.8 x 10^{-4}	1.1 x 10^4	1.6 x 10^7	
[Ru(bpy)(Metpp)(CH$_3$CN)]$^{3+}$	3.3 x 10^{-4}	1.1 x 10^4	1.6 x 10^7	1.7 x 10^7

[a] Measured in deoxygenated acetonitrile solution at room temperature.

[b] Reference 8.

- 0.1, - 0.49, and - 1.0 eV for X = C(O)OEt, H, and NH_2 respectively. Contrary to the first two systems, when X = NH_2, the MLCT emission is completely quenched in solution at room temperature and still occurs in the glass at 77 K. Thus, intramolecular electron quenching can occur in a glass if the process is thermodynamically favored.

Meyer and coworkers have shown that in addition to the driving force , conformational changes are also important in determining whether intramolecular electron transfer will occur.[87] In this study, the question of the ring-ring dihedral angle and its effect on intramolecular electron transfer was addressed using crystallographic data for $[(bpy)Re(CO)_3(MQ^+)](PF_6)_2$ as well as spectral and electrochemical comparisons with Os(II), Re(I), and Ru(II) complexes. In the crystal structure of the rhenium complex, the dihedral angle was found to be $47°$. It is believed that this results as a "compromise" between the nonplanar conformation adopted to minimize steric repulsions and the planar conformation favored due to π-π interactions between the rings. In solution, a nonplanar conformation would occur. However, upon reduction, the electronic coupling between the rings is sufficient to overcome the steric repulsions and the ion would be planar. In both electrochemical and emission experiments, an electron is added to the monoquat acceptor and the two pyridyl rings are coplanar, $\theta = 0°$. It was concluded that the dihedral angle has a significant effect on the energies and intensities of the MQ^+ based MLCT transitions. In addition, changes in the dihedral angle determine whether quenching will occur. Appendix Figure A-XXII (page 191), a minimized picture of $Metpp^+$, demonstrates the rotation of the electron accepting moiety. The dihedral angle has been calculated to be $53°$ for $Metpp^+$.

In the dyads studied in this work, the emission energy and intensity in absorbance matched samples at 77 K are not the same in the methylated and nonmethylated systems. In an ethanolic glass, the integrated peak area of $[Ru(tpy)(tpp)]^{2+}$ is 4.8 times that of $[Ru(tpy)(Metpp)]^{3+}$, as shown in Appendix Figure A-XX (page 189). For $[Ru(bpy)(tpp)(CH_3CN)]^{2+}$, the peak area is 6.8 times that of $[Ru(bpy)(Metpp)(CH_3CN)]^{3+}$, as shown in Appendix Figure A-XXI (page 190). Analysis of the vibrational structure of the emission bands yields frequency modes of 1100, 1200,

1300, and 1000 cm^{-1} for [Ru(tpy)(tpp)]$^{2+}$, [Ru(tpy)(Metpp)]$^{3+}$, [Ru(bpy)(tpp)(CH$_3$CN)]$^{2+}$, and [Ru(bpy)(Metpp)(CH$_3$CN)]$^{3+}$, respectively. This corresponds to the averaged value for the C-C and C-N pyridine based ring modes as reported previously for MLCT excited states of similar types of complexes.[88] This similarity in vibronic structure would indicate that the same states are involved in the emission bands of the two sets of methylated and nonmethylated complexes. In addition, the lifetime of the methylated complex [Ru(tpy)(Metpp)]$^{3+}$ at 77 K is not the same as [Ru(tpy)(tpp)]$^{2+}$. This has also been reported for similar types of dyad systems incorporating MQ$^+$ based electron acceptors.[72,85,86] The results of the 77 K studies indicate that the intramolecular electron transfer is not completely quenched in the glass.

Using the equations discussed in the introduction (page 8), the radiative rate constants can be calculated. The quantum yield for emission is equal to k_R times the lifetime of the complex. Since Φ_{EM} and the lifetime of the complex have been measured, the radiative rate constant can be calculated. The nonradiative rate constant, k_{NR}, can be calculated knowing k_R and Φ_{EM} since the quantum yield for emission in the nonmethylated complexes is equal to the radiative rate constant divided by the sum of the radiative and nonradiative rate constants. These rate constants are summarized in Table XI. As expected, the systems synthesized in this study have higher k_{NR} values than [Ru(bpy)$_3$]$^{2+}$. This is a result of the LF state being in communication with the MLCT state enhancing our apparent k_{NR}. The values we obtain for k_{NR} are actually the sum of k_{IC} to the LF state and k_{NR} to the ground state. As shown in Figure 39, the emitting state is the same for both the methylated and nonmethylated complexes. Consequently, the radiative and nonradiative rate constants for the methylated complexes will be the similar to those of the nonmethylated complexes. Using the values for Φ_{EM}, k_R and k_{NR} that have been calculated, k_{ET}, the rate of electron transfer, for the methylated complexes can also be calculated. The quantum yield for emission in the methylated complexes is equal to k_R divided by the sum of k_R, k_{NR}, and k_{ET}. From these calculations, it appears that the rate of electron transfer is faster in [Ru(tpy)(Metpp)]$^{3+}$ than [Ru(bpy)(Metpp)(CH$_3$CN)]$^{3+}$ as expected due to the increased driving force of [Ru(tpy)(Metpp)]$^{3+}$.

To determine whether these values for k_{ET} are the same as those predicted by Marcus theory, a series of calculations must be performed. As discussed in the introduction, it is possible to calculate the thermodynamic driving force, ΔG, for forward and back electron transfer. To do this, an estimate of the $Ru*^{2+/3+}$ potential is made, the difference between $E_{1/2}$ for the ruthenium oxidation and E_{00}. E_{00} can be estimated by adding 0.13 to the energy of emission (in eV).[33] From the redox potentials given in Tables II and III (pages 65 and 66), ΔG_{ET} and ΔG_{BET} can be calculated. Table XII gives E_{00}, ΔG_{ET}, and ΔG_{BET} for $[Ru(tpy)(Metpp)]^{3+}$ and $[Ru(bpy)(Metpp)(CH_3CN)]^{3+}$.

To calculate k_{ET}, a value for the reorganization energy must first be determined. The reorganization energy, λ, has both inner, λ_i, and outer, λ_o, sphere components. λ_o can be calculated using the equation given in the introduction (page 16), the Marcus-Hush two sphere dielectric continuum model. The values of ε_{op} and ε_s are 1.80 and 36.7, respectively, in acetonitrile. Using a molecular modeling program, r_D, r_A, and r_{DA} for the methylated complexes are estimated(4.05 Å, 4.21 Å, and 5.80 Å, respectively). Using these values, λ_o is calculated to be 0.528 eV in acetonitrile. The inner sphere component, λ_i, can be assumed to be 0.2 eV as reported previously.[83,85] The reorganizational energy, λ, is calculated to be 0.728 eV. Elliott et. al., as well as Schanze et. al., have found that the estimated values using the calculations described are larger than the experimental data in a $\log k_{ET}$ versus ΔG_{ET} plot.[83,85] These values are generally 20 - 30 % larger than the experimental values. To calculate k_{ET} according to Marcus theory, a value of 0.546 eV will be used (25 % of 0.728).

To determine a value for H_{AB}, the donor-acceptor electronic coupling matrix, Elliott and coworkers created a plot of $\ln k_{ET}$ (1/sec) versus ΔG (mV) from a study of a series of linked tris(2,2'-bipyridine)ruthenium(II)/diquat complexes in room temperature acetonitrile solutions (where diquat = N,N'-diquaternary-2,2'-bipyridiniumyl salt).[85] Assuming this will be similar to that of the systems discussed here, a value of 2.8×10^{-3} eV will be used to calculate k_{ET} for these systems. This is a reasonable model for the systems studied here due to the structural similarities and excited state properties

Table XII. Estimates of the Electron Transfer Rates According to Marcus Theory for the Nonmethylated and Methylated Complexes $[Ru(tpy)(tpp)]^{2+}$, $[Ru(tpy)(Metpp)]^{3+}$, $[Ru(bpy)(tpp)(CH_3CN)]^{2+}$, and $[Ru(bpy)(Metpp)(CH_3CN)]^{3+}$ (where bpy = 2,2'-bipyridine, tpy = 2,2':6',2''-terpyridine, tpp = 2,3,5,6-tetrakis(2-pyridyl)pyrazine, and Metpp = 2-[2-(1-Methylpyridiniumyl)]-3,5,6-tris(2-pyridyl)pyrazine).

Compound	E_{00} (eV)	ΔG_{ET} (mV)	k_{ET} (s^{-1})	ΔG_{BET} (mV)	k_{BET} (s^{-1})
$[Ru(tpy)(tpp)]^{2+}$	1.99				
$[Ru(tpy)(Metpp)]^{3+}$	1.90	- 300	6.1×10^{10}	- 2200	1.7×10^{11}
$[Ru(bpy)(tpp)(CH_3CN)]^{2+}$	1.90				
$[Ru(bpy)(Metpp)(CH_3CN)]^{3+}$	1.87	- 180	1.6×10^{10}	- 2050	1.7×10^{11}

of the complexes. Using these values for λ and H_{AB}, k_{ET} for $[Ru(tpy)(Metpp)]^{3+}$ is calculated to be 6.1×10^{10} s^{-1}. Similarly, a value for $[Ru(bpy)(Metpp)(CH_3CN)]^{3+}$ is calculated to be 1.6×10^{10} s^{-1}.

The spectroelectrochemical results for the one electron reduced species of $[Ru(tpy)(Metpp)]^{3+}$ give an idea of what the photoinduced excited state should look like. The major differences between the one electron reduced species of $[Ru(tpy)(tpp)]^{2+}$ and $[Ru(tpy)(Metpp)]^{3+}$ was the appearance of the band at 485 nm for the methylated system. Transient absorbance measurements were performed on $[Ru(tpy)(Metpp)]^{3+}$ and the results are shown in Appendix Figure A-IX (page 178). No evidence of a charge separated state was observed. Only evident are the transient associated with the MLCT excited state and kinetic decay associated with recovery of the ground state. This could be a result of the rapid rate of back electron transfer. Because the intramolecular electron transfer cannot be monitored by transient absorbance spectroscopy, k_{BET} is not available. The values for k_{BET} in Table XII are those obtained through calculations similar to that of k_{ET}. Following the same method as in the calculation of k_{ET}, k_{BET}, the rate of back electron transfer, is calculated to be 1.7×10^{11} s^{-1} and 1.7×10^{11} s^{-1}, for $[Ru(tpy)(Metpp)]^{3+}$ and $[Ru(bpy)(Metpp)(CH_3CN)]^{3+}$, respectively.

The value of k_{ET} is moderately affected by the reduction potential of the viologen portion of the Metpp ligand. The faster rate of electron transfer for $[Ru(tpy)(Metpp)]^{3+}$ relative to $[Ru(bpy)(Metpp)(CH_3CN)]^{3+}$ is consistent with the fact that ΔG_{ET} is more exothermic for $[Ru(tpy)(Metpp)]^{3+}$ (-300 mV versus -180 mV). In Table XII it is shown that k_{ET} increases as ΔG_{ET} becomes more exothermic while k_{BET} remains the same as ΔG_{BET} becomes less exothermic. The forward electron transfer is weakly exothermic whereas back electron transfer is strongly exothermic. As a result, forward electron transfer falls in the Marcus "normal" free energy region. Back electron transfer would be expected to fall in the Marcus "inverted" region. However, without being able to get a measure of k_{BET} experimentally, the results are inconclusive.

Whether the charge separated state exists in these complexes is not totally apparent. There is evidence for the quenching process occurring, however, if it does, the

charge separated state is not long lived. Regardless, the results from this study are significant. A method for the preparation of complexes containing a covalently attached electron acceptor has been accomplished via the methylation of the remote nitrogen on the tpp ligand. Insight into the ground and excited state properties of these types of complexes has been achieved. As reported by Meyer in MQ^+ systems, intramolecular electron transfer can be inhibited as a result of the dihedral angle of the viologen acceptor. As shown in Appendix Figure A-XXII (page 191) the minimized picture of $Metpp^+$ demonstrates the rotation of the electron accepting moiety. This could be eliminated through the synthesis of a planar tpp ligand that could be methylated.
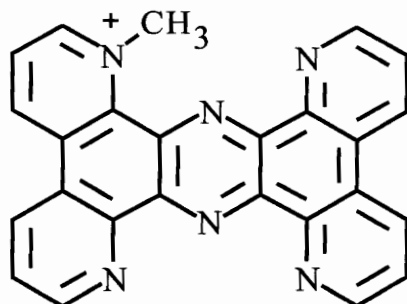
[Ru(tpy)(dpp)Cl]$^+$ and all [Ru(tpy)(BL)(py)]$^{2+}$ systems emit in fluid solution at room temperature. The dpq and dpb based chloride systems may display red shifted emissions beyond the detection limit of our system. The emission of our complexes is in marked contrast to [Ru(tpy)$_2$]$^{2+}$ which has an excited-state lifetime of less than 1 ns and does not display an emission under our conditions.[48-53] The short lifetime of [Ru(tpy)$_2$]$^{2+}$ at room temperature has been attributed to a thermally accessible ruthenium based ligand field excited state that decays rapidly.[60] The presence of more stabilized π^* orbitals on our bridging ligands give rise to a lowering of the energy of the MLCT state preventing thermal population of the ligand field state. This is similar to what is shown in the Jablonski diagrams in Figure 40 (page 138) for [Ru(tpy)(tpp)]$^{2+}$ and [Ru(tpy)$_2$]$^{2+}$. The Ru(dπ) $\rightarrow$ BL(π^*) MLCT excited-state emission occurs at 760 nm (20 ns) for [Ru(tpy)(dpp)Cl]$^+$, 700 nm (80 ns) for [Ru(tpy)(dpp)(py)]$^{2+}$, 800 nm (28 ns) for

$[Ru(tpy)(dpq)(py)]^{2+}$, and 860 nm (< 20 ns) for $[Ru(tpy)(dpb)(py)]^{2+}$ (lifetimes given in parentheses). The short excited-state lifetime for these complexes may be due to the LF state being somewhat thermally accessible giving rise to a quenching of the MLCT excited-state.

Bimetallic Complexes

In general, a shift in emission to lower energy in going from a monometallic to a bimetallic complex is observed. As would be predicted by the energy gap law, a decrease in the emission energy generally results in a decrease in the excited state lifetime.

On the basis of the monometallic emissions, one would expect the emitting state in $[(tpy)Ru(tpp)IrCl_3]^{2+}$ to be ^{3}MLCT Ru($d\pi$) $\rightarrow$ tpp(π^*) excited state. The relatively short excited state lifetime of this complex (22 ns) is consistent with a ruthenium and inconsistent with an iridium based emission. The lowest energy absorption in the electronic spectrum of the bimetallic complex, $[(tpy)Ru(tpp)IrCl_3]^{2+}$, is an iridium based ^{3}MLCT transition whereas the emissive state appears to be a ruthenium based ^{3}MLCT excited state. Excitation into either the Ir($d\pi$) $\rightarrow$ tpp(π^*) ^{3}MLCT or the Ru($d\pi$) $\rightarrow$ tpp(π^*) ^{1}MLCT gives rise to the same emission centered at 810 nm, indicating communication between these states and the ruthenium based ^{3}MLCT emitting state. Energy transfer from the iridium based to the ruthenium based moiety is efficient, Φ_{ISC} and $\Phi_{IC} = 1$. This is shown schematically in Figure 41.

Both $[(tpy)Ru(tpp)Ru(tpp)]^{4+}$ and $[(tpy)Os(tpp)Ru(tpp)]^{4+}$ emit in fluid solution at room temperature. The complexes $[(tpy)Ru(tpp)RuCl_3]^+$ and $[(tpy)Os(tpp)RuCl_3]^+$ may display red shifted emissions beyond the detection limits of our system. The lack of an emission from the (tpy)M^{II}(tpp) unit in the $[(tpy)M(tpp)RuCl_3]^+$ systems indicates efficient quenching of this M $\rightarrow$ tpp charge transfer state by the (tpp)$Ru^{II}Cl_3$ moiety. This again indicates a relatively strong coupling through the tpp bridge.

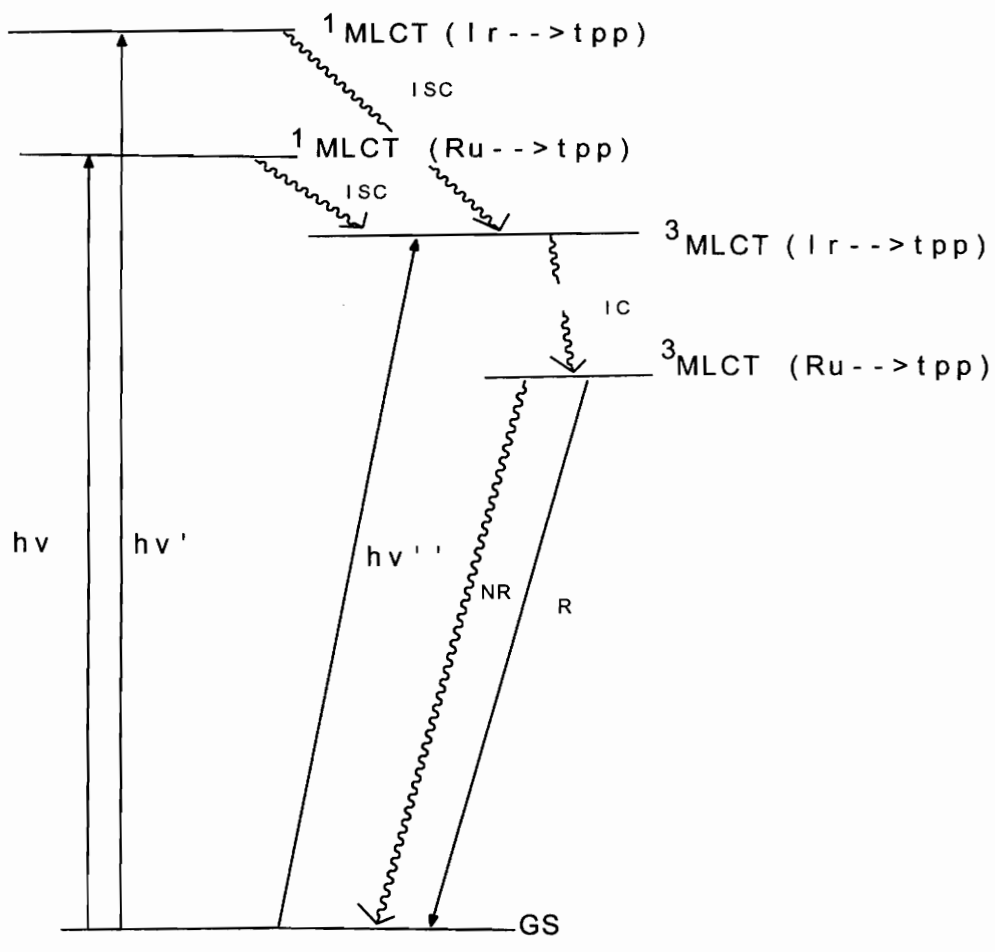Figure 41. Jablonski Diagram for [(tpy)Ru(tpp)IrCl$_3$]$^{2+}$.

Formation of the bimetallic [(tpy)Ru(tpp)Ru(tpp)]$^{4+}$ leads to a system that emits at 833 nm with a lifetime of 100 ns. This is a very long excited state lifetime for a polymetallic polyazine ruthenium complex. Considering the decrease in the energy gap relative to [Ru(tpy)(tpp)]$^{2+}$ one would expect that the emissive lifetime for [(tpy)Ru(tpp)Ru(tpp)]$^{4+}$ to decrease relative to [Ru(tpy)(tpp)]$^{2+}$. In fact, this bimetallic system has a longer lifetime than the [Ru(tpy)(tpp)]$^{2+}$ monometallic at room temperature. In Table X (page 134) the excited-state lifetime of [(tpy)Ru(tpp)Ru(tpp)]$^{4+}$ and [Ru(tpy)(tpp)]$^{2+}$ at room temperature and 77 K is given. As predicted by the energy gap law, at 77 K the lifetime of the bimetallic complex is shorter than the monometallic complex consistent with the decrease in the energy of the excited-state. In this bimetallic complex, the MLCT state is greatly stabilized relative to the ligand field state at room temperature. This prevents thermal population of the LF state at room temperature in the bimetallic complex. This results in the lifetime of the chromophore in the bimetallic complex to be enhanced relative to the monometallic [Ru(tpy)(tpp)]$^{2+}$ when measured at room temperature. This is unprecedented in the literature. At 77 K, thermal population of the ligand field state does not occur, hence the "normal" trend of a bimetallic system having a shorter lifetime than the monometallic analog is observed. This is shown schematically in Figure 42.

The osmium based bimetallic [(tpy)Os(tpp)Ru(tpp)]$^{4+}$ emits from an Os based ^{3}MLCT state with a λ_{max}^{em} of 820 nm and a lifetime of 120 ns. The osmium based chromophores are not expected to have low lying LF states. Hence formation of a bimetallic should result in the normal trend of a decreased lifetime due to a decrease in the energy gap between the ground and excited state. This is observed as the excited state lifetime is decreased from 260 to 120 ns upon bimetallic formation. The 120 ns excited state lifetime for an osmium polymetallic complex is far in excess of any systems studied to date.[25,43,46] Table X (page 134) summarizes the results of the excited-state lifetime studies at room temperature and 77 K. The lifetime of the [(tpy)Os(tpp)Ru(tpp)]$^{4+}$ bimetallic complex is increased to 460 ns at 77 K. The Ru/Ru analog has an excited-state lifetime of 480 ns. The electronic absorption spectroscopic
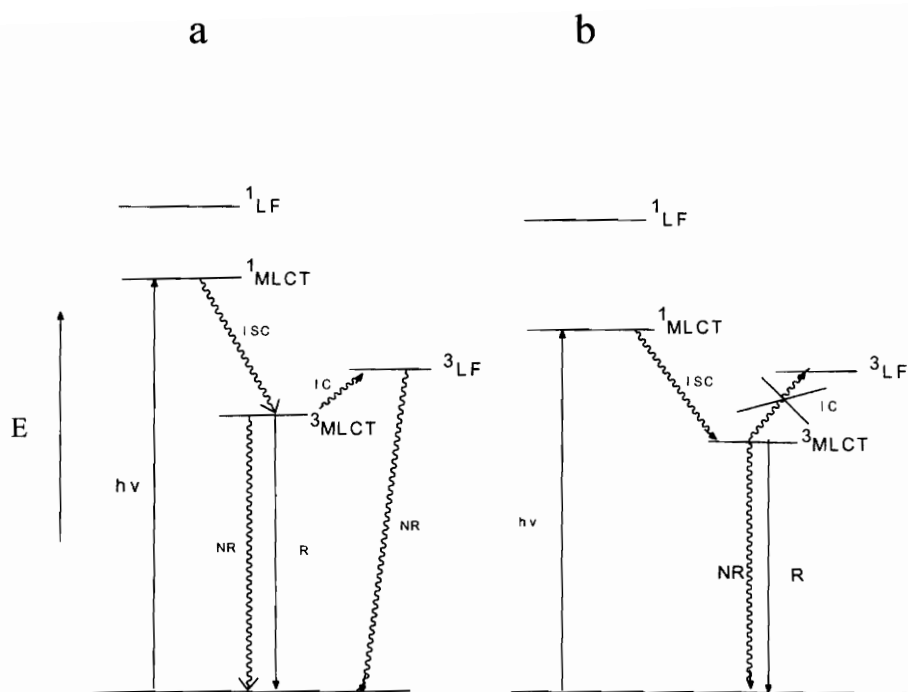
Figure 42. Jablonski Diagram for (a) $[Ru(tpy)(tpp)]^{2+}$ and (b) $[(tpy)M(tpp)Ru(tpp)]^{4+}$.

results state that the lowest energy absorbance for both the Ru/Ru and Os/Ru complexes is similar in energy, 548 nm versus 546 nm, respectively. The emission energy for these complexes is also comparable, 833 and 820 nm, with room temperature lifetimes of 100 and 120 ns respectively. The similarities of these properties is unusual and seems to be unique to these tpp bridged systems.

X-ray Crystallography

The determination and analysis of the x-ray crystal structure was performed by Dr. Brian Scott with the assistance of Dr. Roger Willett and has been reported previously.[55] The iridium monometallic fragment, Ir(tpp)Cl$_3$, forms large blood-red crystals upon slow evaporation of a dimethylformamide solution. A diagram of Ir(tpp)Cl$_3$ showing thermal ellipsoids is given in Figure 43. The iridium atom has a distorted octahedral geometry. The equatorial plane is defined by the three nitrogens of the tpp ligand and a chlorine atom. The other two chlorine atoms occupy the axial positions. An axis of 2-fold symmetry bisects the tpp ligand, the Ir atom, and the equatorial Cl atom. Bond lengths and angles are given in Table XIII. As can be seen from the bond distances and angles, the geometrical constraints of the tpp ligand cause a distortion from octahedral coordination. The "bite" angle of tridentate diimine ligands, such as tpp, gives rise to bond angles less than ideal as illustrated by the N(1)-Ir-N(11) angle of 80.8(2)$^\circ$ and differing metal to nitrogen bond distances within the tpp ligand.

Examination of the conformation of the coordinated tpp ligand within the Ir(tpp)Cl$_3$ framework shows large distortions from planarity. The four pyridine rings are not expected to be coplanar due to steric repulsions that would be present between ring hydrogens on the 3-pyridyl positions. For this reason, it is somewhat surprising that the two coordinated rings are 33.4° out-of-plane with respect to the pyrazine ring in tpp. This can be seen in Appendix Figure A-X (page 179). In addition, the pyrazine ring is expected to have marked effects on the metal-metal communication in the polymetallic

Table XIII. Selected Bond Lengths and Bond Angles for Ir(tpp)Cl$_3$ (where tpp = 2,3,5,6-tetrakis(2-pyridyl)pyrazine).

<u>Bond Lengths (Å)</u>

Ir-Cl(1)	2.349(2)	Ir-N(1)	1.917(8)
Ir-Cl(1A)	2.349(2)	Ir-N(11)	2.032(5)
IrCl(2)	2.363(3)	Ir-N(11A)	2.032(5)

<u>Bond Angles (deg)</u>

Cl(1)-Ir-Cl(2)	90.1(1)	Cl(1)-Ir-N(1)	89.9(1)
Cl(2)-Ir-N(1)	180.0(1)	Cl(1)-Ir-N(11)	90.4(1)
Cl(2)-Ir-(N11)	99.2(2)	N(1)-Ir-N(11)	80.8(2)
Cl(1)-Ir-Cl(1A)	180.0(2)	Cl(2)-Ir-Cl(1A)	90.1(1)
N(1)-Ir-Cl(1A)	89.9(1)	N(11)-Ir-Cl(1A)	89.6(1)
Cl(1)-Ir-N(11A)	89.6(1)	Cl(2)-Ir-N(11A)	99.2(2)
N(1)-Ir-N(11A)	80.8(2)	N(11)-Ir-N(11A)	161.5(3)
Cl(1A)-Ir-N(11A)	90.4(1)		
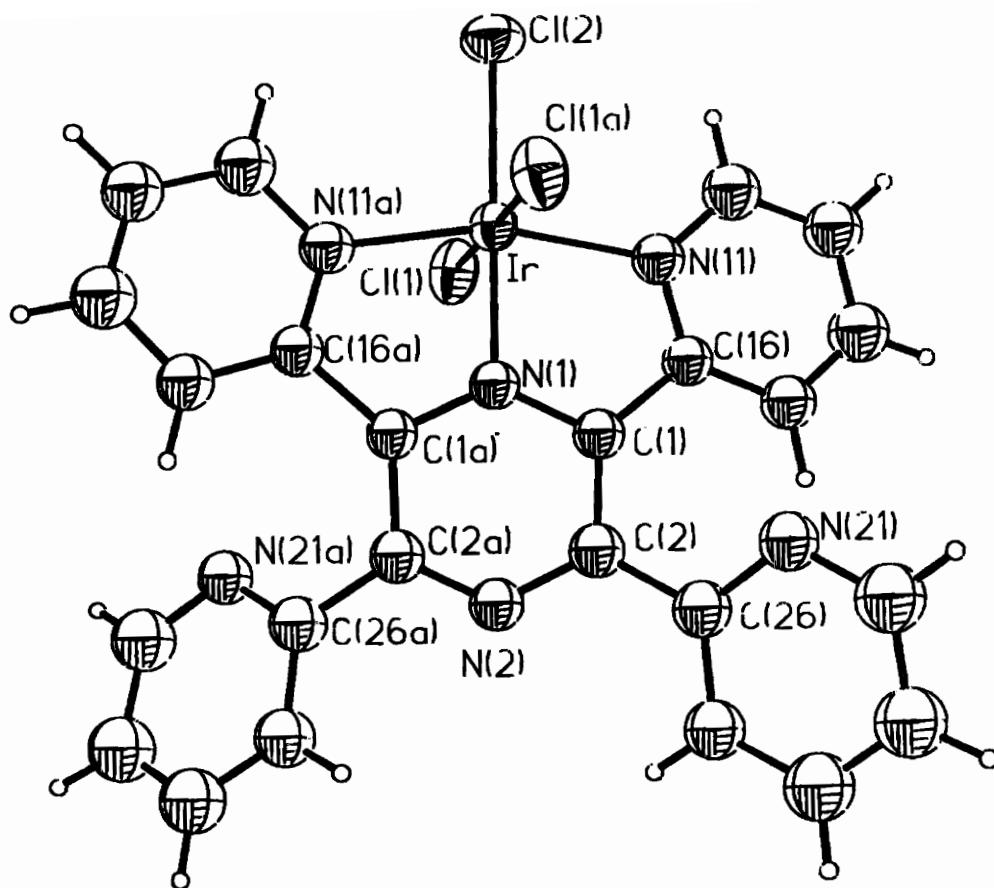
Figure 43. Diagram of Ir(tpp)Cl₃ showing thermal ellipsoids
(50 % thermal ellipsoids and where tpp = 2,3,5,6-tetrakis(2-
pyridyl)pyrazine).

systems bridged using tpp.

Catalysis

It has been shown that complexes of the type $[Rh(BL)_2Br_2]^+$ and $[Ir(BL)_2Cl_2]^+$ are catalytic for the reduction of CO_2 to formate (where BL = bpm, dpp, dpq, and dpb).[37] These systems have low current efficiencies of approximately 40 %. Reduction of the iridium metal from Ir(III) to Ir(I) was found to be necessary to activate these complexes towards reduction of CO_2. This iridium reduction is followed by the loss of the two chloride ligands.

In the cyclic voltammogram of $[(tpy)Ru(tpp)IrCl_3]^{2+}$ shown on page 83, and summarized in Table V, page 81, there are two reversible reductions that have been assigned as sequential reductions of the tpp bridging ligand and an irreversible reduction that can be attributed to the Ir(III)/Ir(I) reduction. The potential where this iridium reduction occurs is taken as the electrolysis potential for the catalysis experiment. Performing a cyclic voltammogram after purging the solution with CO_2 lead to an increase in the cathodic current beginning at - 1.30 V, the region of the Ir(III)/Ir(I) couple. This is consistent with the complex being catalytic toward the reduction of CO_2. This was verified by performing the electrocatalytic experiment in which the entire solution was reduced to -1.60 V, a potential after the iridium reduction.

In collaboration with Girlie Nallas, controlled potential electrolysis was carried out for two hours. In the course of the experiment the color of the catalyst solution changed from dark purple to brown. From the current-time plot it appears that the catalyst is still active beyond two hours since the electrocatalytic current continues to drop. The drop in current results from the completion of the electrocatalysis of the complex. The charge-time plot from electrolysis showed a linear increase of the amount of charge passed with time. The bimetallic catalyzed the reduction of carbon dioxide to formate with a current efficiency of 60.7 % and turnover number of 12 and to carbon monoxide with a current efficiency of 34.8 % and turnover number of 7.

The formation of carbon monoxide is accompanied by water production. The production of formate from CO_2 reduction typically requires the aqueous solvents.[87] Meyer and coworkers have reported that the electrocatalytic reduction of CO_2 by cis-$[Os(bpy)_2(CO)H](PF_6)$ produces CO under anhydrous conditions and formate in the presence of water. It appears that the carbon monoxide produced in our system shifts to formate as water is produced by the system. In the presence of water, the competitive reduction to produce formate limits the formation of CO. A similar effect has been observed by Nallas and Brewer on systems of the type $\{[(bpy)_2Ru(BL)]_2IrCl_2\}^{5+}$ where (BL = dpq and dpb).[74] This could account for the higher current efficiency for formate versus carbon monoxide in this system.

Chapter V
Conclusions and Future Work

The work reported in this thesis involves the synthesis of a series of monometallic and polymetallic complexes incorporating the tridentate bridging ligand tpp as well as an investigation of their ground and excited state properties. Systematic variation of the ligands coordinated to the metal center, variation of the metal center, incorporation of a covalently attached electron acceptor and the formation of bimetallic systems have allowed for a wide variety of complexes to be studied. The preparation of these systems and investigation of the spectroscopic, electrochemical, spectroelectrochemical, and photochemical properties of these systems allows for the understanding of the ground and excited state properties of metal complexes incorporating tpp. The use of the tridentate polypyridyl ligands such as tpy and tpp eliminates the Δ and Λ stereoisomers possible in synthesizing metal complexes incorporating bidentate ligands. The use of tridentate ligands will control the stereochemistry in multimetallic systems incorporating the new monometallic light absorbers.

The procedures for the synthesis of the monometallic and bimetallic complexes has been discussed. The first step in the synthesis of all complexes is the coordination of the terminal ligand tpy or bpy to the ruthenium or osmium metal center assembling the terminal part of the molecule. This is followed by the addition of the bridging ligand required to synthesize the desired material. The bridging ligands used in this study are the tridentate ligand tpp and the bidentate ligands dpp, dpq, and dpb. To synthesize the complexes containing a covalently attached electron acceptor, methylation of one of the remote nitrogens on the tpp ligand forms a covalently coupled viologen. In synthesizing the bimetallic complexes a building block approach was used. After the synthesis of the monometallic complexes $[Ru(tpy)(tpp)]^{2+}$ and $[Os(tpy)(tpp)]^{2+}$, the next step was the attachment of a $RuCl_3$ moiety to form bimetallic complexes of the type $[(tpy)M(tpp)RuCl_3]^+$ where M is either Ru(II) to Os(II). The attachment of a second tpp ligand was accomplished replacing the chlorides making the $[(tpy)M(tpp)Ru(tpp)]^{4+}$

complexes. The stepwise approach to the synthesis of these bimetallic complexes will allow for the systematic design of supramolecular complexes of variable but known length.

Two types of synthetically useful bimetallic complexes have been synthesized, $[(tpy)M(tpp)RuCl_3]^+$ and $[(tpy)M(tpp)Ru(tpp)]^{4+}$ where M = Ru(II) or Os(II). In the first set of complexes it is found that the HOMO is based on the $Ru^{II}Cl_3$ moiety and the LUMO is based on the bridging tpp ligand. In the second set of complexes, the LUMO is still localized on the bridging tpp ligand whereas the HOMO is now localized on the metal being varied, either ruthenium or osmium that is coordinated to both tpp and tpy. The synthetic methodologies developed in this study will allow for the construction of larger polymetallic systems of this type. Both $[(tpy)Ru(tpp)Ru(tpp)]^{4+}$ and $[(tpy)Os(tpp)Ru(tpp)]^{4+}$ emit in fluid solution at room temperature and are quite unique in the class of polymetallic polyazine bridged complexes in that they have lifetimes ca. 100 ns. The long lifetimes of these chromophores make them extremely useful components in the design of supramolecular complexes. These studies indicate that the tpp ligand holds great promise by providing efficient coupling of the bridged metal center within a stereochemically defined framework while maintaining a long-lived excited state. The complexes of the type $[(tpy)M(tpp)Ru(tpp)]^{4+}$ contain a tpp ligand possessing three remote nitrogens. This remote site of coordination could be utilized to incorporate these unique long-lived polymetallic chromophores into molecular devices of interest. In addition, these systems could be methylated and would then contain a covalently attached electron accepting moiety and could be applicable in the area of photoinitiated electron transfer. Because of the increased separation distance, the rate of charge recombination of the charge separated state will decrease.

The mixed-metal bimetallic system $[(tpy)Ru(tpp)IrCl_3]^{2+}$ is an interesting system to study. The lowest lying absorbance is iridium based whereas the lowest lying emission is ruthenium based. It appears from the emission studies that the tpp ligand provides excellent communication between MLCT states centered on different metals. This complex undergoes intramolecular energy transfer upon excitation. Electrocatalysis

studies have shown that this complex is catalytic towards the reduction of CO_2 to formate and carbon monoxide. This complex could also be photocatalytic towards the reduction of CO_2. In addition to this complex, the rhodium analog, $[(tpy)Ru(tpp)RhCl_3]^{2+}$ should also possess similar properties and possibly be catalytic towards CO_2 reduction at lower potentials. Based on the studies performed previously on rhodium and iridium monometallic complexes, both types of complexes are catalytic with the rhodium analogs having a higher current efficiency for the production of formate.[37] Because of the energy of the orbitals of rhodium compared to iridium, this complex should contain the rhodium reduction at a more positive potential than the iridium complex. Thus, reduction of CO_2 using this Ru/Rh mixed metal complex should occur at lower potentials and be more efficient for the production of formate.

The preparation of the ruthenium complexes containing a covalently attached electron acceptor has been accomplished via the methylation of the remote nitrogen on the tpp ligand. The methylation of tpp leads to perturbations of the electrochemical and spectroscopic properties. The electronic absorption spectroscopy upon methylation remains the same as the nonmethylated analogs and lowest energy transition is assigned as a ^{1}MLCT Ru(dπ) $\rightarrow$ tpp(π*) transition localized on the pyrazine ring of the ligand. This excited state is emissive in fluid solution at room temperature. The experimental results are inconclusive as to whether the MLCT emission is quenched in the methylated systems due to intramolecular electron transfer to the viologen acceptor. A possible explanation would be that the lower energy emission in the methylated systems relative to the nonmethylated systems results from the lowering of the ^{3}MLCT energy upon methylation. This would have an increased k_{NR} which would decrease the intensity of the band as well as the lifetime of the complex. Further investigation into these types of complexes is warranted. The synthesis of a planar tpp type ligand with a N site available for methylation would eliminate rotation of the viologen ring. This could facilitate electron transfer. Larger polymetallic complexes can be constructed which incorporate this Metpp ligand by substitution of the remote tpy or bpy with a polyazine bridging ligand. By synthesizing larger, multimetallic complexes with more remote oxidizable

moieties, the rate of charge recombination in the photogenerated charge separated state will be decreased and the charge separation distance will be increased. The presence of the coordinated acetonitrile ligand facilitates synthetic modification of these systems. Replacement of this ligand with an electron donor would result in the synthesis of a monometallic molecular triad complex consisting of an electron donor, light absorbing metal center, and electron acceptor covalently linked. Polymetallic complexes using this same principle would also be useful in photoinitiated electron transfer processes.

In the series of complexes of the type $[Ru(tpy)(BL)Cl]^+$ and $[Ru(tpy)(BL)(py)]^{2+}$ (where BL = dpp, dpq, or dpb) that were synthesized, $[Ru(tpy)(dpp)Cl]^+$ and all the $[Ru(tpy)(BL)(py)]^{2+}$ complexes emit in fluid solution at room temperature. These complexes clearly show that ruthenium terpyridine systems can be designed which have reasonable lifetimes. It has been illustrated that the chloride ligand provides a site for synthetic modification within this framework. This establishes that covalent attachment of electron donors or acceptors is possible. These substituted complexes can then be used in the synthesis of multimetallic systems capable of intramolecular electron transfer. This is currently being performed in this laboratory.

In summary, the building block approach to the design of bimetallic complexes has resulted in the synthesis of bimetallic complexes of the form $[(tpy)M(tpp)Ru(tpp)]^{4+}$ (where M = Ru or Os) with long-lived excited state lifetimes. In the course of synthesizing these bimetallic complexes, the various monometallic and bimetallic precursor complexes have been investigated giving insight into the ground and excited state properties of these types of complexes. This new understanding can be applied to the design of supramolecular complexes where the different components have specific functions. These complexes could have applications in the area of photoinitiated charge separation and catalysis of CO_2 reduction.

References

(1) Drago, R. S. *Physical Methods For Chemists*, 2nd ed., W. B. Saunders Company, Philadelphia, **1992**.

(2) Cotton, F. A.; Wilkinson, G.; Gaus, P. L. *Basic Inorganic Chemistry*, John Wiley & Sons, New York, **1987**.

(3) Jolly, W. L. *Modern Inorganic Chemistry*, McGraw-Hill Book Company, New York, **1976**.

(4) Huhey, H. E. *Inorganic Chemistry*, 3rd ed., Harper & Row, New York, **1983**.

(5) Wehry, E. L. *Physical Methods of Chemistry*, 2nd ed., Vol. VIII, Rossiter, B. W.; Baetzold, R. R., eds., John Wiley & Sons, New York, **1993**.

(6) (a) Kavarnos, G. J. *Fundamentals of Photoinduced Electron Transfer*, VCH Publishers, New York, **1993**. (b) Kavarnos, G. J. *Top. Curr. Chem.* **1990**, *156*, 21.

(7) Purcell, K. F.; Kotz, J. C. *Inorganic Chemistry*, W. B. Saunders Company, Philadelphia, **1977**.

(8) (a) Balzani, V.; Carassiti, V. *Photochemistry of Coordination Compounds*, Academic Press, London, **1970**. (b) Balzani, V.; Boletta, F.; Gandolti, M. T.; Maestri, M. *Top. Curr. Chem.* **1978**, *75*, 1. (c) Juris, A.; Balzani, V.; Campagna, S.; Denti, G.; Serroni, S.; Frei, G.; Gudel,U. *Inorg. Chem.* **1994**, *33*, 1491.

(9) Gilbert, A. and Bagott, J. *Essentials of Molecular Photochemistry,* CRC Press, Boca Raton, **1991**.

(10) Demas, J. N. *J. Chem. Ed.* **1983**, *60*, 797.

(11) Horvath, O. and Stevenson, K. L. *Charge Transfer Photochemistry of Coordination Compounds*, VCH Publishers, Inc., New York, **1993**.

(12) Adamson, A. W.; Fleischauer, P. D. *Concepts of Inorganic Photochemistry*, Wiley Interscience, New York, **1975**.

(13) Fleischauer, P. D.; Adamson, A. W.; Sartori, G. *Prog. Inorg. Chem.* **1972**, *17*, 1.

(14) (a) Juris, A.; Balzani, V.; Barigelletti, F.; Campagna, S.; Balser, P.; von Zewelsky, A. *Coord. Chem. Rev.* **1988**, *84*, 85. (b) Denti, G.; Serroni, S.; Campagna, S.; Ricevuto, V.; Balzani, V. *Coord. Chem. Rev.* **1991**, *111*, 227. (c) Balzani, V.; Ballardini, R.; Bolletta, F.; Gandolfi, M. T.; Juris, A.; Maestri, M.; Manfrin, M. F.; Moggi, L.; Sabbatini, N. *Coord. Chem. Rev.* **1993**, *125*, 75.

(15) Balzani, V.; Boletta, F.; Gandolti, M. T.; Maestri, M. *Top. Curr. Chem.* **1978**, *75*, 1.

(16) Young, R. C.; Nagle, J. K.; Meyer, T. J.; Whitten, D. G. *J. Am. Chem. Soc.* **1978**, *100*, 4773.

(17) Brown, G. M.; Chan, S. F.; Creutz, C.; Scharz, H. A.; Sutin, N. *J. Am. Chem. Soc.* **1979**, *101*, 7638.

(18) Roth, H. D. *Top. Curr. Chem.* **1990**, *156*, 1.

(19) Wrighton, M.; Markham, J. *J. Phys. Chem.* **1973**, *77*, 3042.

(20) Curtis, J. C.; Bernstein, J. S.; Schmehl, R. H.; Meyer, T. J. *Chem. Phys. Letts*. **1981**, *81*, 48.

(21) Sutin, N.; Creutz, C. *J. Chem. Ed.* **1983**, *60*, 814.

(22) Demas, J. N.; DeGraff, B. A. *Anal. Chem.* **1991**, *63*, 829.

(23) Kober, E. M.; Caspar, J. V.; Sullivan, B. P.; Meyer, T. J. *Inorg. Chem.* **1988**, *27*, 4587.

(24) Denti, G.; Serroni, S.; Sabatino, L.; Ciano, M.; Ricevuto, V.; Campagna, S. *Gazz. Chim. Ital.* **1991**, *121*, 37.

(25) Kalyanasundaram, K. *Photochemistry of Polypyridine and Porphyrin Complexes*; Academic Press: London, **1992**.

(26) Gafney, H. D.; Adamson, A. W. *J. Am. Chem. Soc.* **1972**, *94*, 8238.

(27) (a) Bock, C. R.; Meyer, T. J.; Whitten, D. G. *J. Am. Chem. Soc.* **1974**, *96*, 4710. (b) Bock, C. R.; Connor, J. A.; Gutierrez, A. R.; Meyer, T. J.; Whitten, D. G.; Sullivan, B. P.; Nagle, J. K. *J. Am. Chem. Soc.* **1979**, *101*, 4815.

(28) Navon, G.; Sutin, N. *Inorg. Chem.* **1974**, *13*, 2159.

(29) Laurence, G. A; Balzani, V. *Inorg. Chem.* **1974**, *13*, 2936.

(30) (a) Demas, J. N.; Crosby, G. A. *J. Am. Chem. Soc.* **1971**, *93*, 2841. (b) Demas, J. N.; Taylor, D. G. *Inorg. Chem.* **1979**, *18*, 3177. (c) Demas, J. N.; Adamson, A. W. *J. Am. Chem. Soc.* **1972**, *94*, 7587.

(31) Bolletta, F.; Juris, A.; Maestri, M.; Sandrini, D. *Inorg. Chim. Acta* **1980**, *44*, L175.

(32) Sutin, N.; Creutz, C. *Adv. Chem. Ser.* **1978**, *168*, 1.

(33) Lin, C. T.; Bottcher, W.; Chou, M.; Creutz, C.; Sutin, N. *J. Am. Chem. Soc.* **1976**, *98*, 6536.

(34) Vogler, L. M.; Franco, C.; Jones, S. W.; Brewer, K. J. *Inorg. Chim. Acta* **1994**, *221*, 55.

(35) Richter, M. M.; Brewer, K. J. *Inorg. Chim. Acta* **1991**, *180*, 125.

(36) Molnar, S. M.; Neville, K. R.; Jensen, G. E.; Brewer, K. J. *Inorg. Chim. Acta* **1993**, *206*, 69.

(37) Rasmussen, S. C.; Richter, M. M.; Yi, E.; Place, H.; Brewer, K. J. *Inorg. Chem.* **1990**, *29*, 3926.

(38) (a) Denti, G.; Campagna, S.; Sabatino, L.; Scolastica, S.; Ciano, M.; Balzani, V. *Inorg. Chem.* **1990**, *29,* 4750. (b) Barigelletti, F.; DeCola, L.; Balzani, V.; Hage, R.; Haasnoot, J. G.; Reedijk, J.; Vos, J. G. *Inorg. Chem.* **1989**, *28*, 4344. (c) Serroni, S.; Juris, A.; Campagna, S.; Venturi, M.; Denti, G.; Balzani, V. *J. Am. Chem. Soc.* **1994**, *116*, 9086. (d) Denti, G.; Campagna, S.; Serroni, G.; Ciano, M.; Balzani, V. *J. Am. Chem. Soc.* **1992**, *114*, 2944. (e) Denti, G.; Serroni, S.; Campagna, S.; Ricevuto, V.; Juris, A.; Ciano, M.; Balzani, V. *Inorg. Chim. Acta* **1992**, *98*, 507. (e)

Campagna, S.; Denti, G.; Serroni, S.; Ciano, M.; Juris, A.; Balzani, V. *Inorg. Chem.* **1992**, *31*, 2982.

(39) Baiano, J. A.; Carlson, D. L.; Wolosh, G. M.; DeJesus, D. E.; Knowles, C. F.; Szabo, E. G.; Murphy, W. R. *Inorg. Chem.* **1990**, *29*, 2327.

(40) Brauenstein, C. H.; Baker, A. D.; Strekas, T. C.; Gafney, H. D. *Inorg. Chem.* **1984**, *23*, 857.

(41) (a) Rillema, D. P.; Mack, K. B. *Inorg. Chem.* **1982**, *21*, 3849. (b) Rillema, D. P.; Callahan, R. W.; Mack, K. B. *Inorg. Chem.* **1982**, *21*, 2589.

(42) Wallace, A. W.; Murphy, Jr., W. R.; Petersen, J. D. *Inorg. Chim. Acta.* **1989**, 166, 47.

(43) Kalyanasundaram, K. Nazeeruddin, Md. K. *Chem. Phys. Lett.* **1989**, *158*, 45.

(44) Fuchs, Y.; Lofters, S.; Dieter, T.; Shi, W.; Morgan, R.; Strekas, T. C.; Gafney, H. D.; Baker, A. D. *J. Am. Chem. Soc.* **1987**, *109*, 2691.

(45) (a) Meyer, T. J. *Acc. Chem. Res.* **1978**, *11*, 94. (b) Meyer, T. J. *J. Am. Chem. Soc.* **1982**, *104*, 630.

(46) (a) Richter, M. M.; Brewer, K. J. *Inorg. Chem.* **1993**, *32*, 7827. (b) **1992**, *31*, 1594. (d) **1993**, *32*, 5762.

(47) (a) Molnar, S. M.; Jensen, G. E.; Vogler, L. M.; Jones, S. W.; Laverman, L.; Bridgewater, J. S.; Richter, M. M.; Brewer, K. J. *J. Photochem. Photobiol. A: Chem.* **1994**, *80*, 315. (b) Bridgewater, J. S.; Vogler, L. M.; Molnar, S. M.; Brewer, K. J. *Inorg. Chem. Acta* **1993**, *208*, 179.

(48) Pfeiffer, F. R.; Case, F. H. *J. Org. Chem.* **1966**, *31*, 3384.

(49) (a) Ruminski, R. R.; Letner, C. *Inorg. Chim. Acta* **1989**, *162*, 175. (b) Ruminski, R.; Kiplinger, J.; Cockroft, T.; Chase, C. *Inorg. Chem.* **1989**, *28*, 370.

(50) Petersen, J. D. in *Supramolecular Photochemistry,* NATO ASI Series **1987**, 214, 135 and references therein.

(51) Winkler, J. R.; Netzel, T. L.; Creutz, C.; Sutin, N. *J. Am. Chem. Soc.* **1987**, *109*, 2381.

(52) Young, R. C.; Nagle, J. K.; Meyer, T. J.; Whitten, D. G. *J. Am. Chem. Soc.* **1978**, *100*, 4773.

(53) (a) Berger, R. M.; McMillin, D. R. *Inorg. Chem.* **1988**, *109*, 2381. (b) Berger, R. M.; McMillin, D. R. *Inorg. Chem.* **1988**, *27*, 4245.

(54) (a) Hecker, C. R.; Gushurst, A. K. I.; McMillin, D. R. *Inorg. Chem.* **1991**, *30*, 538. (b) Phifer, C. C.; McMillin, D. R. *Inorg. Chem.* **1986**, *25*, 1329.

(55) Vogler, L. M.; Scott, B.; Brewer, K. J. *Inorg. Chem.* **1993**, *32*, 898.

(56) Brewer, R. G.; Jensen, G. E.; Brewer, K. J. *Inorg. Chem.* **1994**, *33*, 124.

(57) (a) Sauvage J. P.; Collin, J. P.; Chambron, J. C.; Guillerez, S.; Coudret, C. *Coord. Chem. Rev.* **1994**, 993. (b) Barigelletti, F.; Flamigni, L.; Balzani, V.; Collin, J. P.; Sauvage, J. P.; Sour, A.; Constable, E. C.; Cargill Thompson, A. M. W. *J. Chem. Soc., Chem. Commun.* **1993**, 942. (c) Collin, J. P.; Laine, P.; Launay, J. P.; Sour, A. *J. Chem. Soc., Chem. Commun.* **1993**, 434. (d) Constable, E. C.; Cargill Thompson, A. M. W. *J. Chem. Soc. Dalton Trans.* **1992**, 3467.

(58) Thummel, R. P.; Chirayil, S. *Inorg. Chim. Acta* 1988, 154, 77.

(59) Arana, C. R.; Abruña, H. D. *Inorg. Chem.* **1993**, *32*, 194.

(60) Lumpkin, R. S.; Carlson, D. L.; Satpathy, A. K.; Petersen, J. D.; Murphy, N. R. *J. Am. Chem. Soc.* **1995** manuscript in preparation.

(61) (a) Brandt, W. W.; Dweyer, F. P.; Gyarfas, E. C. *Chem. Rev.* **1954**, 960. (b) Constable, E. C. *Adv. Inorg. Chem. Radiochem.* **1986**, *30*, 69.

(62) Goodwin, H. A.; Lions, F. *J. Am. Chem. Soc.* **1959**, *81*, 6415.

(63) Escuer, A.; Comas, T.; Ribas, J.; Vicente, R.; Solans, X.; Zanchini, C.; Gatteschi, D. *Inorg. Chim. Acta* **1989**, *162*, 97.

(64) Buu-Hoi, N. P.; Saint-Ruf, G. *J. Chem. Soc.* **1961**, 2259.

(65) Sullivan, B. P.; Calvert, J. M.; Meyer, T. M. *Inorg. Chem.* **1980**, *19*, 1404.

(66) Buckingham, D. A.; Dweyer, F. P.; Sargeson, A. M. *Aust. J. Chem.* **1961**, *14*, 250.

(67) Krause, R. A. *Inorg. Chim. Acta* **1977**, *22*, 209.

(68) Serroni, S.; Denti, G. *Inorg. Chem.* **1992**, *31*, 4251.

(69) Barigelletti, F.; Flamigni, L.; Balzani, V.; Collin, J. P.; Sauvage, J. P.; Sour, A.; Constable, E. C.; Cargill Thompson, A. M. W. *J. Am. Chem. Soc.* **1994**, *116*, 7692.

(70) (a) Marcus, R. A. *J. Chem. Phys.* **1956**, *24*, 966. (b) Marcus, R. A. *Discuss. Faraday Soc.* **1960**, *29*, 21. (c) Siders, P.; Marcus, R. A. *J. Am. Chem. Soc.* **1981**, *103*, 748. (d) Suppan, P. *Top. Curr. Chem.* **1992**, *163*, 95.

(71) (a) Hush, N. S. *Coord. Chem. Rev.* **1985**, *64*, 135. (b) Hush. N. S. *Trans. Faraday Soc.* **1961**, *57*, 557. (c) Hush, N. S. J. Chem. Phys. 1958, 28, 962.

(72) (a) Young, R. C.; Meyer, T. J.; Whitten, D. G. *J. Am. Chem, Soc.* **1975**, *97*, 4781. (b) Chen, P.; Curray, M.; Meyer, T. J. *Inorg. Chem.* **1989**, *28*, 2271. (c) Olmsted, J.; McClanahan, S. F.; Danielson, E.; Younathan, J. N.; Meyer, T. J. *J. Am. Chem. Soc.* **1987**, *109*, 3297. (d) Rillema, D. P.; Nagle, J. K.; Barringer, L. F.; Meyer, T. J. *J. Am. Chem. Soc.* **1981**, *103*, 56. (e) Danielson, E.; Elliott, C. M.; Merkert, J. W.; Meyer, T. J. *J. Am. Chem. Soc.* **1987**, *109*, 2519. (f) Nagle, J. K.; Berstein, J. S.; Young, R. C.; Meyer, T. J. *Inorg. Chem.* **1981**, *20*, 1760. (g) Jones, W. E.; Bignozzi, C. A.; Chen, P.; Meyer, T. J. *Inorg. Chem.* **1993**, *32*, 1167. (h) Younathan, J. N.; Jones, W. E.; Meyer, T. J. *J. Phys. Chem.* **1991,** *95*, 488. (i) Allen, G. H.; White, R. P.; Rillema, D. P.; Meyer, T. J. *J. Am. Chem. Soc.* **1984**, *106*, 2613.

(73) (a) Collin, J. P.; Guillerez, S.; Sauvage, J. P.; Barigelletti, F.; Flamigni, L.; DeCola, L.; Balzani, V. *Coord. Chem. Rev.* **1991**, *111*, 291. (b) Collin, J. P.; Guillerez, S.; Sauvage, J. P.; Barigelletti, F.; Flamigni, L.; Balzani, V. *Inorg. Chem.* **1991**, *30*, 4230. (c) Collin, J. P.; Guillerez, S.; Sauvage, J. P.; Barigelletti, F.; DeCola, L.;

Flamigni, L.; Balzani, V. *Inorg. Chem.* **1992**, *31*, 4112. (d) Sauvage, J. P.; Collin, J. P.; Chambion, J. C.; Guillerez, S.; Coudret, C. *Chem. Rev.* **1994**, *94*, 995. (e) Collin, J. P.; Guillerez, S.; Sauvage, J. P. *J. Chem. Soc., Chem. Commun.* **1989**, 776.

(74) Nallas, G. N. A.; Brewer, K. J. Inorg. Chem. 1995, submitted for publication

(75) (a) Crystallography performed at Washington State University. Sheldrick, G. SHELXTL; Nicolet Analytical instruments: Madison, WI, 1986. (b) Campana, C. F.; Shepard, D. F.; Litchman, W. M. *Inorg. Chem.* **1981**, *20*, 4039.

(76) (a) DeArmond, K.; Hillis, J. *J. Chem. Phys.* **1971**, *54*, 2247. (b) Kahl, J. L.; Hanck, W.; DeArmond, M. K. *J. Phys. Chem.* **1978**, *82*, 540.

(77) (a) Albinati, A.; Jiang, Q.; Ruegger, H.; Vananzi, L. M. *Inorg. Chem.* **1993**, *32*, 4940.

(78) Hallman, P. S.; Stephenson, T. A.; Wilkinson, G. *Inorg. Syn.* **1970**, *12*, 238.

(79) Caspar, J. V.; Meyer, T. J. *J. Am. Chem. Soc.* **1983**, *105*, 5583.

(80) Jensen, G. E. Ph.D. Dissertation, Virginia Polytechnic Institute and State University, in preparation.

(81) Gagne, R. R.; Koval, C. A.; Lisensky, G. C. *Inorg. Chem.* **1980**, *19*, 2855.

(82) Berger, R. M. *Inorg. Chem.* **1990**, *29*, 1920.

(83) (a) Wang, Y.; Schanze, K. S. *Chem. Phys.* **1993**, *176*, 305. (b) Schanze, K. S.; MacQueen, D. B.; Perkins, T. A.; Cabana, L. A. *Coord. Chem. Rev.* **1993**, *122*, 63.

(c) MacQueen, D. B.; Schanze, K. S. *J. Am. Chem. Soc.* **1991**, *113*, 7470. (d) Schanze, K. S.; Cabana, L. A. *J. Phys. Chem.* **1990**, *94*, 2740.

(84) (a) Dodsworth, E. S.; Lever, A. B. P. *Chem. Phys. Letts.* **1986**, *124*, 152.
   (b) Lever, A. B. P. *Inorg. Chem.* **1990**, *29*, 1271.

(85) (a) Cooley, L. F.; Headford, C. E. L.; Elliott, C. M.; Kelley, D. F. *J. Am. Chem. Soc.* **1988**, *110*, 6673. (b) Larson, S. L.; Cooley, L. F.; Elliott, C. M.; Kelley, D. F. *J. Am. Chem. Soc.* **1992**, *114*, 9504.

(86) Scandola, F.; Argazzi, R.; Bignozzi, C. A.; Indelli, M. T. *J. Photochem. Photobiol. A: Chem* **1994**, *82*, 191.

(87) Bruce, M. R. M.; Megehee, E.; Sullivan, B. P.; Thorp, H.; O'Toole,T. R. O.; Downard, A.; Meyer, T. J. *Organometallics* **1988**, *7*, 238.

(88) (a) Caspar, J. V.; Westmoreland, T. D.; Allen, G. H.; Bradley, P. G.; Meyer, T. J.; Woodruff, W. H. *J. Am. Chem. Soc.* **1984**, *106*, 3492. (b) Caspar, J. V.; Meyer, T. J. *Inorg. Chem.* **1983**, *22*, 2444. (c) Klassen, D. M.; Crosby, G. A. *J. Chem. Phys.* **1968**, *48*, 1853. (d) Demas, J. N.; Crosby, G. A. *J. Am. Chem. Soc.* **1971**, *93*, 2841.

APPENDIX
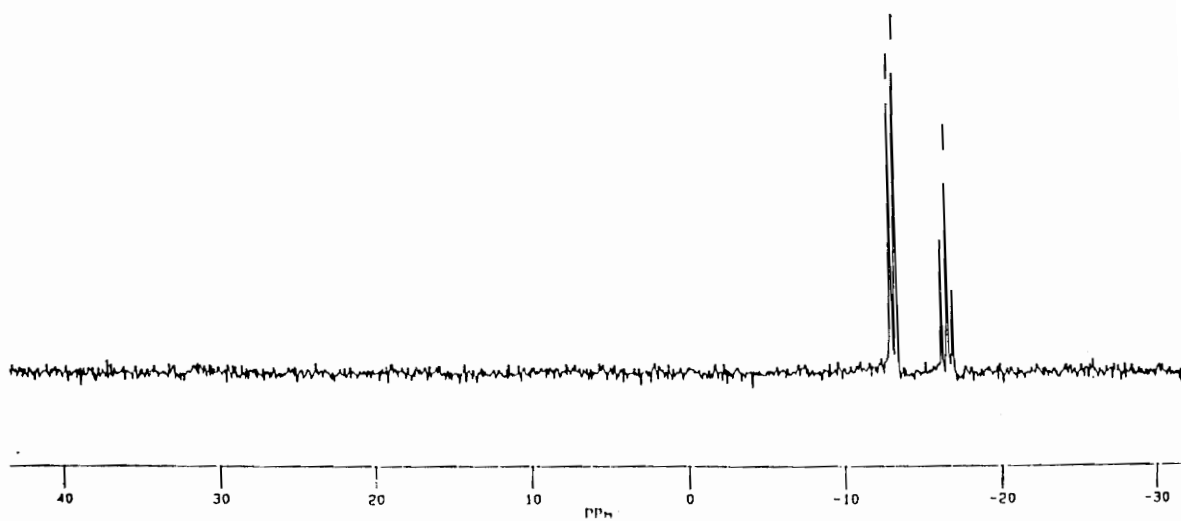
Figure A-I. ^{31}P NMR spectrum of PPP (where PPP = (bis(2-diphenylphosphinoethyl)phenylphosphine).
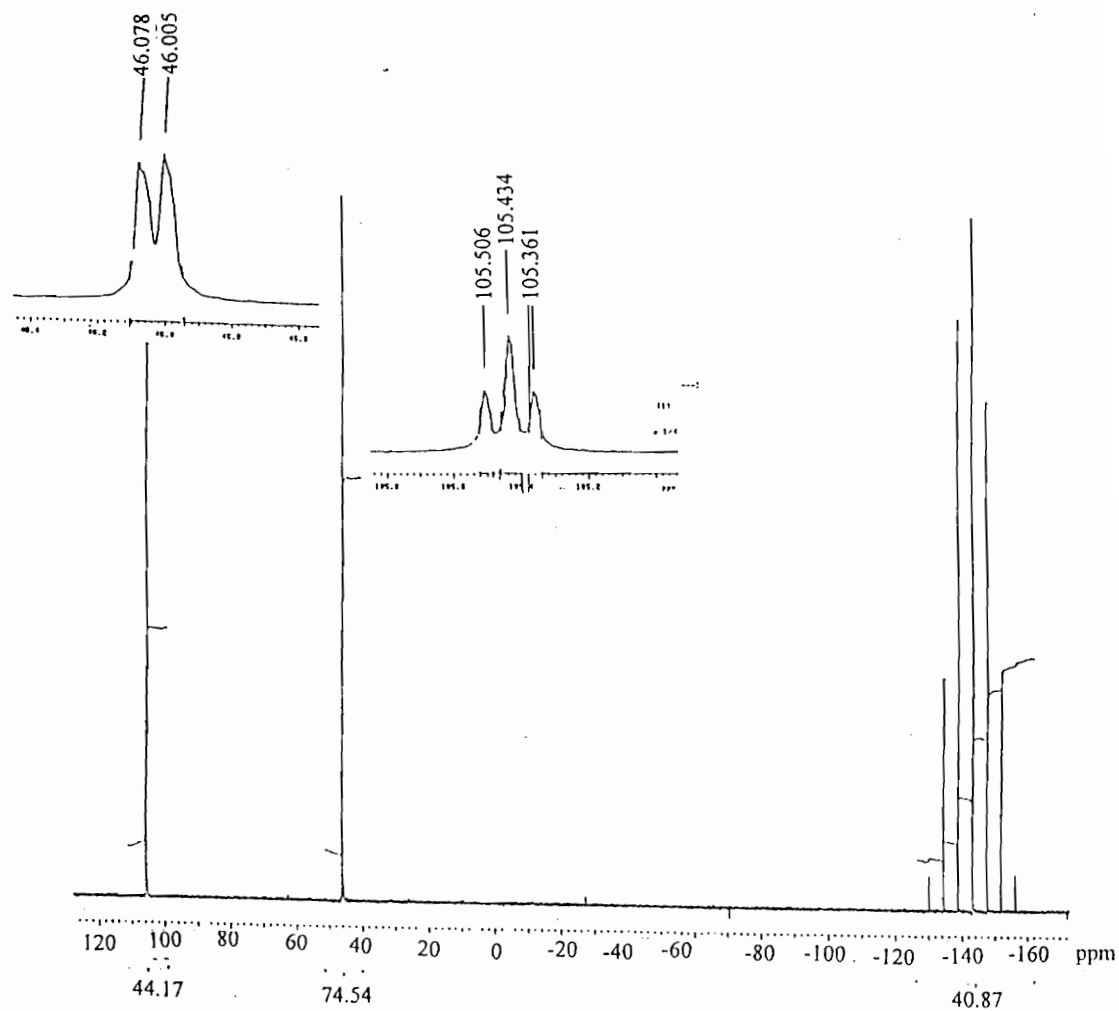
Figure A-II. ^{31}P NMR Spectrum of $[Ru(tpy)(PPP)]^{2+}$ (where tpy = 2,2':6',2''-terpyridine and PPP = (bis(2-diphenylphosphinoethyl) phenylphosphine).
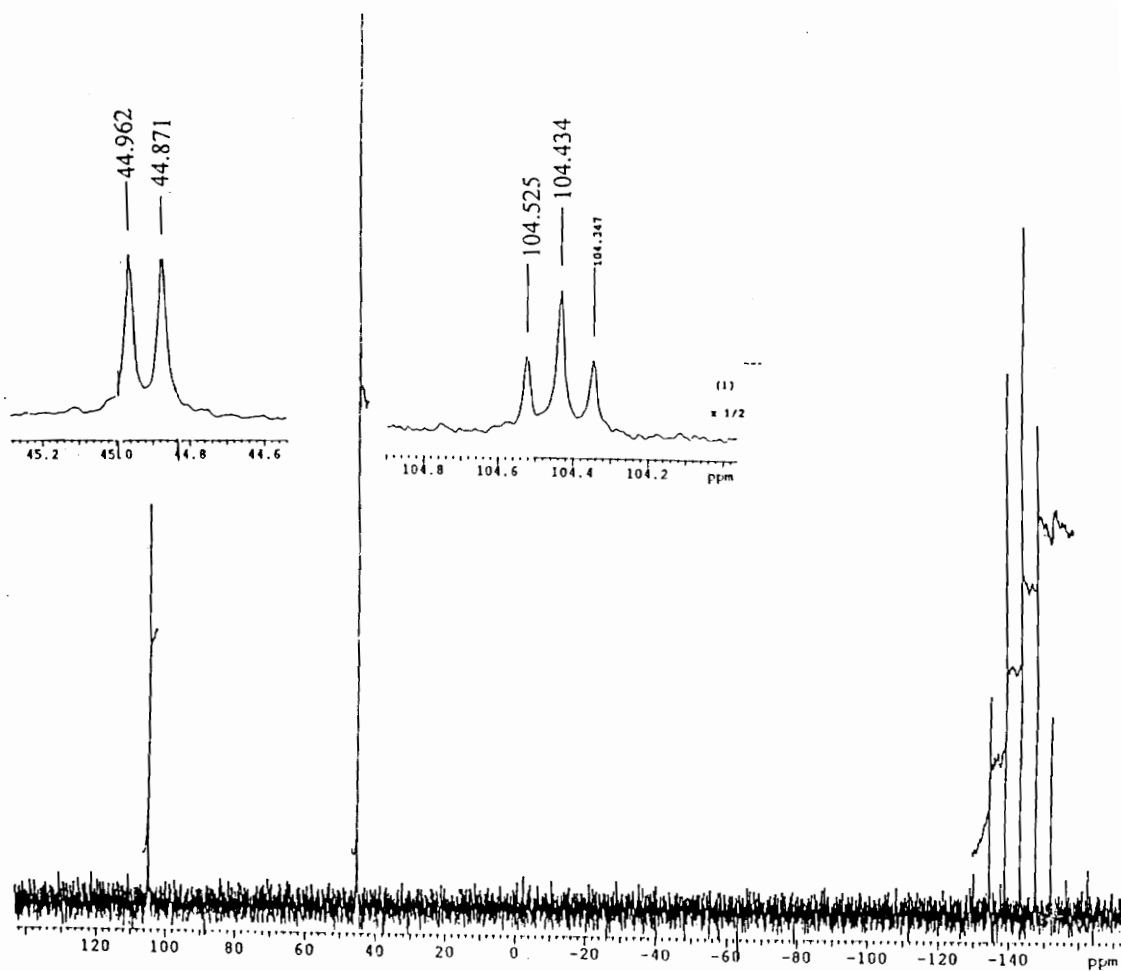
Figure A-III. ^{31}P NMR Spectrum of [Ru(tpp)(PPP)]$^{2+}$ (where tpp = 2,3,5,6-tetrakis(2-pyridyl)pyrazine and PPP = (bis(2-diphenylphosphinoethyl)phenylphosphine).
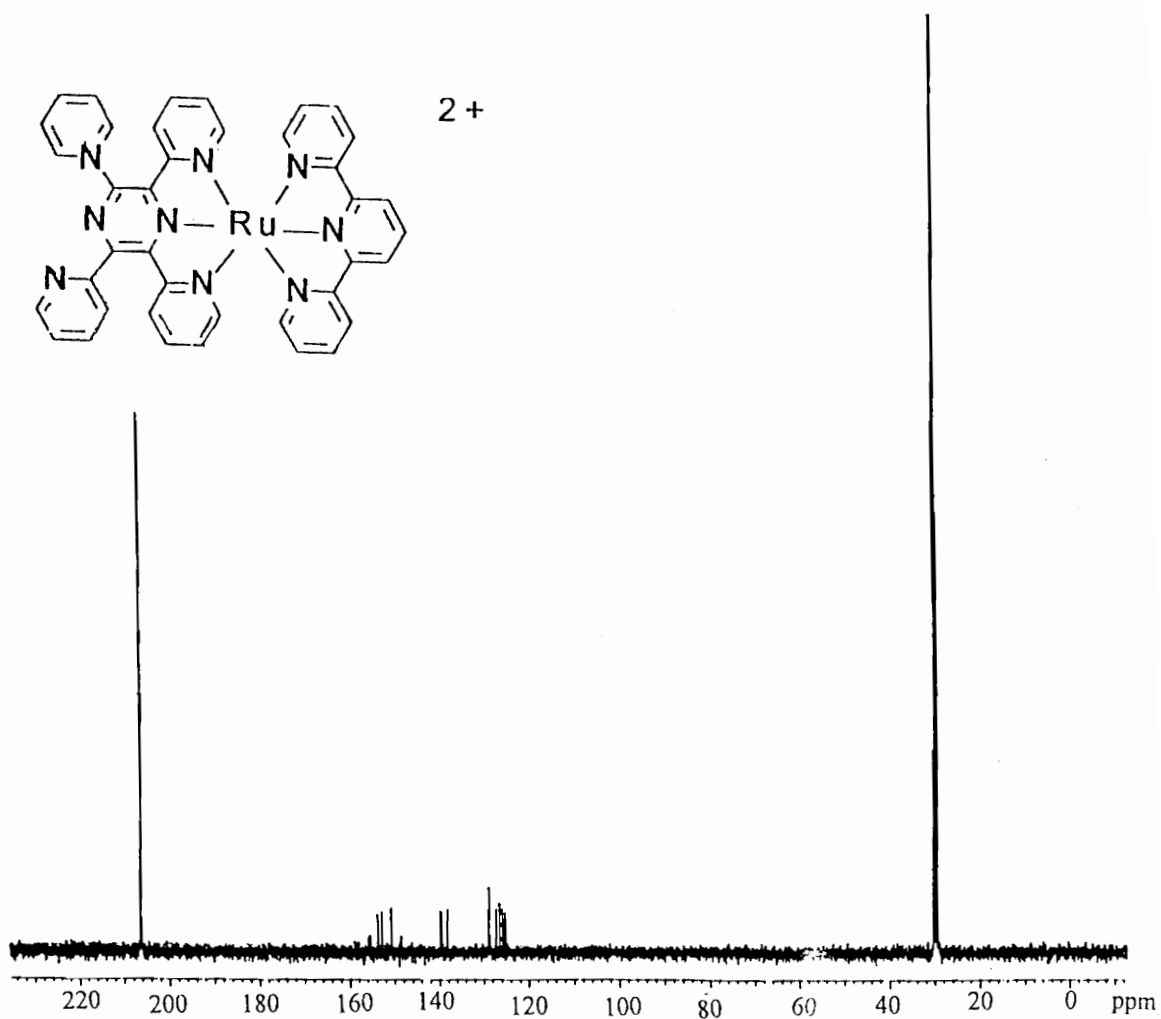
Figure A-IV. ^{13}C NMR Spectrum of [Ru(tpy)(tpp)]$^{2+}$ (where tpy = 2,2':6',2''-terpyridine and tpp = 2,3,5,6-tetrakis(2-pyridyl)pyrazine).
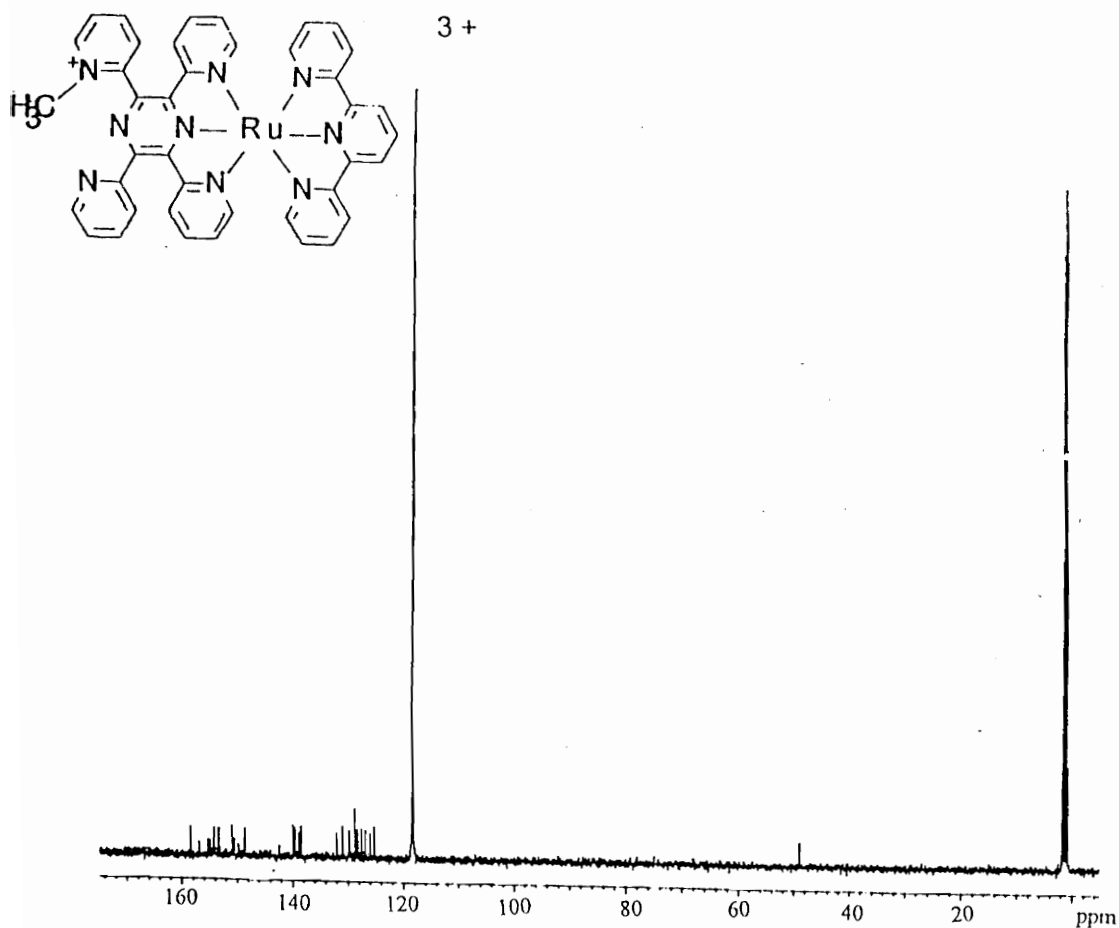
Figure A-V. ^{13}C NMR Spectrum of [Ru(tpy)(Metpp)]$^{2+}$ (where tpy =
2,2':6',2''-terpyridine and Metpp = 2-[2-(1-Methylpyridiniumyl)]-3,5,6-
tris(2-pyridyl)pyrazine).
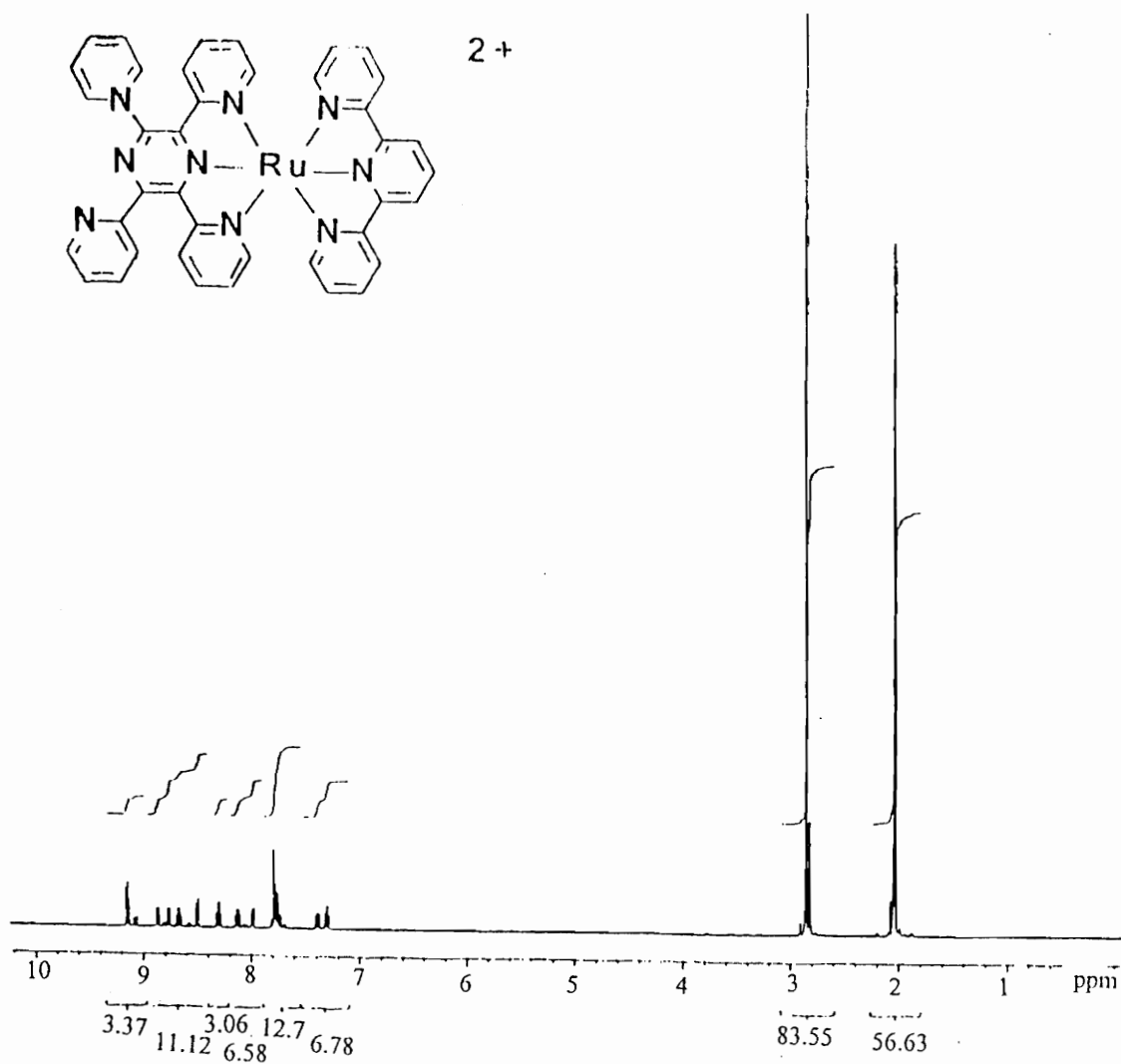
Figure A-VI. ^{1}H NMR Spectrum of [Ru(tpy)(tpp)]$^{2+}$ (where tpy = 2,2':6',2''-terpyridine and tpp = 2,3,5,6-tetrakis(2-pyridyl)pyrazine).
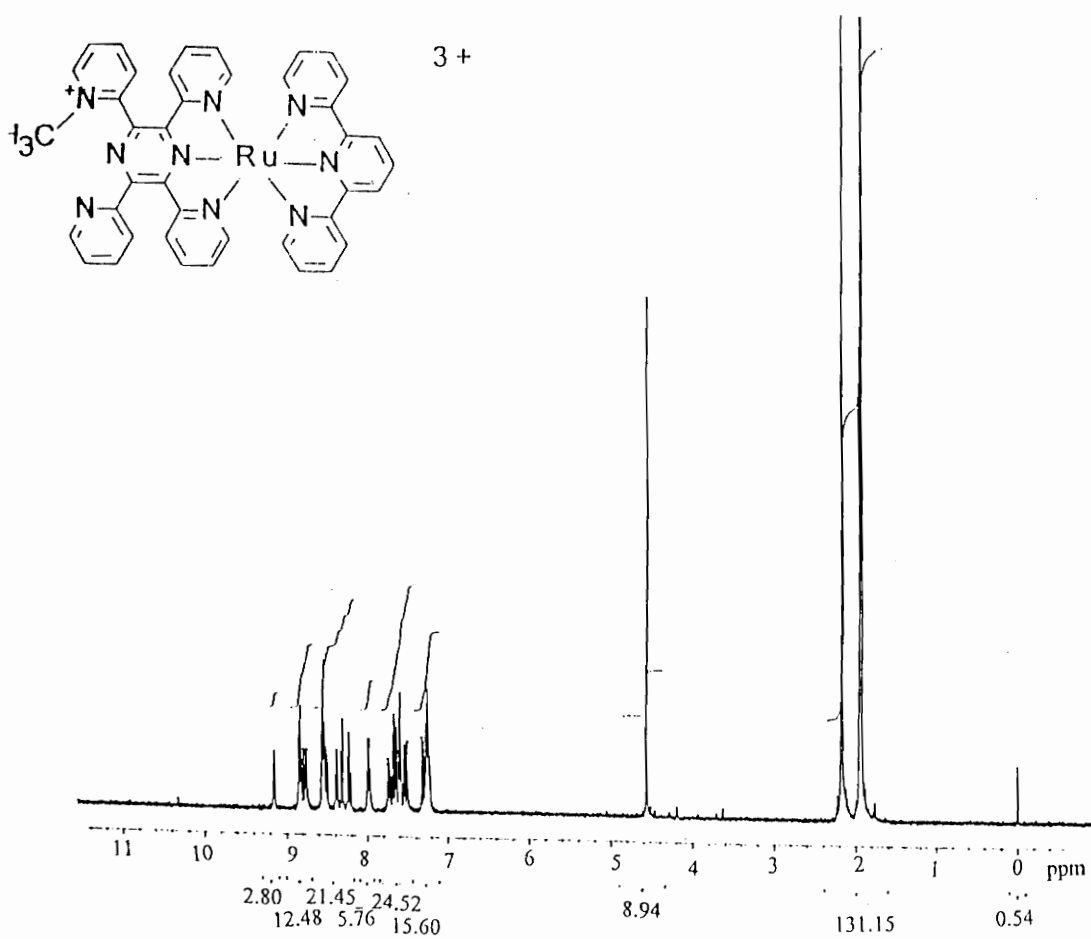
Figure A-VII. ^{1}H NMR Spectrum of [Ru(tpy)(Metpp)]$^{2+}$ (where tpy = 2,2':6',2''-terpyridine and Metpp = 2-[2-(1-Methylpyridiniumyl)]-3,5,6-tris(2-pyridyl)pyrazine).
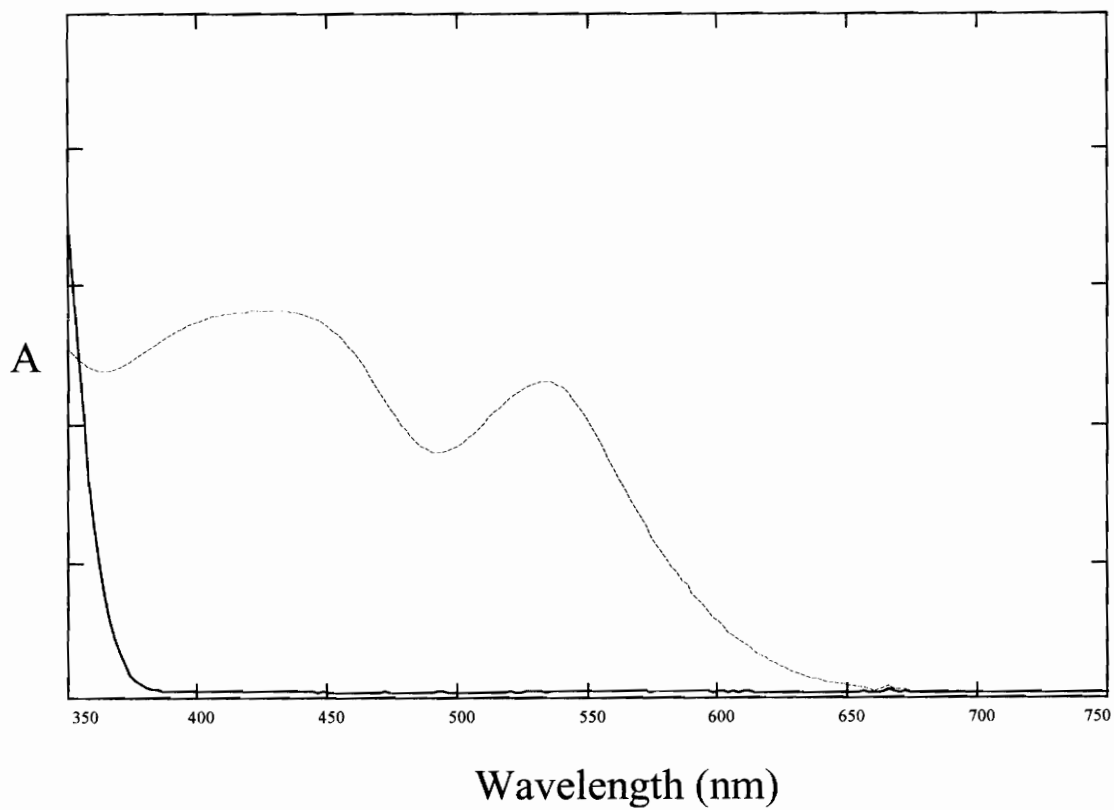
Figure A-VIII. Reductive Spectroelectrochemical results for tpp (where tpp = 2,3,5,6-tetrakis(2-pyridyl)pyrazine).
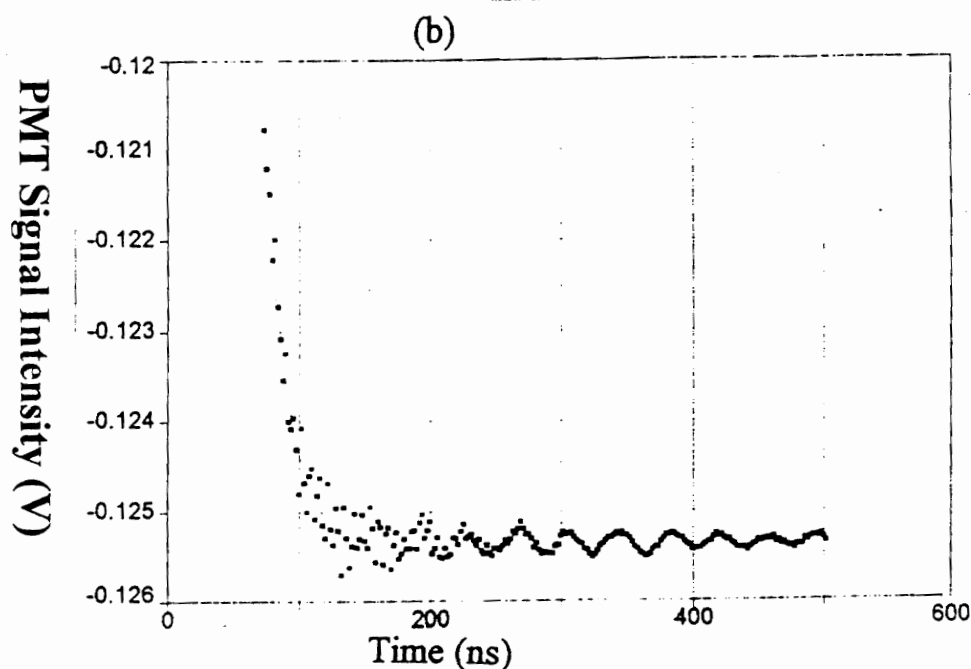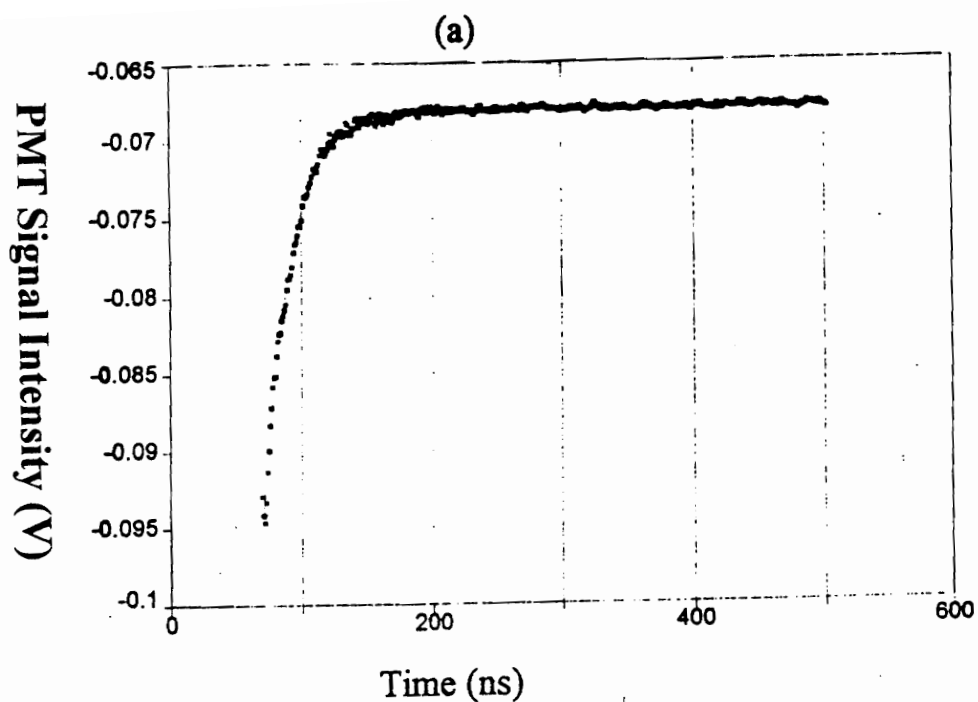
Figure A-IX. Transient Absorbance Spectra for [Ru(tpy)(Metpp)]$^{3+}$:
(a) excite at 532 nm, monitor at 655 nm and (b) excite at 532 nm, monitor
at 390 nm (where tpy = 2,2',2''-terpyridine and Metpp = 2-[2-(1-
Methylpyrindiniumyl)]-3,5,6-tris(2-pyridyl)pyrazine).
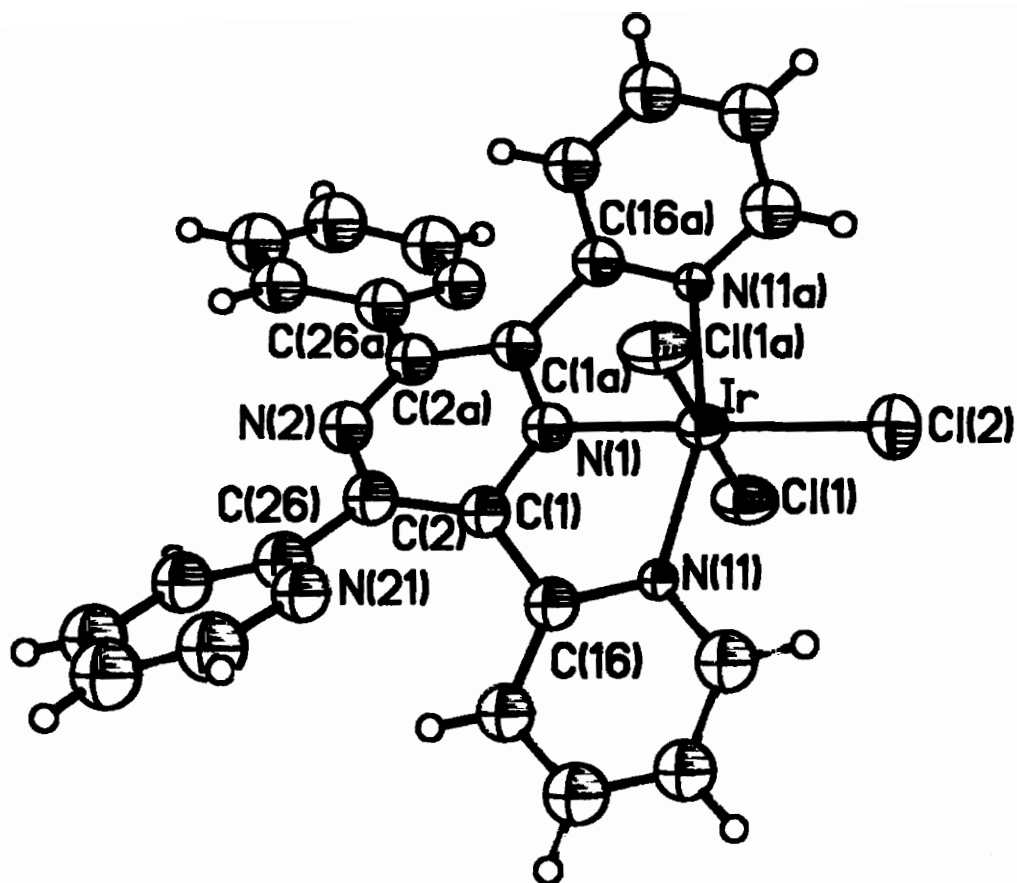
Figure A-X. X-ray crystal structure of Ir(tpp)Cl$_3$ (50 % thermal ellipsoids).
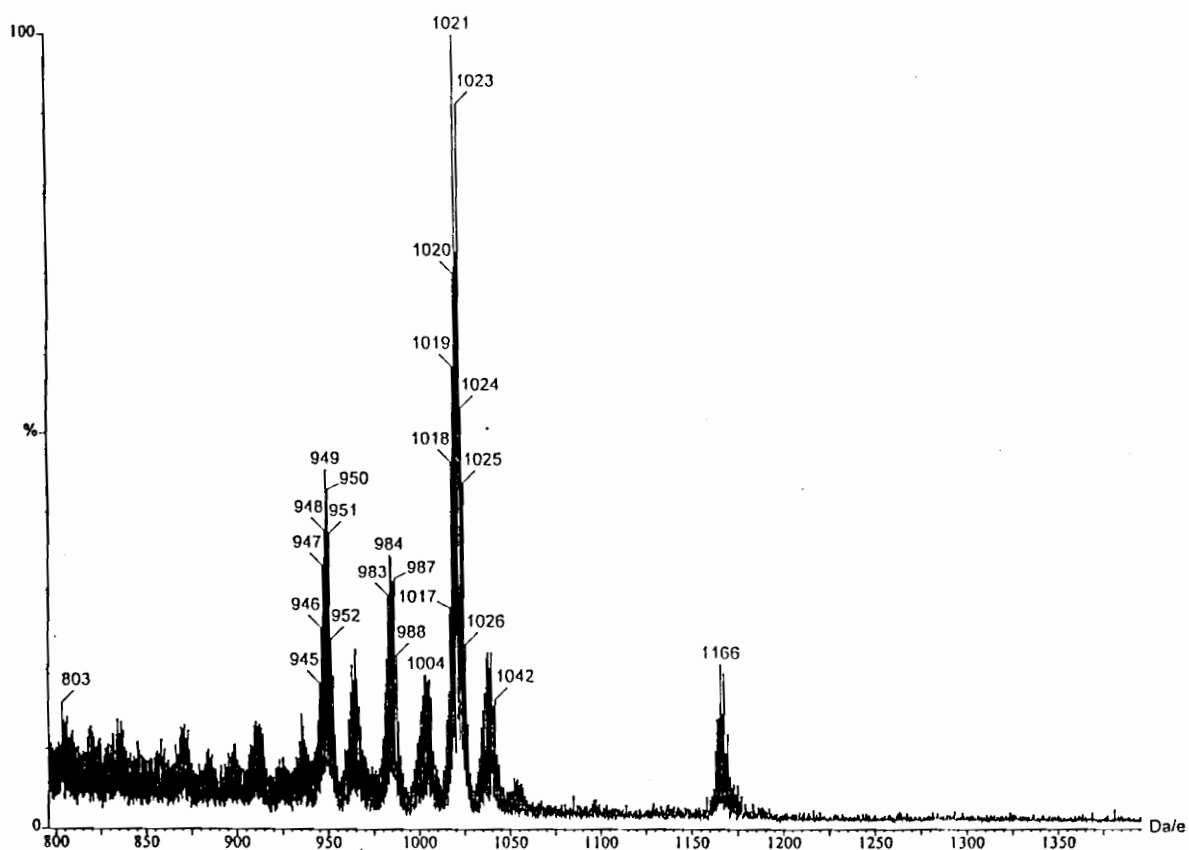
Figure A-XI. Fast Atom Bombardment Mass Spectrum of [(tpy)Ru(tpp)IrCl$_3$](PF$_6$)$_2$ (where tpy = 2,2':6',2''-terpyridine and tpp = 2,3,5,6-tetrakis(2-pyridyl)pyrazine, liquid matrix of neat 3-nitrobenzyl alcohol, Fisions VG Quattro Triple-Stage Quadupole Mass Spectrometer, electron impact ionization energy of 70 eV, 200° C source energy, methane as the reagent gas for chemical ionization and 20 kV Cesium ions for liquid secondary ionization).
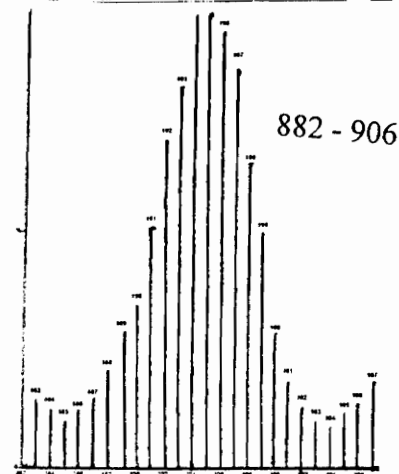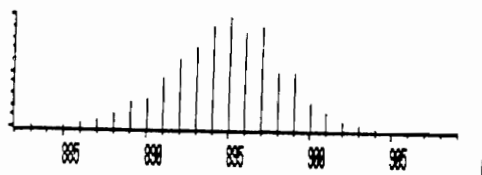
180
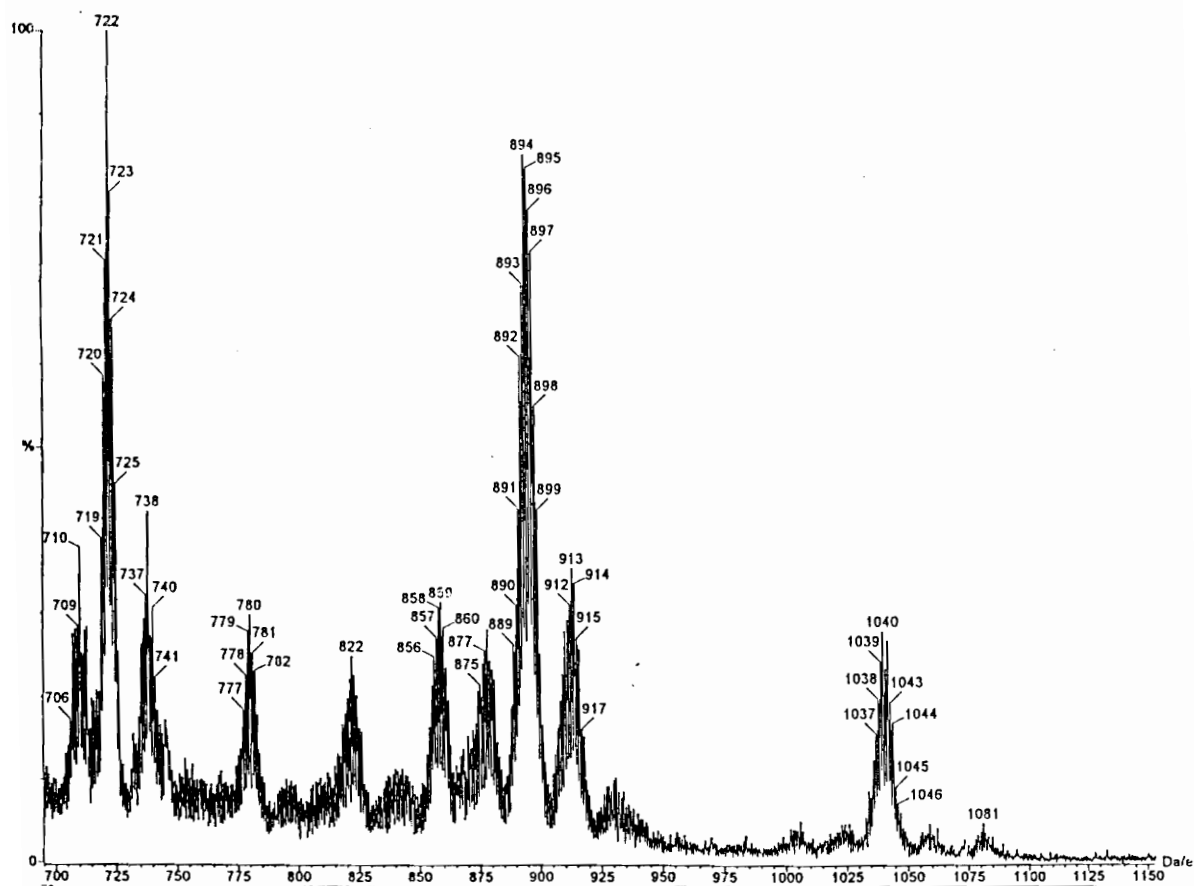
Figure A-XII. Fast Atom Bombardment Mass Spectrum of [(tpy)Ru(tpp)RuCl$_3$](PF$_6$) (where tpy = 2,2':6',2''-terpyridine and tpp = 2,3,5,6-tetrakis(2-pyridyl)pyrazine, liquid matrix of neat 3-nitrobenzyl alcohol, Fisions VG Quattro Triple-Stage Quadupole Mass Spectrometer, electron impact ionization energy of 70 eV, 200° C source energy, methane as the reagent gas for chemical ionization and 20 kV Cesium ions for liquid secondary ionization).
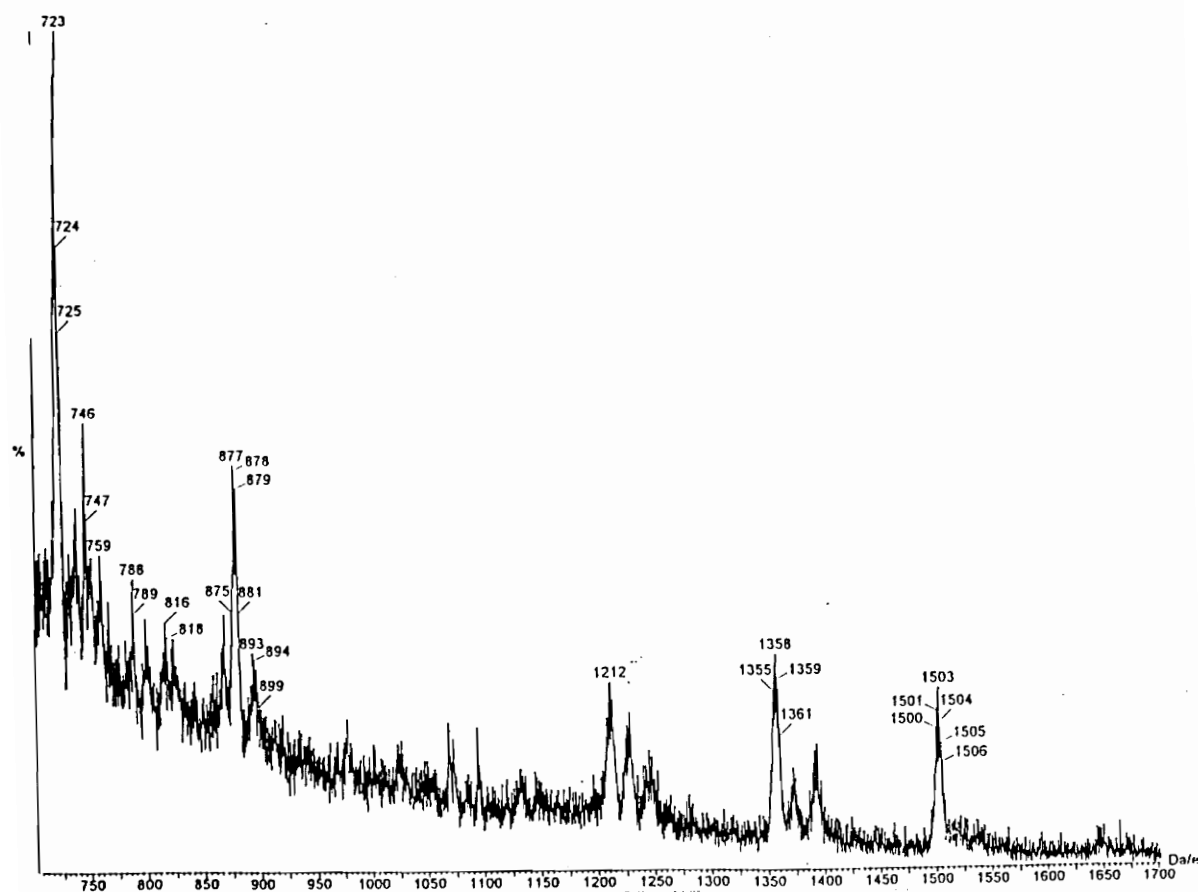
Figure A-XIII. Fast Atom Bombardment Mass Spectrum of
[(tpy)Ru(tpp)Ru(tpp)](PF$_6$)$_4$ (where tpy = 2,2':6',2''-terpyridine and
tpp = 2,3,5,6-tetrakis(2-pyridyl)pyrazine, liquid matrix of neat 3-nitrobenzyl
alcohol, Fisions VG Quattro Triple-Stage Quadupole Mass Spectrometer,
electron impact ionization energy of 70 eV, 200° C source energy, methane
as the reagent gas for chemical ionization and 20 kV Cesium ions for liquid
secondary ionization).
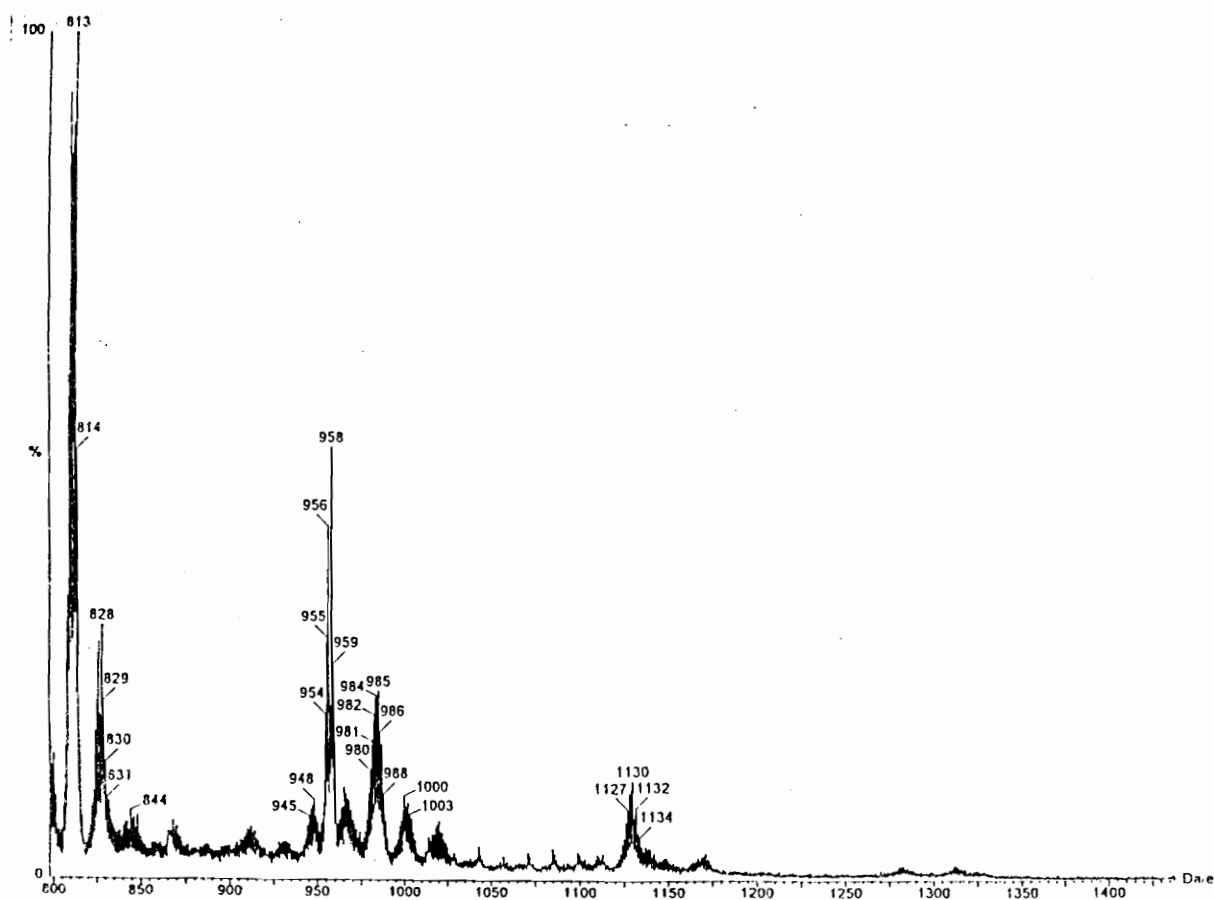
Figure A-XIV. Fast Atom Bombardment Mass Spectrum of [(tpy)Os(tpp)RuCl₃](PF₆) (where tpy = 2,2':6',2''-terpyridine and tpp = 2,3,5,6-tetrakis(2-pyridyl)pyrazine, liquid matrix of neat 3-nitrobenzyl alcohol, Fisions VG Quattro Triple-Stage Quadupole Mass Spectrometer, electron impact ionization energy of 70 eV, 200° C source energy, methane as the reagent gas for chemical ionization and 20 kV Cesium ions for liquid secondary ionization).

183
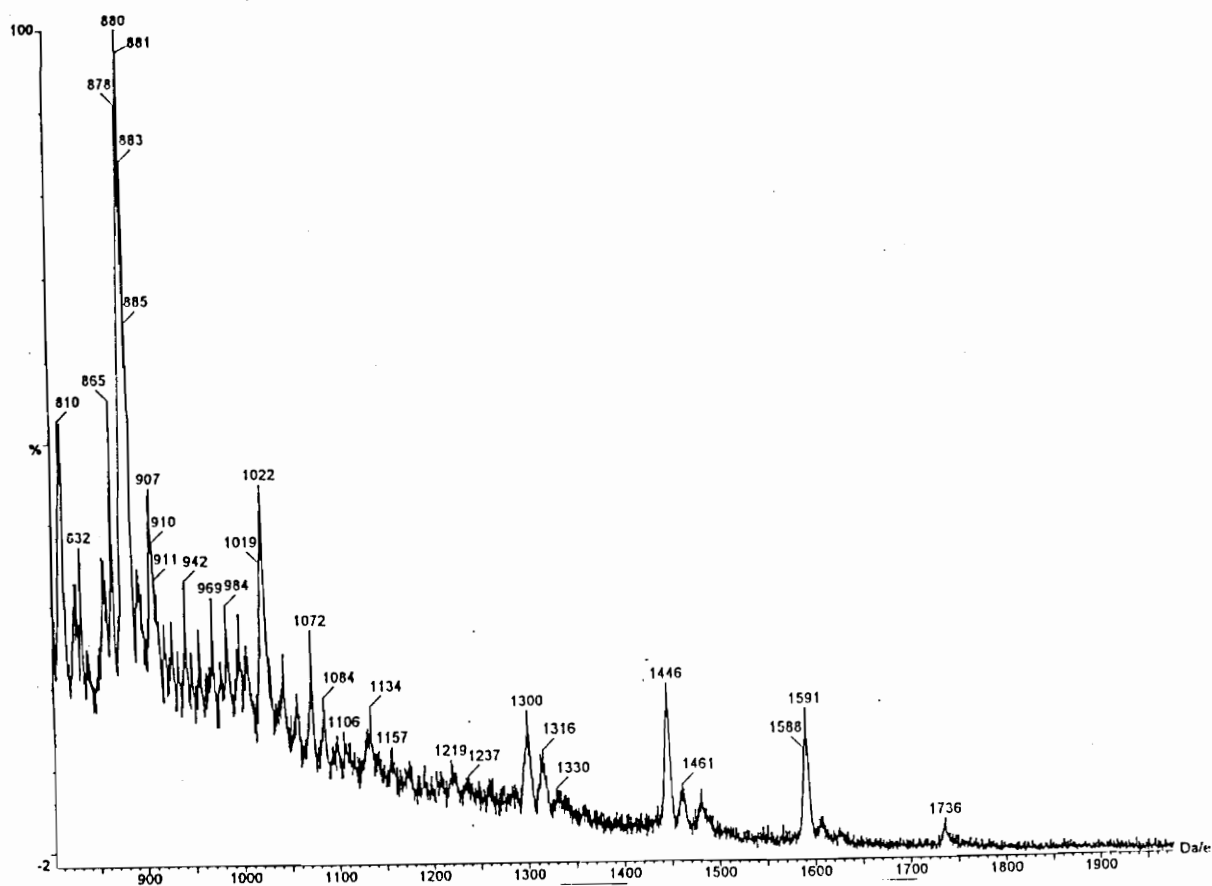
Figure A-XV. Fast Atom Bombardment Mass Spectrum of [(tpy)Os(tpp)Ru(tpp)](PF$_6$)$_4$ (where tpy = 2,2':6',2''-terpyridine and tpp = 2,3,5,6-tetrakis(2-pyridyl)pyrazine, liquid matrix of neat 3-nitrobenzyl alcohol, Fisions VG Quattro Triple-Stage Quadupole Mass Spectrometer, electron impact ionization energy of 70 eV, 200° C source energy, methane as the reagent gas for chemical ionization and 20 kV Cesium ions for liquid secondary ionization).

184
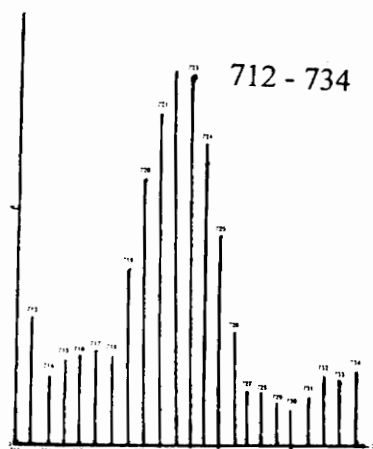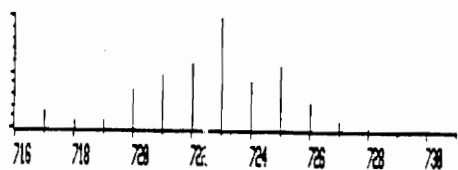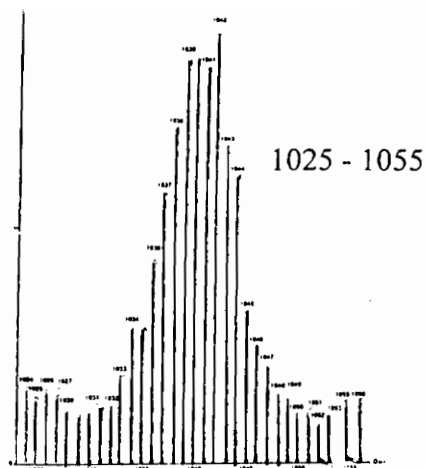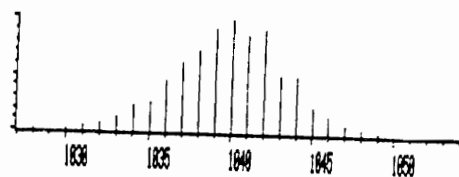
Calculated Isotropic Distributions   Experimental Distributions

Figure A-XVI. Isotropic Distribution Calculations versus Experimental
Results of the Assigned Peaks for [(tpy)Ru(tpp)RuCl₃](PF₆) (where tpy =
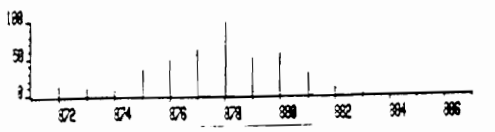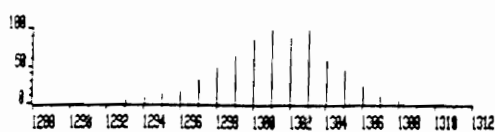2,2':6',2''-terpyridine and tpp = 2,3,5,6-tetrakis(2-pyridyl)pyrazine).
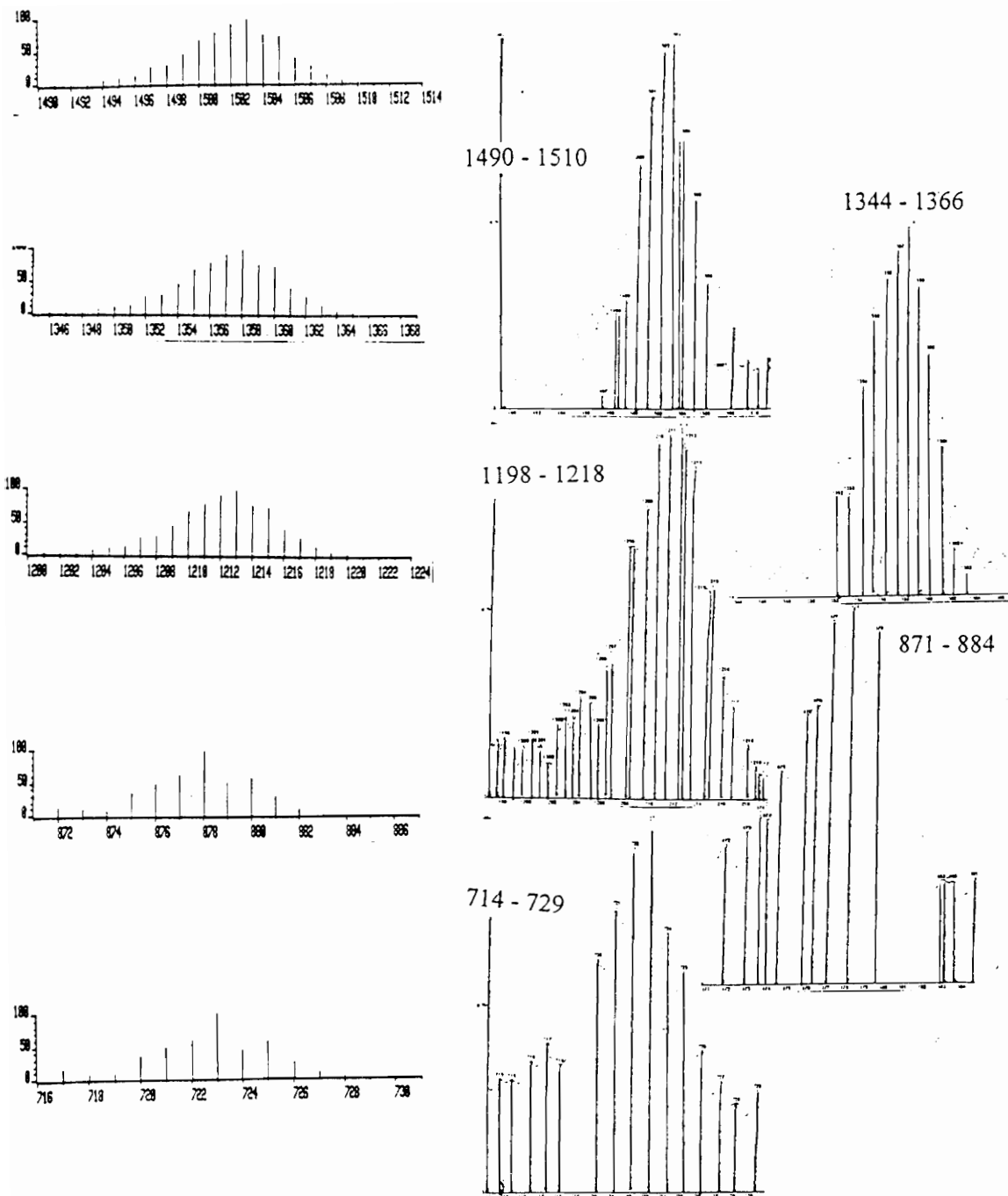
Calculated Isotropic Distributions   Experimental Distributions
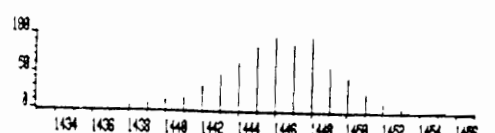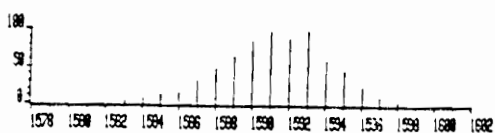
Figure A-XVII. Isotropic Distribution Calculations versus Experimental Results of the Assigned Peaks for [(tpy)Ru(tpp)Ru(tpp)](PF$_6$)$_4$ (where tpy = 2,2':6',2''-terpyridine and tpp = 2,3,5,6-tetrakis(2-pyridyl)pyrazine).
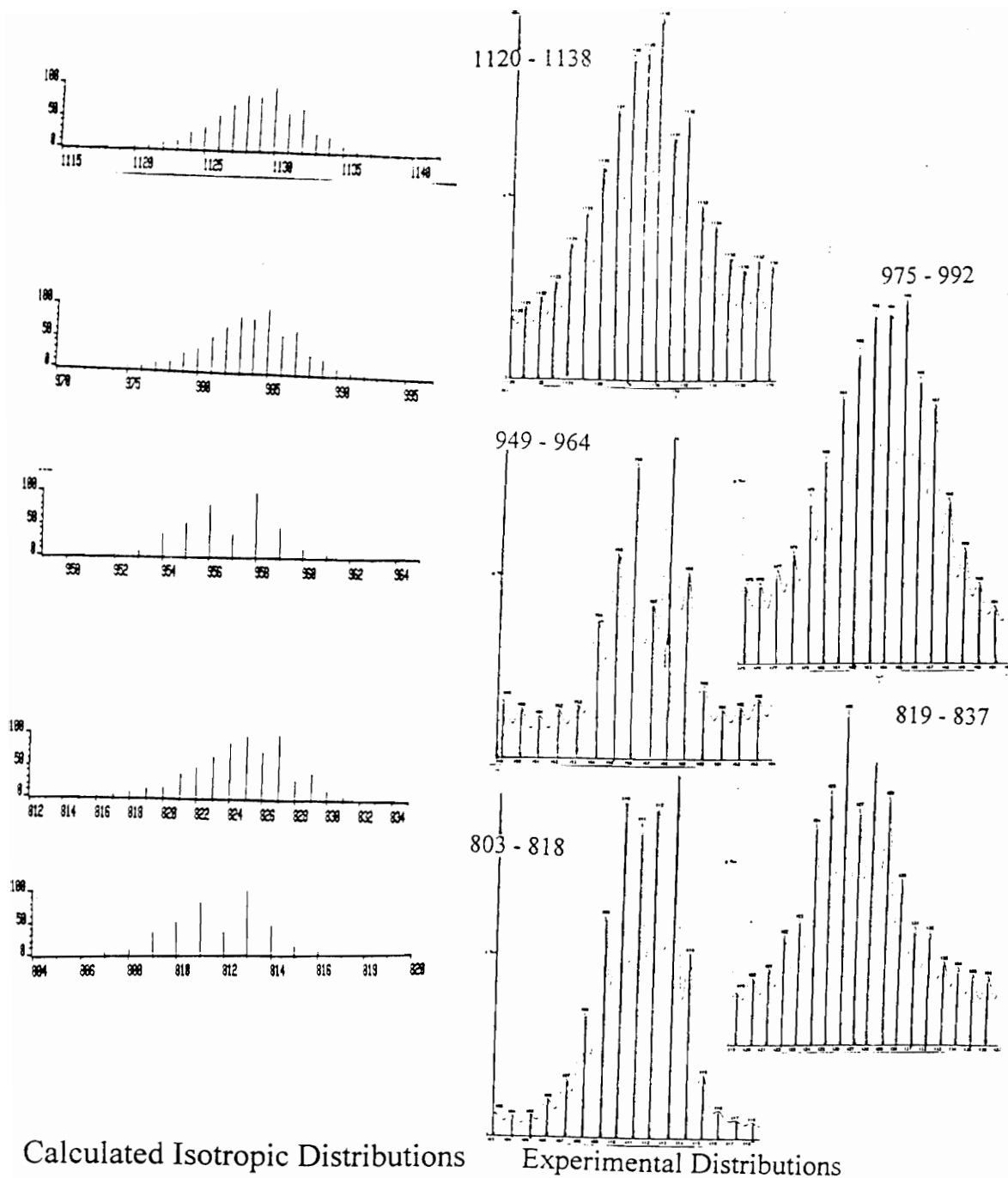
Calculated Isotropic Distributions   Experimental Distributions
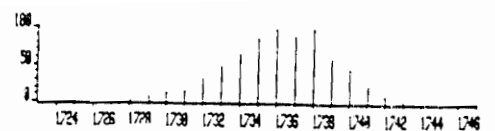
Figure A-XIII. Isotropic Distribution Calculations versus Experimental
Results of the Assigned Peaks for [(tpy)Os(tpp)RuCl$_3$](PF$_6$) (where tpy =
2,2':6',2''-terpyridine and tpp = 2,3,5,6-tetrakis(2-pyridyl)pyrazine).
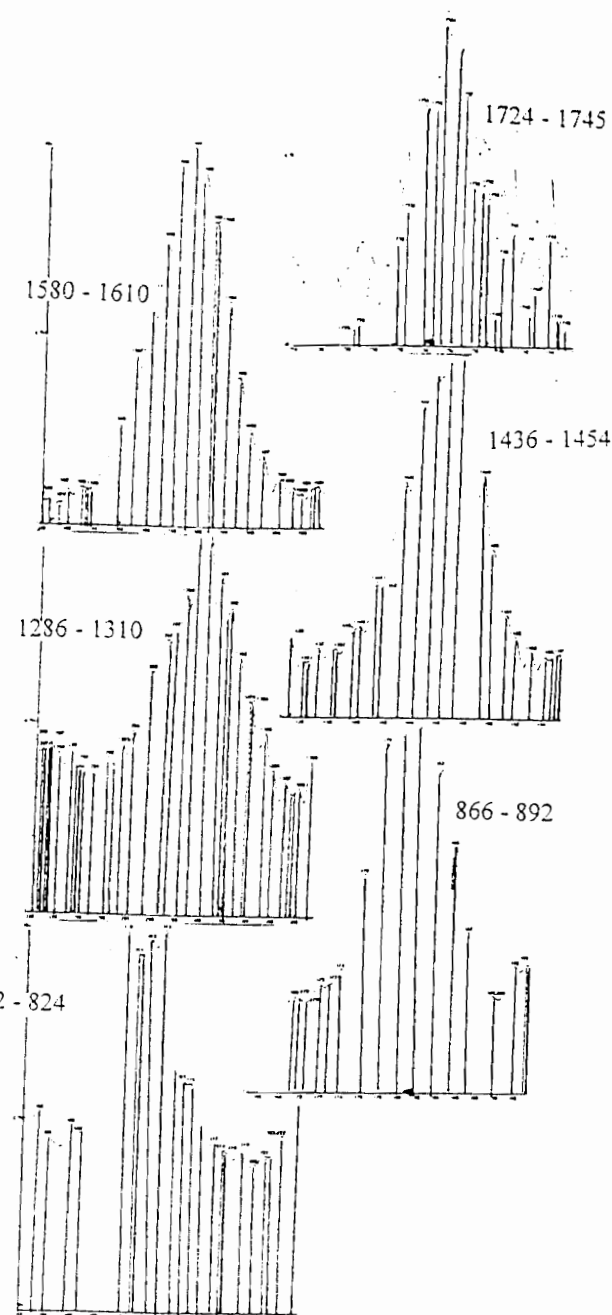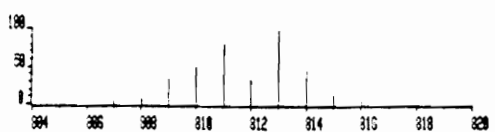
Calculated Isotropic Distributions   Experimental Distributions

Figure A-XIX. Isotropic Distribution Calculations versus Experimental Results of the Assigned Peaks for [(tpy)Os(tpp)Ru(tpp)](PF$_6$)$_4$ (where tpy = 2,2':6',2''-terpyridine and tpp = 2,3,5,6-tetrakis(2-pyridyl)pyrazine).
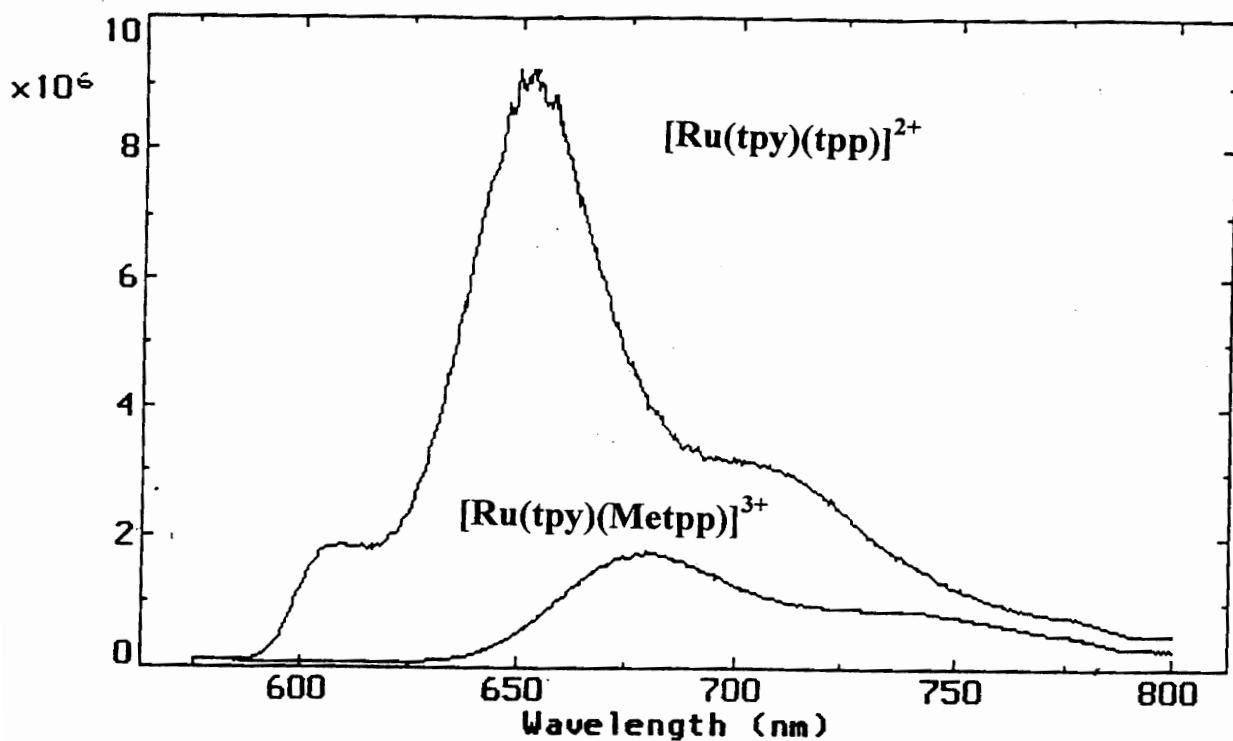
Figure A-XX. Emission spectra of absorbance matched samples of [Ru(tpy)(tpp)]$^{2+}$ and [Ru(tpy)(Metpp)]$^{3+}$ at 77 K (where tpy = 2,2':6',2''-terpyridine, tpp = 2,3,5,6-tetrakis(2-pyridyl)pyrazine), and Metpp = 2-[2-(1-Methylpyridiniumyl)]-3,5,6-tris(2-pyridyl)pyrazine).

Figure A-XXI. Emission spectra of absorbance matched samples of [Ru(bpy)(tpp)(CH$_3$CN)]$^{2+}$ and [Ru(bpy)(Metpp)(CH$_3$CN)]$^{3+}$ at 77 K (where tpy = 2,2':6',2''-terpyridine, tpp = 2,3,5,6-tetrakis(2-pyridyl)pyrazine), and Metpp = 2-[2-(1-Methylpyridiniumyl)]-3,5,6-tris(2-pyridyl)pyrazine).
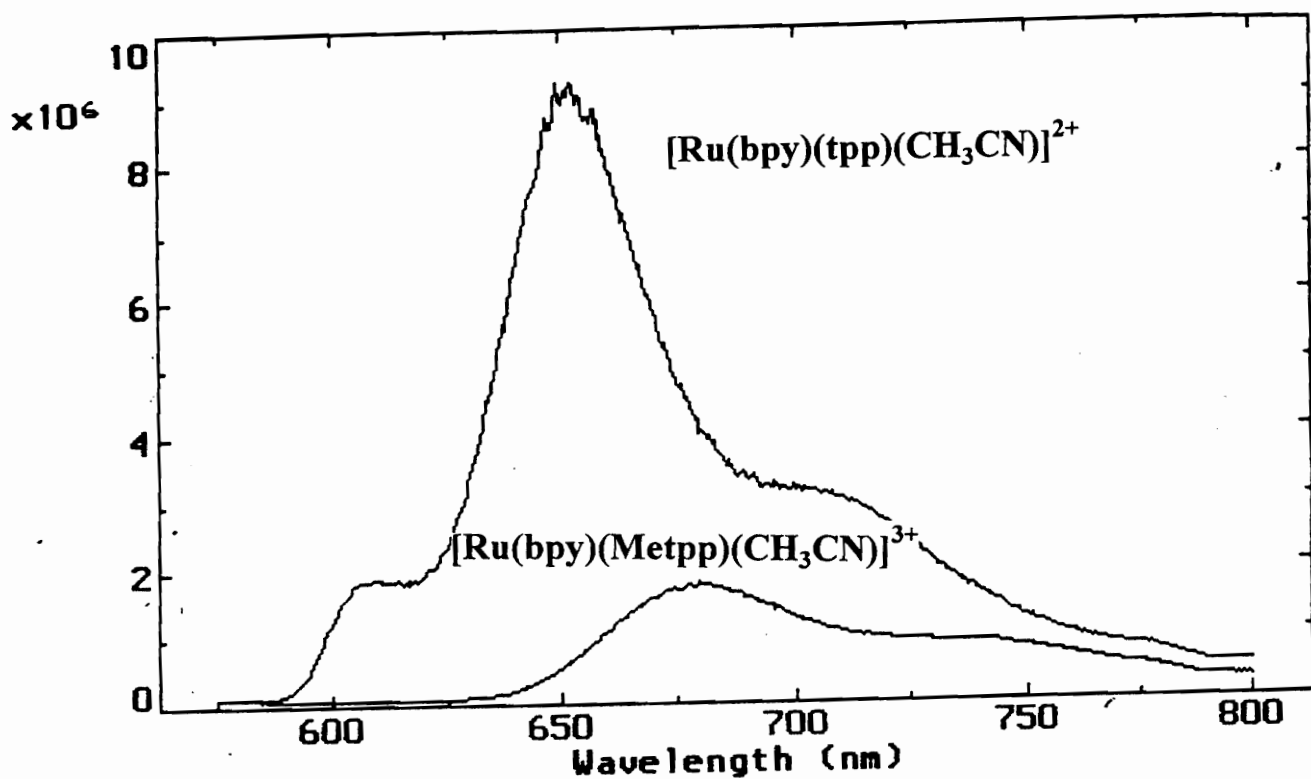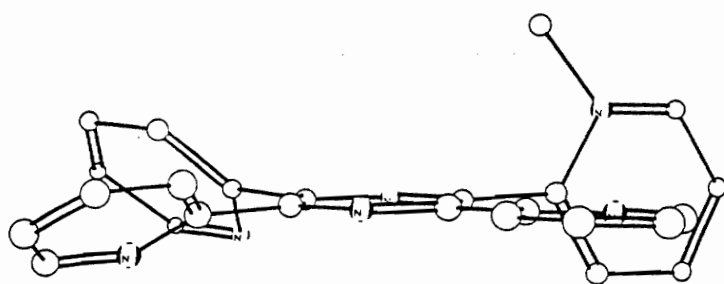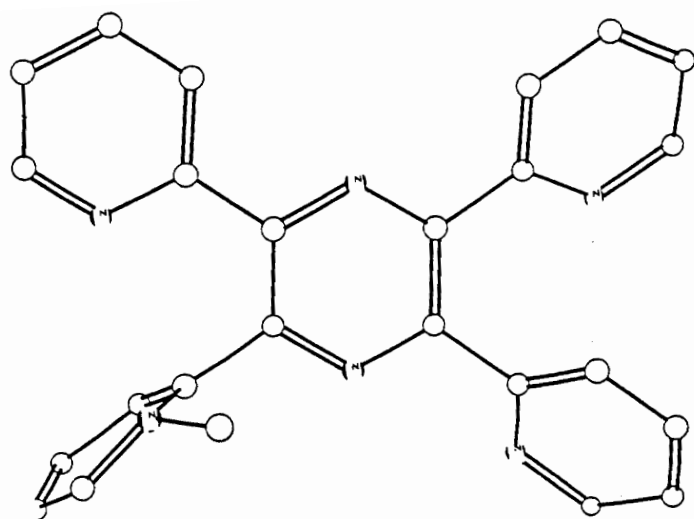
Figure A-XXII. Minimized Picture of Metpp Showing the Rotation of the Electron Accepting Moiety (where Metpp$^+$ = 2-[2-(1-Methylpyridiniumyl)]-3,5,6-tris(2-pyridyl)pyrazine and the dihedral angle is 53°).

Table A-1. Fast Atom Bombardment Mass Spectral Data for [(tpy)Ru(tpp)IrCl$_3$](PF$_6$)$_2$, [(tpy)Ru(tpp)RuCl$_3$](PF$_6$), [(tpy)Ru(tpp)Ru(tpp)](PF$_6$)$_4$, [(tpy)Os(tpp)RuCl$_3$](PF$_6$), and [(tpy)Os(tpp)Ru(tpp)](PF$_6$)$_4$ (where tpy = 2,2':6',2''-terpyridine and tpp = 2,3,5,6-tetrakis(2-pyridyl)pyrazine).

Complex	m/z	Relative Abundance	Assignment
[(tpy)Ru(tpp)IrCl$_3$](PF$_6$)$_2$	1166		[(tpy)Ru(tpp)IrCl$_3$](PF$_6$)$^+$
	1020		[(tpy)Ru(tpp)IrCl$_3$]$^+$
	985		[(tpy)Ru(tpp)IrCl$_2$]$^+$
	950		[(tpy)Ru(tpp)IrCl]$^+$
	915		[(tpy)Ru(tpp)Ir]$^+$
	722		[(tpy)Ru(tpp)]$^+$
[(tpy)Ru(tpp)RuCl$_3$](PF$_6$)	1039	28	[(tpy)Ru(tpp)RuCl$_2$](PF$_6$)$^+$
	894	85	[(tpy)Ru(tpp)RuCl$_2$]$^+$
	722	100	[(tpy)Ru(tpp)]$^+$
[(tpy)Ru(tpp)Ru(tpp)](PF$_6$)$_4$	1501	17	[(tpy)Ru(tpp)Ru(tpp)](PF$_6$)$_2$$^+$
	1356	21	[(tpy)Ru(tpp)Ru(tpp)](PF$_6$)$^+$
	1211	18	[(tpy)Ru(tpp)Ru(tpp)]$^+$
	877	45	[(tpp)Ru(tpp)]$^+$
	722	100	[(tpy)Ru(tpp)]$^+$

Complex	m/z	Relative Abundance	Assignment
[(tpy)Os(tpp)RuCl$_3$](PF$_6$)	1128	13	[(tpy)Os(tpp)RuCl$_2$](PF$_6$)$^+$
	985	23	[(tpy)Os(tpp)RuCl$_2$]$^+$
	956	50	[(tpy)Os(tpp)](PF$_6$)$^+$
	825	30	[Os(tpp)Ru](PF$_6$)$^+$
	811	100	[(tpy)Os(tpp)]$^+$
[(tpy)Os(tpp)Ru(tpp)](PF$_6$)$_4$	1735	4	[(tpy)Os(tpp)Ru(tpp)](PF$_6$)$_3$$^+$
	1590	15	[(tpy)Os(tpp)Ru(tpp)](PF$_6$)$_2$$^+$
	1445	20	[(tpy)Os(tpp)Ru(tpp)](PF$_6$)$^+$
	1300	16	[(tpy)Os(tpp)Ru(tpp)]$^+$
	877	100	[(tpp)Ru(tpp)]$^+$
	811	52	[(tpy)Os(tpp)]$^+$

Samples analyzed by dissolving directly in a 3-nitrobenzyl alcohol matrix using a Fisions VG Quattro Triple-Stage Quadupole Mass Spectrometer with an electron impact ionization energy of 70 eV, 200° C source energy, using methane as the reagent gas for chemical ionization and 20 kV Cesium ions for liquid secondary ionization.

Vitae

Lisa Michelle Vogler was born July 5, 1968, in Salem, Oregon, to Anne and Martin Vogler. After moving various places in the United States, in 1978 she moved to Anchorage, Alaska, with her mother, step father, Roger, and two sisters, Kristina and Julie. In 1986, she graduated with honors from A. J. Dimond High School.

August 1986, Lisa moved to Austin, Texas, to begin her undergraduate education at Saint Edward's University.. After her first year she decided to be a Biology major but continued taking chemistry classes for enjoyment. After her second year, she saw the light and switched to a Chemistry major. During her senior year, she studied the photolysis of copper complexes and gave a senior seminar on her research. In May 1990, she received a Bachelor of Science degree from Saint Edward's University with honors.

In June of 1990, Lisa moved to Pullman, Washington to begin a research program with Dr. Karen Brewer at Washington State University. During that summer she performed research that led to this project. In 1992, she received a Teaching Excellence Award from Washington State University. In May of 1992, Dr. Karen Brewer accepted a teaching position at Virginia Polytechnic Institute and State University that resulted in a move for the research group to Blacksburg, Virginia. In the summer of 1995, she received a Ph. D. in Chemistry from Virginia Polytechnic Institute and State University. In August of 1995, Lisa will be moving to Columbus, Ohio with Mark Vrana where she will begin her search for employment.